THE TRANSCRIPTIONAL AND EPIGENETIC ROLE OF BRD4 IN THE REGULATION OF THE CELLULAR STRESS RESPONSE

INAUGURAL-DISSERTATION

to obtain the academic degree

Doctor rerum naturalium

(Dr. rer. nat.)

submitted to the Department of Biology, Chemistry and Pharmacy
of Freie Universität Berlin

by

Michelle Hussong

from Zweibrücken

2015

Die vorliegende Arbeit wurde im Zeitraum von Juli 2012 bis September 2015 am Max-Planck-Institut für Molekulare Genetik in Berlin sowie an der Universität zu Köln unter der Leitung von Frau Prof. Dr. Dr. Michal-Ruth Schweiger angefertigt.

1. Gutachter: Prof. Dr. Dr. Michal-Ruth Schweiger

2. Gutachter: Prof. Dr. Rupert Mutzel

Disputation am 07.12.2015

ACKNOWLEDGMENT

This dissertation would not have been possible without the guidance and the help of many people who in one way or another contributed to the preparation and completion of this study.

Firstly, I would like to express my sincere gratitude to my advisor Prof. Dr. Dr. Michal-Ruth Schweiger, for her continuous support throughout my PhD study, for her patience, motivation, and immense knowledge. I am eminently thankful for the multiple possibilities she gave me to work on this interesting and challenging field of research.

I also want to thank Professor Dr. Rupert Mutzel for taking the time of being my second supervisor.

My sincere thanks also goes to Prof. Dr. Hans Lehrach for having given me the opportunity to do my PhD thesis in the extraordinary and inspiring environment at the Max-Planck-Institute for Molecular Genetics in Berlin. Especially, the multitude of technologies and knowledge in his department made my work successful.

This thesis would not have been possible without the help of many people. Many thanks to Prof. Dr. Monica Hirsch-Kauffmann for her never-ending support, inspiring suggestions and interesting discussions. A special thanks to Dr. Martin Kerick, who performed all the sequencing data analysis. This work would not have been possible without his invaluable knowledge and support. In this regard I also want to say thanks to the sequencing core facility around Dr. Bernd Timmermann.

I'd especially like to thank Dr. Christian Kähler and Dr. Sylvia Krobitsch for their huge knowledge in the field of heat stress research, for performing the immunofluorescence experiments and for their feedback and suggestions on the manuscript. Furthermore, I'd like to thank Dr. Jörg Isenssee for conducting the quantitative high-content screening microscopy.

I want to thank all former members of the Schweiger lab, especially Dr. Stefan Börno and Dr. Andrea Wunderlich for their support in experiments, for interesting and fruitful discussions and for their contribution and comments on the manuscript. Many thanks also to Nada Kumer who was always a great help in the lab.

I’m very grateful to my present colleagues for the friendly atmosphere in the lab. Many thanks to Christina Grimm, Sabrina Grasse, Susann Siebert and Anne Steinbach who all contributed to making our lab a happy place.

My special thanks go to Sabrina Grasse for all the fun we have had in the last three years. I am especially grateful to get such a good friend even outside of work.

I also gratefully acknowledge the “Studienstiftung des Deutschen Volkes” for their financial support throughout my PhD study.

Last but not the least, my deepest debt is to my family, my parents and my sister for their everlasting support and encouragement throughout writing this thesis and my whole life in general.

ZUSAMMENFASSUNG

Die zelluläre Stressantwort umfasst die Anpassung eines Organismus auf umweltbedingte und endogene Stressfaktoren, welche durch eine Vielzahl von molekularen Prozessen gesteuert wird. Eine Deregulierung dieser Antwort ist ein Indikator und möglicher Auslöser vieler Krankheiten, insbesondere Tumorerkrankungen, und bietet daher einen interessanten Angriffspunkt für Therapien.

Ein sehr wichtiges und für die Tumorforschung auch aus therapeutischer Sicht äußerst vielversprechendes Protein ist das Bromodomänen enthaltende Protein 4, kurz BRD4. BRD4 spielt in sehr vielen Bereichen der Zelle eine wichtige Rolle, unter anderem als epigenetischer Sensor sowie transkriptioneller Regulator und ist damit ein wichtiges Bindeglied zwischen dem transkriptionellen Prozess und epigenetischen Mustern.

Ziel dieser Arbeit war es, die Rolle von BRD4 bei der epigenetischen, als auch der transkriptionellen Regulation im Verlauf von zellulären Stressantworten zu untersuchen. Durch Genexpressionsanalysen in BRD4-defizienten Zellen, sowie Chromatin-Protein-Interaktionsstudien konnte ich 52 BRD4-regulierte Zielgene identifizieren, welche vor allem für Proteine der oxidativen Stressantwort sowie der Hitzestressantwort kodieren.

Weiterführende Analysen identifizierten BRD4 als einen wichtigen Modulator eines der wichtigsten, mit oxidativem Stress assoziierten Signalwege, dem KEAP1/NRF2 Signalweg.

Durch eine transkriptionelle Regulierung von KEAP1 kontrolliert BRD4 die Aktivität des Transkriptionsfaktors NRF2, welche wiederum die Expression zytoprotektiver Gene induziert. Eine Hemmung der BRD4 Aktivität führt unter Stress-Bedingungen zu einer Verringerung an reaktiven Sauerstoffspezies (ROS) in der Zelle und zu einem Schutz der Zellen vor oxidativem Stress-vermittelten Zelltod.

Zudem konnte ich anhand einer Vielzahl von molekularbiologischen Experimenten zeigen, dass BRD4 direkt die Expression von HMOX1, einem ROS-regulierendes Protein, über eine Bindung an den Transkriptionsfaktor SP1, reguliert. Dieses transkriptionelle Regulationsnetzwerk scheint bei Prostatakrebs gestört zu sein, was möglicherweise eine zentrale Rolle beim malignen Prozess der Tumorentstehung spielt.

Zusätzlich zu seiner Funktion bei der transkriptionellen Regulation gibt es bereits einige Hinweise, die eine Rolle von BRD4 bei dem zellulären Spleißprozess wahrscheinlich machen.

Im Rahmen meiner Arbeit konnte ich zeigen, dass BRD4 eine wichtige Rolle bei dem Spleißvorgang unter Hitzestress spielt. So fördert es das, unter Hitzestress beeinträchtigte, Herausschneiden von Introns.

Weitere molekularbiologische Analysen zeigten, dass unter diesen Stressbedingungen BRD4 in sub-nukleären Strukturen, den sogenannten „nuclear stress bodies“, rekrutiert wird. Dort aktiviert BRD4, zusammen mit dem Hitzeschock Faktor HSF1, die Transkription von nicht-kodierenden *Sat III* RNAs. Diese werden als wichtige Modulatoren der Stress-induzierten Spleißreaktion diskutiert.

Zusammenfassend konnte ich zeigen, dass BRD4 sowohl in die Transkiption, als auch in den Spleissprozess unter zellulärem Stress involviert ist. Dies stellt eine weitere Grundlage dar, Pathomechanismen der Tumorentstehung besser zu verstehen, aber auch, um neue Therapieansätze zu entwickeln.

SUMMARY

The cellular stress response describes the adaptation of an organism to environmental stressors by a variety of molecular changes. Deregulation of this response is an indicator and possible promoter of many diseases, in particular cancers, and therefore offers an interesting target for tumor therapies. A for the tumor therapy very promising target is the bromodomains containing protein 4 (BRD4). BRD4 plays a significant role in many cellular processes: It is an epigenetic reader and transcriptional regulator and therefore links the transcription process to epigenetic patterns.

The aim of this study was to further understand the role of BRD4 in the epigenetic and transcriptional regulation of cellular stress responses. Through genome-wide gene expression profiling in BRD4-deficient cells, and chromatin-protein interaction studies, I was able to identify 52 BRD4-regulated target genes, mainly encoded for proteins of the oxidative stress - and heat stress response. Further analyses highlighted BRD4 as regulator of the oxidative stress-induced KEAP1/NRF2 signalling pathway.

By regulating the transcription of *KEAP1*, BRD4 modulates the activity of the transcription factor NRF2 and, in turn, the expression of cyto-protective genes under stress. An inhibition of BRD4 resulted in decreased reactive oxygen species (ROS) production and protected cells from oxidative stress mediated cell death. In addition, BRD4 also interacts with the transcription factor SP1 and directly regulates the expression *of HMOX1*, a ROS reducing protein. Remarkably, this regulatory network is disrupted in prostate cancer and thus might play a central role in tumorigenesis.

Furthermore, using RNA-sequencing analyses of BRD4-deficient and heat treated cells I showed that a reduction of *BRD4* expression increased the heat shock-mediated splicing inhibition, in particular intron retentions.

Subsequent experiments revealed that under heat stress BRD4 binds to the heat shock factor 1 (HSF1), which leads to the recruitment of BRD4 to sub-nuclear structures, the so-called "nuclear stress bodies". The translocation of BRD4 is associated with the transcriptional activation of non-coding *Sat III* RNA expression. *Sat III* RNAs, in turn, are discussed as important modulators of the stress-induced splicing process.

Taken together, my results link BRD4 not only to the transcription machinery, but also to the splicing process under oxidative or heat stress, respectively. This gives additional insights into the mode of action of BRD4 inhibitors and could lay the foundation for the development of new therapeutic strategies.

TABLE OF CONTENT

ABBREVIATIONS

ARE: antioxidant response elements.

BET: bromodomain and extra terminal.

BRD4: bromodomains containing protein 4.

BSA: bovine serum albumin.

Co-IP: Co-Immunoprecipitation.

CoPP: cobalt protoporphyrine.

DHR: dihydrorhodamine 123.

E1: enhancer 1.

FCS: fetal calf serum.

GSTP1: *glutathione S-transferase pi*. ,

HMOX1: heme oxygenase 1.

HS: heat shock.

HSE: heat shock elements. ,

HSF1: heat shock factor 1.

HSP: heat shock protein.

IgG: Immunglobulin G.

IPA: Ingenuity pathway analysis.

IR: intron retention.

KEAP1: Kelch-like erythroid cell derived protein with CNC homolgy-associated protein 1.

MAPK: Mitogen Activated Protein Kinase.

MEME: Multiple EM for Motif Elicitation.

mRNA: messenger RNA.

MYC: V-Myc Avian Myelocytomatosis Viral Oncogene Homolog. ,

NF-κB: nuclear factor–κB.

NRF2: nuclear factor erythroid 2-related factor 2.

nSB: nuclear stress bodies.

PCa: prostate cancer.

Pol II: RNA Polymerase II.

PRG: primary response genes. ,

PSI: percent spliced in.

p-TEFb: positive transcriptional elongation factor b.

RPKM: reads per kilobase per million mapped reads.

Sat III: satellite III.

seq: sequencing.

shRNA: small hairpin RNA.

siRNA: small interfering RNA.

SOD2: *superoxid dismutase 2*. ,

SP1: specific protein 1.

SR: Serine/arginine-rich.

SRSF: Serine/arginine-rich splicing factors.

WT: wild type.

1 Introduction

1.1 The hallmarks of cancer

With approximately 14 million new cases and 8.2 million cancer related deaths in 2012, cancer is a leading cause of death worldwide [1]. The transformation of healthy cells to tumor cells is a complex, multi-stage process from a pre-cancerous lesion to malignant tumors that includes the shutdown or circumvention of many cellular control mechanisms. In addition to genetic predisposition further external mutagens including physical (i.e. ultraviolet and ionizing radiation), chemical (i.e. tobacco smoke and arsenic) and biological carcinogens (i.e. viral, bacterial or parasites infections) increases the risk to develop cancer.

In 2000, Doug Hanahan and Bob Weinberg published a tumor model in which they explained and summarize the main and common features of tumor transformation [2]. Originally, these tumor characteristics, the hallmarks of cancer, included the (1) self-sufficiency in growth signals, (2) the resistance to anti-growth signals, (3) the circumvention of apoptosis, (4) the unlimited replication potential, (5) the continuous stimulation of blood vessels (angiogenesis) and (6) the massive tissue invasion and metastasis potential. Ten years later, in 2011 a follow-up review was published that expanded the primary six hallmarks on the basis of new scientific findings to a list of ten as there are: (7) the tendency towards genomic instability, (8) the ability to avoid the immune system, (9) the presence of inflammation which can induce many types of cancer and (10) the deregulation of metabolic processes in cancer cells [3]. Interestingly, the latter hallmark, the fact that most cancer cells use abnormal metabolic pathways to generate energy was already postulated in the early 20th century by Otto Warburg [4,5]. The so called Warburg effect describes, in general, the adaptation to low-oxygen (hypoxic) environments within tumors due to an insufficient cellular respiration caused by insults to mitochondria.

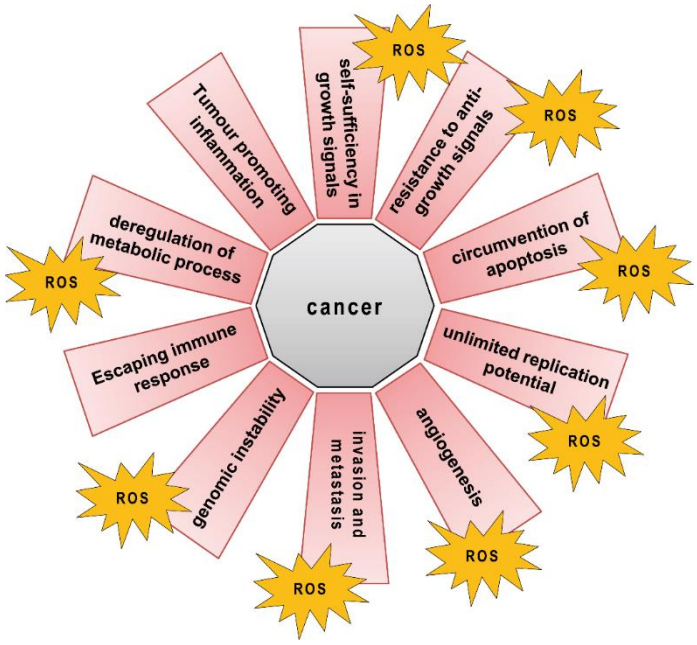

Figure 1 Hallmarks of cancer and the contribution of cellular stress. Oxidative stress plays multiple roles in the development of cancer by influencing several hallmarks of cancer, including the bypassing of apoptosis, the deregulation of metabolic processes or genomic instability (for details see section 1.2.1).

Several cancer-associated genes or cellular pathways can be involved in more than one hallmark, for example oxidative stress [6-10]. Studies from breast [11-14], prostate [15,16], and colon carcinoma [17-21] have shown that the oxidative stress pathway is deregulated in many tumor entities and affects critical steps of cancer initiation and progression, by deregulating cell proliferation, bypassing apoptosis, increasing de novo angiogenesis, and by influencing invasion and metastasis via metabolic and epigenetic mechanisms (Figure 1). Furthermore, the resistance to oxidative stress seems to be an important factor in the development of cancer therapy resistance [22-26].

1.2 The cellular stress response

Cellular stress describes an imbalance of the cellular homeostasis, triggered by environmental stressors, including elevated temperatures, exposure to toxins, reactive oxygen species (ROS) or mechanical damage that result in a broad range of molecular changes. A deregulation of stress response pathways can result in the development of aging related diseases, including neurodegenerative diseases [9,27-29], diabetes [8], heart diseases [6] and cancer [30]. The response to external stimuli is evolutionary highly

conserved among species from prokaryotes to mammalians and can be divided in three main mechanisms: (1) activation of cell repair mechanisms, (2) induction of stress signalling cascades that result in temporary adaptation to stressors and (3) triggering apoptosis.

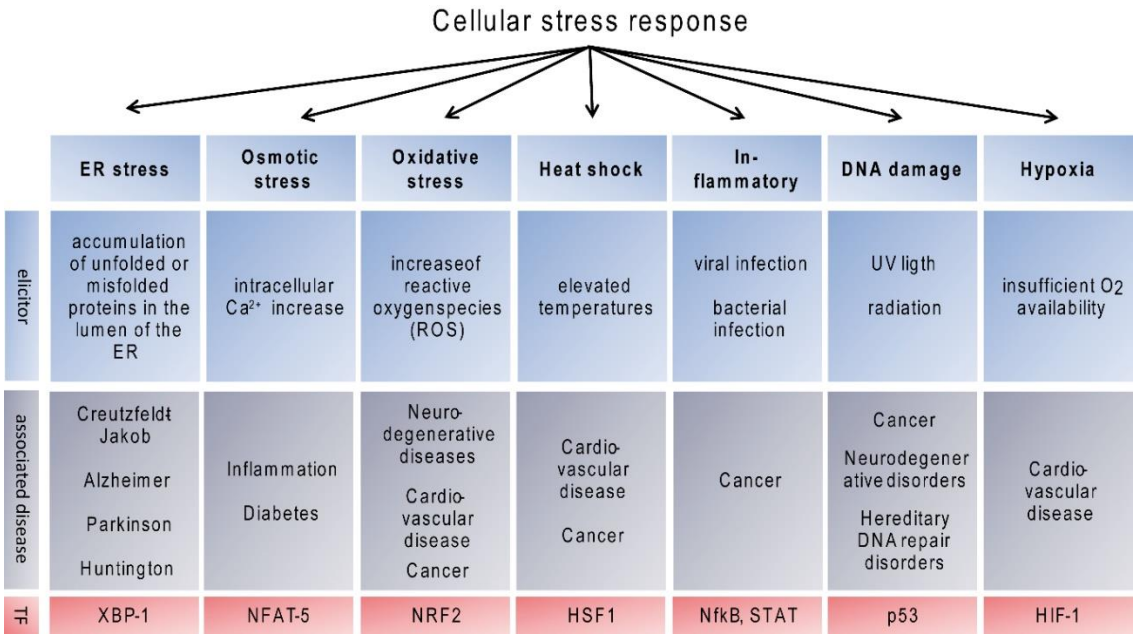

Figure 2 Overview of the main cellular stress response pathways. For each stress response pathway the major exogenous stimuli (elicitor), the main associated diseases and the main transcriptional regulator (TF) are shown.

The response of cells to these external stressors is regulated by multiple signalling cascades helping to maintain or rearrange cellular homeostasis and to repair stress-induced damage [31]. The general cellular stress response can be classified in several subgroups of stress response pathways, including the response to oxidative stress, to heat stress or inflammation. Each pathway has its major transcriptional regulator which is important for the induction of cyto-protective genes. However, these transcription factors are not exclusive for one stress response, in contrast, the stress response pathways interact with each other. Figure 2 summarizes the main stress response pathway in humans and their associated diseases.

1.2.1 Oxidative stress response

Oxidative stress is caused by an imbalance of production and clearance of reactive oxygen species (ROS) (chemical species with one unpaired electron), including superoxide anion, hydrogen peroxide, singlet oxygen, hydroxyl radical, peroxy radical, as well as the second messenger nitric oxide and can be produced by intracellular as well as extracellular sources. Mitochondria are the major endogenous source of ROS [32]. The mitochondrial electron transport chain is able to generate superoxide anions which are precursors of most other ROS by the reduction of molecular oxygen. External and endogenous stimuli, which cause the generation of ROS are for example cigarette smoke, drugs, inflammation or heavy metals [33,34]. Endogenous ROS are important for a wide range of biological functions. Amongst others, ROS act as cellular messengers and are involved in signalling pathways to maintain cellular homeostasis and regulate many cellular and metabolic processes, including proliferation, migration and gene expression [35].

However, a high level of free radicals causes damage to all major classes of biological macromolecules, including nucleic acids, proteins, carbohydrates, and lipids. Oxidative stress is linked to a wide spectrum of diseases, including cardiovascular disease [36], pulmonary diseases [37], diabetes [38], neurodegenerative diseases [39] and a wide range of different tumor entities [40]. In tumor cells the production of ROS is clearly elevated compared to non-transformed cell lines [41]. Oxidative stress is involved in many steps of cell transformation, such as cancer initiation, promotion and progression [42] and plays critical roles in cell adhesion [43], cell proliferation [44], cellular senescence [45], angiogenesis [46] and apoptosis [47] (Figure 1). For example, the regulation of cell proliferation by ROS may be due to the activation of MAPK (Mitogen-Activated Protein Kinases) pathway an essential inducer of cell proliferation [48-51]. High concentrations of ROS permanently induce the ubiquitination of MKP3 (mitogen-activated protein kinase phosphatase 3), a phosphatase that negatively regulates ERK1/2 activity [48,52], a regulator of cell proliferation, cell differentiation, cell cycle and cell adhesion. By modulating integrin-transduced signals, ROS can influence cellular adhesion and by increasing the production of angiogenic factors like IL-8 (Interleukin-8) [53,54] and VEGF (Vascular Endothelial Growth Factor) [55,56] ROS promote vessel growth within the tumor microenvironment. Furthermore, ROS also have been described to mediate cellular senescence by regulating S- and G2-phase checkpoint [57]. In addition to initiation and progression of tumor cells, ROS also influence increased tumor invasion and metastasis formation by promoting pathways associated with cell migration, such as FAK (Focal adhesion kinase) [58,59] or MAPK pathway [60], respectively.

To ensure low levels of ROS in the cell an efficient antioxidant defence system is needed [33]. Under normal conditions, ROS-metabolizing enzymes, such as catalase, glutathione peroxidase and superoxide dismutase (SODs) as well as non-enzymatic antioxidants such as glutathione (GSH), thioredoxin (TX) and vitamin C and E hold the cellular homeostasis in its equilibrium and counterbalance the production of ROS. Members of the superoxide dismutase family are important to reduce superoxide anions to hydrogen peroxide which is further catalysed by glutathione peroxidases and the enzyme catalase. Non-enzymatic antioxidants are important to capture free radicals in the cell. To regulate the antioxidant defence, several signalling cascades are activated upon the induction of oxidative stress. Besides many other signalling cascades, such as the NF-κB signalling [61], the most important signalling pathway in the response to elevated ROS level is the NRF2/KEAP1 signalling system [62].

1.2.1.1 NRF2/KEAP1 pathway

The NRF2 (nuclear factor erythroid 2 [NF-E2]-related factor 2 [NRF2]) – KEAP1 (Kelch-like erythroid cell-derived protein with CNC homology [ECH]-associated protein 1) signalling pathway is the major regulator of oxidative stress. The main signalling proteins within the pathway are the transcription factor NRF2, which is a heterodimer of an erythroid-specific 45 kDa subunit (p45) and the “small” Maf proteins (small avian musculoaponeurotic fibrosarcoma oncogene) [63-65] and its repressor KEAP1. NRF2 belongs to the Cap ‘N’ Collar (CNC) transcription factor family and binds to antioxidant response elements (ARE) [66,67] and NF-E2/Maf-recognition elements (MARE) [68], respectively. NRF2 is a highly unstable protein that is targeted for selective degradation via the ubiquitin pathway [69,70]. Under basal conditions, NRF2 is found to interact with KEAP1 that promotes its ployubiquitination and facilitates its degradation via the 26S proteasome [62,71-73]. Here, KEAP1 acts as a substrate adaptor for the Cullin 3 (Cul3)-dependent E3 ubiquitin ligase complex, in which the polyubiquitination of the NRF2 protein on its lysine residue is catalyzed [74] and its degradation initialized. In contrast, in response to several electrophilic stimuli including ROS, cysteine residues in the KEAP1 protein are covalently modified that results in a conformation change in the KEAP1 protein. This in turn allows NRF2 to liberate from KEAP1-dependent degradation. The release of NRF2 results in nuclear accumulation and activation of transcription of cytoprotective genes such as NAD(P)H quinone oxidoreductase 1 (NQO1), heme oxygenase 1 (HMOX1), glutamate-cysteine ligase (GCL) and glutathione S transferases (GSTs) [75] (Figure 3). HMOX1 is an evolutionary conserved enzyme which catabolizes the

degradation of heme into equimolar quantities of iron (Fe), carbon monoxide (CO) and biliverdin. HMOX1 plays a crucial role in the maintenance of homeostasis under stress conditions. It is expressed ubiquitously in response to various stimuli, including UV irradiation, heavy metals, oxidative stress and inflammatory cytokines, like TNF-α [76]. The induction of HMOX1 expression occurs at the transcriptional level and involves many transcriptional regulators and – elements depending on the type of stimulation, including NRF2, AP1, NF-κB, SP1 and HSF1.

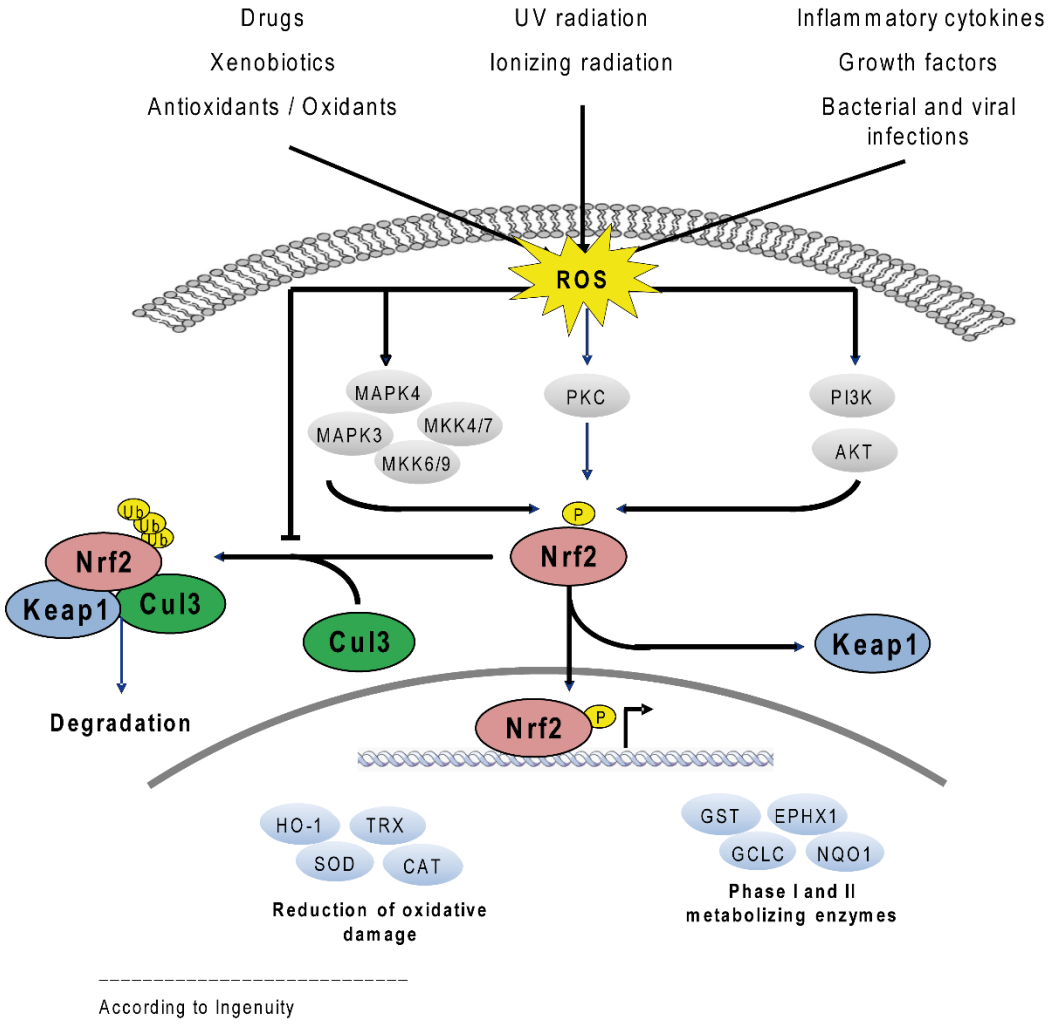

Figure 3 KEAP1/NRF2 signalling pathway. External stimuli, such as UV radiation or xenobiotics results in conformational changes in the KEAP1 protein which normally targets NRF2 for degradation. The liberation of NRF2 from KEAP1 results in its translocation in the nucleus and activates the transcription of cyto-protective genes.

The autophagy-related protein p62 was also shown to affect the stability of NRF2 by disrupting the competitive binding between KEAP1 and NRF2. p62, a substrate for autophagy dependent protein degradation, directly interacts with KEAP1 and leads to its degradation via the autophagy pathway [77]. In addition to the above-described KEAP1 dependent regulation of NRF2, several other mechanisms have been described to alter the activity of NRF2. For example, covalent phosphorylation and acetylation of NRF2 regulate its nuclear accumulation and transcriptional activity [78-82]. In this regard the MAPK signalling pathway plays a role in the stabilization and activation of NRF2 through its phosphorylating capacity [69]. MAPK3, also known as ERK1, is a member of the mitogen activated kinase family and regulates various cellular processes such as proliferation [83], differentiation [100] and cell cycle progression in response to a variety of extracellular and endogenous signals, including elevated levels of ROS [101]. For example, oxidative stress activates MAPK3 signalling and the inhibition of MAPK3 phosphorylation blocks the oxidative stress induced apoptosis [102].

Despite of the cyto-protective function of NRF2 in the cell, NRF2 has a dual role in tumorigenesis. In various cancers it is persistently activated resulting in a growth advantage by promoting tumor growth and resistance to anticancer drugs [82]. Otherwise, in several cancer types it was shown that the activation of NRF2 can suppress carcinogenesis [83-85].

The increased activation of NRF2 in tumor cells can be triggered by several mechanisms. Somatic mutations in KEAP1 [86-89] or NRF2 [90-92], for example, disrupt their interaction and decrease the degradation of NRF2 [93]. Notably, in lung cancer the NRF2/KEAP1 pathway is, according to the cancer genome atlas research network, with 34% one of the most frequently mutated pathways [94]. Furthermore, epigenetic silencing and post-translational modifications of KEAP1 [95,96] or accumulation of p62 [97] may result in insufficient repression of NRF2. Additionally, several studies described an abundant expression of NRF2 induced by oncogenes, such as K-RAS, BRAF and c-MYC [98]. Under normal conditions, NRF2 maintains the cellular homeostasis and inhibits tumor initiation by eliminating cancer-inducing agents, such as ROS. During carcinogenesis, the hyper-activation of NRF2 results in the resistance to high level of ROS and chemotherapeutics, prevents apoptosis and enhances tumor growth. Thus, high levels of NRF2 are associated with poor prognosis which makes the NRF2 system an important and attractive target for anti-cancer therapies.

1.2.2 Heat stress response

The cellular response to heat stress is an ancient and highly conserved defence mechanism characterised by the transcriptional up-regulation of cyto-protective genes encoding the heat shock proteins (HSPs). The heat shock response can be induced by various external stimuli, including elevated temperature, exposure to toxic chemicals, and viral or bacterial infections [107]. Most HSPs act as molecular chaperones to protect damaged proteins from aggregation or to unfold or refold damaged proteins for efficient degradation [108]. Many HSPs are constitutively expressed under normal conditions and function in protein folding, transport, regulation, and degradation [109]. HSPs are classified into different families according to their molecular weight: HSP100, HSP90, HSP70, HSP60, HSP40 and small heat shock proteins. Heat shock proteins are overexpressed in a wide range of human cancers [110-112] and are implicated in tumor progression, prognosis and in therapy response. For example, the expression of the small heat shock protein HSP27 is associated with poor prognosis in gastric [113], liver [114], and prostate carcinoma [115], while HSP70 is correlated with poor prognosis in breast [116], bladder [117] and cervical cancer [118]. The induction of HSPs requires the activation of specific transcription factors, the so called heat shock factors (HSF). In vertebrates and plants at least four members of the HSF gene family have been described [119] and in *Saccharomyces cerevisiae* only one Hsf is expressed [120]**.** In human cells, three HSFs (HSF1, HSF2, and HSF4) have been characterized with HSF1 being currently the best investigated regulator which is also constitutively overexpressed in many cancer types [121]. In breast cancer, for example, an increased expression as well as an enhanced activity of HSF1 is associated with a poor prognosis [122]. HSF1 is ubiquitously expressed and exists in unstressed cells as a monomer that is captured in the cytoplasma by the chaperone complex HSP90 and HSP40/HSP70, respectively. HSF1 remains unbound to DNA, while after heat shock it oligomerizes into a transcriptional active trimer, which binds to heat shock elements (HSE) of heat shock inducible genes [123]. Multiple phosphorylations and sumoylations of regulatory domains in the HSF1 protein further modulate its transcriptional activity [124,125]. The active HSF1 recruits the positive transcriptional elongation factor b (p-TEFb) complex via its transactivation domain to the start sites what, in turn, activates RNA Polymerase II (Pol II) [126].

1.2.2.1 Nuclear stress bodies

Nuclear stress bodies (nSB) are sub-nuclear organelles, with a maximum diameter of 2 - 2.5 µm. They were originally identified as the main site of HSF1 accumulation after cellular stress induction. The formation of nSB is triggered by a direct interaction of HSF1 with pericentric heterochromatic regions, for example at the 9p12 locus [127-129]. This region contains multiple long tandem sequences of satellite III (*Sat III*) repeats (GGAAT) [130]. Therefore, it is not surprising that the number of nSB correlates with cell ploidy. Although the *Sat III* DNA sequences do not harbour the typical HSE elements, HSF1 activates the transcription of these *Sat III* repeat regions into long non-coding RNAs, the *Sat III* RNAs. In human cells, knockdown of HSF1 inhibits the induction of nSB and *Sat III* transcription after heat stress [123]. It is thought the *Sat III* transcripts, after being transcribed upon cellular stress, remain associated with the genetic locus and form, together with HSF1, the nSB. Furthermore, the overexpression of *Sat III* transcripts has been shown to initiate the formation of nSB suggesting an essential function for the formation of these structures. The expression of polyadenylated *Sat III* RNA is inducible by a wide range of stresses including heat, DNA damaging agents (MMS and etoposide), oxidative stress (H_2O_2), hypoxia (Cobalt chloride and low O_2), hyper-osmotic stress (sorbitol) and heavy metals (cadmium) [131]. Besides HSF1, HSF2 that is also present in nSB, as well as the tonicity enhancer binding protein (TonEBP) regulate the production of *Sat III* RNAs in response to hyper-osmotic stress [123,131]. These findings illustrate an important and general role of *Sat III* expression in the cellular response to stress.

The function of nSB is still largely unknown, however, it is assumed they participate in epigenetic and transcriptional control of gene expression and mRNA processing during heat stress [132]. nSB are enriched in acetylated histones (histone H4, especially, H4K8 and H4K16) which are an epigenetic mark of transcriptionally active chromatin and are depleted from heterochromatin markers, such as H3 tri-methylation on lysine 9 (H3K9me3) [133,134]. Moreover, in addition to HSF1 and *Sat III* RNA, further transcriptional regulators, such as CREB (cAMP response element-binding protein) - binding protein (CBP) and Pol II (but not Pol I or Pol III) are found in the nSB, indicating that nSB are large transcription factories.

The best inducer of nSB formation is heat shock. The exposure to elevated temperatures leads to an almost complete shutdown of important cellular processes (see 1.2.2). Besides the up-regulation of chaperones, the block of translation and nucleo-cytoplasmatic shuffle, the inhibition of pre-mRNA splicing is a further characteristic of the heat stress response.

The mechanism underlying the global splicing defect in heat treated cells is still not clear. However, nSB are thought to play an essential role in the alterations of splicing functions. During heat stress, a subset of splicing factors, including the Src-associated in mitosis 68 kDa protein (Sam68) and several SRSF family members, SRSF1, SRSF7 and SRSF9 (see for details 1.3) are efficiently recruited to nSB. Interestingly, *Sat III* RNAs are required for the recruitment and localization of these proteins to the nSB [135]. Down-regulation of *Sat III* RNAs reduces the recruitment of RNA processing factors to nSB, without affecting HSF1 localisation [136]. In this context it is proposed that the accumulation of splicing factors in the nSB may recruit the splicing process toward specific transcripts which are involved in the cellular defence to stress and, at the same time, lead to global deficiency of splicing.

1.3 Cellular stress and pre-mRNA splicing

The transcriptional response to stress is a multistep process which occurs at several levels including transcription, mRNA-processing, -degradation and -export. The cell has the ability to control the gene expression at each of these levels to modulate the protein diversity in response to exo- or endogenous factors. One of the best investigated stress responses, regarding mRNA splicing, is the heat shock response. During elevated temperatures, pre-mRNA splicing is blocked and alternative splicing is severely affected. Importantly, this change does not affect the expression of HSP genes because most of them do not contain introns. Recently, it was shown that under severe as well as mild heat shock conditions, a widespread splicing inhibition occurs in transcripts which are normally spliced post-transcriptionally. Transcripts which undergo the splicing process co-transcriptionally remained almost unaffected.

In nearly all eukaryotic organisms, protein-coding genes are transcribed into precursor-messenger RNAs (pre-mRNAs) which contain non-coding intronic sequences, called introns which are not present in mature mRNAs. This pre-mRNA must undergo a RNA processing reaction, called splicing, that removes introns and ligates the coding segments, called exons, to generate a mature translatable mRNA [137].

The regulation of mRNA splicing during heat shock was first reported in fly, but similar observations have been made in yeast, mammalian cells, and other systems on single gene level. Quite recently, these observations were extended to a global level by using next generation sequencing technologies. To better understand the regulation of splicing

during heat stress in the following sections, the process of mRNA splicing will be discussed in detail.

1.3.1 Spliceosome assembly pathway

The numbers of intron-containing genes vary amongst different species. In budding yeast, *Saccharomyces cerevisiae,* only about 5% of the yeast genes contain intronic regions, by contrast, in humans more than 95% of protein-coding genes have been found to undergo splicing by generating more than 90,000 different mRNAs.

Splicing is catalysed by the spliceosome, a large multi-component ribonucleoprotein (RNP) complex consisting of five small nuclear ribonucleoproteins (snRNP) U1, U2, U4, U5, and U6 as well as non-snRNP associated proteins such as the U2 small nuclear RNA auxiliary factor 1 (U2AF35 and U2AF65) and splicing factor 1 (SF1 or SRSF1) [138-140]. The factors of the spliceosome are assembled on the pre-mRNA substrate in a stepwise manner, traversing different complexes from the pre-spliceosome E, A, B to the catalytic-spliceosome C complex (Figure 4). Reactive regions that are important for a correct mRNA splicing, are short consensus sequences at 5' splice site (ss), 3'ss, branch point site (BPS) and the polypyrimidine tract (PPT) [140].

The first step of pre-mRNA splicing is the formation of the pre-spliceosome complex E. Here, the U1 snRNP interacts with the 5' ss of the intron, while SRSF1 binds to the intron BPS and the U2AF heterodimers U2AF65 and U2AF35 bind to the PPT and 3′ ss, respectively. Subsequently, the U2 snRNP displaces SRSF1 from the BPS to form complex A. In the following reaction the preassembled U4/U6/U5 tri-snRNPs are recruited to the spliceosome to form the pre-catalytic spliceosome complex B. The dissociation of U1 and U4 snRNPs leads to the interaction of the U6 snRNP with the 5′ ss and the U2 snRNA (complex B*). In the last step of the splicing reaction, the formation of the catalytic spliceosome complex C, the U6/U2 snRNPs catalyse a cleavage of the 5′ end of the intron followed by a simultaneous formation of a covalent bond between the first nucleotide of the intron and the BPS to form the intron-lariat. In the second step, the 3' end is cleaved and the exons are ligated in an ATP-dependent manner and the spliced mRNA is released. Figure 4 schematically summarizes the spliceosome assembly process.

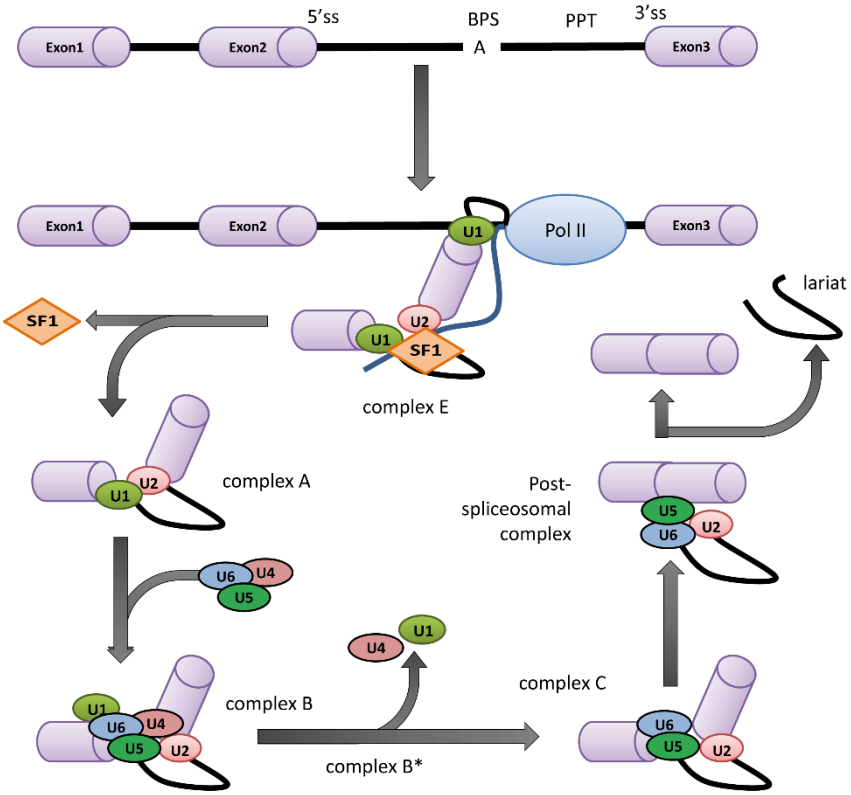

Figure 4 Mechanism of the U2-dependent spliceosome assembly. The splicing process is regulated by multiple steps of assembling and disassembling of snRNPs (circles) including U1, U2, U4 and U6 as well as non-snRNPs (diamond), such as SF1. Exon and intron sequences are indicated by boxes and lines, respectively. Modified after Will and Luhrmann, 2011 [140].

In addition to the main splice-site regions on exon/intron junctions, flanking *cis*- regulatory elements are present in the pre-mRNA to facilitate splice site recognition and selection. Based on their position in the mRNA and their function, these elements can be classified into four subtypes: exonic splicing enhancers (ESEs), exonic splicing silencers (ESSs), intronic splicing enhancers (ISEs) and intronic splicing silencers (ISSs) [141,142]. These cis-regulatory elements initialize the binding of *trans*-regulatory factors, such as members of serine/arginine-rich proteins (SR) and hnRNP (heterogeneous ribonucleoprotein particles) protein families. ESE or ISE are mainly bound by the SR protein family and play a major role in constitutive splicing. In contrast, ESS and ISS elements are preferably bound by the hnRNP family members and are mainly required for alternative splicing [142].

1.3.2 Alternative splicing

In humans more than 95% of protein-coding genes have been found to undergo alternative splicing in a development- and cell type specific manner [143-146]. Alternative pre-mRNA splicing is a fundamental part of gene regulation and expands the proteomic diversity in eukaryotes. Alternative splicing can be classified in seven major events: (1) alternative 5' splice sites, (2) alternative 3' splice sites, (3) mutually exclusive alternative exons, (4) cassette exon inclusion or skipping, (5) intron retention, (6) alternative promoter and first exon and (7) alternative poly A site and last exon [147] (Figure 5). The most predominant mode in mammalians, with about 30% frequency, is the cassette exon skipping and inclusion while in lower metazoans and plants it is the retention of introns [148].

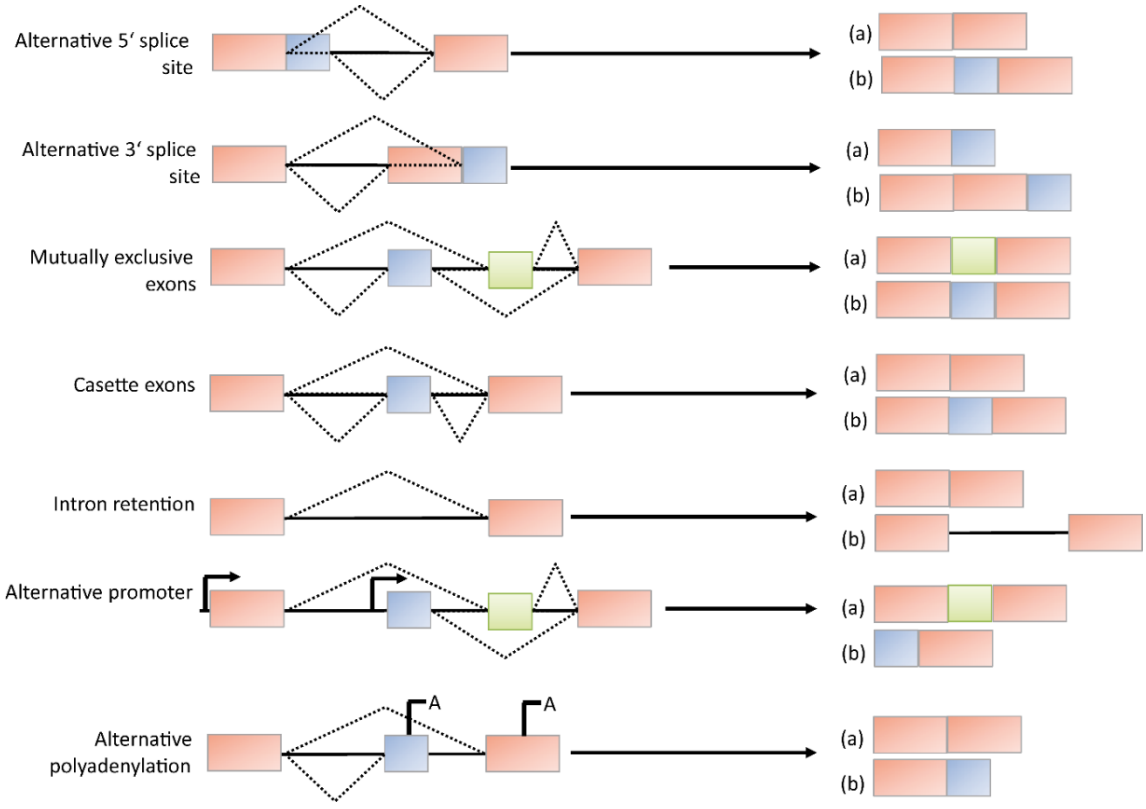

Figure 5 Alternative splicing events. All known alternative splicing events are represented. Red bars represent the constitutive exons, blue and green the exclusive exons and the black line represents introns. Each alternative splicing event can result in two different spliced transcripts, shown as (a) and (b). Modified after Rajan et al. 2009 [149].

In general, intron retention characterizes a lack of splicing. Mutually exclusive exons describes exons where either one or the other are retained in the transcript but never both

exons in the same mRNA. Alternative 5' splice site describes a change of the 3' boundary of the upstream exon, while alternative 3’ splice sites depict a change of the 5' boundary of the downstream exon. Alternative promoter and alternative poly A sites arise from changes in first exons or last exons usages, respectively.

1.3.3 Co-transcriptional splicing

Pre-mRNA splicing can be carried out during the process of transcription, called co-transcriptional splicing, while the elongating Pol II is still active, as well as after transcription termination, called post-transcriptional splicing. A key player in the coordination of transcription with the splicing process is Pol II itself. Depending on the posttranslational modifications of its C-terminal domain (CTD) Pol II actively participates in splicing or not. The main modifications of the CTD of Pol II are phosphorylation on serines 2 and 5 that have been identified to help coupling transcription and RNA processing events [150]. Truncation or mutations of the CTD result in splicing defects [151,152]. The phosphorylation on serine 5 is important for transcription initiation, whereas the serine 2 phosphorylation, mediated by the transcription elongation factor p-TEFb, regulates promoter clearance and transcriptional elongation. It was shown that splicing proteins such as U2AF65 and members of the SR family interact directly with the phosphorylated CTD to stimulate the association of Pol II with the spliceosome complex [153,154].

Another complex, the mediator complex, was identified to regulate alternative mRNA processing by linking transcriptional activators or repressors, which interact with splicing silencers (i.e. hnRNPs) or enhancers (i.e. SR proteins), with transcriptionally active promoters [155,156]. SR proteins themselves associate co-transcriptionally with the Pol II and thereby influence transcription as well as splicing regulation. A depletion of SRSF2 (also known as SC35) results in drastic effects on transcriptional elongation by inhibiting p-TEFb recruitment [157]. Based on these observations, two models were described to explain co-transcriptional splicing: (1) the kinetic model [158] and (2) the recruitment model [159]. The kinetic model uses the process of transcriptional elongation to explain splicing regulation. A decreased elongation rate or a pausing of Pol II leads to an increase in exon and/or intron inclusion, while a fast transcription rate could cause exon skipping [160]. In contrast, the recruitment model posits a physical interactions between the transcription machinery - in particular the CTD of Pol II - and the spliceosome which alter alternative splicing [152,161-163]. Importantly, these models are not at all mutually exclusive. Both,

the recruitment model as well as the kinetic model play important roles in the regulation of pre-mRNA splicing.

In addition to modifications of the CTD of Pol II the transcribed DNA template itself, seems to be modulator of splicing regulation. DNA as well as histone modifications were found to influence the efficiency of pre-mRNA splicing by affecting the process of exon definition. Genome wide sequencing studies revealed that several histone marks are enriched at exonic sequences, such as trimethylation of H3 lysine 36 (H3K36me3), dimethylation of H3 lysine 27 (H3K27me2) and monomethylation H3 lysine 79 (H3K79me1) [164-168]. Notably, the mark of active gene expression, H3K36me3, is more frequently found on exons that are always included in mRNA compared to alternative exons, enhancing an important role in pre-mRNA splicing [164,169]. Interestingly, splicing itself influences histone modifications as well. Inhibition of the splicing process leads to a reduction of the endogenous level of the H3K4 tri-methylation signal and a reduction and redistribution of H3K36me3 [170,171]. In addition to histone marks, genome-wide methylome analysis revealed a correlation between alternative splicing and DNA methylation, suggesting a direct role in exon definition. Exons with a higher inclusion rate show a higher level of DNA methylation relative to those that are mainly excluded from transcripts [172]. Furthermore, methylation levels are significantly enhanced at exonic relative to intronic regions. Importantly, these epigenetic alterations can adopt to both splicing models, the kinetic and the recruitment model, by either influence on the Pol II elongation rate, or by site-specific recruitment of RNA-binding proteins.

1.4 BET family

The BET (bromodomain and extra terminal) family of proteins is an evolutionary highly conserved class of epigenetic readers and transcriptional regulators. In the last years, BET proteins have emerged as strong therapeutic targets in a multiplicity of human disorders including cancer, viral infections and inflammatory and autoimmune diseases [173,174]. They are defined by the presence of bromodomains, one in plants or two in yeast and mammalians, followed by the conserved extra terminal (ET) domain [175]. Bromodomains are conserved regions which are capable of binding acetylated lysine residues in histones or other proteins. They consist of 110 amino acids that form four antiparallel alpha-helices (*αZ*, *α*A, *α*B and *α*C) and two loops linking these helices [176]. Interestingly, the bromodomains, called BDI and BDII, share less sequence homology in one protein compared to their homologous domains in other BET family members [177]. Similar to the

bromodomains, the extraterminal domains form *α*-helices that result in two adjacent pockets which may be utilized for protein–protein interactions [178]. Even though the bromo- and the extra terminal domains are the main characteristics for the BET family proteins, other domains such as the SEED (Ser/Glu/Asp-rich region) domains recognizes regulatory elements in the DNA and are also highly conserved throughout species [176].

Additionally to their domain organization and protein structure, the members of the BET family share several functional properties that are often conserved from yeast to human BRD proteins. The interaction between BRD proteins and chromatin creates functional roles in a variety of cellular processes such as transcriptional regulation, cell cycle regulation or DNA damage response [179]. For example the BET family member in yeast, the bromodomain factor 1 (Bdf1p) preferentially binds - similar to its mammalian homologues - to acetylated histone H4 tails throughout the cell cycle that can be efficiently blocked by mutations in the bromodomains [180]. Bdf1p links transcription initiation and chromatin remodelling by interacting with the transcription factor TFIID [181]. *Bdf1* deletions also lead to global splicing defects by diminishing the transcription of the small nuclear ribonucleic acid (snRNA), the core components of the spliceosome [182,183]. Further genetic analyses revealed functions in the regulation of apoptosis and DNA replication [184]. The absence of Bdf1p results in increased sensitivity to DNA damaging agents and leads to mitochondrial dysfunction under stress conditions followed by an accumulation of ROS and chromatin fragmentation and condensation [185] which are typical marker of apoptosis.

Another representative of the BET family is the female sterile homeotic (fsh) gene of *Drosophila melanogaster* fs(1)h that plays important roles in embryogenesis and development [186]. Unlike the yeast protein Bdf1p, fs(1)h encodes two BET isoforms generated by alternative splice sites [187]. Both isoforms share main cellular functions, such as the transcriptional regulation, but the DNA binding profile and the genomic location of these two isoforms allows to distinguish between the shorter isoform (fs(1)h-S) and longer (fs(1)h-L. The shorter isoform is mainly found at sites that are marked as enhancers or promoters whereas the longer one is located at insulator sites which describes intergenic regions that are responsible for intra- or inter-chromosome interactions [188].

In humans the BET family consists of four members (BRD2, BRD3, BRD4 and BRDT). Except of BRDT, a testis specific protein, all other BRD proteins are expressed ubiquitously and exhibit similar functional properties: The first described human member of the BET family BRD2, formerly named RING3 (really interesting new gene 3), was

described in 1996 as a mitogen-stimulated nuclear protein [189]. As shown for its homologues in yeast and fly, BRD2 plays a role in transcriptional regulation [190,191], cell cycle regulation [189], embryonic development [192] and splicing [193]. BRD2 interacts with the transcriptional regulator E2F1 and promotes the expression of several E2F dependent cell cycle genes including Cyclin D1, A and E [189]. In addition, BRD2 seems to be a critical regulator of the inflammatory response through the transcriptional regulation of a broad spectrum of inflammatory cytokines such as IL-1B and IL6 [194,195]. BRD3 and BRDT are less well characterized members of the BET family in humans. BRD3 has been reported to interact with the transcription factor GATA1, suggesting a role in transcriptional regulation as well [196]. BRDT is an important regulator of spermatogenesis. Deletions of the *Brdt* genes in mice models lead to defects in chromatin structure and gene expression [197,198]. Microarray analysis of control and *Brdt* mutant has demonstrated that a significant change in transcription occurs in the absence of BRDT during spermatogenesis. Together with functions in transcription, BRDT is also discussed to be part of the splicing machinery [198]. Deletions of BRDT in spermatids results in longer transcripts as well as in alterations in the 3′-UTR definition correlated with clearly reduced protein levels. Moreover, mass spectrometry analysis of overexpressing full-length *BRDT* in human cells showed that BRDT interacts with a variety of spliceosome components including SRSF2, DDX5, HNRNPK, and TARDBP [198]. Table 1 summarizes the functions of the main members of the BET family. However, the best investigated and most promising target for clinical therapies is the human BRD4 protein. Its functions and properties are described in the following section.

Table 1 Overview of the function of BET proteins in *Saccharomyces cerevisiae*, Arabidopsis Thaliana, Drosophila melanogaster and Homo sapiens.

Organism	***Gene***	***Function***
Saccharomyces cerevisiae	*bdf1*	Transcriptional regulation [181], Cell cycle [180], Regulation of apoptosis [184], DNA Damage prevention [185], Replication [180], mRNA splicing [182,183]
Arabidopsis Thaliana	Gte4, Gte6	Cell cycle [199], Development [200], Transcriptional regulation [199]
Drosophila melanogaster	*fs(1)h*	Transcriptional regulation [188], Development [186], Chromatin architecture [188]
Homo sapiens	*BRD2*	Cell cycle [189], Inflammatory response [174,195], Transcriptional regulation [190,191], Splicing [193], Development [192]
	BRDT	Transcriptional regulation [196], Splicing [198]
	BRD4	Cell cycle [201-203], Inflammatory response [204], Transcriptional regulation [205-207], Development [208], DNA Damage [209], Replication [210], Chromatin architecture [211]

1.4.1 The human BRD4 protein

BRD4, formerly named MCAP (mitotic chromosome-associated protein), is an ubiquitously expressed nuclear protein which exists in two isoforms generated by alternatively spliced transcripts differing at their 3' ends [212]. BRD4 is involved in many cellular activities, such as transcription, DNA replication, cell cycle progression and epigenetic memory. A depletion of BRD4 leads to growth inhibition and lethality as shown in several *in vivo* models including knockout mouse models as well as embryonic stem cells [212,213]. Furthermore, a deregulation of BRD4 expression results in abnormal cell cycle arrests, mediated by an altered expression of certain cell cycle G1 related genes, such as cyclins D1 and D2 (CCND1, CCND2) [201-203].

As described for all other BET family members, BRD4 binds to acetylated histone. It specifically shows preferences for acetylated lysine 14 on histone H3 (H3K14) as well as lysine 5 and 12 on histone H4 (H4K5 and H4K12), and remains associated with chromosomes even throughout mitosis [204,214]. Heterozygotious depletions of the *BRD4* gene result in a reduction of histone acetylation upon drug-induced mitotic stress [213].

Histone modifications are part of the epigenetic regulation. At least eight distinct types of modifications are found on histones including acetylation, methylation, phosphorylation and sumolyation. In a proteomic analysis several proteins involved in histone modification were found to interact with the ET domain of BRD4, including NSD3 (nuclear receptor SET domain-containing 3), CHD4 (chromodomain helicase DNA binding protein 4) or JMJD6 (jumonji domain containing 6) [215]. For example NSD3, also known as WHSC1L1 (Wolf-Hirschhorn syndrome candidate 1-like 1), is a histone methyltransferase. A reduced interaction of NSD3/BRD4 results in a decrease of H3K36 methylation, enhancing a putative role of BRD4 in the regulation of histone modifications.

Additionally, the protein- protein interaction with JMJD6 potentially connects BRD4 with the splicing process [215,216]. JMJD6 acts as a regulator of RNA splicing by mediating 5-hydroxylation of the splicing factor U2AF65, thereby affecting its pre-mRNA splicing capacity [217]. On the other hand, the splicing factor SC35 (also named SRSF2) utilizes, under certain conditions, BRD4 to enhance the recruitment of p-TEFb to Pol II [157].

In addition, an *in situ* single cell chromatin imaging and micrococcal nuclease (MNase) assay revealed a participation of BRD4 in the maintenance of higher-order chromatin structure [211]. Here, a reduced expression of BRD4 results in a loosened chromatin condensation. Further studies have shown that BRD4 influences DNA replication as well as cell division. For example, by the interaction with the largest subunit of replication factor C (RFC-140) BRD4 inhibits the RFC-dependent DNA replication [210]. Based on the interaction with the signal-induced proliferation-associated protein (SIPA1) BRD4 increases the RAP activity (GTP hydrolysis on RAP1 and RAP2) of SIPA1 which is important for cell division [218].

Early on, BRD4 has been implicated in transcriptional regulation processes. BRD4 interacts with p-TEFb, a heterodimer composed of Cyclin T1,T2 or K and cyclin dependent kinase 9 (CDK9). P-TEFb plays a critical role during the transition from abortive to productive elongation of Pol II by hyper-phosphorylation of the CTD of Pol II by CDK9 [205,206]. In its inactive form, p-TEFb persists in a complex with the 7SK small nuclear RNA (7SK snRNA) and HEXIM1. The interaction of BRD4 and p-TEFb via the bromodomains results in the release of the inhibitory subunit, the activation of p-TEFb and promotion of Pol II phosphorylation [207]. Furthermore, it was shown that BRD4 associates with TRAP220, a component of the mediator complex. These findings picture an important role of BRD4 in the regulation of gene expression.

To date, an increasing number of studies identified BRD4 as part diverse transcriptional regulation processes. As such BRD4 was described to regulate the papillomavirus E2 transcriptional activation function [219] and to activate the regulation of inflammatory genes. A chromatin immunoprecipitation analysis of several primary response genes (PRG) indicates that BRD4 detects the lipopolysaccharide (LPS) induced acetylation on histone H4 at the promoters of several PRGs. Subsequently, BRD4 recruits p-TEFb to PRG promoters and activates the following induction of PRGs [204].

Furthermore, recent work has also discovered that BRD4 binds to the so-called 'super-enhancers' [220,221]. Super-enhancers are characterized by a large size (more than 10,000 bp [222]), high transcription factor density and content, increased binding of the mediator complex and increased chromatin accessibility [223,224]. In addition to the mediator complex, a number of other general transcriptional regulators are enriched at super-enhancer regions compared to normal enhancers, including Pol II, RNA from transcribed enhancer loci (eRNA), the histone acetyltransferases p300 and CBP. Super-enhancers were found to regulate the expression of key oncogenic drivers in many tumor cells for example within the *MYC* locus [222]. Inhibition of BRD4 in multiple myeloma tumor cells led to a loss of BRD4 binding at super-enhancers and consequently to a decreased expression of *MYC* [225]. These observations were discussed as a potential explanation for why cancer cells are specifically sensitive to BRD4 inhibition, despite the ubiquitous expression of BRD4 in a wide range of tumor cells.

1.4.2 BRD4 as therapeutic target in disease

The crucial role of BRD4 in cell cycle progression and proliferation suggests an important role of BRD4 for the development of diseases, especially cancer. Moreover, BRD4 has been shown to promote transcription of known oncogenic drivers such as MYC and RAS enhancing its role as therapeutic target for anticancer treatment. There is increasing interest in the inhibition of BET proteins for a variety of therapeutic applications and diseases. To date, ten different BET inhibitors have been developed and used for research or for clinical usage [226]. BET inhibitors are specific for the first or second bromodomains of BET proteins, but are unspecific for different BET family members. The majority of BET inhibitors reversibly blocks one or both bromodomains, which are essential for the binding to acetylated peptides and thereby cause a displacement of all the BET proteins from chromatin [227,228]. In 2010 the first small-molecule inhibitors of BET proteins were developed, JQ1 and I-BET151 [229,230]. Both inhibitors are widely used in different

research applications and are used in pre-clinical studies for NUT midline carcinoma, acute leukaemia, lymphoma and other solid tumors.

The genomic rearrangement between BRD4 (and to a lesser extent BRD3) with the nuclear protein in testis (NUT) gene was first reported in 1991 and results in a rare and lethal squamous cell carcinoma known as NUT midline carcinoma (NMC). The fusions impair normal BRD4 and BRD3 functions, inhibit cellular transcriptional activation and might have a broad effect on cell proliferation, metastasis or invasiveness. Treatment of patient-derived xenograft models with JQ1 has shown to induce growth arrest of malignant cells [229].

Further implications of a role of BRD4 in human disease were published in 2006, in studies from cervical carcinoma. Here, BRD4 was identified as a key interacting partner of the viral E2 protein of HPV-16 (human papillomavirus-16) and BPV-1 (bovine papillomavirus-1), which is the main transcriptional regulator of viral gene expression [231]. Furthermore, BRD4 also interacts with the latency-associated nuclear antigen 1 (LANA-1) of the Kaposi's sarcoma-associated herpesvirus (KSHV) [232] and the Epstein-Barr virus (EBV) nuclear antigen 1 (EBNA1) [233]. In all cases, BRD4 is required for transcriptional regulation and the maintenance of viral infection. Recently, BRD4 has been additionally identified to directly interact with the Merkel cell polyomavirus (MCV) protein large T antigen (LT) which is found in 80% of all Merkel cell tumors, a rare and highly aggressive type of tumor [234]. BRD4 has also be found to be associated with the HIV provirus where it inhibits HIV latency, by blocking the recruitment of the viral Tat protein to HIV promoter [173].

As mentioned in the previous section, BRD4 was identified as a transcriptional regulator of MYC expression. The possibility to manipulate MYC expression by treatment with the BET inhibitors rise a huge application potential for many MYC associated cancers [235-241]. Thus, a suppression of BRD4 using RNAi or BRD4 inhibitors in acute myeloic leukaemia cells results in cell cycle arrest and apoptosis due to a rapid decrease of the MYC mRNA level [242]. Moreover, studies in several leukaemia, lymphoma and melanoma cell lines have shown for the BET inhibitors JQ1, and I-BET 151, respectively, an anti-tumorigenic effect [243-246]. Furthermore, BRD4 seems to act also via other oncogenic drivers such as FOSL1, RAS and the hedgehog signalling pathway, shown for lung adenocarcinoma, malignant peripheral nerve sheath tumor (MPNST) and medulloblastoma, respectively (Figure 6) [247-249].

A recently published study on castration-resistant prostate cancer discovered BRD4 to regulate androgen receptor (AR) responsive genes [250]. Moreover, in *TMPRSS2* - (transmembrane protease, serine 2) ERG (ETS-related gene) fusion positive cell lines the inhibition of BRD4 by JQ1 inhibits the expression of ERG through the reduction of AR and BRD4 binding to the *TMPRSS2* promoter and/or enhancer. A tumor promoting function of BRD4 was also described for hepatocellular carcinoma, glioblastoma and osteosarcoma [251-253].

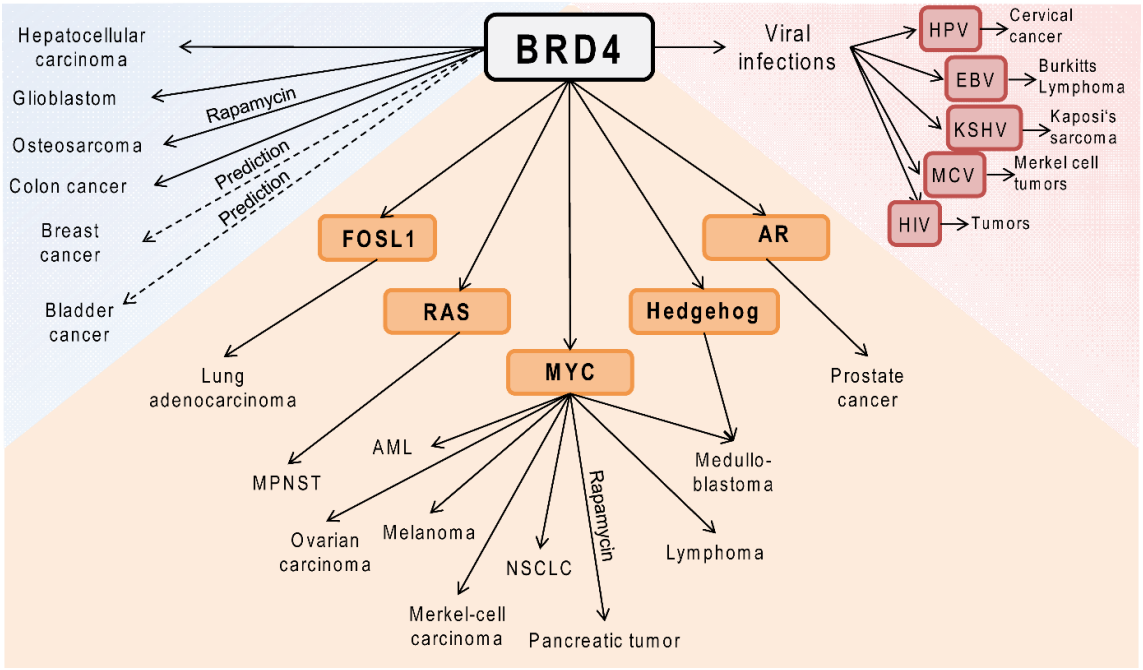

Figure 6 BRD4 implications in cancer and diseases. BRD4 is involved in a multiplicity of cancer types and cancer associated diseases, by acting via oncogenic drivers such as c-myc (orange), or viral protein interactions (red). For several cancers (blue) the mechanism underlying the therapy success of BRD4 inhibition is not yet clarified.

In addition to the oncogenic effects of BRD4 it was also shown that BRD4 possesses a tumor and metastasis suppressor activity *in vivo*. In human colon cancer cell lines, as well as in primary tumors it was shown that BRD4 is often down-regulated by an abnormal hypermethylation of its promoter [254]. An up-regulation of BRD4 in these colon cancer cell lines results in a reduction of tumor growth that enhances the tumor and metastasis suppressor activity of BRD4 [255]. Furthermore, BRD4 may also play an important role in tumor progression of breast cancer. Here, BRD4 activation reduces the invasiveness and mobility of a highly metastatic cell line [256,257]. Furthermore, for breast and bladder cancer, BRD4 was also shown as prognostic marker. In bladder cancer tissue an elevated

BRD4 expression predicts a lower survival rate compared to cells with lower BRD4 expression [258]. In 2008 Crawford et al. described also a negative correlation between BRD4 protein levels and the disease outcome in breast cancer patients [256]. Higher BRD4 levels correlated with a better prognosis. Figure 6 and Table 2 summarizes BRD4s implications in cancer.

Taken together, BRD4 seems to be a potential universal target for therapy in numerous human cancers and other diseases. Due to the promising effects of BET inhibitors in pre-clinical trials, in 2013 the first clinical phase I studies have been started for NUT midline carcinoma (GSK525762; 'NCT01587703'), acute leukaemia, lymphoma (CPI-0610; 'NCT01949883') and other solid tumors (OTX015; 'NCT02259114') [259].

Table 2 Overview of BRD4 implications in cancer and the application of BET inhibitors. Shown are cancer type, BET inhibitor used in research, the proposed mode of action, clinical studies and the corresponding BET inhibitor and the associated references.

Tumor entity	Compound	Mode of action	Clinical study	Ref.
acute myeloic leukemia (AML)	JQ1 OTX015	down-regulation of c-MYC	CPI0610[b] OTX015[b]	[260], [261], [242]
Breast Cancer	JQ1	lowered PI3K signalling; down-regulation of EGFR family	OTX015[c]	[262]
Burkitts Lymphoma	JQ1	down-regulation of c-MYC		[263]
Colon Cancer	MS417	regulation of EMT proteins		[255]
Glioblastoma	I-BET151 JQ1	regulation of c-MYC, BCL-2, BCL-XL	OTX015[a]	[252], [264], [265]
Kaposi's Sarcoma	I-BET151 JQ1 PFI-1	down-regulation of c-MYC		[265]
Lung Cancer	JQ1	inhibition of ASCL1; down-regulation of FOSL1	OTX015[c]	[266], [247], [241], [267]
Lymphoma	JQ1	inhibition of NF-κB	CPI0610[b]	[268]
Medullo-blastoma	JQ1 I-BET151	down-regulation of c-MYC ; suppression of HH		[269], [236], [235], [270]
Melanoma	I-BET151 MS436 MS417	down-regulation of BIM; down-regulation of SKP2, ERK1, c-MYC		[246], [245], [271]
Merkel cell tumors	JQ1	down-regulation of c-MYC		[240]
MLL	I-BET 151	down-regulation of c-MYC, *BCL2, CDK6*		[230], [272]
MPNST	JQ1	induction of BIM; regulation of PRC2 targets		[273], [248]
Multiple Myeloma	CPI203	N/A	CPI0610[b]	[274]
Nut Midline carcinoma	JQ1	down-regulation of *SOX2*	I-BET762[b] OTX015[c]	[275]
Osteosarcoma	JQ1 I-BET151 I-BET762	suppression of FOSL1; down-regulation of RUNX2; activation of NFATC1		[276], [253], [277]
Ovarian cancer	JQ1	down-regulation of c-MYC		[278]
Pancreatic tumors	CPI203	down-regulation of c-MYC	OTX015[c]	[239], [253]
Prostate Cancer	JQ1	suppression of AR	OTX015[c]	[279]

EMT = *epithelial-to-mesenchymal transition*; HH = *Hedgehog signalling pathway*; AR = *androgen receptor*; MPNST = *malignant peripheral nerve sheath tumor;* MLL = *mixed* lineage *leukemia;* [a]Trial; [b]Phase I; [c]Phase IB;

1.5 Aim of the work

Cellular stress is a hallmark of many tumors and describes an imbalance of the cellular homeostasis, triggered by environmental stressors. The cellular response to stress is regulated on multiple levels and a deregulation affects critical steps of cancer initiation and progression.

The cellular bromodomain containing protein 4 (BRD4) is a transcriptional regulator which was already linked to cellular responses to inflammatory signals and is discussed to be involved in the splicing regulation upon LPS stimulation.

The aim of this study was to enhance the knowledge about BRD4's function in the regulation of gene expression during cellular stress. Using genome wide mRNA expression and chromatin immunoprecipitation sequencing analyses I identified key BRD4 associated target genes that revealed BRD4 as a new regulator of the cellular stress response. To further understand the role of BRD4 in the regulation of stress induced pathways I investigated the influence of BRD4 in the response to oxidative and heat stress using different molecular biological approaches. On the other side, I analysed a novel function of BRD4 in the splicing process during heat stress using genome-wide transcriptome analyses and protein-biochemical methods.

The elucidation of a role of BRD4 in these regulatory mechanisms may potentially pave the way for novel therapeutic strategies and applications for a clinical usage of BET inhibitors.

2 Results

2.1 Identification of BRD4 regulated stress pathways

During the last years several studies demonstrated an important and crucial role of BRD4 for tumor progression. In addition, the therapeutic potential of BRD4 inhibitors was proved in many cancer entities. Presumably, these therapeutic successes arise mainly from BRD4's role in the transcriptional regulation by mediating the activation of Pol II. However, it is still not clear whether BRD4 is generally involved in the transcription of active genes, or if it is selectively associated with a subset of genes of specific pathways. In a couple of studies BRD4 was associated with signal induced changes on transcriptional as well as chromatin level [204,213,280-282].

To get further inside into the transcriptional role of BRD4 – especially in signal or stress induced gene expression regulation – I performed an integrated analysis of data from chromatin immunoprecipitation sequencing (ChIP-Seq) and RNA-sequencing (RNA-Seq) data to nominate key BRD4 regulated signalling pathways. Therefore, previously generated RNA-seq expression data of two BRD4 knockdown experiments and two BRD4 ChIP-seq experiments were used to identify the top BRD4 regulated target genes and associated pathways. First, both data sets were analysed separately before they were integrated.

For the transcriptome analyses (RNA-seq) a knockdown of BRD4 was achieved by using home-made small hairpin RNAs (shRNAs), which were previously designed and described by Schweiger et al. [283] and which target both isoforms of the BRD4 protein. The transcriptomes of BRD4-depleted cells as well as of control cells were analysed using paired-end polyA-selected RNA-sequencing. The isolated RNA was reverse transcribed into complementary DNA (cDNA) and the library preparation was done using the TrueSeq RNA Sample Preparation Kit from Illumina. To enrich mRNAs that contain poly(A)-tails oligo-dT coated beads were used to select the poly-A-tail containing transcripts. The transcriptome was analysed on an Illumina HighSeq 2500. The raw reads were mapped against the human genome GRCh37/hg19 using BWA version 0.5.9-r16 with default parameters. Exon-wise read counts were calculated by counting all reads that overlapped with exons by at least one nucleotide. The read counts were summed across all exons of a given transcript. The alignment and counting of raw reads was performed by Dr. Martin Kerick. To nominate significant differentially regulated genes, the mean expression value

for each gene was calculated. The analyses identified 1844 genes differentially regulated in both knockdown approaches with a mean fold change (FC) above 1.41 or under 0.7 (log2FC ± 0.5). Of these regulated transcripts, 970 transcripts showed an up-regulation, whereas 887 transcripts were down-regulated in BRD4 depleted cells. To elucidate the transcriptional activating role of BRD4, I mainly focused in my thesis project, on significantly down regulated transcripts. For the validation of the RNA-sequencing experiments a subset of genes were selected by chance and their expression after BRD4 knockdown was analysed using quantitative PCR. To exclude method dependent artefacts, and to rule out cell type or tissue specific regulations, mRNA expression experiments were carried out in two unrelated cell lines, HEK293T and WI38.

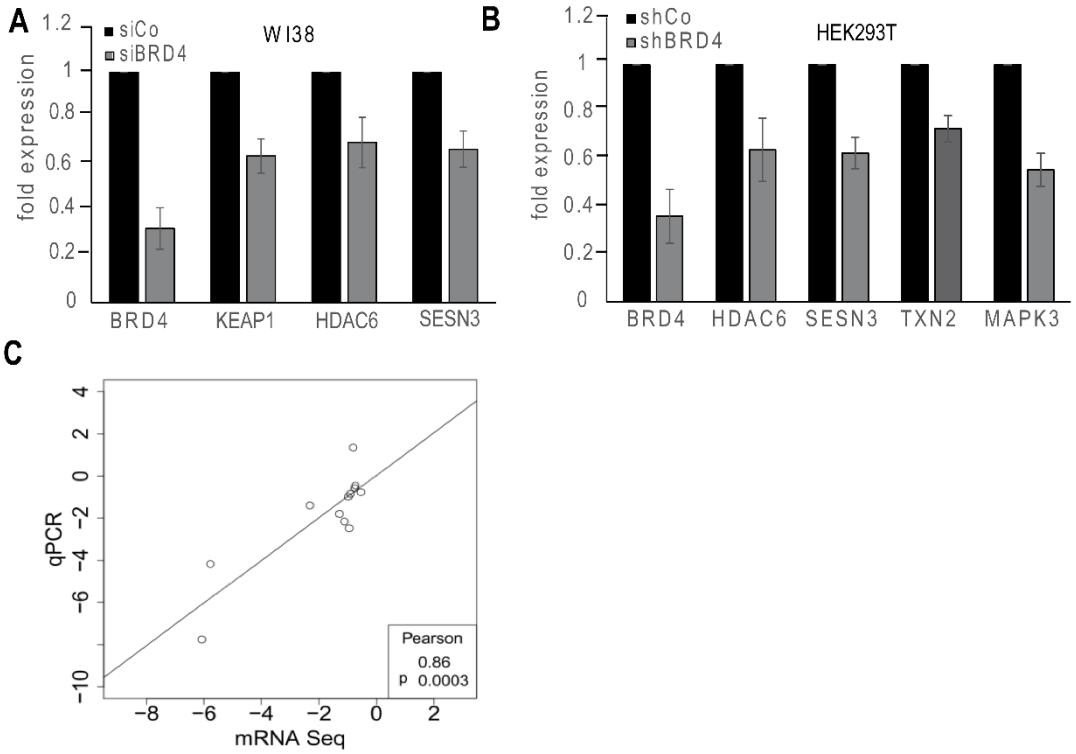

Figure 7 RNA-Seq expression validations. (A, B) ***Validation of identified differentially regulated mRNAs in BRD4 knockdown cells using qPCR.*** BRD4 knockdown was performed using **(A)** ***siRNA in WI38 cells or using*** **(B)** ***shRNA in HEK293T cells***. Both small interfering RNAs targeted both isoforms of BRD4. As normalisation β-tubulin (*TUBB*) was used. **(C)** ***Spearman correlation of mRNA Seq values and qPCR data of all tested transcripts***. Figure was provided by Dr. Martin Kerick. The mean expression values (log2 fold change) of the qPCR experiments are plotted on the y-axis and the mean expression values (log2 fold change) of the mRNA-Seq experiments are shown on the x-axis. (Figure taken from Hussong et al. 2014)

HEK293T cells were treated with the above described RNA interference constructs shBRD4 to down-regulate BRD4 expression. On the other site, WI38 cells were transfected with a commercial available pool of four different small interference RNAs (siRNA) that target the N-terminal end of BRD4 transcripts which is present in both isoforms. All tested target genes showed a significant down-regulation upon BRD4 knockdown achieved by small interfering RNAs (siRNA) as well as small hairpin RNAs (shRNA) in both cell lines. Both RNA interference constructs efficiently diminished *BRD4* expression down to 30% (Figure 7A, B). Taken together, the qPCR experiments confirmed the sequencing data, resulting in a Spearman correlation coefficient of 0.86 ($p = 0.0003$) (Figure 7C).

It is already known that BRD4 regulates a subset of transcriptional regulators, such as MYC and RAS. To exclude side-effects in my BRD4 knockdown experiments due to BRD4 regulated genes, ChIP experiments, previously performed by Dr. Andrea Wunderlich, were used to identify direct BRD4 targets. Additionally, a Pol II ChIP was also performed once to validate the success of the ChIP-method. The BRD4-, Pol II- as wells as IgG -precipitated DNA was analysed on the Illumina Genome Analyzer IIx. The alignment and counting of reads was performed by Dr. Martin Kerick. Peaks of the enriched DNA were called with MACS version 1.4. The BRD4-binding peaks were normalized to the IgG-control ChIP that was used as background control. PeakSplitter version 1 was used with default parameters to call subpeaks that were subsequently annotated to transcription start sites (TSS). A subpeak was associated to a TSS if at least one nucleotide of the peak was within the range of 500 bp upstream of a TSS. For visualisation, the results of the ChIP-seq experiments were loaded in the UCSC Genome Browser. Figure 8A shows a representative visualisation of the ChIP-seq data for the *KEAP1* gene. Enrichment peaks of BRD4 (blue) were clearly visible in the promoter region of *KEAP1* and overlay with the binding sites of Pol II (red), as expected. As control, the IgG control (brown) didn't show any enrichment peaks.

In two independent ChIP experiments 1885 significant BRD4 binding-sites peaks with FDR (false discovery rate) under 5% were identified in at least one of the ChIP experiments. To exclude cell type specific artefacts the validations of the ChIP-seq data were performed in the prostate cancer cell line DU145 as well as the human embryonic lung fibroblast cell line WI38. The BRD4-binding was calculated for 6 genes using qPCR. Therefore, I used primers that amplify the promoter region of the genes under examination. These regions, detected by qPCR, correspond to the regions of the BRD4-binding peaks identified in the ChIP-seq data. As background control, an intergenic non-coding region (NCR) as well as

an IgG-ChIP control were used. The NCR corresponds to a 78 bp long region located on chromosome 12 (chr12:61,667,719-61,667,796) in a gene depleted region. The nearest regulatory unit that is associated with a transcribed gene is located 400,000 bp upstream of the NCR. The specific BRD4 binding enrichment was normalized to the input and the IgG-ChIP controls.

As shown in Figure 8B, all identified BRD4 target genes displayed at least a 2-fold increased BRD4 binding to promoters compared to the IgG-ChIP control and displayed no enrichment to the NCR background control. Moreover, the chromatin binding of BRD4 could be validated in WI38 as well as in DU145 cells, excluding cell type specific artefacts.

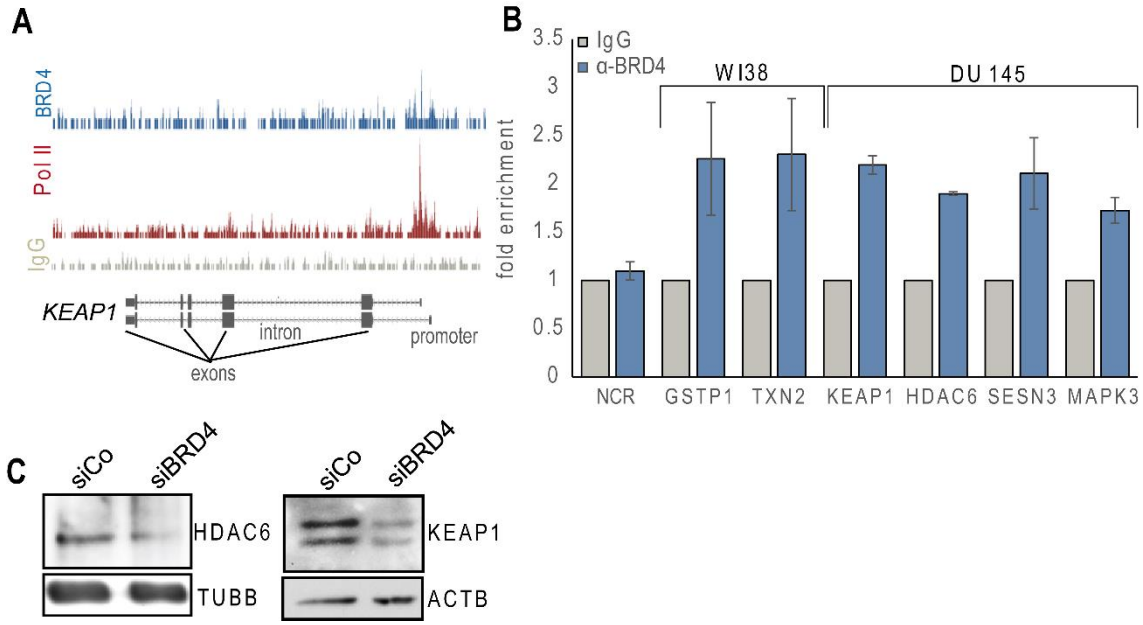

Figure 8 Validation of ChIP-Seq data. (A) ***Visualisation of BRD4 and Pol II binding sites in the ChIP-Seq data represented within the KEAP1 gene region.*** BRD4 (blue), Pol II (red) and IgG (brown) enrichment was visualized in the UCSC genome browser for the gene region of *KEAP1*. Enrichment of BRD4 and Pol II were detected in the promoter region as shown by the peaks. **(B)** ***Validation of ChIP-Seq data.*** BRD4 enrichment to the promoter regions of the indicated genes were analysed using two further ChIP-qPCR experiments with region-specific primers and an intergenic non-coding region (NCR) as negative control in DU145 as well as in WI38 cells. The specific BRD4-ChIP signals were normalized to IgG-ChIP control. **(C)** ***Western blot of* HDAC6 *and* KEAP1 *after BRD4 knockdown.*** HEK293T cells were transfected with either siBRD4 or a control siRNA (siCo) and harvested 72 h post transfection. As loading control β-actin (ACTB) and β-tubulin (TUBB) were used.

The integration of both data sets – data obtained by the RNA-seq and ChIP-seq experiments – resulted in 52 commonly activated target genes of BRD4 (Supplement Table S 1). Interestingly, several key regulators of cellular stress response, such as *KEAP1, HDAC6, SESN3, MAPK3, MDM2, TXN2, SOD2, GSTP1, GPX1, DNAJB2* are part of these 52 target genes, enhancing the hypothesized role of BRD4 in signal inducible pathways. Furthermore, pathway analyses using the free available software "Consensuspath DB" [284] revealed many cellular stress response pathways as significantly enriched in the data set. Most importantly, the response to reactive oxygen species was one of the most significantly enriched pathways with a p-value of $1.21*10^{-06}$. Interestingly, the cellular response to heat stress was also significantly enriched ($p = 1.27*10^{-02}$), suggesting a general role of BRD4 in the regulation of stress pathways (Table 3)

Table 3 Pathway analysis of the identified top 52 BRD4 target genes using ConsensusPath DB (version 28).

pathway	*Source*	*p-value*[a]	*q-value*[b]	*members_input_overlap*
Detoxification of Reactive Oxygen Species	Reactome	$1.21*10^{-6}$	$1.29*10^{-4}$	*GPX1; TXN2; GSTP1; SOD2*
Cellular responses to stress	Reactome	$2.04*10^{-6}$	$1.29*10^{-4}$	*GPX1; SOD2; HDAC6; UBE2E1; TXN2; MAPK3; GSTP1; MDM2*
Oxidative Stress	Wikipathways	$1.27*10^{-4}$	$4.02*10^{-4}$	*TXN2; GPX1; SOD2*
Signalling by NGF	Reactome	$2.15*10^{-3}$	$2.54*10^{-4}$	*ABR; MAPK3; ITGB3BP; MDM2; ARHGEF3*
Metabolism of nucleotides	Reactome	$2.29*10^{-3}$	$2.54*10^{-4}$	*GPX1; UCK1; UCK2*
Prostate cancer	KEGG	$3.10*10^{-3}$	$2.62*10^{-2}$	*MAPK3; MDM2; GSTP1*
Oncogene Induced Senescence	Reactome	$4.36*10^{-3}$	$2.92*10^{-2}$	*MAPK3; MDM2*
Cellular response to heat stress	Reactome	$1.27*10^{-2}$	$5.20*10^{-2}$	*MAPK3; HDAC6*

[a]p-values are corrected for multiple testing using the false discovery rate method; [b]the minimum false discovery rate at which the test may be called significant

To validate these data and to see whether the oxidative stress response pathway in general is affected by BRD4, an enrichment analysis of the RNA-seq expression data after BRD4 knockdown was performed using a list of oxidative stress responsive genes (Supplement Table S 2). The list of 37 genes was extracted out of the online available pathway database “Gene Ontology” (GO:0034599, ‘cellular response to oxidative stress’). Indeed, the expression data showed a significant enrichment of these genes, enhancing a functional role of BRD4 in the defence against oxidative stress. The calculated odds ratios (OR) show an enrichment of 3.9-fold of genes out of the GO:0034599 gene list in the group of significantly down-regulated genes after BRD4 depletion (OR = 3.9; p-value = $2.7*10^{-5}$).

The functional relevance of BRD4 knockdown was further approved on protein level by Western blotting. For this, blots for HDAC6 and KEAP1 protein, two identified BRD4 target genes and important genes of the cellular stress response, were performed in BRD4 knockdown and control cells. HEK293T cells were transfected with either siBRD4 or a control siRNA (siCo) and harvested 72 h post-transfection. Comparable to RNA-seq and qPCR experiments, the protein levels of HDAC6 as well as of KEAP1 were significantly decreased upon BRD4 depletion (Figure 8C) compared to wild type control cells. In contrast, the protein levels of the house-keeping proteins β-actin (ACTB) and β-tubulin (TUBB) were unaffected.

2.2 BRD4 as part of the oxidative stress response

The expression analysis combined with ChIP experiments suggested a role of BRD4 in the regulation of the oxidative stress response. Interestingly, using the Ingenuity pathway analysis (IPA) software for further pathway analysis (IPA®, Qiagen Redwood City, www.qiagen.com/ingenuity), the “NRF2-mediated Oxidative Stress Response” was identified as the most significant enriched pathway (p = $4.27*10^{-06}$) in the BRD4 target gene list (Table 4 and Figure 9).

Table 4 IPA analysis of the 52 identified BRD4 target genes. Canonical pathways are listed according to their p-value and the ratio of listed genes.

Ingenuity Canonical Pathways	p-value[a]	Ratio[b]	Molecules
NRF2-mediated Oxidative Stress Response	$4.27*10^{-06}$	$3.3*10^{-02}$	*DNAJB2,SOD2,EPHX1,GSTP1, KEAP1, MAPK3*
Prostate Cancer Signalling	$1.00*10^{-03}$	$3.6*10^{-02}$	*MDM2,GSTP1,MAPK3*
Chronic Myeloid Leukaemia Signalling	$1.45*10^{-03}$	$3.2*10^{-02}$	*HDAC6,MDM2,MAPK3*
Melanoma Signalling	$4.57*10^{-03}$	$4.7*10^{-02}$	*MDM2,MAPK3*

[a]the p-value is calculated using the right-tailed Fisher Exact test. [b]number of molecules in a given pathway that meet cut criteria, divided by total number of molecules provided by the software that make up that pathway.

The NRF2 signalling pathway is the major regulator of oxidative stress. In addition to downstream targets of NRF2, such as *SOD2, GSTP1* and *EPHX1*, two important regulators of NRF2 activity were found in the BRD4 target list: *KEAP1* and *MAPK3* (*ERK1/2*). This leads to the assumption that BRD4 may be an upstream regulator of the NRF2-mediated stress response by regulating a key modulator of the NRF2 activity, such as KEAP1.

Oxidative stress induces conformational changes in the KEAP1 protein, resulting in the liberation of NRF2 and its activation. Disruptions of this sensible regulatory network result in a defective stress response and can lead to cell transformation and cancer development. Keeping these relations in mind, I focused my following work on the elucidation of the influence of BRD4 in the KEAP1/NRF2 mediated regulation of oxidative stress.

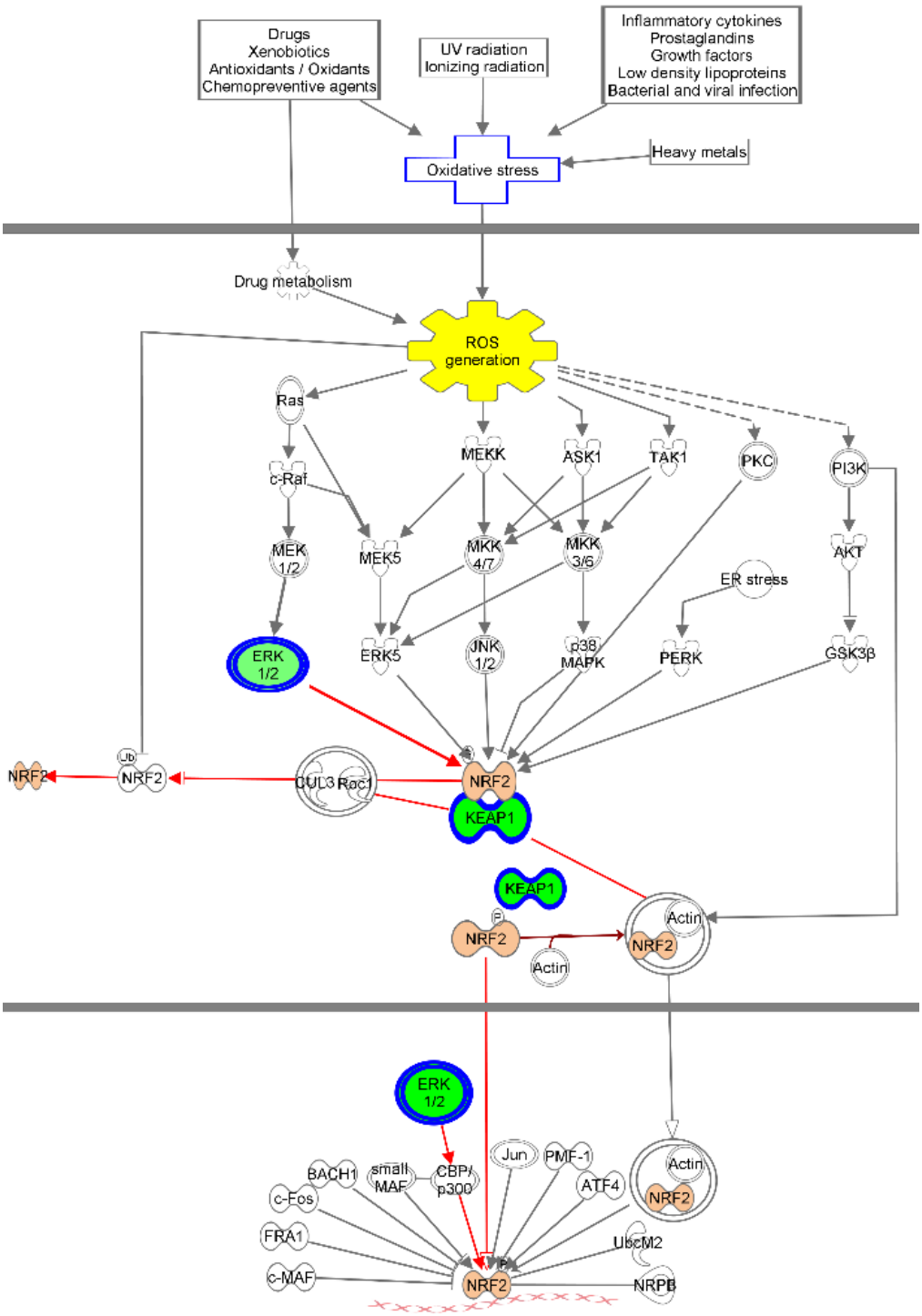

Figure 9 Ingenuity pathway analysis revealed the NRF2-mediated oxidative stress response as the major enriched pathway of the BRD4 target genes. The upstream-regulators of NRF2 (orange), KEAP1 and MAPK3 (ERK1/2), represented in green, are direct targets of BRD4.

2.2.1 BRD4 depletion increases the transcriptional activity of NRF2

My analyses have shown that the expression of the oxidative stress sensing protein KEAP1 is directly regulated by BRD4 (Figure 8). Since KEAP1 is the main regulator of the transcriptional activity of NRF2, the question arose, if BRD4 might influence the oxidative stress mediated regulation of NRF2 signalling pathway. To measure the NRF2 activity, the induction of HMOX1 (heme oxygenase 1) following oxidative stress treatment was used as readout. To focus on the role of BRD4 in the NRF2-mediated induction of HMOX1 in my experiments, the oxidative stress inducer cobalt protoporphyrine (CoPP) was used to specifically induce the NRF2/KEAP1 signalling pathway.

CoPP is a potent and effective inducer of HMOX1 expression. The up-regulation of HMOX1 by CoPP is mediated by the transcriptional regulators BACH1 (BTB and CNC homology 1) and NRF2. BACH1 is a heme binding protein which represses transcription of HMOX1 by binding to the heme-responsive elements (HeRE) in the 5' UTR of the HMOX1 promoter. Treatment with CoPP leads to a posttranscriptional destabilization of the BACH1 protein and, at the same time, to a stabilization of the NRF2 protein due to its decreased KEAP1-dependent proteosomal degradation [285]. Specifically, CoPP decreases the BACH1 protein half-life over 6-fold and, in contrast, increases the half-life of NRF2 up to 4-fold. However, the underlying mechanism is still not clarified.

Having observed that BRD4 depletion in unstressed cells significantly repressed KEAP1 expression, I asked whether the CoPP mediated induction of HMOX1 may be promoted by BRD4 depletion. Therefore, the expression level of HMOX1 following CoPP treatment was measured in BRD4-depleted (shBRD4) as well as in control cells (shCo, treated with an unspecific shRNA). First, the HMOX1 protein level (Figure 10A) and mRNA level (Figure 10B) were analysed in HEK293T cells treated for 72 h with shBRD4 or shCo, followed by a stimulation with 20 µM CoPP for 6 h, 10 h or 14 h. Protein as well as RNA was isolated after the indicated time points and analysed by Western blotting and qPCR, respectively. Indeed, under these conditions BRD4 knockdown experiments in combination with CoPP induction showed that a reduced BRD4 level resulted in an elevated HMOX1 expression on protein as well as on mRNA level, in a time-dependent manner of CoPP stimulation (Figure 10A, B). Already after 6 h, the stimulation with 20 µM CoPP resulted in an enhanced induction of HMOX1 in BRD4-deficient cells compared to the control cells. This effect was even more visible after 10 h. However, after 14 h of treatment the effect was compensated again.

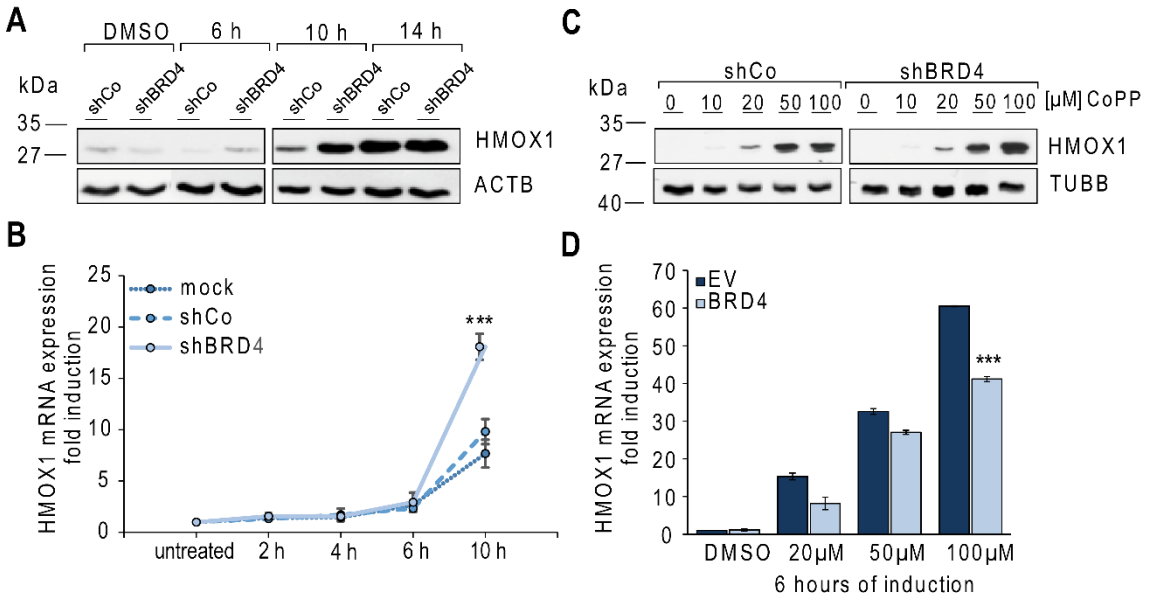

Figure 10 BRD4 regulates the stress-mediated expression of *HMOX1*. (A) ***HMOX1 protein expression in BRD4-deficient cells after CoPP treatment at different time points.*** HEK293T cells were transfected with either shBRD4 or shCo and stimulated with 20 µM of CoPP for 6, 10 and 14 h for Western blot analysis. As loading control ACTB was used. (Figure taken from Hussong et al. 2014) **(B)** ***HMOX1 mRNA expression in BRD4-deficient cells after CoPP treatment at different time points.*** HEK293T cells were transfected with either shBRD4 or shCo and stimulated with 20 µM CoPP for 2, 4, 6 and 10 h for qPCR experiments. *HMOX1* expression was normalized to *TUBB*. (Figure taken from Hussong et al. 2014) **(C)** ***HMOX1 protein expression in BRD4-deficient cells after CoPP treatment with different concentrations.*** HEK293T cells were transfected with either shBRD4 or shCo and stimulated with 20, 50 and 100 µM for 14 h for Western Blot analysis. As loading control TUBB was used. **(D)** ***BRD4 overexpression during CoPP induction decreases the HMOX1 levels***. HEK293T cells were transfected with either the BRD4 overexpressing plasmid or the empty vector (EV) control and stimulated with 20, 50 and 100 µM of CoPP for 6 h. The expression of *HMOX1* was measured using qPCRs. As reference gene β-tubulin was used. (***p-values <0.01 according to two-tailed t-tests)

To further investigate the influence of BRD4 in the CoPP mediated induction of HMOX1, HEK293T cells were transfected with shBRD4 or shCo and were stimulated after 72 h for 14 h with 20, 50 or 100 µM CoPP. Proteins were extracted and analysed on Western blot. Interestingly, the stimulation with varying concentrations of CoPP didn't show a significant enhanced HMOX1 protein induction in BRD4-depleted cells compared to control cells (Figure 10C), indicating a time- rather than a dose dependent influence of BRD4 reduction.

However, a transfection with a BRD4 overexpression plasmid and simultaneous CoPP treatment with 20, 50 and 100 µM CoPP for 6 h led to a significantly attenuated activation of *HMOX1* mRNA expression (40-fold induction) compared to the corresponding mock

control (60-fold induction) (Figure 10D), enhancing and verifying the observed repressive function of BRD4 in the CoPP mediated induction of *HMOX1.*

To explore whether the enhanced induction of HMOX1 by BRD4 knockdown after stimulation was due to an increase in NRF2 level caused by a decreased *KEAP1* expression, the NRF2 protein level was measured in BRD4-deficient and control HEK293T cells after stimulation with 20 µM CoPP. The endogenous NRF2 protein level was analysed after 6, 10 and 14 h of CoPP induction in shBRD4 and shCo treated cells. Similar to the induction rate of HMOX1, NRF2 protein level clearly increased in CoPP treated cells, as expected, but showed a further up-regulation in cells with diminished BRD4 expression (Figure 11A).

As seen for HMOX1, already 6 h after CoPP induction, the NRF2 protein level showed a significant increased stabilization in BRD4-deficient cells. Analysis of *NRF2* mRNA expression indicated that this increased NRF2 protein level was not due to an enhanced gene expression of *NRF2* (Figure 11B). The expression of *NRF2* transcripts were measured in HEK293T cells treated with shBRD4 or shCo for 72 h, with or without simultaneous treatment with 20 µM CoPP for 6 h. The relative *NRF2* expression was calculated by normalizing to the untreated knockdown control (shCo). Neither the knockdown of BRD4 (shBRD4) nor the simultaneous treatment with CoPP had a significant influence on *NRF2* mRNA expression (Figure 11B), pointing to a reduced degradation of NRF2 by KEAP1.

In the classical regulation model, an increased NRF2 results in nuclear accumulation and activation of transcription. Using immunofluorescence microscopy the nuclear accumulation of NRF2 was analysed in WI38 cells. BRD4-depleted and control cells were treated with 50 µM CoPP for 6 h. The NRF2 protein was stained with an antibody against the endogenous protein. Simultaneously, nuclei were stained with Hoechst to analyse the nuclear localisation of NRF2. Actually, under unstimulated conditions NRF2 was mainly detected in the cytoplasma and show only a marginal overlap with Hoechst staining. After treatment with 50 µM CoPP NRF2 showed an increased accumulation in the nucleus, as expected, that was further intensified in shBRD4 treated cells, supporting the proposed regulation through a diminished KEAP1 protein (Figure 11C).

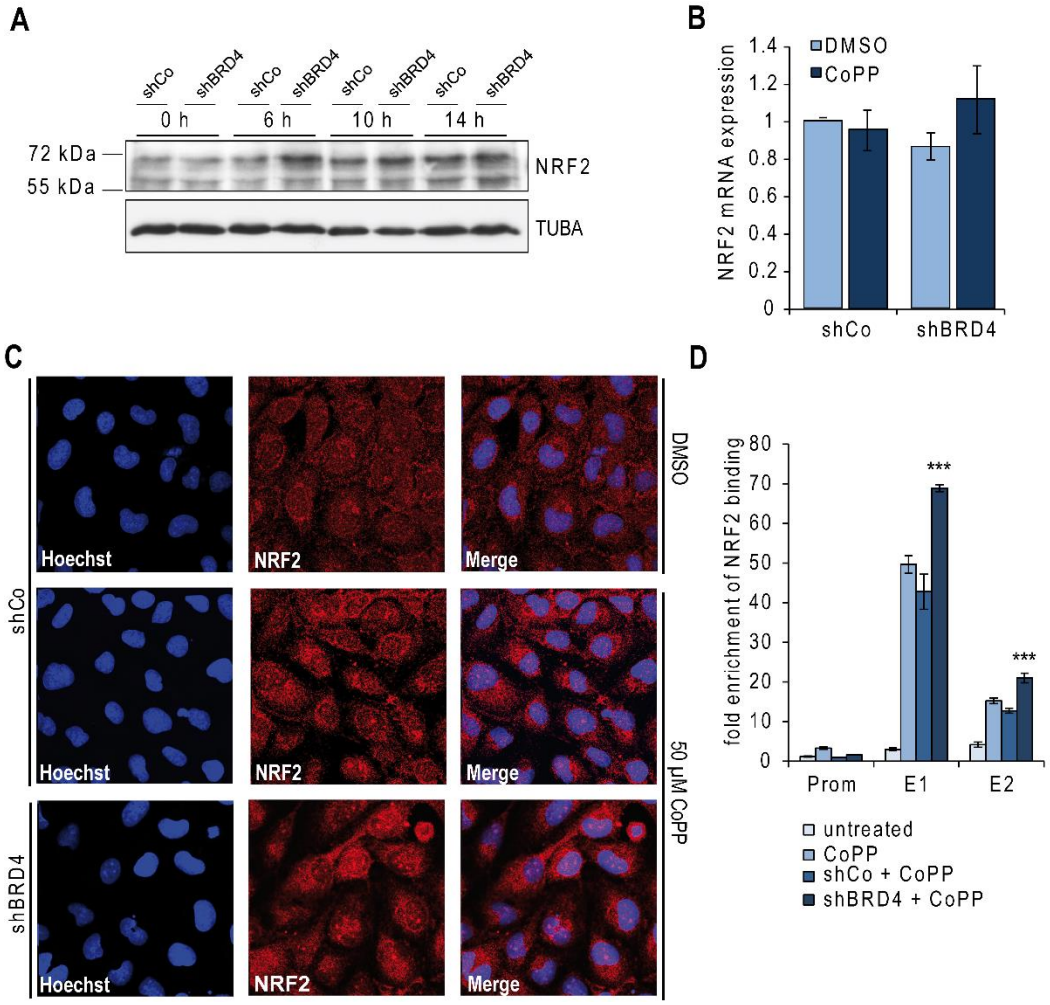

Figure 11 BRD4 knockdown increases NRF2 activity. (A) ***Western blot analysis of the NRF2 expression after CoPP treatment.*** NRF2 (MW = 60,000) protein levels were measured after treatment with 20 µM CoPP in BRD4 knockdown cells (shBRD4, 72 h) or control cells (shCo, 72 h) after 6, 10 and 14 h, as indicated. TUBA (α-tubulin) was used as a loading control. **(B)** ***NRF2 expression in BRD4-deficient and CoPP treated cells.*** *NRF2* mRNA expression was calculated in untreated (DMSO) or treated (CoPP, [20 µM] for 6 h) BRD4 knockdown (shBRD4, 72 h) and control (shCo, 72 h) cells. The expression was normalized to *TUBB* and to untreated (DMSO) and shCo treated cells. **(C)** ***Immunofluorescence of NRF2 after CoPP stimulation.*** WI38 cells were transfected with either shRNAs against BRD4 (shBRD4) or an unspecific control shRNAs (shCo) and treated after 72 h with 50 µM CoPP or DMSO for 6 h. Cells were stained with an antibody against NRF2 and Hoechst and examined with a confocal fluorescence microscope (LSM 510 meta, Zeiss). **(D)** ***ChIP analyses of the NRF2 binding to enhancer regions as well as to the promoter of the HMOX1 gene.*** ShBRD4 knockdown or shCo cells were treated after 72 h with 50 µM CoPP or DMSO for 6 h. The NRF2 binding to the *HMOX1* promoter as well as to both enhancers was analysed with qPCRs using region-specific primers. Specific BRD4-ChIP signal was normalized to the IgG-ChIP control. (*p-values < 0.1, **p-values < 0.05 and ***p-values < 0.01 according to two-tailed t-tests) (Figures taken from Hussong et al. 2014)

To further investigate, whether the increased NRF2 accumulation also resulted in an enhanced transcriptional activity, caused by an increased DNA binding of NRF2, ChIP experiments in CoPP-treated and -untreated BRD4 knockdown (shBRD4) and control knockdown (shCo) cells were performed. The ChIP experiments were carried out in HEK293T cells. NRF2 binds to antioxidant-responsive elements and NF-E2/Maf recognition elements, respectively, that are mainly found in the enhancer regions E1 and E2, located ~3 kb and ~10 kb upstream of the transcription-initiation site of *HMOX1*. The NRF2 binding to both *HMOX1* enhancers E1 and E2 as well as on the promoter region was analysed using qPCR. The promoter region of *HMOX1* was detected with primers that amplify a region of the 5' UTR of the *HMOX1* promoter. The enrichment at E1 was measured by using primers that are located in the first enhancer region, around 4,000 bp upstream of the TSS and the enrichment at E2 by using primers that are located in the second enhancer region, approximately 10,000 bp upstream of the TSS. Under unstressed conditions, NRF2 was found neither at the promoter region, nor at the enhancer regions E1 and E2 of *HMOX1*. The treatment with 50 µM CoPP for 6 h that leads to stabilization and nuclear accumulation of NRF2, resulted in a clear enrichment at both enhancer regions, but not on the promoter, as already described in the literature. Interestingly, BRD4 reduction significantly increased NRF2 binding to both *HMOX1* enhancers, after CoPP induction, but did not increase the binding to the promoter. The enrichment of both enhancers was more than 1.6-fold increase in BRD4-depleted and CoPP treated cells compared to the CoPP treated knockdown control cells. This explains the increased expression of *HMOX1* by enhancing the transcriptional activity of NRF2 (Figure 11D).

2.2.2 BRD4 protects cells against high levels of ROS

So far, I was able to show that a diminished expression of BRD4 leads to the down-regulation of KEAP1, a reduced degradation of NRF2, followed by the transcriptional induction of cyto-protective genes, such as HMOX1. To test if the increased HMOX1 induction in BRD4 knockdown cells results in a decreased ROS level and an enhanced cell survival the bromodomain and extra-terminal (BET) inhibitor JQ1 was used. JQ1 blocks the bromodomains of BET proteins and leads to a dissociation of BRD4 from chromatin, resulting in a reduced transcriptional activity.

First, to determine if the inhibition with JQ1 has the same effects on the transcriptional regulation as the down-regulation of the BRD4 protein with RNA interference, the expression level of *KEAP1* in JQ1 treated cells was analysed. WI38 cells were stimulated

with various concentration of JQ1 (0.5, 1, 2.5 and 5 µM) for 72 h and the RNA was isolated and analysed using qPCR. Similar to BRD4 knockdown, a down-regulation of *KEAP1* was found in a dose-dependent manner upon JQ1 treatment (Figure 12A). With an increased concentration of JQ1, the expression of *KEAP1* mRNA went down. The treatment with 5 µM JQ1 for 72 h reduced significantly the expression of *KEAP1* down to 60% compared to the DMSO-treated control cells. Subsequently, to investigate if the level of ROS may be influenced by a deregulation of BRD4 activity, a dihydrorhodamine 123 (DHR) flow cytometry assay was performed. Dihydrorhodamine 123 is an uncharged and non-fluorescent indicator of ROS. In the presence of ROS the non-fluorescent DHR molecule is oxidized to the highly fluorescent product rhodamine 123 which localizes in the mitochondria. The formation of the green fluorescent rhodamine 123 can be measured by flow cytometry. WI38 cells, treated with various concentrations (1, 2.5 and 5 µM) of the BRD4 inhibitor JQ1 were stimulated after 72 h with or without 1 mM hydrogen peroxide (H_2O_2) for 4 h to induce the generation of ROS. Under unstimulated conditions, no differences in the amount of ROS could be detected between DMSO and JQ1 treated cells. However, in DMSO control cells, the stimulation with H_2O_2 clearly induced the generation of ROS in 4,729 cells in average. When stimulated by H_2O_2, the inhibition of BRD4 in those cells resulted in a significantly reduced number of high ROS containing cells (Figure 12B). For example, the treatment with 1 µM JQ1 reduced the number of high ROS containing cells from 4,729 to 1,869 in average. The treatment with 2.5 and 5 µM resulted in an induction of ROS in 1,577 and 1,456 cells, respectively. In summary, treatment with JQ1 reduced the number of cells with high level of ROS from 35% to 18% (Figure 12C).

To test a functional consequence of the diminished ROS level, cell viability assays were performed in BRD4-deficient as well as in JQ1 treated WI38 cells with the Alamar Blue® assay. The Alamar Blue® reagent contains the nontoxic, cell permeable and blue-coloured compound resazurin. In viable, metabolizing cells, resazurin is reduced to resorufin, which produces very bright red fluorescence signals that can be measured and quantified using an UV-Vis spectrophotometer at 570 nm. WI38 cells were treated with siBRD4 or siCo and were stimulated after 24 h with 100 µM H_2O_2 for 30 min. The cell survival rate and the viability of these cells was observed over 72 h. Accordingly, cells with diminished BRD4 expression displayed an increased cell survival upon H_2O_2 treatment compared to control cells (Figure 12D) that increased with the time after H_2O_2 stimulation. After 72 h the cell viability increased up to 20% in BRD4-depleted compared to control cells.

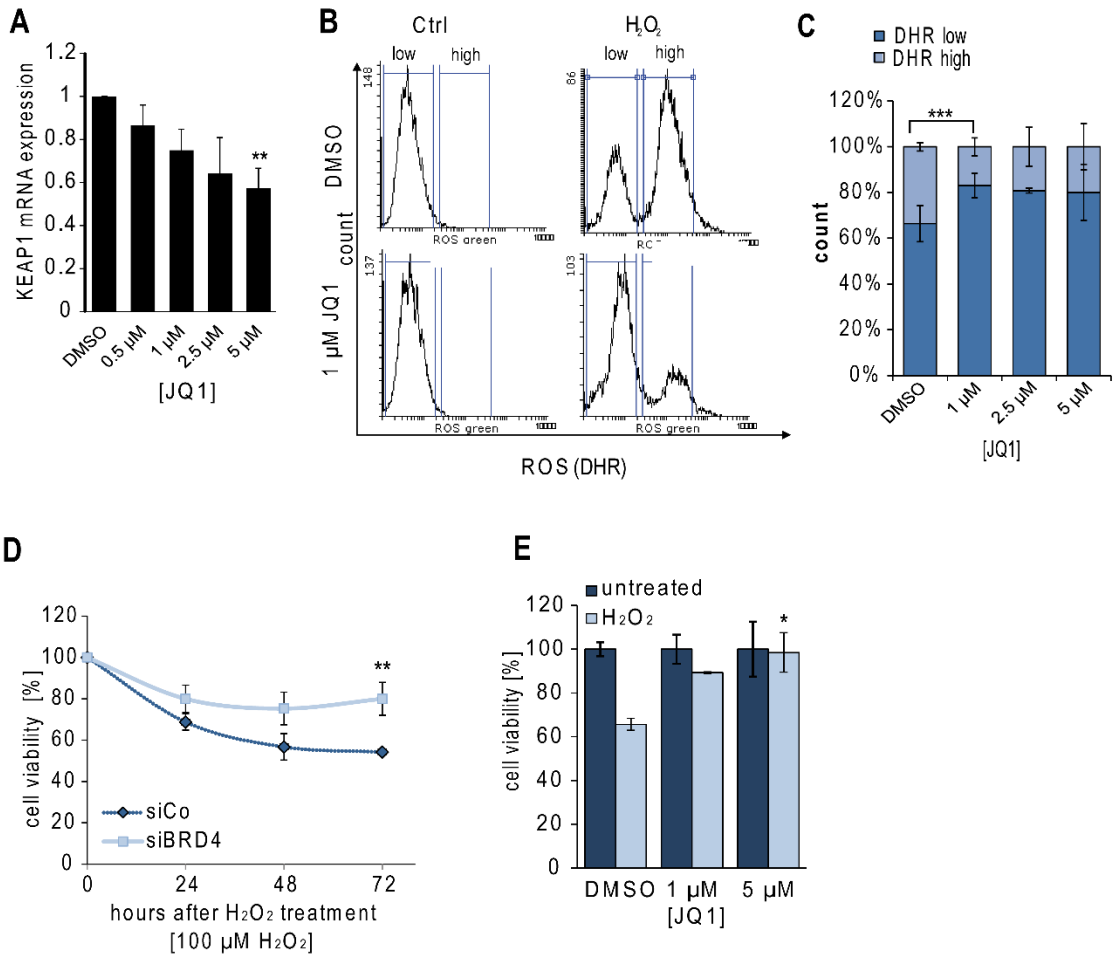

Figure 12 BRD4 inhibition decreases ROS and enhances cell survival under oxidative stress. (A) ***KEAP1 mRNA expression was analysed in WI38 cells after 72 h of JQ1 or DMSO treatment using qPCR.*** As a reference gene, β-tubulin was used. The results represent the averages of two independent experiments. **(B)** ***Determination of ROS in WI38 cells.*** Cells were treated with 1 µM JQ1 or DMSO for 72 h. 4 h before measurement, 1 mM H_2O_2 was used to stimulate ROS production. The intensity of intracellular ROS was measured with a flow cytometer using the fluorescence substrate DHR. The intensity of the green fluorescent DHR is plotted on the x-axis and represents the level of ROS. On the y-axis, the number of cells are shown. **(C)** ***Flow cytometry analysis using the Flowing Software 2 in cells treated with various concentrations of JQ1.*** The distribution of cells with high and low intensity of DHR was calculated and plotted as relative cell number. Low intensity of DHR represents low level of ROS, whereas high fluorescence indicates high level of ROS. **(D)** ***Cell viability assay of BRD4 knockdown.*** WI38 cells were transfected either with siBRD4 or non-targeting control siRNA. After 24 h, cells were treated with 100 µM H_2O_2 for 30 min. Cell viability was measured after 24, 48 and 72 h using the Alamar Blue reagent. **(E)** ***Cell viability assay of BRD4 inhibition.*** WI38 cells were incubated with various concentrations of JQ1 for 72 h. 48 h before determination of cell viability, the cells were treated with 100 µM H_2O_2 for 30 min. (*p-values < 0.1, **p-values < 0.05 and ***p-values < 0.01 according to two-tailed t-tests) (Figures taken from Hussong et al. 2014)

Similarly, the cell viability of WI38 cells treated with or without JQ1 (1 and 5 µM) for 72 h confirmed this observation of a decreased cell death after oxidative stress induction (Figure 12E). The inhibition of BRD4 using 5 µM of JQ1 resulted in a 35% increased cell survival 48 h after oxidative stress induction (100 µM H_2O_2 for 30 min).

Thus, the inhibition of BRD4 lowers intracellular ROS levels after exposure to stress, due to an increased NRF2 activity, which also might be the explanation for the increased cell viability.

2.2.3 BRD4 directly regulates *HMOX1* expression

Besides the function of BRD4 under H_2O_2 stress conditions, I was also interested if BRD4 also directly regulates HMOX1 under normal conditions. For this, I investigated the expression of HMOX1 in BRD4 knockdown and control cells without the exposure to stress. HEK293T cells were treated with RNA interference constructs that target both isoforms of BRD4 (siBRD4 and shBRD4-1) as well as a construct that only down-regulates the longer isoform. To down-regulate both BRD4 transcripts I used, on the one hand, the previously described siRNA-pool that target the N-terminal end of the BRD4 transcript which is present in both isoforms and the small hairpin RNA (shBRD4-1) that was already used for the previously performed knockdown approaches. To distinguish between both isoforms of BRD4 a second small hairpin RNA construct (shBRD4-2) was used that targets a region in the C-terminus of BRD4 that is only present in the longer transcript.

First, the expression of *HMOX1* mRNA level was quantified in HEK293T cells treated for 72 h with siBRD4 or shBRD4-1. The down-regulation of BRD4 using both RNA interference constructs significantly reduced the expression of *HMOX1* mRNA (Figure 13A). The treatment with siBRD4 reduced the expression of *HMOX1* down to 70% compare to the knockdown control. An even stronger down-regulation could be observed in the cells treated with shBRD4-1. In this case the down-regulation of both isoforms of BRD4 significantly reduced the expression of *HMOX1* down to 40%. Similar results were observed on protein level. HEK293T cells were transfected with either shBRD4-1, shBRD4-2 or the corresponding knockdown control (shCo). 72 h post-transfection the cells were harvested and the protein level of BRD4, HMOX1 and ACTB was analysed on Western Blot. The down-regulation of BRD4 with both shRNAs drastically decreased the HMOX1 protein level, but did not influenced the level of ACTB (Figure 13B). The same results were detected using the pool of four different small interference RNAs. HEK293T cells were treated with siBRD4 and the corresponding knockdown control for 72 h. The

protein level of BRD4, HMOX1 and ACTB were again measured by Western blotting. As seen for the treatment with both shRNA constructs, the down-regulation of BRD4 using siRNA diminished clearly the HMOX1 protein level, but has no impact on the expression of ACTB (Figure 13C). Consistent with the knockdown experiments, an overexpression of BRD4 in HEK293T cells for 48 h resulted in an up-regulated HMOX1 protein level (Figure 13D). The protein level of ACTB was unaffected.

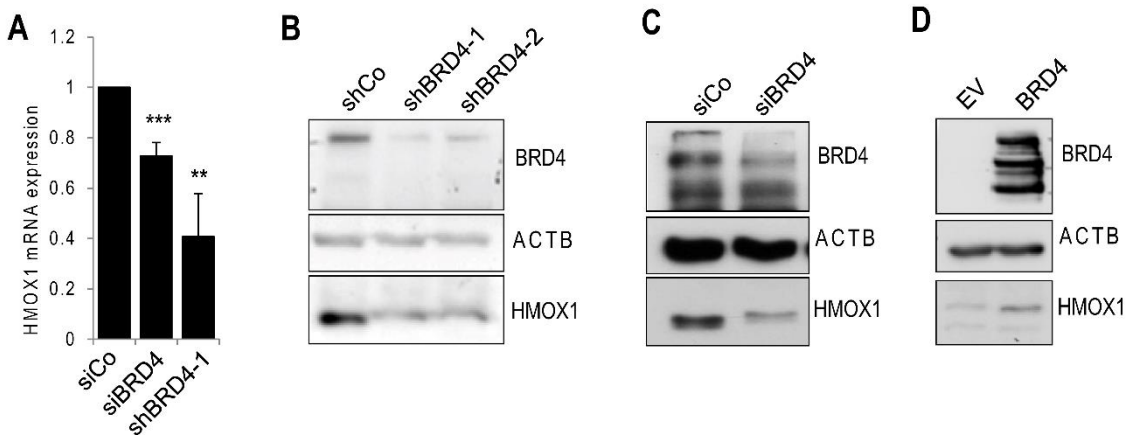

Figure 13 BRD4 regulates the transcription of *HMOX1* in the absence of stress. (A) ***HMOX1 expression in BRD4 deficient cells.*** mRNA expression analysis of *HMOX1* after BRD4 knockdown using siRNA as well as shRNA against human BRD4 in HEK293T cells. Cells were transfected with siBRD4, shBRD4-1 and the corresponding knockdown control. 72 h after transfection, cells were harvested, RNA isolated and the mRNA expression level was quantified using qPCR with primers targeting the *HMOX1* mRNA. As normalization *TUBB* was used. **(B, C)** ***Western blot of BRD4 and HMOX1 after BRD4 knockdown.*** HEK293T cells were transfected with either shBRD4 **(B),** siBRD4 **(C)** or with their corresponding knockdown control and harvested 72 h post transfection. Proteins were analysed on Western Blot. As loading control ACTB was used. (Figure taken from Hussong et al. 2014) **(D*) HMOX1 protein level after BRD4 overexpression.*** HEK293T cells were transfected with either BRD4-pcDNA overexpressing plasmid or with the corresponding empty vector (EV) control and harvested 48 h post transfection. Proteins were analysed on Western Blot. As loading control ACTB was used. (**p-values < 0.05 and ***p-values < 0.01 according to two-tailed t-tests)

Since these results cannot be explained by the previously identified regulation of KEAP1 by BRD4, further experimental analyses were performed to elucidate this discrepancy.

To illuminate the underlying regulatory mechanism, luciferase reporter assays of the *HMOX1* promoter were performed in the absence of stress. As already mentioned,

HMOX1 expression is regulated over several transcriptional regulatory elements and transcription factor binding sites in the promoter and in the enhancer regions E1 and E2 located upstream of the *HMOX1* promoter. Among these transcription factors, members of the heat-shock factor (HSF), nuclear factor - κB (NF-κB), nuclear factor–erythroid 2 (NF-E2), and activator protein - 1 (AP1) families are the most important and the best studied regulators of the *HMOX1* expression and are found in the promoter region as well as in the enhancer regions.

To elucidate which regulatory sequence is essential for the BRD4 dependent regulation of *HMOX1* different luciferase constructs were generated. They either contained E1 in addition to a 2- kb region of the *HMOX1* promoter, including the 5'UTR (E1-HMOX1-WT (wild type)) or fragments of different sizes of the promoter region alone (HMOX1-WT, HMOX1-367, HMOX1-228). The construct E1-HMOX1-WT contains all important regulatory regions, including the binding sites of NRF2, whereas the construct without the enhancer region only includes binding sites for the transcription factors HSF1, NF-κB, AP1 and SP1 (Figure 14).

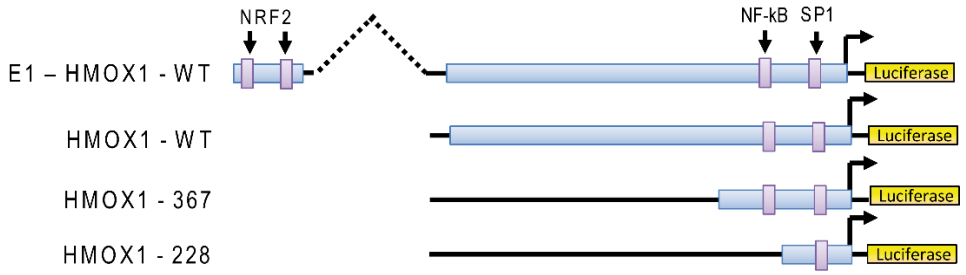

Figure 14 Schematics of the *HMOX1* luciferase reporter constructs. Blue bars represent the cloned promoter and enhancer fragments, respectively. In violet the binding sites of NRF2, NF-κB and SP1 are marked. (Figure taken from Hussong et al. 2014)

The promoter activity of the constructs was analysed using the Dual- Luciferase® Reporter Assay System from Promega. The plasmids containing the *HMOX1* promoter fragments, express the firefly-luciferase, while the co-transfected "control" reporter plasmid express the renilla-luciferase. In each experiment, the firefly-luciferase activity was normalized to the renilla-luciferase signal that serves as the baseline response. First, the renilla luciferase control construct and the firefly-luciferase constructs E1-HMOX1-WT and HMOX1-WT were transfected into HEK293T cells together with either a BRD4 overexpression-, an NRF2 overexpression-construct or the corresponding negative control

(empty vector, EV). An overexpression of NRF2 revealed a more than 2-fold increase of the luciferase signal with E1-HMOX1-WT but changes with HMOX1-WT, confirming the transcriptional enhancement by NRF2 through the enhancer regions (Figure 15A). Interestingly, a transfection with BRD4 increased the reporter activity of the E1-HMOX1-WT construct up to 2-fold but showed an even stronger luciferase activity with the HMOX1-WT promoter construct (Figure 15A). The promoter activity of the HMOX1-WT promoter increased more than 4-fold compared to the empty vector control. This suggests an additional transcriptional regulation mechanism of BRD4 besides the KEAP1/NRF2 pathway on *HMOX1*.

To validate the observed regulation of *HMOX1* by BRD4, the activity of the wild type promoter containing luciferase construct was measured in BRD4-deficient HEK293T cells, using both shRNAs, shBRD4-1 and shBRD4-2 (Figure 15B). Indeed, a BRD4 knockdown significantly decreased the promoter activity of the HMOX1-WT construct to 68% (p-value (shBRD4-1) = 0.007) and 53% (p-value (shBRD4-2) = 0.013), respectively (Figure 15B). Of the same cells, the corresponding protein lysates were analysed on Western blots to check the efficiency of the BRD4 knockdown. The Western blot showed an efficient down-regulation of BRD4 on protein level whereas the protein level of ACTB was unchanged.

To investigate, whether BRD4 directly activates the *HMOX1* transcription by direct association to the promoter, additional BRD4-ChIP, and as control IgG-ChIP experiments in untreated HEK293T cells were performed (Figure 15C). The precipitated DNA was analysed with qPCRs using primers including the *HMOX1* 5'UTR (Prom), or primers that bind to the first enhancer region (E1). In addition, primers for a non-coding intergenic region (NCR) on chromosome 12 (chr12:61,667,719-61,667,796) were used. The qPCR analyses showed that the NCR as well as E1 were not enriched in the ChIP-experiments, neither in the BRD4-ChIP nor in the IgG-ChIP control. In contrast, the *HMOX1* promoter was 2-fold increase in the BRD4 precipitated samples compared to IgG control.

To further clarify how BRD4 may regulate the *HMOX1* transcription, the *HMOX1* promoter was shortened to curtail the regulatory elements. In 2009 it was published by Huang and colleagues [281] that BRD4 binds to the transcription factor NF-κB over the acetylated lysine 310 of RelA and thereby regulates the transcription of inflammatory stress responsive genes. To investigate an NF-κB dependent regulation of *HMOX1* in unstimulated cells by BRD4 two reporter constructs, with (HMOX1-367) or without (HMOX1-228) the NF-κB binding site, located 230–250 bp upstream of the TSS, were used.

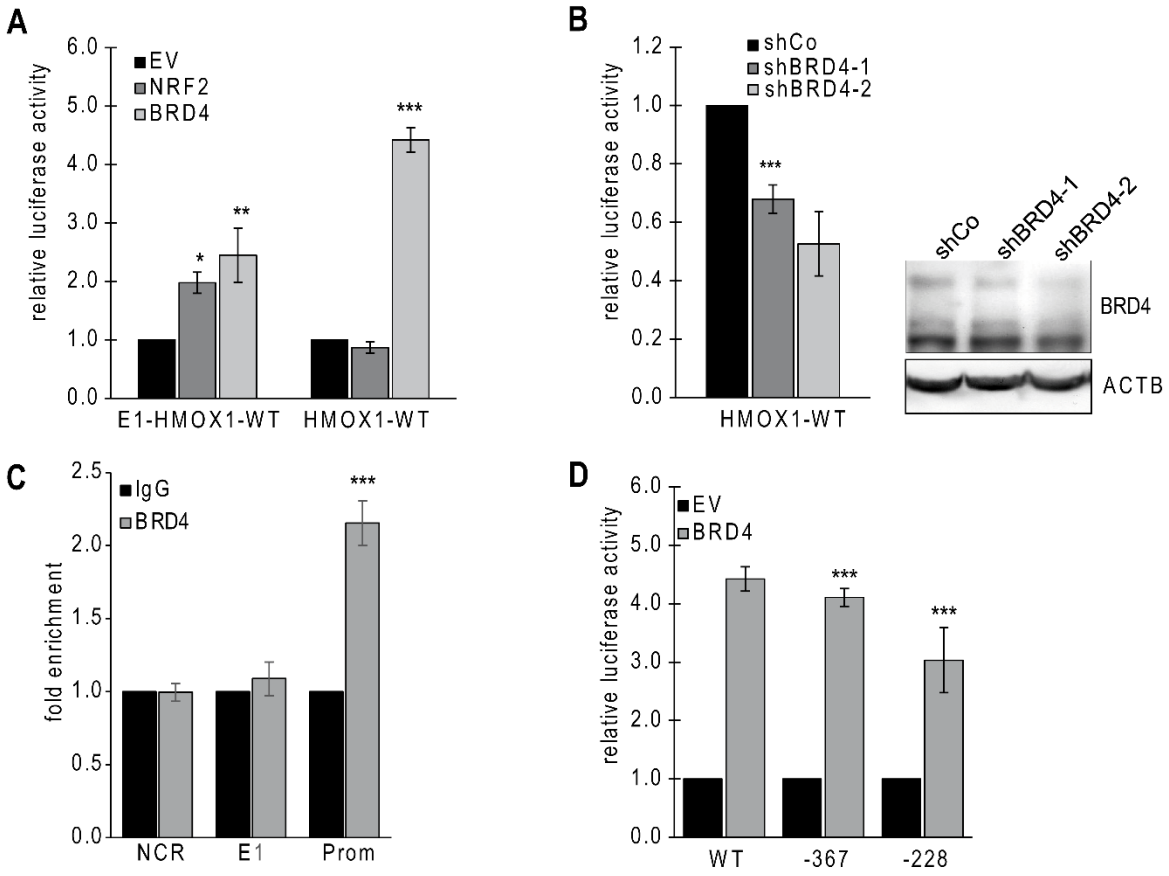

Figure 15 BRD4 regulates *HMOX1* promoter activity. (A) ***HMOX1 reporter assays with BRD4 and NRF2 overexpression.*** BRD4 (pcDNA-BRD4-FL), NRF2 (pTL-Flag-NRF2) expressing constructs or empty vectors (EV) were co- transfected with a luciferase reporter plasmid carrying the *HMOX1* promoter either with (E1-HMOX1-WT) or without (HMOX1-WT) the first enhancer region of the *HMOX1* gene. After 24 h, the promoter activity was normalized to EVs and the co-transfected renilla luciferase activity. Results represent the averages of three independent experiments. **(B)** ***HMOX1 reporter experiments in BRD4 knockdown cells.*** HEK293T cells were co-transfected with either shBRD4-1, shBRD4-2 or shCo as control with the luciferase reporter carrying the *HMOX1* promoter (HMOX1-WT). 72 h post transfection, the cells were harvested for measuring the luciferase activity, normalized to renilla luciferase activity, or for Western blot analysis. As loading control ACTB was used. Results represent two biological replicates. **(C)** ***Binding of BRD4 to the HMOX1 promoter.*** ChIP analyses were performed with an antibody against BRD4 or with rabbit IgG as a negative control. The enrichment was analysed with qPCRs for the promoter (Prom) and for the enhancer region 1 (E1) of *HMOX1* and an intergenic non-coding region (NCR). Values were normalized to the input and IgG controls. **(D)** ***Mapping of the BRD4 responsive region on the HMOX1 promoter.*** BRD4 (pcDNA-BRD4-FL) or empty vector (EV) were co-transfected with a luciferase construct carrying the full-length *HMOX1* promoter (HMOX1-WT), a 367-bp long (HMOX1-367) or a 228-bp (HMOX1-228) long fragment of the *HMOX1* promoter. 24 h post transfection, the promoter activity was determined and normalized to the renilla luciferase and the EV signals. Results represent the averages of three independent experiments. (*p-values < 0.1, **p-values < 0.05 and ***p-values < 0.01 according to two-tailed t-tests) (Figures taken from Hussong et al. 2014)

The promoter activity was determined after an overexpression of BRD4 for 24 h in HEK293T cells. Whereas the 367-bp long promoter construct showed only a marginal reduced promoter activity compared to the WT promoter, the activity of the 228-bp long construct was attenuated compared to the full-length promoter. Nevertheless, the luciferase experiments revealed that the 367-bp long as well the 228-bp long construct showed still an activating function of BRD4, suggesting an of NF-κB independent regulation (Figure 15D).

2.2.4 BRD4 regulates *HMOX1* expression via SP1

To identify regulatory sequences in the *HMOX1* promoter required for the BRD4-mediated regulation under unstressed conditions the binding regions from the ChIP-seq experiments were used to perform Multiple Expectation Maximization for Motif Elicitation (MEME) [286] analysis. The online available motif searching tool identifies common sequence patterns in the BRD4 binding regions and compares these patterns with known transcription factor binding motifs. Among others, the motif search depicted significant enrichments for several transcriptional regulators including YY1, SMAD3 and SP1 (Table 5).

A comparison of the identified transcription factor binding sites with the *HMOX1* promoter sequence showed that SP1 (specific protein 1) - binding sites are also located in the *HMOX1* promoter region. The SP1-binding motif, identified as one of the top sequence motifs for BRD4 binding (p-value of $2.67*10^{-04}$), is located 180 – 196 bp upstream of the TSS in the *HMOX1* promoter and thereby is situated in all promoter fragments. SP1 is a zinc finger transcription factor that binds to GC-rich motifs (5'-(G/T)GGGCGG(G/A)(G/A)(C/T)-3' (GC box element)) (Figure 16A) of numerous stress related promoters and is involved in many cellular processes, including cell differentiation, cell growth, apoptosis, immune responses, response to DNA damage, and chromatin remodelling.

To investigate if the BRD4 dependent regulation of HMOX1 acts over SP1, point mutations were inserted in the SP1-binding site in the HMOX1-WT luciferase reporter plasmid. The GC-rich consensus sequence of the SP1 binding motif was disrupted by the insertion of two thymine nucleotides instead of a guanine duplex (GG → TT) (Figure 16B).

Table 5 MEME/TOMTOM analysis of BRD4 ChIP-Seq data.

TF[a]	*p-value*[b]	*E-value*[c]	*q-value*[d]	*Target consensus*
ABI4	$1.42*10^{-5}$	$1.22*10^{-2}$	$2.40*10^{-2}$	CGGTGCCCCC
NKX3-1	$1.84*10^{-5}$	$1.59*10^{-2}$	$3.17*10^{-2}$	TAAGTAT
EGR1	$3.79*10^{-5}$	$3.26*10^{-2}$	$3.20*10^{-2}$	TCCGCCCCCGCATT
ZFX	$7.28*10^{-5}$	$6.28*10^{-2}$	$4.10*10^{-2}$	GGGGCCGAGGCCTG
YY1	$2.07*10^{-4}$	$1.79*10^{-1}$	$3.00*10^{-1}$	GATGGC
SP1	**$2.67*10^{-4}$**	**$2.31*10^{-1}$**	**$1.02*10^{-1}$**	**CCCCGCCCCC**
SRF	$2.79*10^{-4}$	$2.40*10^{-1}$	$2.40*10^{-1}$	GTTAAAAAAAAAAATTT
ELF3	$2.79*10^{-4}$	$2.40*10^{-1}$	$2.40*10^{-1}$	GTTCAAAAAAAAAATTC
STP1	$3.03*10^{-4}$	$2.61*10^{-1}$	$1.02*10^{-1}$	GCGCCGCA
SMAD3	$3.48*10^{-4}$	$3.00*10^{-1}$	$3.00*10^{-1}$	CAGAGTGGCGGGGCGTA
ID1	$3.52*10^{-4}$	$3.03*10^{-1}$	$6.06*10^{-1}$	CGAAAAGGAAAA
SUM1	$5.08*10^{-4}$	$4.37*10^{-1}$	$8.75*10^{-1}$	AAAAATTTT
ZEB1	$5.23*10^{-4}$	$4.51*10^{-1}$	$9.02*10^{-1}$	CAGGTG

[a]transcription factor; [b]gives the probability of a random string (generated from the background letter frequencies); [c]describes the number of hits one can "expect" to see by chance, [d]the minimum false discovery rate at which the test may be called significant.

The promoter activity of the mutated construct was tested following SP1 overexpression in HEK293T cells. As expected, the overexpression of SP1 increased the promoter activity of the wild type construct up to 2-fold compared to the empty vector control (EV) (Figure 16C). In contrast, the insertion of the point mutations in the *HMOX1* promoter significantly abolished the promoter activation in SP1 overexpressing cells. The expression of SP1 did not further enhance the promoter activity, indicating a disrupted SP1-binding site. A subsequent overexpression of BRD4 in these cells resulted in the expected activation of the WT-luciferase reporter, whereas the SP1-mutated promoter showed a significant lower activation after BRD4 expression (Figure 16C). Accordingly, the promoter activation of the wild type promoter (HMOX1-WT) after BRD4 overexpression was more than 2-fold

reduced when the promoter harbours the SP1 binding site mutations, suggesting a regulation of the *HMOX1* gene promoter over the SP1-binding sites.

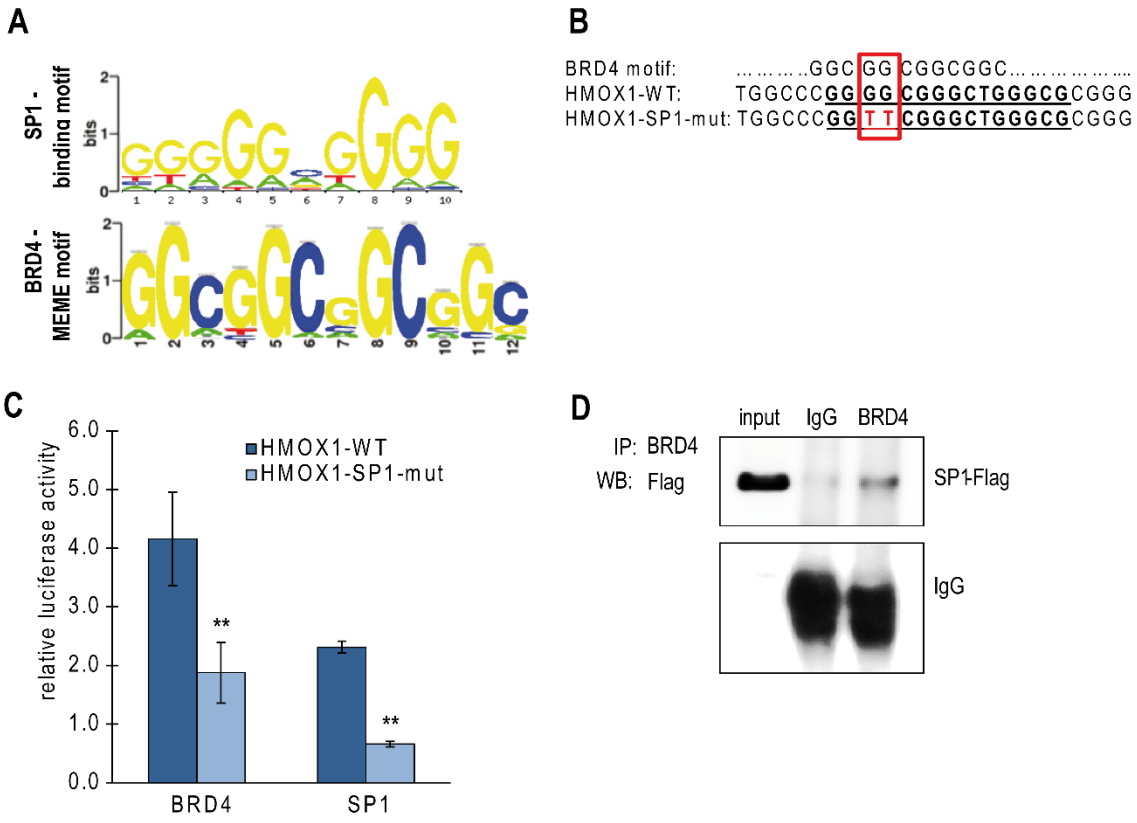

Figure 16 BRD4 regulates the *HMOX1* expression over the SP1 binding sites. (A) ***MEME analyses of BRD4 ChIP-Seq data.*** The binding matrix represents the identified BRD4 'binding motif' of the ChIP-sequencing (lower) and the SP1 consensus motif (upper). Using the TOMTOM analysis tool, the SP1-binding motif was identified as one of the top known binding motifs associated with the BRD4-binding site (P-value: 0.00026, E-value: 0.2305; q-value: 0.1024). **(B)** ***Schematics of the SP1-binding site in the HMOX1 promoter (HMOX1-WT) and the inserted mutations (HMOX1-SP1-mut) (red).*** **(C)** ***Reporter assays with wild-type (HMOX1-WT) or SP1-site-mutated (HMOX1-SP1-mut) HMOX1 reporter constructs.*** pTL-FLAG-BRD4 and pTL-FLAG-SP1 expressing constructs were co-transfected with either the *HMOX1* wild-type promoter or with the SP1-binding site mutant. 24 h post transfection, cells were harvested, and the promoter activity was determined and normalized to the renilla luciferase signal. Results represent averages of two independent experiments. (Figures taken from Hussong et al. 2014) **(D)** ***Co-immunoprecipitation of BRD4 and SP1***. Co-IPs were performed using an endogenous BRD4 antibody in HEK293T cells, transfected with pTL-FLAG-SP1 and analysed on a Western Blot using an antibody against the FLAG-tag to detect SP1. (*p-values < 0.1, **p-values < 0.05 and ***p-values < 0.01 according to two-tailed t-tests)

Due to these observations, the question arose if BRD4 and SP1 physically interact. Using co-immunoprecipitation experiments in unstimulated, SP1 overexpressing HEK293T cells,

a potential interaction between BRD4 and SP1 was tested. Indeed, the Western bot analysis showed a pull-down of the overexpressed and Flag-tagged SP1 protein in the BRD4 precipitated lane (Figure 16D). In contrast, the precipitation with the IgG control depicted no specific co-precipitated protein. These experiments strongly suggest a regulation of *HMOX1* by BRD4, even independent of the KEAP1/NRF2 pathway, through the association to the transcription factor SP1. Furthermore, a comparison of the 52 identified target genes with genes that harbour known SP1 binding sites (extracted out of the online available database SAbioscience from Qiagen) revealed that 20 BRD4 target genes contain a SP1-binding sequence in transcription regulatory regions. Amongst others, oxidative stress related genes such as *GSTP1* and *TXN2*, were found to have a SP1-binding site, indicating a general mechanisms of BRD4 regulation in the absence of stress.

2.2.5 BRD4/KEAP1/NRF2 pathway regulation in prostate cancer

The previous sections of my PhD thesis described in detail the influence of BRD4 on the KEAP1/NRF2 mediated response to oxidative stress. Knockdown of BRD4 or treatment with the BRD4 inhibitor JQ1 resulted in decreased ROS production and increased cell viability under H_2O_2 exposure. A deregulation of BRD4 diminished KEAP1 expression led to an increase in the transcriptional activity of NRF2 that, in turn, resulted in a disturbed regulation of the inducible *HMOX1*.

The KEAP1/NRF2 pathway is frequently disrupted by somatic mutations in tumors. As such the question remains what the impact of BRD4 inhibitors on the KEAP1/NRF2-pathway and the tumor growth of different tumor entities would be. To check the *BRD4* mRNA level in different tumor entities the expression of *BRD4* in 16 different cancer cell lines, accounting for 7 tumor entities, was analysed by qPCR experiments (Figure 17A). The used cell lines for each tissue are listed in Supplement Table S 3. The expression was normalized to the human embryonic fibroblast cell line WI38. This analysis depicted an increase of BRD4 expression in colon cancer cell lines ($p = 0.053$) as well as in prostate cancer cell lines ($p = 0.055$) with an average increase of 5 and 10-fold, respectively. To validate these data in a clinical context, gene expression profiles of patient derived prostate tissue samples as well as colon tissue samples, which were already available in the group, were used to investigate the BRD4 expression. The prostate cancer gene expression data had been generated by micro array experiments from 48 normal and 47 tumor prostate tissue samples [287], whereas the colon cancer expression data have been

generated from 12 matched normal and tumor samples by RNA-seq. The gene expression analysis revealed a significant increase of BRD4 expression in prostate tumor samples ($p = 2.8 * 10^{-15}$) (Figure 17B) and nearly no differential expression in colon cancer samples ($p = 0.08$) (Figure 17C).

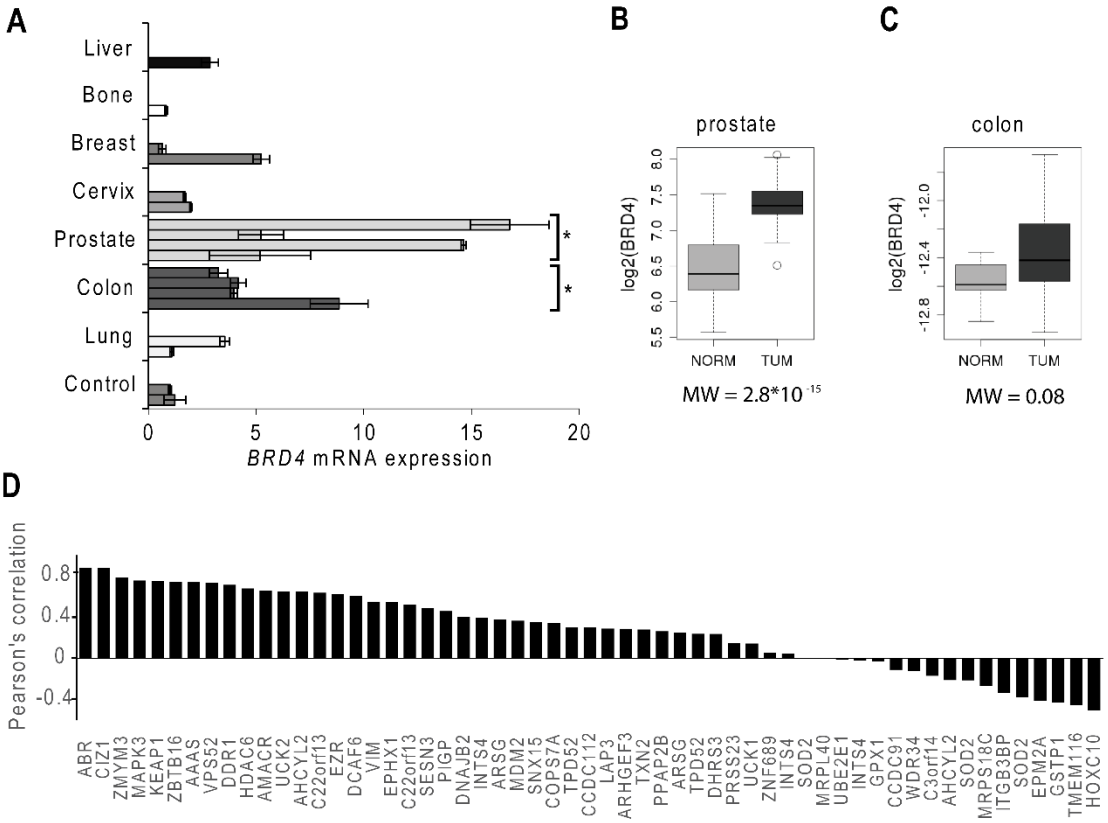

Figure 17 Regulation of *BRD4* and its target genes in cancer. (A) ***mRNA expression analysis of BRD4 in different cancer cell lines using qPCR.*** The expression was normalized to the cell line WI38 and *TUBB*. **(B, C)** ***expression profiles of BRD4*** in **(B)** prostate tumor and normal samples and **(C)** colon tumor and normal samples. P-values were calculated using the Mann-Whitney test (MW). Differential expressions were calculated based on values of 47 tumor and 48 normal samples for prostate cancer and 12 matched normal and tumor samples for colon cancer. Figure and analyses were provided by Dr. Stefan Börno. **(D)** ***Correlation of the expression of the 52 identified BRD4 target genes in prostate cancer to BRD4 expression.*** Bars represent the Pearson correlation coefficient. (*p-values < 0.1, **p-values < 0.05 and ***p-values < 0.01 according to two-tailed t-tests)

Due to the elevated expression level of BRD4 in prostate tumor samples the question was whether the transcriptional regulating role of BRD4 is altered in prostate cancer (PCa). Therefore, the expression values of the 52 BRD4 target genes were correlated with the *BRD4* expression in tumor as well as in normal prostate tissues. Out of the previously

identified 52 BRD4 target genes, 21 genes were found to have a positive correlation above 0.4 to *BRD4* expression. These 21 genes included *MAPK3* (Pearson = 0.75, p-value = $7.74*10^{-19}$), *KEAP1* (Pearson = 0.75, $3.09*10^{-18}$) and *HDAC6* (Pearson = 0.68, $3.99*10^{-14}$) (Figure 17D).

To test the relevance of the identified regulatory network between BRD4/KEAP1/NRF2 in cancer, three prostate cancer cell lines (DU145, LNCaP, PC3) and as control one normal prostate cell line (RWPE-1) were used to determine the expression of *BRD4, KEAP1, NRF2* and *HMOX1* (Figure 18A). All tested prostate cancer cell lines do not contain the TMPRSS-ERG translocation, an in approximately 50% of PCa present genomic alteration. Furthermore, PC3 cells have a higher metastatic potential compared to DU145 cells which have a moderate metastatic potential and to LNCaP cells which show a very low metastatic potential and an androgen-sensitive growth. In contrast, DU145 and PC3 cells are androgen independent. The mRNA expression of *BRD4, KEAP1, NRF2* and *HMOX1* was calculated by qPCR and put into relation to the values obtained with the RWPE-1 cell line.

Again, the expression of *BRD4* was significantly up-regulated in all prostate cancer cell lines compared to the control, with the most significant increase of 3.4-fold found in LNCaP cells followed by DU145 with an increase of *BRD4* expression of 2.9-fold. Similar to the human prostate cancer tissue, the *NRF2* level was decreased in all cancer cell lines. In DU145 cells the *NRF2* expression was down-regulated to 50%, in PC3 cells to 43% and showed in LNCaP cells a down-regulation to 37%. Furthermore, the positive correlation between *BRD4* expression and *KEAP1* expression, found in the human prostate cancer tissue samples, could also be detected in these cell lines. Here, the expression of *KEAP1* showed a 3-fold increased expression in DU145 cells, followed by LNCaP with 2.2-fold and PC3 with a 1.3-fold increased *KEAP1* mRNA level compared to RWPE-1 cells. Interestingly, the expression of *HMOX1* was more variable. *HMOX1* was found to be 3.4-fold up-regulated in DU145, down-regulated in PC3 to 60% and marginal up-regulated in LNCAP cells (fold change = 1.09), suggesting an, at least partly independent regulation of NRF2. In a study published in 2008, Kumar and colleagues demonstrated, that prostate cancer cell lines have a higher H_2O_2 production than normal cells (Figure 18B) [288]. They used as an indicator for ROS CM-H_2DCFDA, a chloromethyl derivative of H_2DCFDA, preferably used for long-term studies. CM-H_2DCFDA is oxidized in the presence of ROS, comparable to dihydrorhodamine 123, that results in a fluorescent adduct that can be quantified by immunofluorescence. They showed that PC3 cells have a much higher ROS amount compared to the DU145 cells (Figure 18B) which seems to have a disrupted NRF2-HMOX1 axis. To validate these observation in our prostate cancer cell lines, I

performed further ROS detection experiments. DU145 and RWEP-1 cell lines were treated with or without 1 mM H_2O_2 for 4 h. The amount of oxidized rhodamine 123 was quantified using a flow cytometry approach as already described in the previous experiments. Indeed, upon stimulation with H_2O_2, DU145 cells showed a 1.6-fold increased ROS production compared to RWPE-1 (Figure 18C), supporting the results of Kumar et al. 2008.

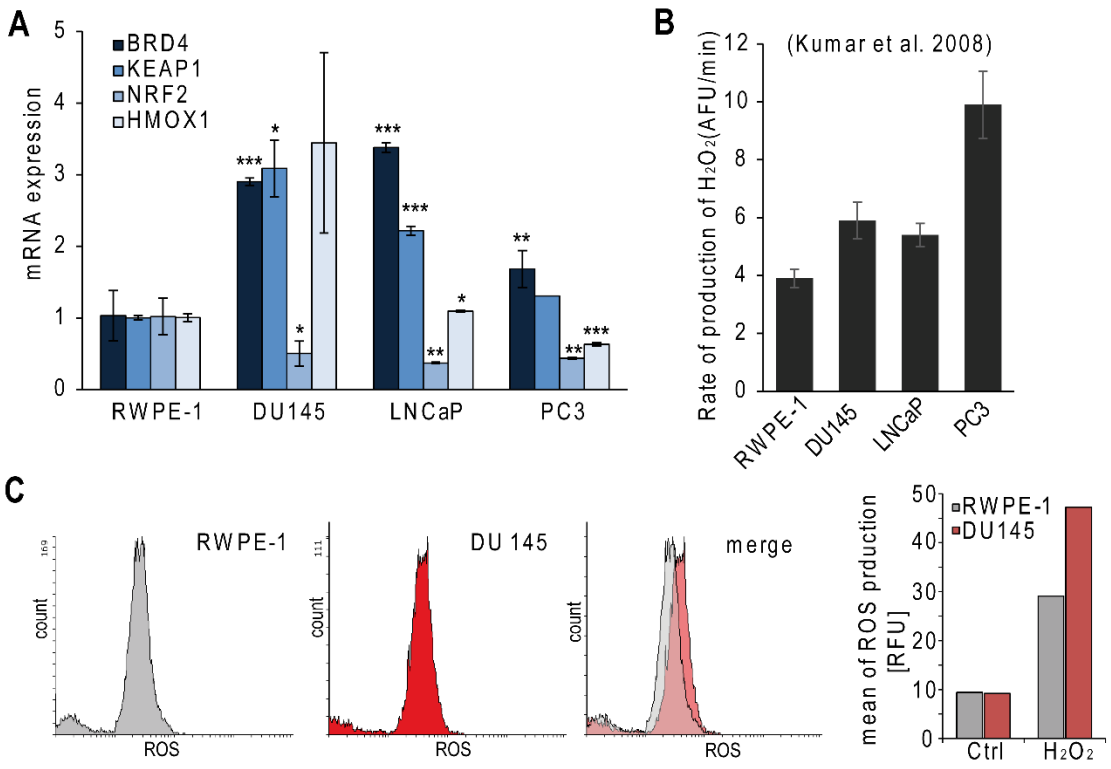

Figure 18 Regulation of the NRF2/BRD4 pathway in prostate cancer cell lines. (A) ***BRD4, KEAP1, NRF2 and HMOX1 mRNA expression in PCa cell lines using qPCR.*** The expression was determined in at least two independent experiments and normalized to *TUBB* and to the normal control cell line RWPE-1. (*p-values < 0.1, **p-values < 0.05 and ***p-values < 0.01 according to two-tailed t-tests) (Figure taken from Hussong et al. 2014) **(B)** ***H_2O_2 production in prostate cancer cell lines from Kumar et al. 2008***. The rate of production of H_2O_2 was measured using the dye CM-H_2DCFDA, a derivative of H_2DCFDA, useful for long-term studies. **(C)** ***Determination of ROS in RWPE-1 and DU145 cells.*** 4 h before detection, 1 mM H_2O_2 was used to stimulate ROS production. The intensity of intracellular ROS was measured using the fluorescence substrate DHR. Summary of the flow cytometry analysis using the Flowing Software 2 is shown on the right site.

Based on these data, I assumed that BRD4 inhibition in DU145 cells may lead to a down-regulation of *HMOX1* and in turn decreased cell viability. DU145 as well as PC3 cells were treated with or without 1 µM JQ1 for 72 h and the RNA was isolated. The expression of *BRD4*, *HMOX1* and *KEAP1* was determined using qPCRs. For each cell line, the

expression values of the genes under examination in JQ1-treated samples were normalized to their expression values in the corresponding DMSO control. The expression analysis of *BRD4* showed no change upon treatment with JQ1, neither in PC3 cells (Figure 19B), nor in DU145 cells (Figure 19A). However, the treatment with JQ1 reduced the expression of *KEAP1* in both prostate cell lines indicating that the regulation of KEAP1 by BRD4 is still functional. The expression of *HMOX1* was only down-regulated down to 40% in DU145 cells, supporting a regulation over BRD4 (Figure 19A). Similar to mRNA expression experiments, Western Blot analysis of the same samples showed a slight decrease in HMOX1 protein level in JQ1 treated DU145 cells, but no change in PC3 cells (Figure 19C). Due to the weak HMOX1 antibody signals in the Western blot, the intensity of each lane was quantified using the free available image editing software Image J [289]. The intensity of each lane of the HMOX1 signal was normalized to its corresponding TUBB signal. The Image J analysis confirmed the decreased HMOX1 expression in DU145 cells after treatment with JQ1. In contrast, the HMOX1 protein level in PC3 cells showed an even slight increase after BRD4 inhibition. Furthermore, the Western blot quantification confirmed the decreased HMOX1 expression in PC3 cells compared to DU145 cells, as seen in the previous described qPCR analyses. Interestingly, the level of NRF2 protein was unchanged in PC3 as well as in DU145 JQ1 treated cells, despite of a down-regulation of *KEAP1 mRNA*, indicating a disrupted KEAP1/NRF2 regulatory network in these prostate cancer cell lines. It should be mentioned that these experiments (mRNA and protein expression analysis in DU145 and PC3 cells) are only performed once. Further validations have to be done.

In a published study by Alaoui-Jamali et al. it was shown that the silencing of the *HMOX1* gene or the exposure to a small molecular HMOX1 inhibitor (OB-24) reduced cell proliferation, tumor growth and metastatic invasion in hormone-refractory prostate cancer [290]. To clarify if the down-regulation of HMOX1, caused by the treatment with JQ1, also results in a reduced cell proliferation, I measured the cell viability of DU145 and RWPE-1 cells upon JQ1 treatment. Both cell lines were treated with equal amounts of BRD4 inhibitor (0.025, 0.05, 0.1, 0.25, 0.5, 2.5, 5 and 10 µM) for 72 h. Cell viability was measured using the Alamar Blue® reagent. Despite the down-regulation of *HMOX1* in DU145 cells no change in cell viability upon JQ1 treatment was detectable (Figure 19D). However, these data go along with data from Wyce et al. who identified for DU145 cells a half maximal inhibitory concentration (IC_{50}) value for the BET inhibitor I-BET762 of more than 3 µM, which indicates a therapy resistance of DU145 cells for BRD4 inhibitors.

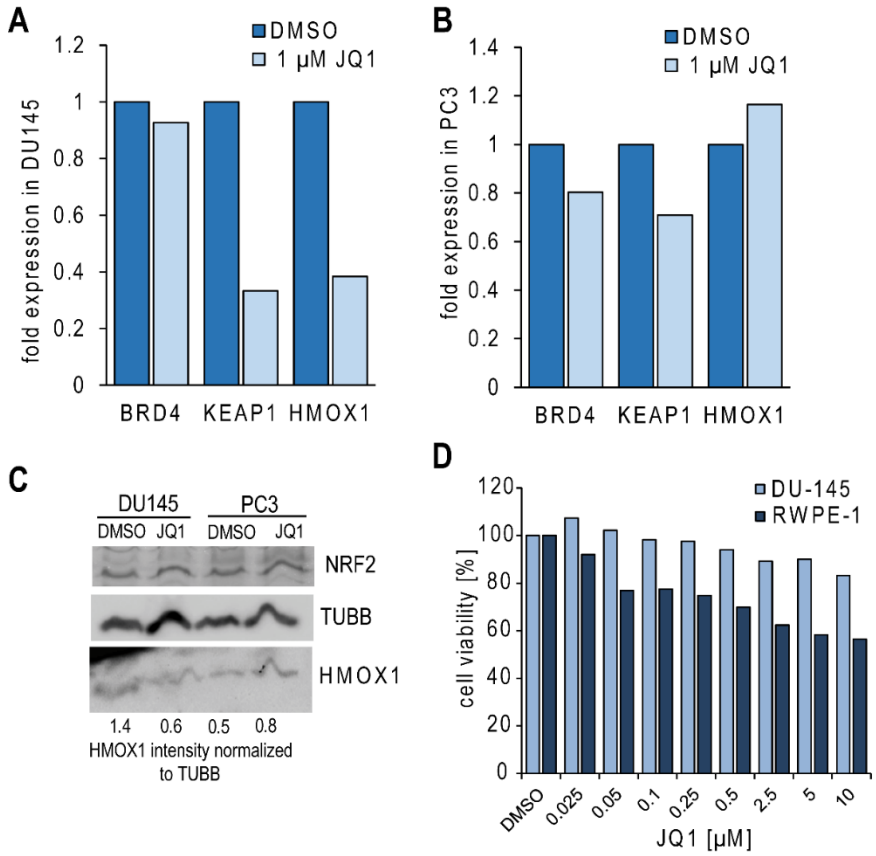

Figure 19 *HMOX1* regulation in DU145 and PC3 cells upon BRD4 inhibition (A*) qPCR expression analysis of BRD4, KEAP1 and HMOX1 in JQ1 treated DU145.* DU145 cells were either treated with 1 µM JQ1 or with the equal amount of DMSO for 72 h. *BRD4, KEAP1* and *HMOX1 mRNA* expression was normalized to *TUBB*. **(B)** ***qPCR expression analysis of BRD4, KEAP1 and HMOX1 in JQ1 treated PC3.*** PC3 cells were either treated with 1 µM JQ1 or with the equal amount of DMSO for 72 h. *BRD4, KEAP1* and *HMOX1 mRNA* expression was normalized to *TUBB*. **(C)** ***Western blot analysis of BRD4, KEAP1 and HMOX1 in JQ1 treated DU145 and PC3 cells.*** Both cell lines were either treated with 1 µM JQ1 or with the equal amount of DMSO for 72 h. BRD4, KEAP1 and HMOX1 level were analysed by Western blotting and normalized to TUBB. Numbers below represents the quantitative analysis of HMOX1 intensity normalized to TUBB intensity for each lane using the Image editing software "Image J". **(D)** ***Cell viability assay of DU145 and RWPE-1 cells***. Cells were treated with various concentration of JQ1 and cell viability was measured using the Alamar Blue reagent 72 h after stimulation.

2.3 The role of BRD4 in the heat shock response

Due to the role of BRD4 in stress related pathways, such as the oxidative stress response, the question arose whether BRD4 is also involved in further stress signalling cascades. Beside the oxidative stress response, the heat shock response is one of the most important inducible protection systems in eukaryotes. In Section 2.2 it was shown that the cellular response to heat stress was significantly enriched ($p = 1.27*10^{-02}$) in the 52 identified BRD4 target genes (Table 3). Based on these results, in the following section, I investigated a potential role of BRD4 in the regulation of the heat shock response.

2.3.1 Influence of BRD4 on the general transcriptional regulation during heat stress

According to Table 3, two very interesting BRD4 target genes are involved in the regulation of heat stress, *MAPK3* and *HDAC6*. Hence, to analyse a possible role of BRD4 during heat shock (HS), BRD4-deficient and control cells were exposed to mild heat stress. The knockdown experiments were performed in WI38 cells using a pool of small hairpin RNAs (siBRD4) that target both isoforms of BRD4. The subsequent exposure to heat was done in a cell culture incubator at 42°C for 4 h. Immediately after HS, cells were harvested and RNA was isolated. The transcriptomes of three independent experiments were analysed using RNA-sequencing. The RNA library was prepared according to the Illumina TrueSeq RNA Sample Preparation Kit protocol. After purification of poly-A-tails containing RNAs using oligo-dT affinity, the transcriptome was analysed on an Illumina HighSeq 2500. The raw reads, obtained from the sequencing, were mapped against the human genome GRCh37/hg19 using BWA version 0.5.9-r16 with default parameters. To investigate gene expression analysis all reads that overlapped with exons by at least one nucleotide were counted and the read counts of a given transcript were divided by its length in kb and the count of all aligned reads of the sample in million, generating RPKM values (reads per kilobase per million mapped reads). The initial alignment and counting of raw reads was performed by Dr. Martin Kerick. To calculate the relative expression value of a given transcript, the RPKM values of BRD4 knockdown and HS-treated samples (siBRD4-HS) or of knockdown control combined with HS samples (siCo-HS) were divided by the RPKM values of the same transcripts of the untreated knockdown control sample (siCo).

First, the knockdown efficiency of *BRD4* was verified in the three replicates. Therefore, the relative expression of *BRD4* mRNA transcripts were extracted out of the RNA-seq data of each experiment and plotted. As pictured in Figure 20A, in all replicates the expression of

BRD4 was efficiently diminished in siBRD4+HS (siBRD4-HS normalized to siCo) cells down to 16 – 40%. Furthermore, the exposure to heat in siCo+HS (siCo-HS normalized to siCo) cells, did not significantly change the *BRD4* mRNA expression level.

Additionally, to ensure a comparable heat stress induction for all replicates, the expression of the major heat shock proteins (HSP) was dissected. The relative gene expression was calculated as mentioned above by dividing the RPKM values of the siBRD4-HS and siCo-HS samples by the RPKM values of the untreated siCo samples. The differential log2 expression changes of each replicate and each sample were plotted in a heat map diagramm (Figure 20B). In blue are shown the expression values of the normalized siCo+HS samples and in red the log2 fold changes of siBRD4+HS. The more intensive the colours are, the stronger was the up-regulation of the given transcript. The comparison of the expression profiles of siCo+HS and of the siBRD4+HS revealed an almost equal induction of all *HSP* mRNAs in siCo+HS as well as in siBRD4+HS experiments. These data confirmed on the one hand the efficiency of the HS treatment and on the other hand indicated no significant influence of BRD4 on the major stress response regulation, represented by the up-regulation of the transcription of HSP. To further analyse if a reduced BRD4 expression, indeed, has no influence on the expression patterns after HS, transcriptome-wide gene expression profiles of siCo+HS as well as of siBRD4+HS cells were performed (Figure 20C). The relative expression of genes with a more than 2-fold up- or down-regulation under HS was analysed. Actually, a depletion of BRD4 under HS (siBRD4+HS) did not influence the global gene expression profile of HS treatment (siCo+HS), depicted by the heat map diagramm. The intensity of the colour correlates with the fold expression change in relation to the siCo samples without HS. Both, the expression profile of the HS cells and the expression profile of HS cells with a simultaneous BRD4 knockdown resemble each other in regard to the number of up-, and down-regulated genes as well as in regard to the expression change values of each transcript.

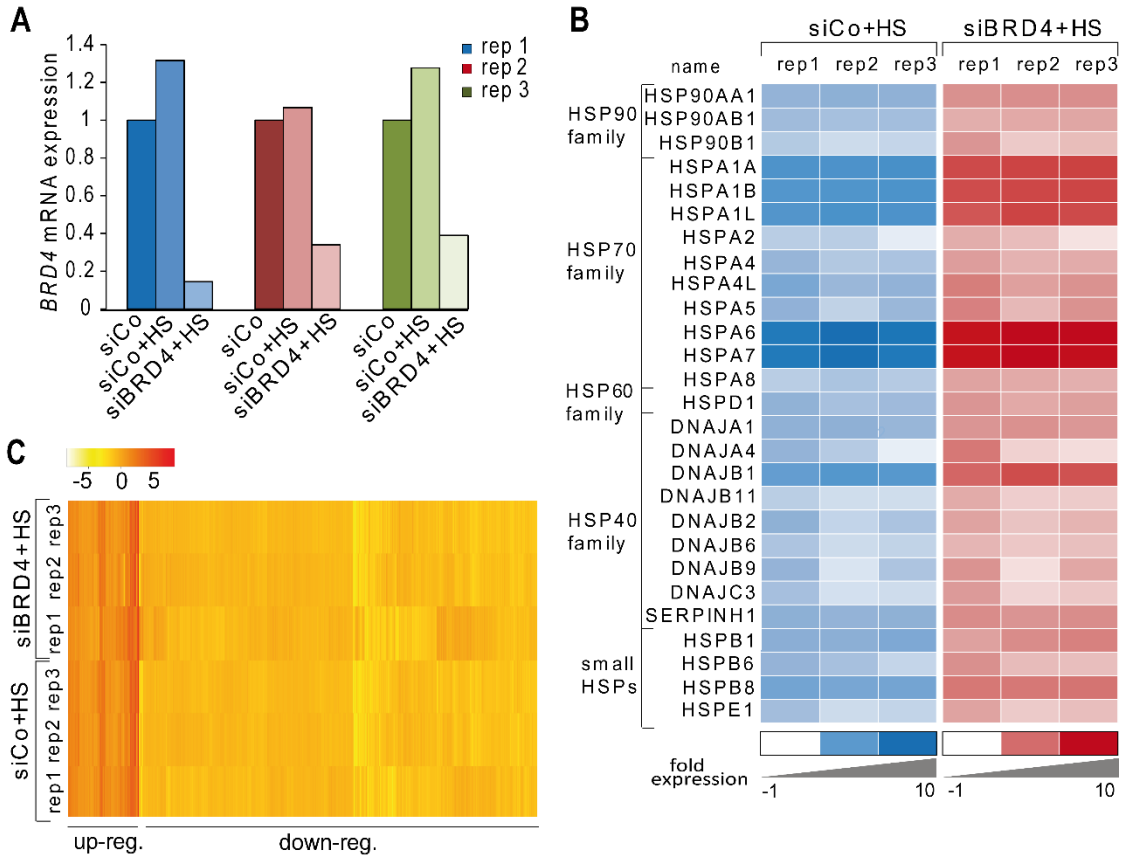

Figure 20 BRD4 depletion in HS cells does not change global gene expression patterns. *BRD4* knockdown was achieved by using the siRNA pool directed against the human BRD4 for 72 h and subsequent HS treatment was performed at 42°C for 4 h. **(A)** ***BRD4 mRNA expression in three mRNA-Seq experiments.*** The relative expression of *BRD4* was calculated by the ratio of the determined RPKM values of siBRD4-HS and the RPKM values of the untreated siCo sample (siBRD4+HS) or by the ratio of the RPKM values of siCo-HS samples and the RPKM values of the untreated siCo sample (siCo+HS). The relative fold change is shown in blue for the first, in red for the second and in green for the third replicate for each condition. **(B)** ***mRNA expression of the major HSP transcripts.*** Gene expression analysis of the RNA transcriptome data of the main heat shock proteins (HSPs) for each replicate in siCo+HS cells (blue) as well as in siBRD4+HS cells (red). HSP were classified into their specific family class. The more intensive the columns are, the stronger was the up-regulation of the corresponding HSP transcript. (Figure taken from Hussong et al. 2015) **(C)** ***mRNA expression of the most significant deregulated transcripts in HS samples.*** Gene expression profiles of transcripts, which showed an expression change of at least 2-fold in all three HS samples. Shown are the relative expression values of siCo+HS as well as siBRD4+HS. Red represents up-regulated transcripts; yellow marks all transcripts that are down-regulated in the respective experiment. (Figure taken from Hussong et al. 2015)

2.3.2 BRD4 regulates splicing of introns during HS

The gene expression profiles of HS and BRD4-deficient cells did not give any indication for an influence of BRD4 on the transcriptional regulation of HS inducible genes. However, besides the transcriptional regulation, pre-mRNA splicing is another important mechanism in the adaptation and survival of stress. Due to evidence of a potential function of BRD4 in the pre-mRNA splicing process in the literature, I investigated, whether BRD4 may take part in the global splicing alterations after HS.

Therefore, the RNA-seq derived transcriptome data were used to estimate changes in splicing patterns. The following bioinformatics analyses on alternative splicing have been performed by Dr. Martin Kerick, but will be presented here for a better understanding of validations and follow-up experiments. For this, aligned reads were extracted which were located at the 5`, 3' splice site (ss)-, at exon- or intron region. Therefore, the Ensembl database version 69 was used to calculate exon intron coordinates. In detail: All reads that overlapped with exon coordinates in the Ensembl annotation were used to calculate the exon expression level. The intron expression was computed for all introns that had a minimal size of 100 bp and that did not overlap with any other Ensembl database entity, such as microRNAs or non-coding RNAs. Constitutive exons were derived from exons that were present in all transcripts of a gene, while exclusive exons had to be associated to only one transcript without overlapping to any other Ensembl entity. Finally, alternative 5' and 3' ss, respectively, were calculated by subtracting constitutive exon regions as well as exclusive exon intervals from each remaining exon sequence.

To calculate differential splicing alterations the "percent spliced in" (PSI) value according to Wang et al. (2008) was used [291]. It estimates the inclusion and exclusion of a specific exon, intron or alternative 3' or 5' ss by dividing the sum of the reads on the region of interest (i.e. exon or intron) by the sum of reads on all constitutive exons of its associated complete transcript. In Box 1A the calculation of the PSI value is depicted schematically. Theoretically, the maximal PSI value of 1 represents an inclusion of this region in all transcripts. In contrast, the other extreme, a value of 0 means that the region of interest is completely skipped.

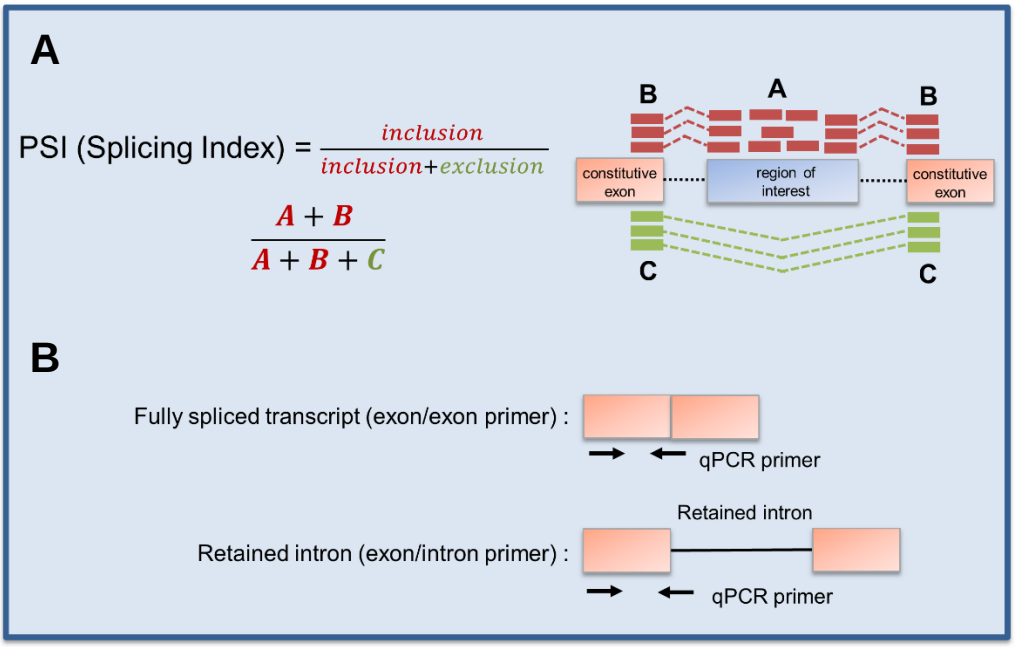

Box 1 Schematic representation of the detection of alternative splicing events in (A*) RNA Seq data analysis using the PSI value according to Wang et al 2008*. "*A"* represents the number of reads that map to the region of interest. "*B"* indicates the number of reads that map to the junctions between the constitutive exons and the region of interest. "*C"* displays the number of split reads that map on both constitutive exons. Red bars represents the reads that are counted for the inclusion level, green highlighted those reads that represents the exclusion level. **(B) *Primers used for splicing validations***. qPCR experiments were performed by using exon/exon primers to detect the fully spliced transcript and exon/intron primer to detect the transcript with the retained intron. The values generated by the exon/intron primers were normalized to the values of the exon/exon primer.

In this study, the PSI values were calculated by dividing the RPKM value of the feature of interest (e.g. constitutive exon or intron) by the RPKM value of its associated gene. The difference (ΔPSI values) were obtained analogous to the calculation of fold expression values, described above, by dividing the PSI values of two samples in log space. The ΔPSI for constitutive exons, exclusive exons, alternative 5` and 3`ss and intron retention (see Figure 5) was calculated for siBRD4 (PSI(siBRD4) vs PSI(siCo)), for siCo+HS (PSI (siCo-HS) vs PSI(siCo)) and for siBRD4+HS (PSI(siBRD4-HS) vs PSI(siCo)). Figure 21A – C demonstrate the global splicing analysis for the first experiment that showed the best HS induction as well as the strongest BRD4 knockdown.

First, the differential splicing pattern of BRD4-depleted cells was analysed. The box plot analyses, summarize the ΔPSI values of each transcript for each splicing event. The mean

of the ΔPSI values of the respective splicing event is represented by a black line in each box plot. As shown in Figure 21A, the depletion of BRD4 alone did not show significant changes of any investigated splicing event. The averaged ΔPSI values were under 0.1 in each splicing event. However, after HS, similar to the data presented by Shalgi et al., a significant increase in intron retention ($p = 7.71 \times 10^{-265}$, mean ΔPSI(siCo+HS) = 0.18) was found (Figure 21B, orange box plots), whereas in all other splicing events, no significant change of the mean ΔPSI value was observed.

Interestingly, a simultaneous BRD4 depletion in heat treated cells further enhanced the observed effect on intron retention but did not alter any other splicing events (Figure 21B, red box plots). The mean ΔPSI value of 0.18 in HS cells was further increased up to 0.25 in HS cells with an additional BRD4 knockdown (siBRD4+HS). These results were also obtained and validated in the other two replicates as shown in the following analyses.

The number of retained introns was calculated for each replicate. Significant intron retention (IR) was detected using the following criteria: (1) RPKM gene expression value of the corresponding transcripts had to be over 0.5; (2) RPKM expression value of the intron in the control sample (siCo) under 0.13; (3) ΔPSI value comparing treatment vs control (siCo) of more than 2-fold and (3) a minimum of 10 reads in the intron of the non-control samples. The number of the introns that cut these criteria were calculated in each replicate and plotted. The box plot analysis in Figure 21D demonstrates that the number of IR in siBRD4+HS was elevated (p=0.07) compared to siCo+HS. In HS samples, 6,915 intron retentions were identified, whereas the simultaneous BRD4 knockdown revealed 8,062 retained introns in average.

To extract IR that are affected by BRD4 depletion under HS conditions, for each replicate and each intron the ΔΔPSI value (ΔPSI siBRD4+HS - ΔPSI siCo+HS) was determined. Significant changes (ΔΔPSI >1.5) in at least two experiments were found for 965 introns (Figure 21E) accounting for 824 genes (Supplement Table S 4). Nearly all introns with IR under siCo+HS and siBRD4+HS are not annotated introns in Ensembl. When analysing the gene expression of the IR introns only 28 showed a down-regulation below 1.5-fold and only 1 gene was up-regulated more than 1.5-fold. The expression of the remaining 794 genes did not change significantly (Figure 21F). This supports a direct effect of BRD4 on the splicing machinery without affecting the transcriptional process.

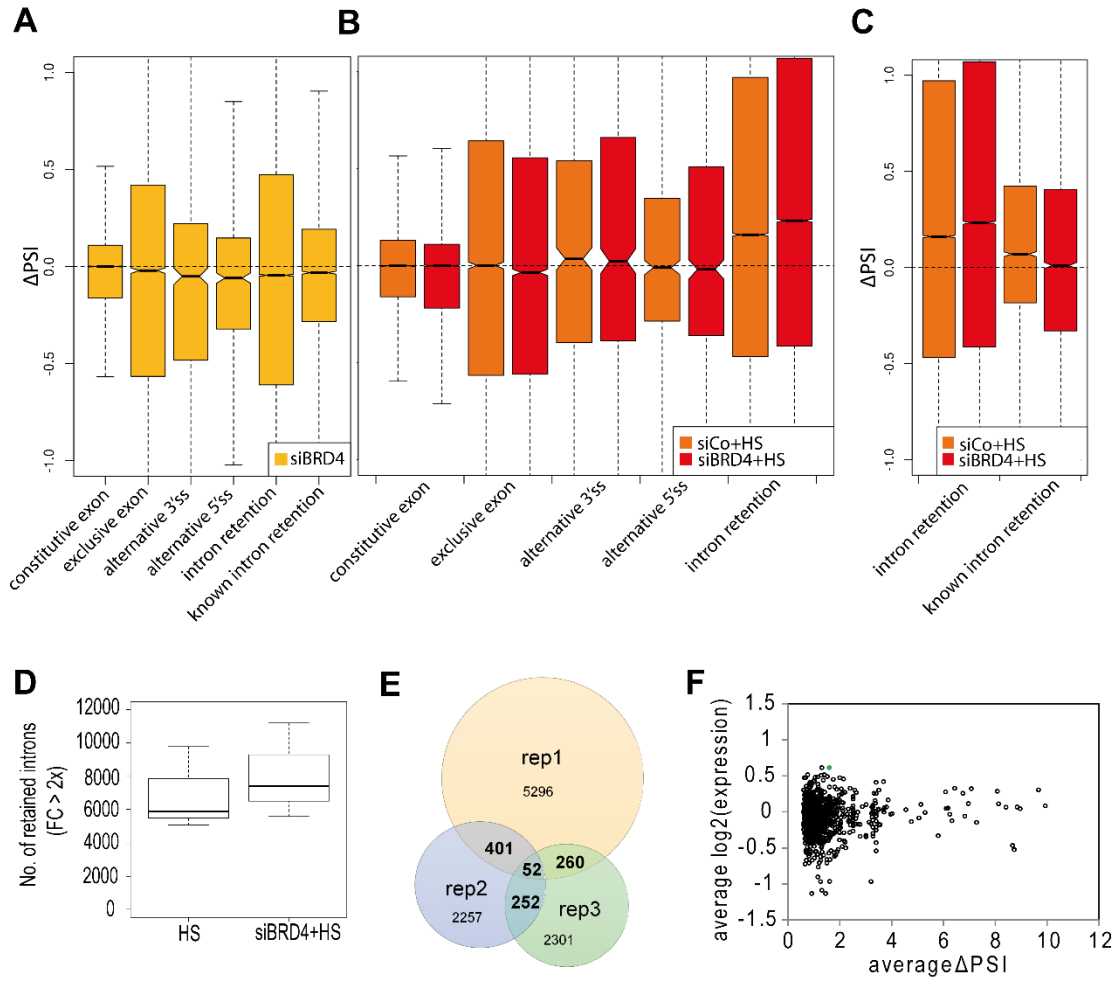

Figure 21 BRD4 knockdown increases the HS mediated splicing defect. (A, B) ***Bioinformatics analyses of alternative splicing events*** in **(A)** siBRD4 treated cells and **(B)** in HS treated cells with (siBRD4+HS) or without (siCo+HS) BRD4 knockdown. Cells were exposed to 42°C for 4 h. Inclusion and exclusion of constitutive and exclusive exons and introns as well as alternative 3' and 5' splice sites were calculated using the "percent spliced in" value corresponding to Wang et. al. 2008. Figures are provided by Dr. Martin Kerick. **(C)** ***Comparison between known retained introns and annotated retained introns in siBRD4+HS and siCo+HS cells.*** Known retained introns represent all introns that are annotated in the Ensembl database as known retained intron. Unknown intron retentions refer to not described before as retained introns. Figures are provided by Dr. Martin Kerick. **(D)** ***Box plot of the average counts of intron retention in siCo+HS cells and in siBRD4+HS cells over all three replicates.*** Introns that show an increase of retention more than 2-fold compared to control cells without knockdown and HS were counted. **(E)** ***Venn diagram depicting the overlap between the identified intron retentions in all three siBRD4+HS replicates.*** **(F)** ***Correlation of intron retention with the gene expression of the corresponding genes.*** Plotted are all transcripts that show an increase of intron retention in at least two replicates of siBRD4+HS in comparison to HS alone. (Figures taken from Hussong et al. 2015)

To get an overview of a potential mechanism of the splicing inhibited genes after siBRD4+HS, I performed pathway analyses of the 824 genes that have at least one IR intron in siBRD4+HS cells in comparison to siCo+HS. I used the Ingenuity Pathway Analysis software and found predominantly cancer-relevant pathways, such as molecular mechanism of cancer ($p = 5.46*10^{-3}$), ERK/MAPK signalling ($p = 9.79*10^{-3}$), FAK Signalling ($p = 2.56*10^{-2}$) and endoplasmatic reticulum stress pathway ($3.1*10^{-2}$) (Table 6) enriched, suggesting a disease-relevant role of the splicing inhibition of BRD4. The molecules of the identified pathways that were found in our data set are listed in Supplement Table S 5.

Table 6 Pathway analysis of the 824 genes that have at least one IR intron in BRD4-deficient and heat treated cells in comparison to HS treated alone. Canonical pathways are listed according to their p-value and the ratio of list genes.

Ingenuity Canonical Pathways	p-value[a]	Ratio[b]
Sonic Hedgehog Signalling	$2.82*10^{-3}$	$1{,}67*10^{-1}$
TNFR1 Signalling	$5.50*10^{-3}$	$1{,}22*10^{-1}$
Molecular Mechanisms of Cancer	$5.50*10^{-3}$	$6{,}03*10^{-2}$
ERK/MAPK Signalling	$9.77*10^{-3}$	$6{,}95*10^{-2}$
Protein Kinase A Signalling	$1.91*10^{-2}$	$5{,}44*10^{-2}$
FAK Signalling	$2.57*10^{-2}$	$8{,}05*10^{-2}$
Adipogenesis pathway	$2.57*10^{-2}$	$7{,}09*10^{-2}$
Nucleotide Excision Repair Pathway	$2.82*10^{-2}$	$1{,}14*10^{-2}$
Endoplasmic Reticulum Stress Pathway	$3.09*10^{-2}$	$1{,}43*10^{-2}$

[a]the p-value is calculated using the right-tailed Fisher Exact test. [b]number of molecules in a given pathway that meet cut criteria, divided by total number of molecules provided by the software that make up that pathway.

To rule out that technical factors such as genomic DNA contamination due to an insufficient DNA digest, for example, would interfere the analyses the relation between inter- and intragenic regions was dissected. A contamination with genomic DNA would be represented by a higher or almost equal number of intergenic regions compared to intronic regions. Therefore, the aligned reads on exons, introns as well as intergenic regions were counted in all experiments. The averaged read density in the intergenic regions (0.04

RPKM) was nearly 2-fold lower than in introns (0.08 RPKM) and even almost 200-fold lower than the averaged read density found in exons (8.0 RPKM), highlighting the quality of sample preparation (Figure 22A).

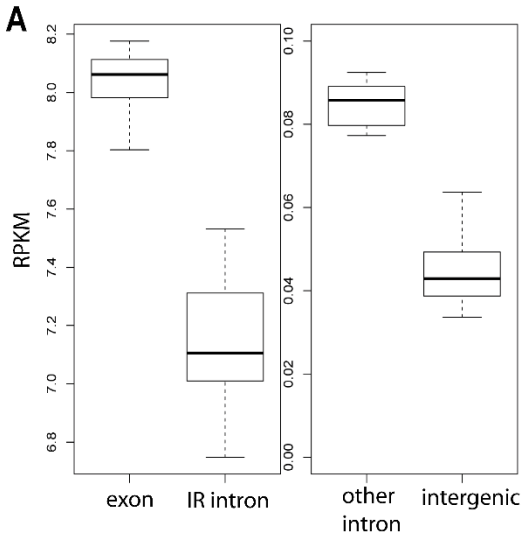

B

Comparison	Pearson: 5'vsCenter	Pearson: 3'vsCenter
siCo+HS vs siCo - rep1	0.38	0.41
siCo+HS vs siCo - rep2	0.39	0.43
siCo+HS vs siCo - rep3	0.37	0.41
siBRD4+HS vs siCo - rep1	0.38	0.45
siBRD4+HS vs siCo - rep2	0.38	0.43
siBRD4+HS vs siCo - rep3	0.39	0.44

Figure 22 Quality control of the splicing calculation (A) ***Average RPKM values of all aligned reads on exons, introns (IR introns) and (other intron) as well as intergenic regions over all samples.*** IR introns are the introns that were identified as retained introns under all conditions. Other introns represent the intronic background noise of introns that were found in only one experiment. (Figure taken from Hussong et al. 2015) **(B)** Comparison and validation of the intron-exon-junction method and the Introns-only-method. Pearson correlation of ΔPSI ratios measured from intron-exon-junction spanning reads with ratios calculated from intron-only-intervals for all indicated comparisons.

Furthermore, to exclude that the increased intron expression results from spliced lariats in the nucleus, ΔPSI values of all introns were correlated with ΔPSI of the corresponding 5' exon/intron as well as 3' exon/intron junctions. Reads on these junctions were only detectable if retained introns were measured. Spliced lariats do not harbour such an exon/intron junction (for detail see section 1.3.1). A positive correlation between the expression of the putative retained intron and the expression of the exon/intron junction indicates the detection of a retained intron. The correlation was calculated in all experiments (siCo+HS and siBRD4+HS) by Dr. Martin Kerick and revealed a significant averaged correlation of 0.37 for 5' exon/intron junction and 0.42 for 3' exon/intron junction, respectively. This positive correlation confirmed the detection of unspliced transcripts rather than lariats (Figure 22B).

2.3.3 Validation of Splicing inhibited genes

To validate the identified retained introns as well as perfectly spliced introns qPCR experiments were used to analyse the splicing events in four additional biological replicates. The introns were classified into three groups according to their intron specific expression pattern under the different conditions. The first group contained all introns that are perfectly spliced under all conditions, meaning, no sequencing reads detectable in the intergenic regions (i.e. *HMOX1*, Figure 23A). The cut-off criteria for the 1st group were: (1) RPKM gene expression value of the corresponding transcripts had to be over 0.5 and (2) RPKM expression value of the intron in all samples under 0.13. In the second group all introns with a retained intron in siCo+HS are found, irrespectively of their expression pattern in siBRD4+HS (i.e. *BAG3*, Figure 23A). In this case all introns are selected that cut the following criteria: (1) RPKM gene expression value of the corresponding transcripts had to be over 0.5; (2) RPKM expression value of the intron in the control sample (siCo) under 0.13; (3) ΔPSI value comparing PSI(siCo-HS) vs PSI(siCo) of more than 1.5-fold and (3) a minimum of 10 reads in the intron of the non-control sample. The last group included introns that showed an increased expression in BRD4-deficient cells following HS treatment compared to HS treatment alone. In this case, more reads in the intronic regions were mapped in siBRD4+HS compared to siCo+HS. The cut-off criteria, in this case, were: (1) RPKM gene expression value of the corresponding transcripts had to be over 0.5; (2) RPKM expression value of the intron in the control sample (siCo) under 0.13; (3) ΔPSI value comparing PSI(siBRD4-HS) vs PSI(siCo) of more than 1.5-fold in at least 2 replicates, (3) a minimum of 10 reads in the intron of the non-control sample and (4) ΔΔPSI value comparing ΔPSI(siBRD4+HS) vs ΔPSI(siCo+HS) of more than 1.5-fold in at least 2 replicates. As example, the *ATF3* gene is shown in Figure 23A.

For each group at least 5 introns (5 introns for 1st, 6 for 2nd and 12 for 3rd group) were selected and analysed using qPCR with primers recognizing the exon/intron junction and as control the fully spliced transcript (exon/exon primer) as shown in Box 1B. The validations revealed a good correlation between the sequencing data and the qPCR experiments. Retained introns under HS conditions showed, comparable to the sequencing data, a significant splicing inhibition ($p = 3.7*10^{-04}$) with a median increase of IR of more than 3-fold compared to the perfectly spliced transcripts (Figure 23B) in siCo+HS cells. Furthermore, in BRD4-deficient and heat treated cells the retention was significantly increased ($p = 0.006$) with an average increase of 1.5-fold compared to the cells only exposed to HS for introns of the 3rd group (Figure 23C).

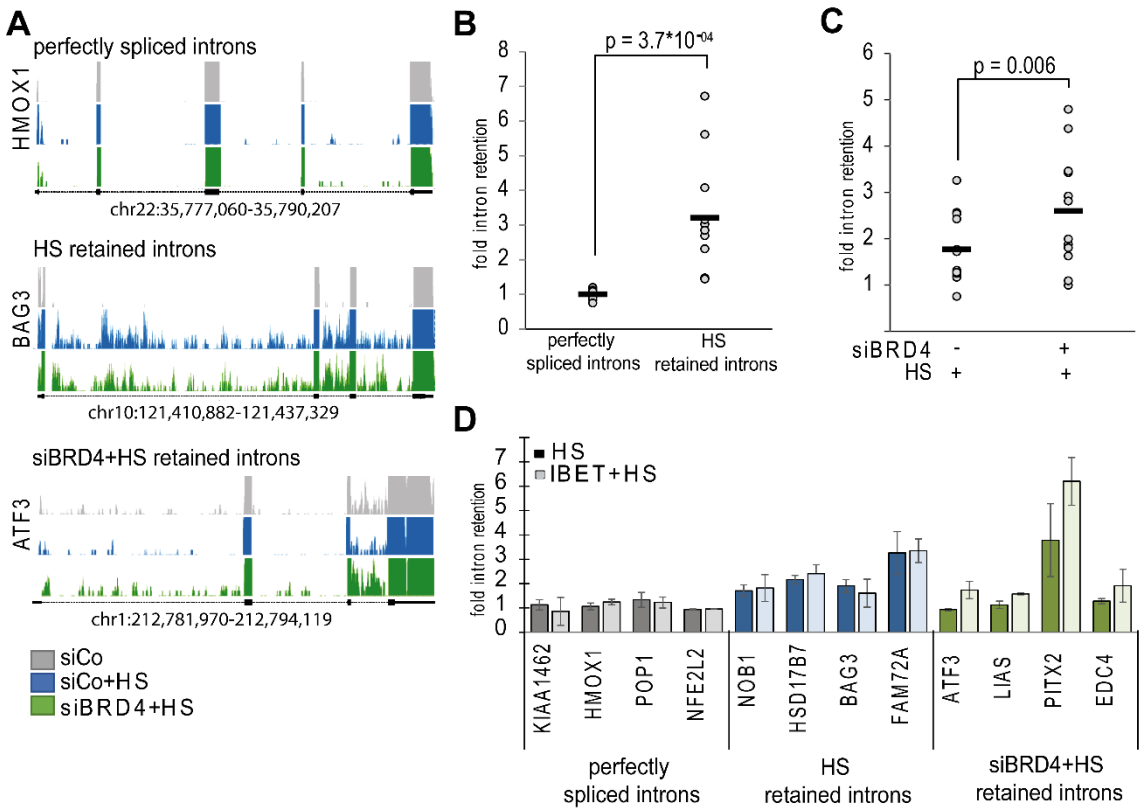

Figure 23 Validation of intron retention. (A) ***Visualization in the UCSC browser of the three groups of transcripts used for validation.*** Perfectly spliced transcripts (*HMOX1*), transcripts with splicing inhibition following HS (*BAG3*) and transcripts with an increased splicing inhibition in siBRD4+HS (*ATF3*) are shown. Exons are marked with a black squares, introns with a black line. **(B, C)** ***Validation of IR using qPCRs in four additional biological replicates.*** To measure the fold intron retention primer were used that detect the exon/intron junction and as control the corresponding exon/exon junction of the same transcript (see Box 1). The values of the exon/intron primers were put into relation to the expression values generated by the exon/exon primers. (p-values are calculated according to two-tailed, paired t-tests). **(B)** ***Validation of introns that show an increased expression following HS***, independent of BRD4 expression (2nd group) compared to the perfectly spliced introns (1st group) in siCo+HS samples. **(C)** ***Expression of introns that are influenced by BRD4 knockdown*** (3rd group) in cells treated either with siBRD4 or siCo following HS**. (D)** ***Intron expression analysis in cells treated with I-BET151 and HS or with HS alone.*** Validation of IR using qPCR in cells treated with 1 µM of the BET inhibitor I-BET 151 for 72 h and subsequently exposed to HS at 42°C for 4 h. For each condition, the expression of introns was calculated in three independent experiments. (Figures taken from Hussong et al. 2015)

Indeed, an elevated intron expression (fold intron inclusion >1.2) of 10 out of the 12 tested introns were validated. Similar results were obtained using the BRD4 inhibitor I-BET151. I-BET151 blocks similar to JQ1 the bromodomains, resulting in a displacement of the BET proteins from chromatin. The treatment of WI38 cells with 1 µM I-BET151 for 72 h increased similar to BRD4 knockdown the HS mediated IR of introns part of the 3rd group, but had no influence on the intron expression profile of introns found in group 1 and 2, respectively (Figure 23D).

2.3.4 The general splicing machinery is unaffected by BRD4 knockdown after HS

BRD4 knockdown as well as BRD4 inhibition after HS result in global splicing defects, represented by an increase of IR. The question arises, how does BRD4 influence or regulate the splicing process during HS. Splicing, in general, is catalysed by the spliceosome, a large multi-component ribonucleoprotein (RNP) complex which accounts for more than 99% of all splicing events. A deregulation of core components of the spliceosome can alter splicing patterns and is associated with the development of cancer [292-295]. Therefore, I wondered if the increased splicing inhibition, described above, is due to expression alterations of splicing factors that are essential for the splicing process. Therefore, the expression data of known splicing regulating genes were extracted out of the RNA-seq data and visualized. Indeed, several splicing regulating proteins are differentially regulated after HS treatment, such as *SRSF2* (fold change = 0.56), *SRSF5* (fold change = 0.42) and *SRSF6* (fold change = 0.47). However, a reduction of BRD4 expression did not further enhance this effect (Figure 24A), making a differential expression pattern of splicing factors as reason for the observed splicing defects unlikely.

Another possible mechanism, how BRD4 may regulate splicing could be directly over the splicing factor SRSF2 (also known as SC35). Studies in human HeLa cells showed that BRD4 co-localizes with SC35 upon treatment with the CDK9-inhibitor flavopiridol. Furthermore, SC35 utilizes BRD4 to enhance the recruitment of p-TEFb to Pol II. Based on these observations, I asked whether HS and/or BRD4 inhibition may lead to a dislocation of SC35 from the so called splicing speckles resulting in a general splicing defect. Using immunofluorescence studies, the localization of BRD4 and SC35 were tested in unstressed as well as heat treated cells. The analyses revealed that in unstressed as well as in cells treated for 1 h at 44°C neither the localization of SC35 in the nuclear splicing speckles nor the co-localization with BRD4 was altered (Figure 24B).

Furthermore, the treatment with 0.2 and 2 µM of the BRD4 inhibitor I-BET151 for 24 h in HS stimulated HeLa cells had no influence on the nuclear distribution of SC35 (Figure 24C). Based on these data, it is unlikely that the observed splicing defects are the consequence of a transcriptional deregulation of the general splicing machinery.

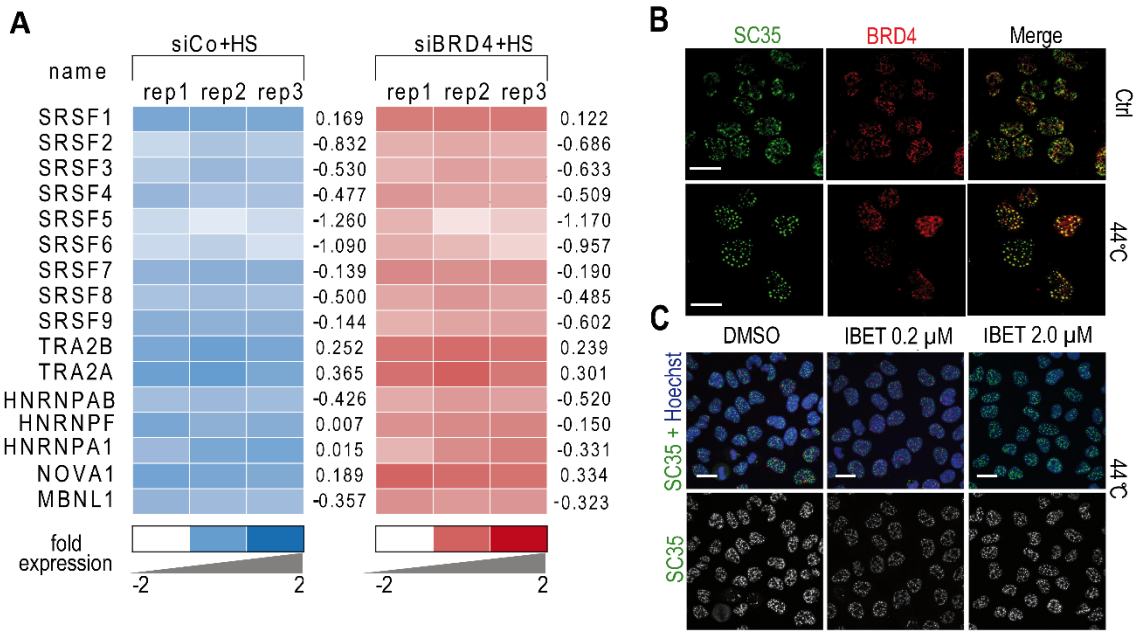

Figure 24 The general splicing machinery is unaffected by BRD4 knockdown after HS. **(A)** ***Gene expression analysis of the RNA transcriptome data of the main proteins involved in spliceosome formation and splicing regulation.*** Expression data for each replicate in siCo+HS (blue) as well as in siBRD4+HS (red) were extracted out of the RNA-Seq data. The intensity of the colour correlates with the fold expression change in relation to the siCo samples without HS. The averaged log2 fold expression is shown on the right side of each condition. **(B)** ***Co-localisation of BRD4 and SC35.*** HeLa cells were treated with 500 nM flavopiridol for 2 h and subsequently exposed to HS at 44°C for 1 h or left untreated, fixed and stained with antibodies directed against BRD4 (red) and SC35 (green). **(C)** ***Cellular localisation of SC25 after I-BET151 and HS treatment.*** HeLa cells were incubated with the indicated concentrations of the BET inhibitor I-BET151 for 24 h. Afterwards, cells were exposed to HS at 44°C for 1 h, fixed and stained with antibodies directed against BRD4 and SC35. Nuclei were stained with Hoechst. (Figures taken from Hussong et al. 2015)

2.3.5 BRD4 is recruited to nSB after HS in an HSF1 dependent manner

The mechanisms underlying co-transcriptional splicing and post-transcriptional splicing inhibition under heat stress is mechanistically not well understood. Upon thermal stress, a subset of hnRNP and various other splicing factors, except SC35, are recruited to specific nuclear sites which are known as nuclear stress bodies or nSB. It is supposed, that this accumulation of splicing ensures a functional splicing of vital genes. Hence, the question came up if BRD4 is recruited to these sub-nuclear structures under HS and thereby regulates the still productive co-transcriptional splicing under HS.

nSB are mainly marked by the heat shock factors HSF1 and HSF2. To investigate the nuclear distribution of BRD4 after HS, human HeLa cells were treated either with mild (42°C) or severe (44°C) HS for 1 h until harvesting to ensure a sufficient induction of nSB. The cells were stained, on the one hand with an antibody against HSF1 to visualize the nSB and on the other hand with an antibody against the endogenous BRD4. The nuclei were stained with Hoechst. Both HS conditions, 42°C as well as 44°C induced the generation of nSB, represented by the generation of distinct HSF1 foci. Indeed, a co-localization of HSF1 and BRD4 could also be observed under both HS conditions, however, the co-localization drastically increased after exposure to 44°C (Figure 25A).

Similar results were obtained by overexpressing BRD4 and HSF1 or BRD4 and HSF2, respectively. In both cases, HeLa cells were transfected with the overexpressing plasmids pTL-FLAG-BRD4 and pTL-HA-HSF1 or pTL-FLAG-BRD4 and pTL-HA-HSF2. 48 h post-transfection, cells were exposed to 44°C for 1 h before they were fixed and stained with antibodies directed against the corresponding protein-tags (FLAG-tag and HA-tag). Nuclei were stained with Hoechst. In heat treated HeLa cells the overexpressed BRD4 formed distinct sub-nuclear foci where it co-localized with the transiently overexpressed HSF1 and HSF2 proteins, respectively (Figure 25B). This co-localisation further supports the translocation of BRD4 to nSB after HS. These co-localisation studies were performed by Dr. Christian Kähler in the group of PD. Dr. Sylvia Krobitsch.

A co-localization in the same nuclear structure suggests also a physical interaction. To investigate a possible association between BRD4 and HSF1, a co-immunoprecipitation in WI38 cells was performed. HSF1 was transiently overexpressed for 48 h to increase the co-localisation rate of both proteins. Subsequently, these cells were exposed to heat for 4 h (HS) or left untreated as control. The precipitation was performed in both samples (untreated and HS) with an antibody against the endogenous BRD4 protein. As control, to exclude background signals, a control-IP with IgG was performed in both samples.

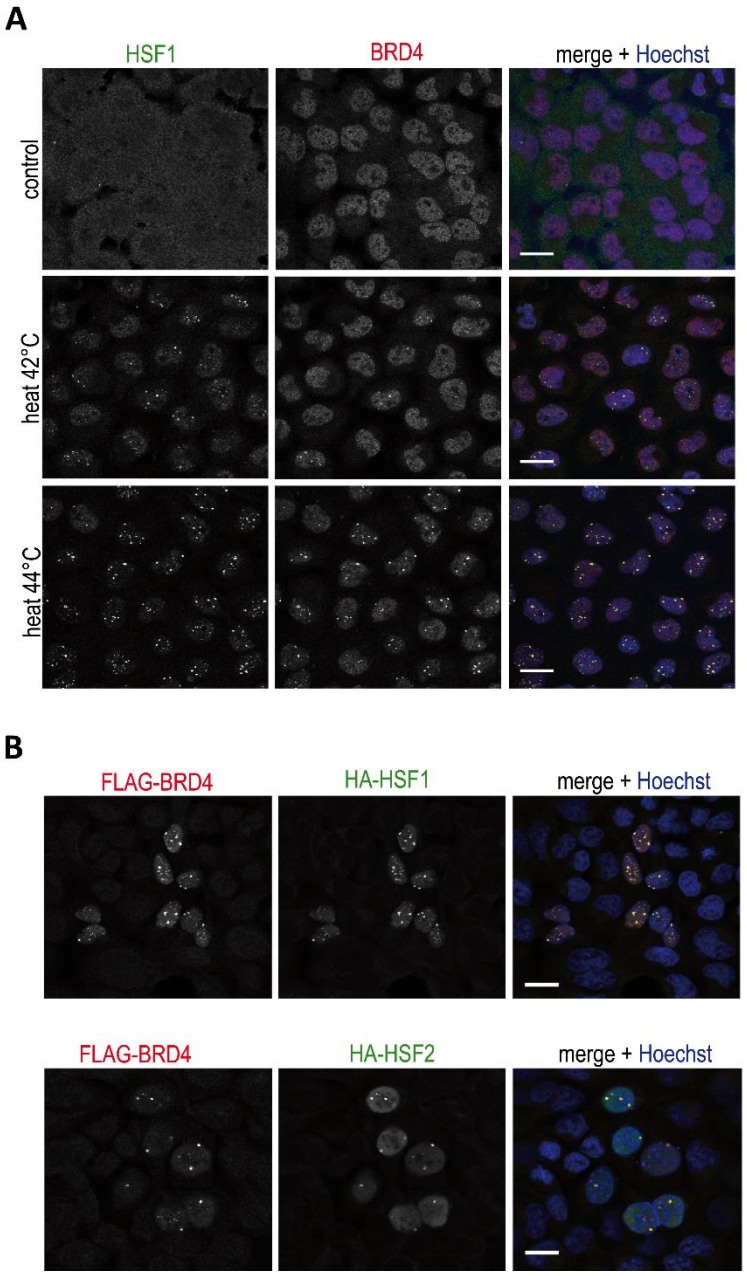

Figure 25 BRD4 is recruited to nSB following HS. (A) ***BRD4 co-localizes with HSF1 in nSB under HS.*** HeLa cells were exposed to HS at 42°C or 44°C for 1 h or left untreated (control) and processed for confocal microscopy to analyse the localization of BRD4 and HSF1. Nuclei were stained with Hoechst. Scale bars represent 20 µm. **(B)** ***Co-localisation of overexpressed BRD4, HSF1 and HSF2 in stressed cells.*** HeLa cells were co-transfected with the expression plasmids pTL-FLAG-BRD4 and pTL-HA-HSF1 or pTL-HA-HSF2 to overexpress the long isoform of human BRD4 together with HSF1 or HSF2, respectively. 48 h post transfection, cells were exposed to HS at 44°C for 1 h, fixed and stained with antibodies directed against the FLAG-tag and the HA-tag. Nuclei were stained with Hoechst. Scale bars represent 20 µm. The analyses were performed by Dr. Christian Kähler. (Figures taken from Hussong et al. 2015)

The Western blot analysis showed a specific pull-down of the overexpressed HSF1 protein in the BRD4 precipitated lane and none in the IgG control lane (Figure 26A), indicating an interaction between BRD4 and HSF1. An immunoprecipitation of HSF1 in BRD4 overexpressing cells confirmed these results (Figure 26B).

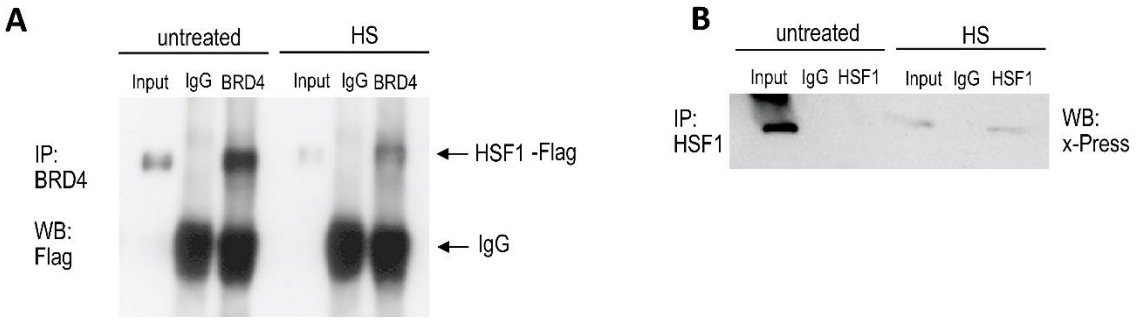

Figure 26 BRD4 interacts with HSF1 under HS. (A) ***WI38 cells were transfected with pTL-FLAG-HSF1 and either treated at 42°C for 4 h or left at 37°C.*** Co-immunoprecipitation was performed using an antibody against the endogenous BRD4 and analysed on Western Blot using an antibody against the FLAG-tag to detect HSF1. **(B)** ***HeLa cells were transfected with pcDNA4C-BRD4-FL and either treated at 42°C for 4 h or left at 37°C.*** Co-immunoprecipitation was performed using an antibody against the endogenous HSF1 protein and analysed on Western Blot using an antibody against the X-Press-tag to detect BRD4. (Figures taken from Hussong et al. 2015)

HeLa cells were transfected with an BRD4 overexpressing plasmid and were exposed 48 h post-transfection to heat at 42° for 4 h. This time, the precipitation was performed by using an antibody directed against the endogenous HSF1 protein. As negative control an immunoprecipitation with IgG was performed as well. The Western blot was developed using an antibody that detects the X-press-tag of the overexpressed BRD4 protein. Interestingly, the precipitation of HSF1 showed an interaction with the overexpressed BRD4 only in heat treated cells even though the overexpression of BRD4 in the untreated cells was stronger than in the HS cells. That in the first experiment a positive interaction was visible without heat exposure, can be explained by the fact that the overexpression of HSF1 per se formed nSB in untreated cells, whereas the sole overexpression of BRD4 may be not sufficient to generate these structures without stress.

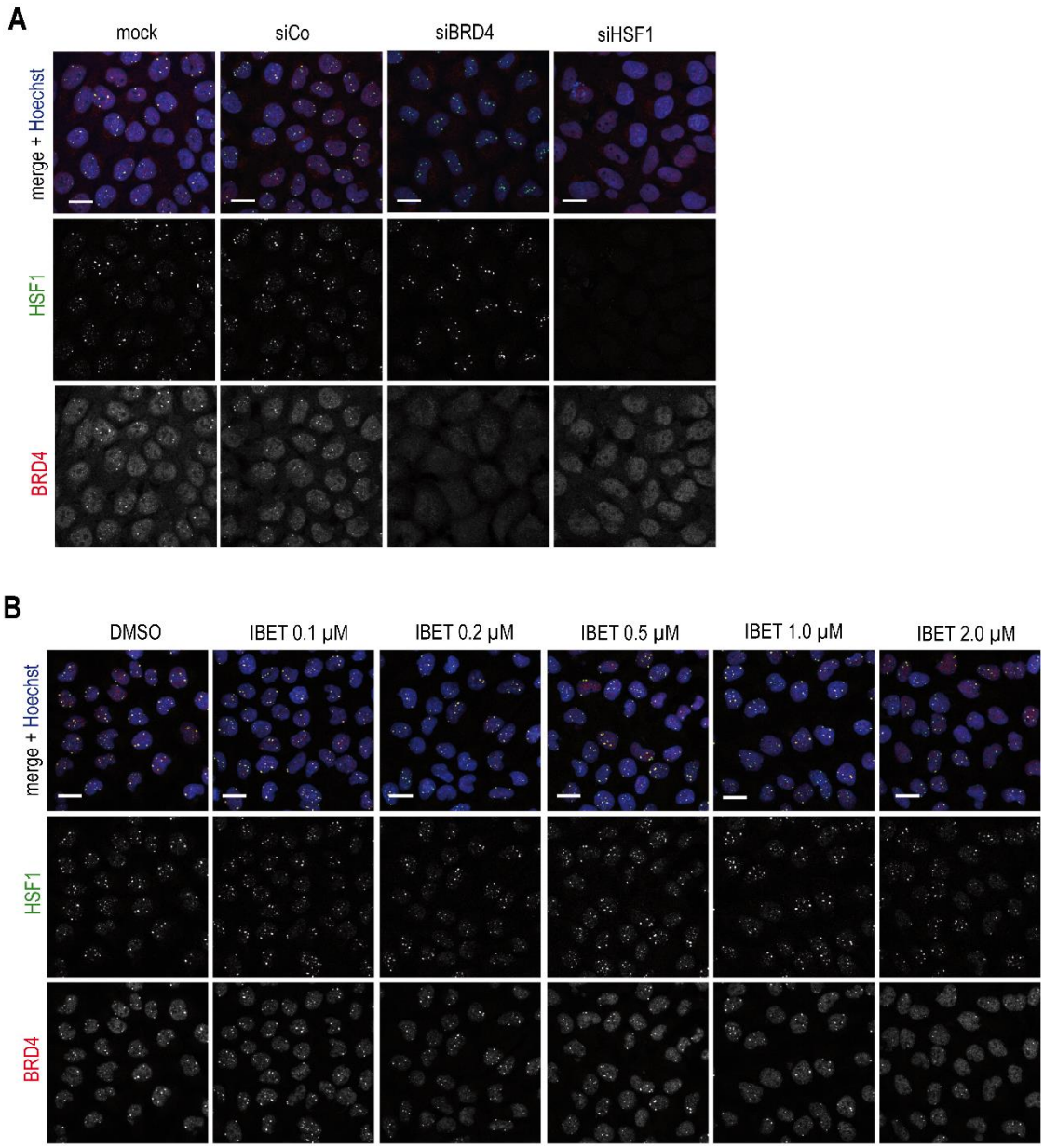

Figure 27 BRD4 recruitment is accomplished in an HSF1 dependent manner. (A) ***Formation of nSB in BRD4- and HSF1-deficient cells.*** HeLa cells were transfected with siRNAs against BRD4 or HSF1 transcripts, or non-targeting control siRNA (siCo). 72 h post transfection cells were exposed to HS at 44°C for 1 h, fixed and processed for immunostaining of BRD4 and HSF1. **(B)** ***Formation of nSB in I-BET151 treated cells.*** HeLa cells were incubated with the indicated concentrations of the BET inhibitor I-BET151 for 24 h. Subsequently, cells were exposed to HS 44°C for 1 h, fixed and stained with antibodies directed against BRD4 and HSF1. Nuclei were stained with Hoechst. Scale bars represent 20 µm. The immunofluorescence analyses were performed by Dr. Christian Kähler. (Figures taken from Hussong et al. 2015)

Additionally, these results suggest that the interaction between HSF1 and BRD4 (by HS or overexpression) could be essential for the recruitment of BRD4 to nSB. To explore this hypothesis, BRD4 knockdown (siBRD4), HSF1 knockdown (siHSF1) and control (siCo) cells were treated for 1 h at 44°C and the localization of HSF1 and BRD4 in the cell was analysed. A diminished BRD4 expression neither influenced the formation of nSB nor the localization of HSF1. In contrast, a reduced HSF1 expression abolished the formation of nSB and the recruitment of BRD4 to these structures (Figure 27A). Similar results were observed in HS cells treated with the BRD4 inhibitor I-BET151. HeLa cells were treated with 0.1, 0.2, 0.5, 1.0, and 2.0 µM I-BET151 for 24 h before they were exposed to heat at 44°C for 1 h. Indeed, the treatment with I-BET151 had no influence on the formation of the nSB itself, but reduced the formation of BRD4 containing nSB. (Figure 27B).

Using an automated microscopy approach based on a Cellomics ArrayScan VTI high-content screening platform, performed by Dr. Jörg Isensee, the number of HSF1 and BRD4 positive foci in I-BET151 treated and control cells upon HS, were measured. HeLa cells were treated again with varying concentration of I-BET151, as indicated, and were subjected to HS at 44°C for 1 h. Cells were fixed and stained with antibodies directed against BRD4 and HSF1. The nuclei were stained with DAPI. For each condition, BRD4 as well as HSF1 foci in 5,000 cells were counted in at least 3 replicates. As seen for the BRD4 knockdown approach the inhibition of BRD4 had no effect on the number of HSF1 positive foci. However, the I-BET151 treatment decreased the number of BRD4 positive foci compared to the DMSO control in a dose dependent manner. With increased concentrations of inhibitor, the number of BRD4 positive foci decreased of more than 50% (Figure 28A).

Furthermore, the analyses showed that BRD4 is only translocated in every second nSB demonstrated by a 50% reduced number of BRD4 positive foci per cell compared to HSF1 positive foci. Similar results were also detected for BRD4 inhibition using JQ1, another well-established BET inhibitor. HeLa cells were treated with varying concentration of JQ1, as indicated, and were subjected to HS at 44°C for 1 h. The numbers of BRD4 positive foci under HS were reduced down to 50% in cells treated with 500 nM JQ1 compared to the DMSO treated control (Figure 28B). These data suggest a HSF1 dependent recruitment of BRD4 to nSB under HS conditions.

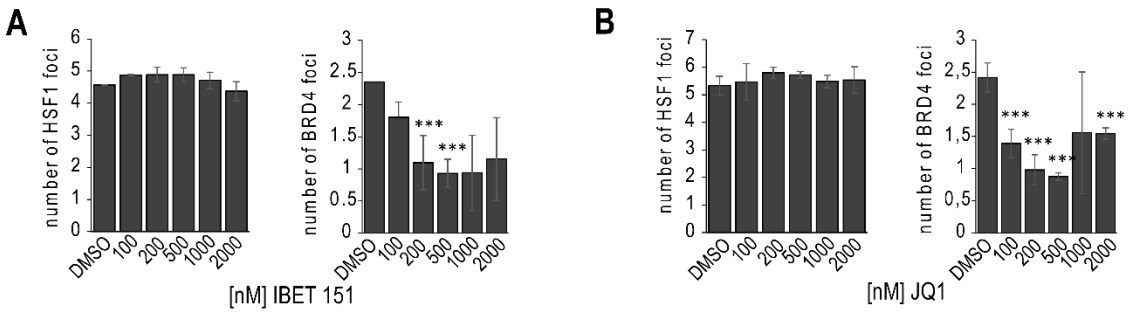

Figure 28 Quantitative high-content microscopy analysis of BRD4 and HSF1 foci in nSB. (A) ***HeLa cells were exposed to 44°C for 1 h with prior treatment of 100, 200, 500, 1000 and 2000 nM I-BET151 for 24 h.*** Cells were fixed and stained with antibodies directed against BRD4 and HSF1. Number of HSF1 as well as BRD4 foci were measured using the Cellomics ArrayScan VTI high-content screening platform and plotted. **(B)** ***HeLa cells were exposed to 44°C for 1 h with prior treatment of 100, 200, 500, 1000 and 2000 nM JQ1 for 24 h***. Cells were fixed and stained with antibodies directed against BRD4 and HSF1. Number of HSF1 as well as BRD4 foci were measured using the Cellomics ArrayScan VTI high-content screening platform, performed by Dr. Jörg Isensee and plotted. (***p-values > 0.01 according to two-tailed t-test) (Figures taken from Hussong et al. 2015)

2.3.6 BRD4 regulates the expression of *Sat III* RNA in an HSF1 dependent manner

The co-localization as well as the interaction between BRD4 and HSF1 suggest a functional interplay of both proteins in nSB. Besides their role in mRNA splicing, nSB also participate in epigenetic and transcriptional control. nSB are enriched in acetylated histone H4, especially, H4K8 and H4K16. In addition to HSF1, they contain additional transcriptional regulators such as CBP (CREB-binding protein) and Pol II. It was shown that the localisation of HSF1 in nSB is responsible for the activation of the transcription of satellite III repeats into stable non-coding RNAs (*Sat III*). *Sat III* RNAs are supposed to play a role in the formation of nSB. *Sat III* transcripts are transcribed by Pol II and are polyadenylated. A recently published study showed a stimulating function of BRD4 on the transcription of noncoding enhancer RNAs (eRNAs) [296] as well as of the noncoding RNA *HOTAIR* [297], indicating a potential role of BRD4 in the regulation of *Sat III* RNA.

To determine whether the BRD4/HSF1 interaction in nSB is important for the HS mediated induction of the *Sat III* transcripts the expression of the non-coding *Sat III* transcripts was analysed using RNA specific primer [131]. WI38 cells were transfected with siBRD4, siHSF1 or siCo constructs and 72 h after transfection, subjected to either HS at 42°C for 4 h or left at 37°C. RNA was isolated and *Sat III* RNAs were reverse transcribed using sequence specific primers that were already described in Valgardsdottir et al. 2008.

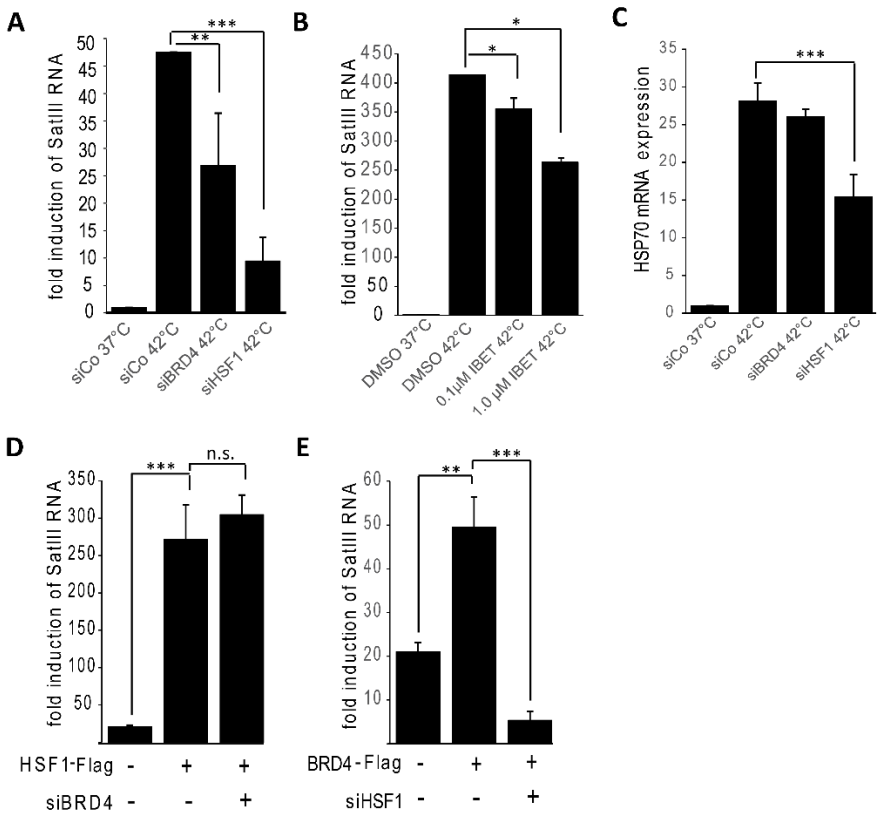

Figure 29 BRD4 regulates *Sat III* transcription. (A) ***Expression analysis of non-coding Sat III RNA in BRD4- and HSF1-deficient cells following HS.*** WI38 cells were transfected with siBRD4, siHSF1 or siCo, and 72 h after transfection, subjected to either HS at 42°C for 4 h or left at 37°C. *Sat III* transcripts were reverse transcribed with the RSM13 and FSM13 primer and amplified in the qPCR reaction with Hur98R and M13 primers, taken from Valgardsdottir et al. 2008. Additionally, the same amount of RNA was reverse transcribed with random hexamer oligos and amplified with primer specific for *TUBB* mRNA. *Sat III* RNA expression was normalized to *TUBB* and put into relation to the unstressed knockdown control. **(B)** ***Expression analysis of Sat III RNA after BRD4 inhibition in HS cells.*** WI38 cells were treated with 1 µm I-BET151 for 72 h. Total RNA was prepared from unstressed (37°C) and HS (4 h at 42°C) cells. *Sat III* transcripts were reverse transcribed, amplified and normalised as described above. **(C)** ***Expression of HSP70 mRNA in BRD4- and HSF1-deficient cells following HS***. WI38 cells were transfected with siBRD4, siHSF1 or siCo and 72 h after transfection, subjected to either HS at 42°C for 4 h or left at 37°C. *HSP70* expression was measured using transcript specific primers and was normalized to *TUBB* expression. **(D)** ***Expression analysis of Sat III RNA cells in HSF1 overexpressing and BRD4-depleted cells***. WI38 cells were transfected with siBRD4 or siCo. 24 h post-transfection cells were transfected with pTL-FLAG-HSF1. After additional 48 h cells were subjected to HS at 42°C for 4 h. *Sat III* transcripts were reverse transcribed, amplified and normalised as described above. **(E)** ***Expression analysis of Sat III RNA cells in BRD4 overexpressing and HSF1-depleted cells***. WI38 cells were transfected with siHSF1 or siCo. 24 h post-transfection, cells were transfected with pTL-FLAG-BRD4. After additional 48 h cells were subjected to HS at 42°C for 4 h. *Sat III* transcripts were reverse transcribed, amplified and normalised as described above. (n.s. = not significant, *p-values = 0.05, **p-values < 0.05, ***p-values < 0.01 according to two-tailed t-tests) (Figures taken from Hussong et al. 2015)

As expected, heat induced *Sat III* transcription up to 45-fold. A reduced expression of HSF1 diminished the heat-induced up-regulation of the *Sat III* RNA transcripts to 10-fold (Figure 29A). Interestingly, the down-regulation of BRD4 (Figure 29A) as well as the inhibition of BRD4 using I-BET151 (Figure 29B) resulted in a decreased induction of the *Sat III* transcripts, similar to HSF1 depletion. BRD4 knockdown reduced the *Sat III* RNA expression to 25-fold. The treatment with 1 µM I-BET151 for 72 h resulted to 38% less expression of *Sat III* RNA. Notably, the transcription of the *HSP70* mRNA, another target of HSF1, seemed not to be significantly affected by BRD4 depletion or inhibition (Figure 29C).

To further elucidate the dependency of BRD4 and HSF1 in regard to the transcriptional regulation of *Sat III* RNA the expression level of the *Sat III* RNA transcripts were analysed in WI38 cells. Cells were transfected with siBRD4 or siCo for 72 h. 24 h post-transfection, a HSF1 overexpressing construct was transfected into the BRD4-deficient as well as into control cells. After additional 48 h cells were exposed to HS at 42°C for 4h (Figure 29D). In the same experimental setup, a BRD4 overexpressing construct was transfected into the HSF1-deficient as well as into control cells that were subsequently exposed to HS at 42°C for 4 h (Figure 29E). Total RNA of both experiments was isolated and the expression of *Sat III* was analysed. Both, HSF1 and BRD4 overexpression alone, resulted in a significant activation of *Sat III* RNA transcription (Figure 29D, E). The increased HSF1 expression enhanced the HS mediated induction of *Sat III* transcripts up to 10-fold. Interestingly, an abolished BRD4 expression did not influence the HSF1 mediated enhanced induction of *Sat III* RNA (Figure 29D). However, overexpression of BRD4 resulted in a 2-fold increased induction of *Sat III* transcription that is completely abrogated with a simultaneous HSF1 knockdown (Figure 29E). These data further support an HSF1 dependent transcriptional role of BRD4 in nSB.

The role of *Sat III* RNA in stressed cells is still not completely clarified. *Sat III* transcripts are known to be responsible for the recruitment of several splicing factors to nSB and are thought to play a role in the altered splicing pattern during cellular stress. Thus, I asked, whether a down-regulation of the BRD4-mediated *Sat III* expression may lead to similar splicing patterns as BRD4 inhibition does. Therefore, *Sat III* RNA was down-regulated using custom designed siRNA (see [136]) and the splicing pattern of a BRD4 regulated intron (*ATF3*) in comparison to an intron not regulated by BRD4 (*BAG3*) was analysed using qPCR in WI38 cells. 24 h after the transfection of *Sat III*- siRNAs into WI38 cells, *Sat III* depleted and control cells were exposed to 44°C for 2 h. *Sat III*-siRNA knockdown abolished the otherwise HS-induced *Sat III* RNA transcription in a concentration

dependent manner by approximately 40% at 44°C and 500 nM *Sat III*-siRNA (Figure 30A). Interestingly, the *ATF3* intron was increasingly retained with increased *Sat III* knockdown (Figure 30B). This resembles the results obtained with siBRD4+HS in previous analyses. In contrast, the *Sat III*-siRNA did not have an impact on the *BAG3* intron (Figure 30C). Again, the same results I had shown in previous experiments in BRD4 knockdown and heat treated cells. These experiments suggest that the observed splicing deregulation in BRD4-deficient cells might be, in part, the consequence of a reduced *Sat III* RNA expression.

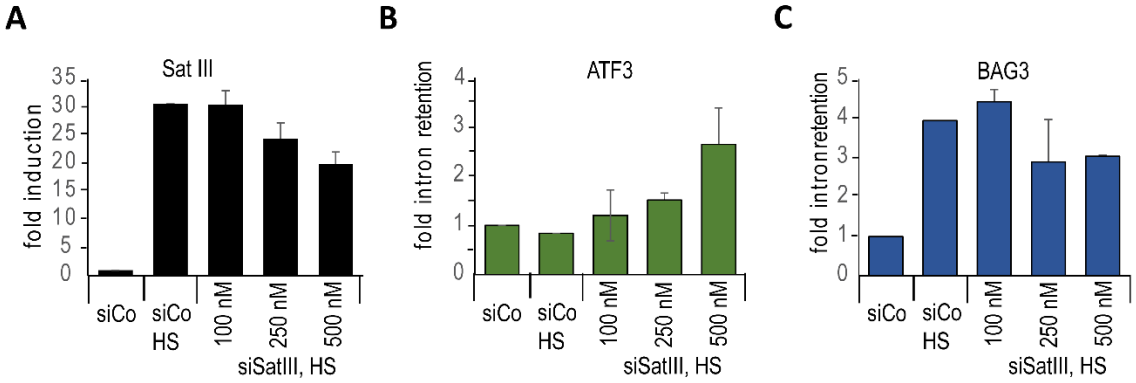

Figure 30 *Sat III* RNA knockdown increases intron retention under HS of BRD4 regulated genes. (A) ***Knockdown efficiency of Sat III RNA.*** WI38 cells were transfected with different concentrations of Sat III-siRNA, as indicated, and as control with a siRNA control pool (siCo). 24 h post-transfection, cells were subjected to HS at 44°C for 2 h or left at 37°C. Subsequently, total RNA was isolated and the expression of *Sat III* RNA was determined as following: *Sat III* transcripts were reverse transcribed with the RSM13 and FSM13 primer and PCR amplified in the qPCR reaction with Hur98R and M13 primers, taken from Valgardsdottir R. et al. 2008. Additionally, the same amount of RNA was reverse transcribed with random hexamer primers and amplified with oligos specific for *TUBB* transcripts. *Sat III* RNA expression was normalized to *TUBB* and put into relation to the unstressed knockdown control. **(B)** ***Intron expression analysis in Sat III-depleted cells of ATF3***. Fold intron retention of *ATF3* was calculated in the same cells by using primers that detect the exon/intron junction and as control the corresponding exon/exon junction of the same transcript (see Box 1). The values of the exon/intron primers were put into relation to the expression values generated by the exon/exon primers. **(C)** ***Intron expression analysis in Sat III-depleted cells of BAG3***. Fold intron retention of *BAG3* was also calculated in the same cells. Calculation and normalisation was performed as described for *ATF3*. (Figures taken from Hussong et al. 2015)

Taken together, in the second part of my studies I was able to elucidate BRD4 as a novel component of the stress induced nSB by interacting with HSF1, the main transcriptional regulator of the heat shock response. My results indicate that the association of BRD4 with HSF1 in nSB is required for the induction of the non-coding *Sat III* RNA that are themselves important factors in the splicing regulatory process during HS.

3 Discussion

The nuclear BET protein BRD4, a protein which binds acetylated histone tails, has been identified as an important component in cell cycle regulation, DNA replication, chromosome segregation DNA damage response, and in gene expression regulation. By compacting the chromatin structure through an interaction with the condensin complex**,** BRD4 promotes cell-cycle checkpoint recovery and attenuates DNA damage response signalling [209]. Thereby it protects cells from irradiation-induced cell death. Moreover, by interacting with the positive elongation factor b (p-TEFb) BRD4 plays a critical role during the transition from abortive to productive elongation of Pol II. The interaction with p-TEFb builds a bridge to other transcription factors and transcriptional modulators that allow BRD4 to act in a diversity of transcription programs. Amongst others, it was shown that BRD4 stimulates the transcription of inflammatory response genes by cooperating with NF-κB or STAT proteins [298]. Additionally, chromatin immunoprecipitation analyses of primary response genes (PRG) showed that BRD4 detects signal induced acetylation changes on histone H4 at the promoters of these PRGs. Subsequently, BRD4 recruits p-TEFb to PRG promoters and activates their induction. PRGs are a group of genes that have been shown to be regulated by BRD4 and are induced in response to both cell-extrinsic and –intrinsic signals. They play crucial roles in a wide range of biological processes, including the stress response, innate and adaptive immune system, glucose metabolism and oncogenic transformation [322]. It is worth noting that the inflammatory response, as part of the cellular stress response, is an important factor during initiation of cancer.

In this regard, BRD4 was shown to act as critical factor in the development and progression for several diseases, including cancer. BRD4 has been shown to promote transcription of known oncogenic drivers such as c-MYC that imposes a large application potential for diverse MYC associated cancers [235-241], including acute myeolic leukemia [242] and mixed lineage leukemia [230]. In addition to the oncogenic effects of BRD4 it was also shown that BRD4 possesses a tumor and metastasis suppressor activity in colon [255] and breast cancer [256,257]. However, detailed mechanisms of these contrary activities are not known.

Due to the large number of cancer relevant implications of the BET proteins, inhibitors for this protein family were developed and showed great therapeutic effects. The majority of these inhibitors share a similar mode of target inhibition. They block the acetyl-binding domains and prevent the association of BRD4 with histone tails in nucleosomes. In

prostate and lung cancer as well as in acute myeloic leukemia, the treatment with the inhibitors JQ1 or I-BET showed a drastic reduction of tumor growth and a significant extension of overall survival of approximately 25% [299].

Becoming aware of BRD4 as a turnstile in tumor pathogenesis, understanding the molecular mechanism of BRD4 action, especially in the response to exogenous as well as endogenous stressors, can help to shed light on the complex deregulation of the transcriptome in cancer and other diseases. Moreover, it can help to better understand the observed therapeutic effect of BRD4 inhibition.

Therefore, the aim of this study was to enhance the knowledge about BRD4's function in the regulation of gene expression during cellular stress.

3.1 BRD4 regulates the transcription of stress response regulators

To gain insight into the transcriptional property of BRD4, integrated RNA-sequencing and ChIP-sequencing analyses were used to nominate key BRD4 regulated target genes and cancer relevant pathways. The integration of transcriptome data in BRD4-deficient cells and data of BRD4-binding profiles revealed 52 key target genes. These genes showed a significant reduced expression in BRD4 depleted cells and an enriched BRD4 binding in their promoter region. Interestingly, these 52 target genes were enriched in several stress associated pathways, including the oxidative stress response (OR = 3.9; p-value = $2.7*10^{-5}$) and the cellular response to heat ($1.27*10^{-02}$) (Table 3). Further evidence for the importance of BRD4 in oxidative stress response pathways was given by pathway analyses using the Ingenuity Pathway Analysis software IPA (IPA®, Qiagen). This analysis revealed the NRF2 signalling cascade as the most significantly affected pathway by BRD4 ($p = 4.27*10^{-06}$). In addition to downstream targets of NRF2, such as *SOD2, GSTP1* and *EPHX1*, two important upstream regulators of NRF2 activity were found in the BRD4 target list: *KEAP1* and *MAPK3* (*ERK1/2*).

These results indicate a role for BRD4 as modulator of the cellular stress response at multiple levels. The RNA-seq as well as ChIP-seq data were validated for a subset of BRD4 target genes using additional quantitative PCR and Western blot analyses. Besides important upstream regulators of the oxidative stress response (*MAPK3* and *KEAP1*), modulators of the inflammatory response (*ITGB3BP* and *VIM*) as well as of the heat shock response (*HDAC6*) were also identified as BRD4 target genes. As mentioned above, BRD4 is an important regulator of the inflammatory response and is essential for the induction of primary response genes upon exposure to LPS [204]. In this context, the

finding that the top target genes of BRD4 are enriched for oxidative and heat stress response genes, further highlight BRD4's function in these mechanisms.

In general, cellular stress describes an imbalance of cellular homeostasis and can be caused by environmental stressors, such as heat or radiation. A deregulation affects critical steps of cancer initiation and progression, by influencing cell proliferation, overcoming apoptosis and increasing de novo angiogenesis [300]. The response to stress is regulated on multiple levels, including the transcriptional up-regulation of cyto-protective genes, the activation of cell repair mechanisms and the induction of apoptosis.

Oxidative stress is one of the best investigated stress response pathways. It represents an imbalance in pro-oxidant/antioxidant homeostasis that leads to the generation of toxic ROS which can cause protein, lipid and DNA damages. The defence against oxidative stress is an important cellular signalling pathway and a hallmark of many tumors [6-10]. In this context, the treatment with anti-oxidants was shown to be beneficial for the prevention of cancer initiation of several tumor entities [301]. Interestingly, amongst others, three important modulators of essential oxidative stress-sensitive transcription factors, are found to be direct regulated by BRD4: *MAPK3, KEAP1* and *MDM2.*

MAPK3, also known as ERK1, is a member of the mitogen activated kinase family and is involved in various cellular processes, such as cell proliferation, adhesion, survival and differentiation [99,302,303]. MAPK3 is activated by oxidative stress and is important for the regulation of oxidative stress induced apoptosis [102]. Furthermore, the MAPK signalling pathway is responsible for the phosphorylation of NRF2 that, in turn, leads to the activation of the transcription factor [304,305]. Interestingly, MAPK3 is also an interesting target for oxidative stress associated anticancer therapies. In doxorubicin resistant hepatocellular carcinoma cells for example, it was shown that the treatment with flavonoid chrysin significantly reduced NRF2 expression by down-regulating the PI3K-Akt and MAPK pathways and thereby restoring chemosensitivity [306].

Another protein that is linked to NRF2-mediated oxidative stress response is KEAP1. KEAP1 is the main regulator of NRF2 protein levels. Under unstressed conditions NRF2 is bound by KEAP1. This interaction facilitates the degradation of NRF2 via the ubiquitin-proteasome pathway which results in the inhibition of nuclear accumulation and the transcriptional activation of NRF2. In contrast, the exposure to oxidizing stress induces conformational changes of the KEAP1 protein, leading to the liberation of NRF2 from the protein complex and to its transcriptional activation [62,71-73]. Disruption of this sensible

regulatory network results in a defective stress response and can lead to cell transformation and cancer development [86-89].

MDM2 (Mouse double minute 2 homolog) is an E3 ubiquitin ligase whose main target is the tumor suppressor protein TP53. MDM2 targets TP53 for degradation by the ubiquitin-proteasome pathway and therefore represses its transcriptional activity [307]. In turn, TP53 plays key and complex roles in the cellular response to oxidative stress [308]. On the one hand TP53 can reduce the intracellular levels of ROS by regulating the expression of many antioxidants, including members of the sestrin or glutathione peroxidase families [309]. On the other hand, in response to high levels of oxidative stress, TP53 represses the expression of NRF2 resulting in an increased sensitivity towards oxidative stress [310]. Interestingly, several human tumor types have been shown to have increased levels of MDM2, supporting a role of *MDM2* as an oncogene [311].

These data suggest a role of BRD4 as upstream regulator of the oxidative stress response, mainly of the NRF2-mediated response to oxidative stress. In various cancers, including lung and prostate cancer [312,313], NRF2 is constitutively activated resulting in a growth advantage by promoting tumor growth and resistance to anticancer drugs [82]. However, in yet other cancer types (especially pulmonary diseases) it was shown that the activation of NRF2 can suppress carcinogenesis, demonstrating a dual and complex role of NRF2 in tumorigenesis [83-85]. Thus, the modulation of NRF2 is a promising strategy for cancer treatment.

3.1.1 BRD4 as regulator of the NRF2/KEAP1 mediated response to oxidative stress

The KEAP1/NRF2 pathway is frequently disrupted by somatic mutations in lung, head and neck, esophagus and skin cancers [86,87,90,91,93,95]. Notably, in lung cancer the NRF2/KEAP1 pathway is, according to the cancer genome atlas research network, with 34% one of the most frequently mutated pathways [94]. Mutations in *NRF2* and *KEAP1* are clustered within the KEAP1–NRF2-binding surface but are mutually exclusive [314]. In regard to the type of mutations 77% of all *KEAP1* mutations and 90% of all *NRF2* mutations which are found in tumors are missense substitutions. *KEAP1* mutations, in contrast to *NRF2* mutations are found, next to abnormally increased DNA methylation, to impair *KEAP1* function.

Since *KEAP1* was identified as one of the top 52 BRD4 target genes I focused my work on the elucidation of the role of BRD4 in the KEAP1/NRF2 network. In ChIP experiments I was able to show that BRD4 binds directly to the *KEAP1* promoter region under basal

conditions. The BRD4-dependent transcriptional regulation of *KEAP1* was validated using several cell biological approaches, including qPCR and Western blot analyses in various cell lines that underlined *KEAP1* as a BRD4 target.

To investigate the impact of BRD4 on the regulation of NRF2 by KEAP1 under stress, Cobalt protoporphyrin (CoPP) was used to induce the NRF2/KEAP1 pathway. CoPP leads to an up-regulation of the NRF2 protein levels by decreasing the KEAP1-dependent degradation of NRF2 [285]. As read-out and to measure the transcriptional activity of NRF2, the inducible and cyto-protective gene *HMOX1* was used. HMOX1 is the rate-limiting enzyme in the heme catabolism and part of the cellular defence against oxidative stress. In this study, I was able to show that the increased NRF2 level after CoPP treatment, which drives the expression of *HMOX1*, is further enhanced by an additional BRD4 depletion, caused by a down-regulation of *KEAP1* and a lack of NRF2 degradation. A reduced BRD4 expression resulted in an enhanced accumulation of NRF2 in the nucleus followed by an increased binding to its regulatory elements in the enhancer regions of *HMOX1*. The increase in *HMOX1* expression in BRD4 depleted and stressed cells goes along with an increased cell viability and a decreased amount of intracellular ROS under H_2O_2 stress. Similar results were obtained with a treatment with the BRD4 inhibitor JQ1, which increases cell viability and reduces ROS. Thus, under exertion of stress, BRD4 indirectly regulates *HMOX1* over the KEAP1/NRF2 pathway resulting in a counteraction of BRD4 and HMOX1 levels.

As mentioned above, the modulation of NRF2 activity is an interesting target for cancer therapy. Over the last few decades, numerous NRF2 inducers as well as inhibitors have been developed. Almost all currently known NRF2 inducers are indirect inhibitors of the KEAP1-NRF2 interaction, resulting in a reduced degradation of NRF2 [315-317]. For example, sulforaphane (SFN), a potent naturally occurring inducer of NRF2 signalling, modifies multiple domains in the KEAP1 protein that results in the stabilisation and nuclear accumulation of NRF2 and subsequently in the induction of NRF2 target genes, such as NQO1 or HMOX1 [318]. Interestingly, in mouse models of prostate cancer, SFN intake decreases tumor growth, increases cancer cell apoptosis and prevents cancer progression [319,320]. Furthermore, the pre-treatment with CoPP and the up-regulation of NRF2 protects human gastric mucosal cells from deoxycholate-induced cell death [321]. Deoxycholate is a hydrophobic bile acid that induces DNA damage and activates oncogenic signalling pathways through the generation of ROS.

Having this in mind, BRD4 might be also an interesting target in regard to chemoprevention by modulating the NRF2/KEAP1 pathway and by up-regulating cyto-protective genes in a stressed environment.

3.1.2 BRD4 as turnstile in ROS regulation

In addition to *KEAP1, MAPK3* and *MDM2*, several downstream targets of NRF2 were found to be directly regulated by BRD4. All of them, including *GSTP1*, *SOD2* and *TXN2* are oxidative stress sensitive enzymes and important for the reduction of cellular ROS.

Due to selection cut-off criteria, *HMOX1* was not part of the initial RNA-Seq candidate list. Nevertheless, *HMOX1* was also found to be deregulated after BRD4 depletion in the absence of stress, comparable to the other identified BRD4 target genes. Furthermore, ChIP-qPCR experiments identified an enrichment of BRD4 at the *HMOX1* promoter. However, without stress, BRD4 appeared to directly regulate HMOX1: Down-regulation of BRD4 resulted in a decreased *HMOX1* transcription and an overexpression of BRD4 increased the level of *HMOX1*.

Using bioinformatics motif analysis combined with mutation and co-immunoprecipitation experiments I showed that BRD4 activates *HMOX1* transcription via an interaction with the transcription factor SP1. Interestingly, Hargreaves and colleagues found that SP1, a zinc finger transcription factor that binds to GC-rich motifs, is associated with promoters of primary response genes (PRG) and facilitates there the phosphorylation of Pol II. PRGs - compared to late responsive genes - usually have short primary transcripts with only a few exons. These characteristic were also found in some of the identified stress responsive BRD4 target genes. For example, the number of exons of the detoxifying enzymes *GSTP1*, *SOD2*, *TXN2* and *HMOX1* do not exceed 7 and all of them harbour a SP1-binding site, supporting the regulation of BRD4 via SP1 as a general mechanism to regulate the expression of stress responsive genes in the absence of stress. It is worth noting that in addition to transcription initiation and elongation, PRG are also regulated at the level of mRNA splicing, a process also regulated by BRD4 during stress response which was uncovered in this study (discussed in section 3.2).

Taken together, the regulatory network between BRD4 and SP1 may be a mechanism for a fast fine-tuning of the cellular reactions towards small ROS deviations, as already described for PRG expression, that do not activate the KEAP1/NRF2 oxidative stress response.

3.1.3 Dual role of BRD4 in prostate cancer

Having identified BRD4 as a regulator of the oxidative stress response either via the NRF2/KEAP1 system or via the interaction with SP1 under unstressed conditions, I asked whether a modulation of BRD4 activation influence the progression of cancers.

Elevated rates of ROS have been detected in many cancer cell lines [323] as well as solid tumors [288,324,325], where they modulate many processes of tumor development and progression. Moreover, the levels of antioxidant proteins have been shown to be altered in malignant cells [326] as well as in primary cancer tissues, including ovarian [327], lung [328] and colorectal cancer [329]. This implicates an aberrant regulation of redox homeostasis and stress adaptation as a hallmark of many cancer types. High levels of ROS regulate cell transformation, proliferation, invasion, angiogenesis and metastasis and promote cancer progression. In contrast, most chemotherapeutic agents suppress tumor progression by increasing oxidative stress in cancer cells. Due to the two-faced role of oxidative stress in tumor pathogenesis, both, pro- and antioxidant-based agents have been evolved for cancer prevention and therapy [330,331].

As already shown for castration-resistant prostate cancers, the inhibition of BRD4 has a strong therapeutic effect in this cancer type by regulating androgen receptor (AR) responsive genes, independent of c-MYC [250,332]. In this case, BRD4 physically interacts with the N-terminal domain of AR. This interaction can be disrupted by JQ1 and leads to a displacement of AR from its target gene loci.

Prostate cancer accounted for more than 1,000,000 new cases and 300,000 deaths per year (2012) and is the second most common cancer among men worldwide [104]. Many factors like diet, environmental carcinogens, inflammatory diseases as well as oxidative stress have been linked to an increased risk of prostate cancer and were discussed as potent drivers in the development and progression of this disease. In regard to NRF2 - as one of the most important regulators of the oxidative stress response - studies from human prostate cancer samples implicated a down-regulation of NRF2 and several of its target genes in tumor cells compared to normal tissue [16,106]. Since several studies from patient samples as well as from prostate cancer cell lines have also shown that prostate cancer have higher levels of ROS than normal controls [105], the therapeutic inhibition of BRD4 might as well function over altered ROS levels. In this study I showed that the expression of BRD4 is constitutively increased in prostate tumor samples, as well as in prostate cancer cell lines, suggesting a potential role of BRD4 in the progression of this cancer type. Furthermore, correlation analysis of *BRD4* expression and its target genes

revealed a significant relation between *BRD4* and *KEAP1* in human prostate cancer samples. Along with *BRD4* expression, *KEAP1* was significantly up-regulated in tumor tissue samples and in prostate cancer cell lines. Due to the already published therapeutic effects of BRD4 and its increased expression in prostate tumors, I investigated the regulation of the BRD4/KEAP1/NRF2 network in prostate cancer cell lines.

As mentioned above, several studies described a down-regulation of *NRF2* in human prostate cancer that could also be validated in our tested prostate cancer cell lines. Interestingly, the expression of *HMOX1* was more variable. In DU145 cells, the expression of *HMOX1* was significantly increased, whereas the level of HMOX1 in PC3 was down-regulated.

Interestingly, treatment of DU145 cells with the BRD4 inhibitor JQ1 reduced the expression of HMOX1 on mRNA as well as on protein level without affecting the level of NRF2, highlighting a direct regulation of *HMOX1* transcription over BRD4 in DU145 cells. In contrast, the endogenous expression level of *HMOX1* in PC3 cells showed a significant down-regulation, despite of the increased expression level of BRD4. Treatment with JQ1 in these cells had no influence on the *HMOX1* expression, indicating a regulation irrespective of BRD4, presumably over NRF2.

Interestingly, the two-sided regulatory mechanism of *HMOX1* transcription, observed in prostate cancer cells, correlates with the internal level of ROS in these cell lines. Kumar and colleagues uncovered an increased level of ROS in PC3 cells compared to DU145 cells [288] and consequently an increased intracellular oxidative stress environment.

In this regard, Alaoui-Jamali and colleagues described an anti-tumorigenic effect of the small molecular HMOX1 inhibitor (OB-24) in AR-independent prostate cancer [290]. However, despite a down-regulation of *HMOX1* by JQ1 in DU145, ROS levels and cell viability were not affected in these cells. Notably, Wyce et al. found for DU145 as well as for PC3 a resistance towards the BET inhibitor I-BET762, supporting a general resistance to BRD4 inhibition. However, Jayakumar and colleagues demonstrated that in DU145 cells a reduction of *HMOX1* expression overcomes radioresistance, but has no impact on cell-viability alone [333]. Since the treatment of JQ1 reduces the *HMOX1* expression, but has no impact on cell viability, it may be possible to combine BRD4 inhibitors with radiotherapy or platinum-based drugs - treatments which induce the generation of ROS [334] - and thereby improve the effect of BRD4 inhibitors.

Taken together, these results illustrate BRD4 as a novel regulator of NRF2 activity during stress response. The fact that hundreds of so-called “survival” genes (in addition to

HMOX1) are modulated by NRF2, makes NRF2 activation to be a very attractive target for oxidative stress associated disorders. Targeting NRF2 activation has been shown to prevent or even inhibit the progression of the major oxidative stress related diseases, such as diabetes, cancer, cardiovascular diseases and neurodegenerative diseases [335-338]. Thus, by regulating several important modulators of NRF2 activity, BRD4 becomes a potent and interesting target for ROS induced diseases.

3.2 BRD4 regulates splicing under heat stress (HS)

Besides KEAP1, several additional stress-associated regulators are part of the identified BRD4 target gene list, including *HDAC6*.

HDAC6 plays a key role in the autophagy pathway [339] as well as in the clearance of misfolded protein aggregates following stress induction [340]. Autophagy can be stimulated by multiple forms of cellular stress, including hypoxia, reactive oxygen species or protein aggregates and is a central component of the cellular stress response [341,342]. Furthermore, due to its ubiquitin-binding activity HDAC6 activates the main transcriptional regulator of the HS response, HSF1. HDAC6 forms hereby a complex with HSF1 and HSP90 that keeps HSF1 in its inactive form. An increase of misfolded proteins leads in a shift of HDAC6 binding to ubiquitinated protein aggregates which in turn results to the dissociation of HDAC6 from the complex and activation of HSF1 [340]. Based on these results I asked whether BRD4 may also play a role in the HS mediated stress response.

The cellular response to HS is an ancient and highly conserved defence mechanism which is also active under proteotoxic stress and activated during tumor development. A broad range of tumors have been shown to express high levels of heat shock proteins (HSPs) [110-112], thus representing a pivotal target of HSP inhibitors. Furthermore, in addition to conventional anti-tumor therapies, such as radiation or chemotherapy, hyperthermia has been shown to be a successful therapeutic approach in a wide range of cancer entities [343].

The HS response is characterized by the transcriptional up-regulation of cyto-protective genes. Having in mind the transcriptional role of BRD4 in the oxidative stress response and the previously described pathway analyses, I investigated whether BRD4 may also be part of the HS response. The expression profiles of BRD4-depleted and HS treated cells were analysed. Interestingly, the reduced BRD4 expression appears to have no functional influence on the main transcriptional response during HS.

Nevertheless, besides changing gene expression levels, the HS response induces also a shift in the exon-intron composition of transcripts [344,345]. The mechanism underlying the inhibition of post-transcriptional splicing and maintenance of co-transcriptional splicing under HS is still not well understood and may play a major role in influencing the cellular transcriptome under stress conditions.

A role in the splicing process is also discussed for BRD4, supporting further investigations of a splicing function of BRD4 during HS. BRD4 interacts with JMJD6 [215] - which affects the pre-mRNA splicing capacity of U2AF65 – and interacts with the splicing factor SC35 (also named SRSF2) [157]. Furthermore, as mentioned in the previous section, a study with lipopolysaccharide stimulated macrophages showed that BRD4 is important for the generation of mature spliced transcripts of PRG [204].

Using transcriptome-wide RNA sequencing experiments under HS, with and without BRD4 knockdown alternative splicing alterations were investigated. Even though, in the absence of stress, BRD4 seemed to have no influence on splicing regulation, under HS conditions a down-regulation of BRD4 expression increased the heat-induced splicing inhibition, represented by an increase of intron retention. Here, 965 introns were affected by BRD4 depletion, including cancer relevant genes, such as *EZH2* and *WHSC1*. Intron retention can have profound functional consequences by introducing premature translation termination codons (PTC) to the mature transcripts that are then targeted by the nonsense-mediated decay (NMD) [346]. Wang and colleagues reported that the majority of NMD targets are members of stress response- and tumor-promoting pathways. Therefore, inhibition of the NMD in tumor cells is found to be an important mechanism to regulate cellular stress response and promote tumorigenesis [347]. Hence, a deregulation of BRD4 that is found in several cancer types - including colon and breast cancer [254,256] - might influence the splicing pattern of tumor promoting transcripts which could be a possible mechanism of cancerogenesis.

3.2.1 BRD4 as novel component of splicing-associated nuclear stress bodies (nSB)

Post-transcriptional splicing inhibition under HS is mechanistically not well understood and it is also not clear why co-transcriptional splicing is still functional under HS. It is proposed that the splicing defects are caused by the assembly of various splicing factors, including SR proteins, hnRNPs, snRNAs and *Sat III* RNA, in nuclear stress bodies (nSB) under HS conditions. This assembly could ensure a functional co-transcriptional splicing of vital

genes despite of a general splicing inhibition. nSB are unique sub-nuclear organelles which were originally identified as the main site of HSF1 accumulation at pericentric heterochromatic tandem repeats of satellite III DNA sequences [127]. Using immunofluorescence analyses I showed that the typically diffuse located BRD4 protein is recruited to these nSB under HS by interacting with HSF1.

After exposure to HS, heterochromatic regions in nSB are reverted to euchromatin as shown by the presence of acetylated histone H4, especially, H4K8 and H4K16 [134]. Notably, Hagreaves and colleagues have shown that the recruitment of BRD4 to promoters of primary response genes after LPS-stimulation requires the histone modifications H4K5/8/12Ac [204]. This mechanism is likely to be a general regulator of inducible gene expression that would also be a conceivable mechanism for the HS induced recruitment of BRD4 to nSB. The reduced recruitment of BRD4 to nSB structure following treatment with the bromodomain inhibitor I-BET151 supports this theory. The BRD4 inhibitor reversibly blocks the bromodomains, which are essential for the binding to acetylated peptides and thereby causes the displacement of BRD4 from chromatin. Interestingly, BRD4 depletion as well as inhibition have no influence on the nuclear distribution of HSF1. In contrast, in HSF1-deficient cells BRD4 recruitment is completely abrogated, indicating an HSF1-dependent translocation of BRD4.

The described interaction- as well as the immunofluorescence studies suggest a stress induced interplay of BRD4 and HSF1. In addition to splicing regulation, nSB are also thought to be the place of active gene transcription, especially of HSF1 target genes. Pol II as well as other transcriptional co-regulators are also recruited to nSB upon HS. Notably, the recruitment of Pol II requires the binding of HSF1 to the pericentric regions of *Sat III* DNA, similar to BRD4. Keeping the interaction of BRD4 with p-TEFb and its role in Pol II phosphorylation in mind, it is conceivable that BRD4 acts as linker between HSF1 and the transcription machinery. This supports the finding that BRD4 inhibition also results in a reduced *Sat III* RNA expression.

Additionally, chromatin organization itself seems to play an important role in the formation of nSB after HS treatment. SWI/SNF chromatin remodelling complexes are located, similar to BRD4, in nSB by interacting with *Sat III* RNA [348]. Depletion of BRG1, a component of the SWI/SNF chromatin remodelling complex, results in an impaired nSB formation in response to HS, implicating an essential role in the non-coding RNA-dependent organization of nSB [348]. For paraspeckles (nuclear structures enriched in characteristic RNA-binding proteins and non-coding RNAs) it was shown that the chromatin remodelling

complex acts as a part of their structural formation by bridging the non-coding RNA *NEAT1* to RNA-binding proteins to build RNP complexes at chromosomal loci. The same mechanism is also thought for the formation of nSB by targeting the non-coding *Sat III* RNA to RNA-binding proteins, in particular to splicing factors. In this regard, SWI/SNF may act as linker between *Sat III* RNA and splicing factors which are recruited to nSB following HS. Interestingly, BRG1 and BRD4 were found to be enriched in a complex at the same regions of super-enhancers in embryonic stem cells [220,221]. Similarly, an interplay between BRD4 and the chromatin remodelling complex SWI/SNF could occur in nSB and might connect BRD4 with the co-transcriptional splicing regulation during HS.

Further implications of BRD4 as part of the co-transcriptional splicing process arise from its homologue Bdf1 in *Saccharomyces cerevisiae*. A deletion of *Bdf1* leads to a global splicing defect. It is speculated that Bdf1 plays a direct role in connecting mRNA splicing with chromatin remodelling and transcription initiation. Chromatin immunoprecipitation data revealed a decrease in U1 snRNP recruitment at intron containing genes, suggesting impairment of co-transcriptional spliceosome recruitment in *bdf1Δ* strains [182,349].

Interestingly, a BRD4 knockdown in unstressed cells did not show a significant alteration in alternative splicing. Under basal conditions BRD4 was shown to interact with the splicing factor SC35 and is located in nuclear splicing speckles. Hence, an involvement of BRD4 in the splicing process under unstressed conditions cannot be ruled out. A large number of proteins and snRNAs are involved in the basal splicing process. Since BRD4 is not a typical splicing factor, it is possible that the putative role of BRD4 in the co-transcriptional splicing regulation in the absence of stress might be compensated by a variety of other splicing associated proteins. In contrast, the exposure to heat turned down the splicing machinery and resulted in an increased intron retention. In this case, some essential splicing factors are recruited – together with BRD4 - to nSB to ensure splicing of vital genes. Under these conditions, the role of BRD4 in the splicing process cannot be compensated again.

RNA splicing is also thought to be influenced by epigenetic modifications, such as DNA methylation and histone modifications. Notably, trimethylation of H3 lysine 36 (H3K36me3), a mark of active gene expression, was shown to be more enriched at constitutive exons rather than at alternative exons [164,169]. Furthermore, recently mutations in the lysine methyltransferase SETD2 have been reported to decrease H3K36me3 and increase intron retention in clear cell renal carcinomas [350]. Interestingly, BRD4 has also been reported to interact with NSD3, a histone methyltransferase that has

been shown to catalyse H3K36 methylation [215]. Both, depletion of BRD4 and NSD3 reduce the level of cellular H3K36me3 and lead to the speculation that BRD4 inhibition might act upstream of H3K36me3 and promote intron retention after HS. To clarify the significance of the H3K36me3 modifying ability of BRD4 in regard to its splicing regulating function, it would be interesting to analyse the distribution of H3K36me3 in BRD4-depleted and HS treated cells using ChIP analyses. It would be expected that H3K36me3 binding regions in these cells overlap with BRD4 regulated introns or with their corresponding up- or downstream located exons under HS.

However, future work will reveal the effect of BRD4 inhibition in cancer therapy on epigenetic patterns and alternative splicing events. Furthermore, it would be interesting to know if, similar to HS, splicing under proteotoxic stress - which is a major stress factor in cancer cells - is maintained over BRD4's recruitment to nuclear stress bodies.

3.2.2 BRD4 regulates stress-induced non-coding RNA expression

As mentioned above, nSB also participate in epigenetic and transcriptional control of gene and noncoding RNA expression. The recruitment of BRD4 to nSB may link HSF1 with the transcriptional machinery, in particular with Pol II. Due to this connection, BRD4 could be involved in the HSF1-dependent transcriptional regulation. Since no significant alterations in the overall gene expression profiles of BRD4-depleted and heat treated cells were detected, the question about a functional role of BRD4/HSF1 interaction in the transcriptional process came up.

The localisation of HSF1 in nSB is responsible for the activation of the transcription of cyto-protective HSF1 target genes and of satellite III repeats into stable non-coding RNAs (*Sat III*). The *Sat III* transcripts are transcribed by Pol II, are polyadenylated and consequently targets of the general mRNA transcription machinery. Here BRD4 may have a role in the regulation of *Sat III* RNA transcription. In another connection, Kanno et al. showed a stimulating function of BRD4 on the transcription of noncoding enhancer RNAs (eRNAs) [296] as well as on the noncoding RNA *HOTAIR* [297]. Indeed, depletion or inhibition of BRD4 efficiently attenuated the induction of *Sat III* RNA in a HSF1-dependent manner.

It is known that a down-regulation of these transcripts blocks the recruitment of splicing factors to nSB [136]. Notably, I was able to show that an abrogation of *Sat III* RNA following HS, resulted in similar splicing defects as BRD4 depletion. In addition to HS, *Sat III* RNAs are also induced by a wide range of other stresses including DNA damaging agents (MMS and etoposide), oxidative stress (H_2O_2), hypoxia (Cobalt chloride and low O_2), hyper-

osmotic stress (sorbitol) and heavy metals (cadmium) [131]. Furthermore, the induction of *Sat III* RNA is in accordance with the formation of nSB under these stressing agents. The transcriptional activation of *Sat III* RNAs and the following recruitment of several transcription and pre-mRNA processing factors to nSB are a general mechanism to sustain essential transcriptional programs and splicing patterns under stress. Furthermore, this recruitment ensures and facilitates a rapid recovery from stress induction. My observations suggests that the observed splicing deregulation in BRD4 depleted cells under HS could be, in part, a consequence of an abrogated *Sat III* induction under stress conditions. In this regard, it would be interesting if a reduction of BRD4 expression after exposure of some of the other *Sat III* RNA inducers, such as H_2O_2, results in similar splicing defects. It has to be mentioned that the induction of *Sat III* transcripts by other stresses is less efficient in comparison to the induction following HS. Detection of splicing defects might be thus more difficult.

The regulation of *Sat III* RNA in HS cells could also be an explanation why BRD4 depletion in absence of stress did not result in alteration of alternative splicing events. *Sat III* RNA transcription is only induced upon stress induction and thereby not influenced by a sole down-regulation of BRD4 under basal conditions.

Having in mind the stimulating role of BRD4 in the transcription of the oncogenic *HOTAIR* RNA under basal conditions and the *Sat III* RNAs under heat, it is plausible that BRD4 has a general function in the transcription of non-coding RNAs which regulate cellular functions. A miss-regulation of non-coding RNA dependent protection programs could result in an ineffective stress response and to the development of stress associated diseases. One of the best characterized and described diseases that is associated with a deregulation of non-coding RNAs and a resulting altered splicing pattern is myotonic dystrophy (MD). This neuromuscular disorder is due to the accumulation of the mutated transcripts of the *DMPK* (dystrophia myotonica-protein kinase) gene that contains numerous additional CUG repeats in the 5'UTR region. [351]. The alternative splicing regulator MBNL1 (Muscleblind-Like Splicing Regulator 1) has a high affinity for such CUG-repeat containing RNAs and co-localizes with these transcripts in distinct nuclear foci. This accumulation, in turn, leads to widespread disruption of alternative splicing events in MD tissues.

3.2.3 Role of BRD4 inhibitors in alternative splicing-associated diseases

Alternative splicing has been found to be associated with various diseases including Frasier syndrome [352], cystic fibrosis [354], myotonic dystrophy (MD) [356], and retinitis pigmentosa [355] as well as neurodegenerative and complex diseases (Parkinson's disease [353] and cancer [357]). Mutations or genetic alterations within spitting distance of splice sites or splicing regulatory sequences, such as splicing enhancers or silencers can alter cell type and gene specific splicing patterns. Moreover, mutations in spliceosomal-associated genes are thought to cause genome-wide splicing alterations that are detected in diverse cancer types [358]. For example, frequent mutations in the spliceosomal protein SF3B1 have been discovered in myelodysplastic syndrome (MDS) [359]. It is worth noting that cancer-specific alternative splicing patterns include all of the main splicing events, such as cassette exons, alternative 5′ and 3' ss intron retention, and mutually exclusive exons [360]. Currently, using novel sequencing and bioinformatics technologies, the characterization of the global splicing pattern in tumorigenesis gains increasing research interest. Quite recently, Dvinge and Bradley analysed, in a genome-wide study, RNA splicing patterns across 805 matched tumor and normal control samples from 16 different cancer types [361]. They identified a widespread diversity of RNA splicing defects, also demonstrated by a predominantly increase of intron retention, in almost all tested tumor entities even in the absence of mutations that directly affect the RNA splicing machinery. Interestingly, the differential intron retention in cancer cells correlates with tumorigenesis and prognosis. Moreover, a study of five lung cancer patients identified possible tumor-specific intron retentions [362]. Mentionable, out these 2340 identified tumor-specific intron retentions, 136 were also found in the BRD4 depleted and heat treated samples, suggesting a role of BRD4 in the observed splicing pattern, at least in lung cancer.

Interestingly, RNA splicing-targeted therapies are becoming a promising and powerful therapeutic approach in monogenic as well as complex genetic diseases. They can be classified in (1) antisense oligonucleotides (ASO), (2) Spliceosomal-Mediated RNA *trans*-splicing (SMaRT), (3) modified snRNAs and (4) Small molecule compounds. The first three approaches, ASO, SMaRT and the modified snRNAs, have similar capabilities due to their specificity to distinct RNA isoforms. These approaches have been designed to target only one specific transcript or splice site to restore normal splicing of this transcript or to knockdown mutated genes. These RNA splicing-targeted therapies have been already used successfully for β-thalassemia [363], cystic fibrosis [364] Fanconi anemia [365] or Duchenne muscular dystrophy (DMD). In this regard, several clinical trials have recently

demonstrated that oligonucleotide-based drugs induces efficiently alternative splicing of the dystrophin pre-mRNA in DMD patients, resulting in the expression of a less pathogen isoform of the dystrophin protein and to an improvement of the disease.

In contrast, therapies based on small molecule compounds influence the general splicing process. For example, the small molecules, spliceostatin A bind the SF3B spliceosomal complex, which is an essential component of the U2 snRNP. Thereby, they induce aberrant splicing and disrupt the metabolic and proliferative activities of cancerous cells. Several of these splicing inhibitors, including spliceostatin A, are already used for cancer therapy [366,367]. Having in mind the splicing inhibitory effects of BRD4 inhibition in heat treated cells, BRD4 inhibitors could be novel RNA splicing anti-cancer drugs. Inhibition of BRD4, maybe in combination with hyperthermia, could affect the altered alternative splicing pattern in cancer, increase the degradation of cancer-relevant genes and thereby disrupt the oncogenic potential of tumors.

3.3 Conclusion

By integrating BRD4-ChIP and gene expression data from BRD4 deficient cells, BRD4 was identified as an essential regulator of the cellular stress response.

In the absence of stress, BRD4 activates the *HMOX1* promoter and regulates the *HMOX1* expression over an interaction with SP1 (Figure 31A). Thus, BRD4 acts as a positive transcriptional activator of *HMOX1*, whereas BRD4 silencing results in decreased *HMOX1* mRNA and protein expression as well as a reduced promoter activity (Figure 31B). This regulatory mechanism may be important for cellular reactions towards small ROS deviations. Furthermore, BRD4 binds to the *KEAP1* promoter in normal and also in prostate cancer cells, highlighting *KEAP1* as a direct target of BRD4 in cancer. Under CoPP treatment, and thus exertion of stress, NRF2 is significantly increased, which drives *HMOX1* expression (Figure 31C). An additional BRD4 knockdown further enhances this mechanism by a down-regulation of *KEAP1* followed by a decreased NRF2 degradation (Figure 31D). This increase in *HMOX1* expression goes along with an increased cell viability and a decreased amount of intracellular ROS under H_2O_2 stress. Thus, under exertion of stress, BRD4's regulation of *HMOX1* is mediated via the KEAP1/NRF2 pathway.

In prostate tumors, these regulatory mechanisms appear to be disturbed. The regulatory network in DU145 seems to be similar to the regulation without stress, meaning a regulation of *HMOX1* direct over BRD4. In contrast, the data in PC3 resemble the

regulation network in stressed cells where *HMOX1* transcription is regulated by the KEAP1/NRF2 signalling pathway.

Taken together, these data provide new insight into the transcriptional regulatory network of BRD4 as it nominates BRD4 as key mediator of *KEAP1* in the oxidative stress response and to directly target SP1-binding sites in the *HMOX1* promoter. The two-sided regulatory mechanism of BRD4 may prevent tumor cells from a loss of *HMOX1*, an increase of ROS and promote cell survival. As outlined above, further studies of the BRD4 transcriptional network and the cooperation between BRD4, KEAP1, NRF2 and NRF2 target genes as transcriptional regulators in prostate cancer have the potential to elucidate important druggable oncogenic dependencies.

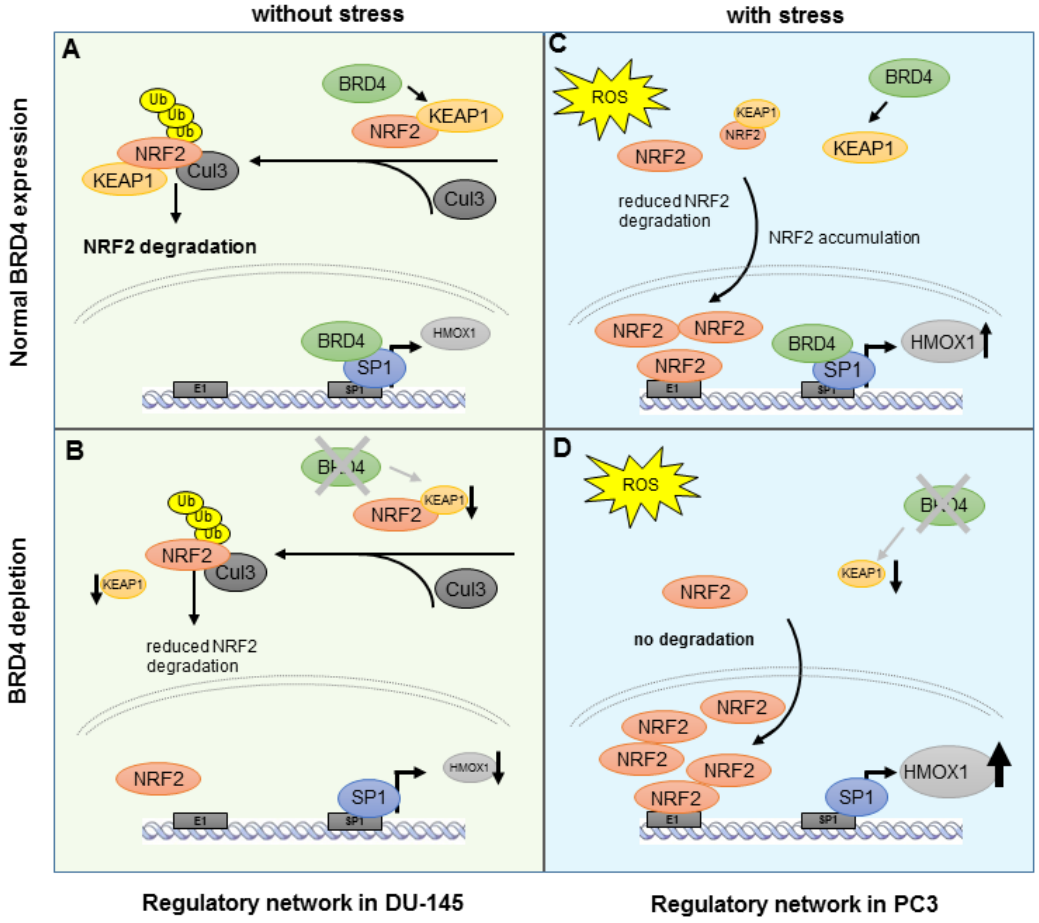

Figure 31 Schematics of the regulation of the HMOX1 expression under normal (A and B) and stress conditions (C and D) and without (A and C) or with (B and D) BRD4 knockdown. Under normal conditions, BRD4 directly activates the HMOX1 promoter over SP1-binding sites. In the presence of stress, HMOX1 expression is mainly regulated over the NRF2/KEAP1 pathway where BRD4 regulates KEAP1.

Besides the above mentioned involvement of BRD4 in the cellular response to oxidative stress, I was also able to elucidate BRD4 as novel component of the cellular response to heat. In particular, I found that BRD4 is involved in alternative splicing events during heat shock. The reduction or inhibition of BRD4 in heat-treated cells increases the HS mediated splicing inhibitory effect, represented by an increase of intron retention.

Given the important role of BRD4 in the regulation of the elongation rate of Pol II that is associated with co-transcriptional splicing, this might be an explanation for the observed splicing defects in BRD4-depleted cells.

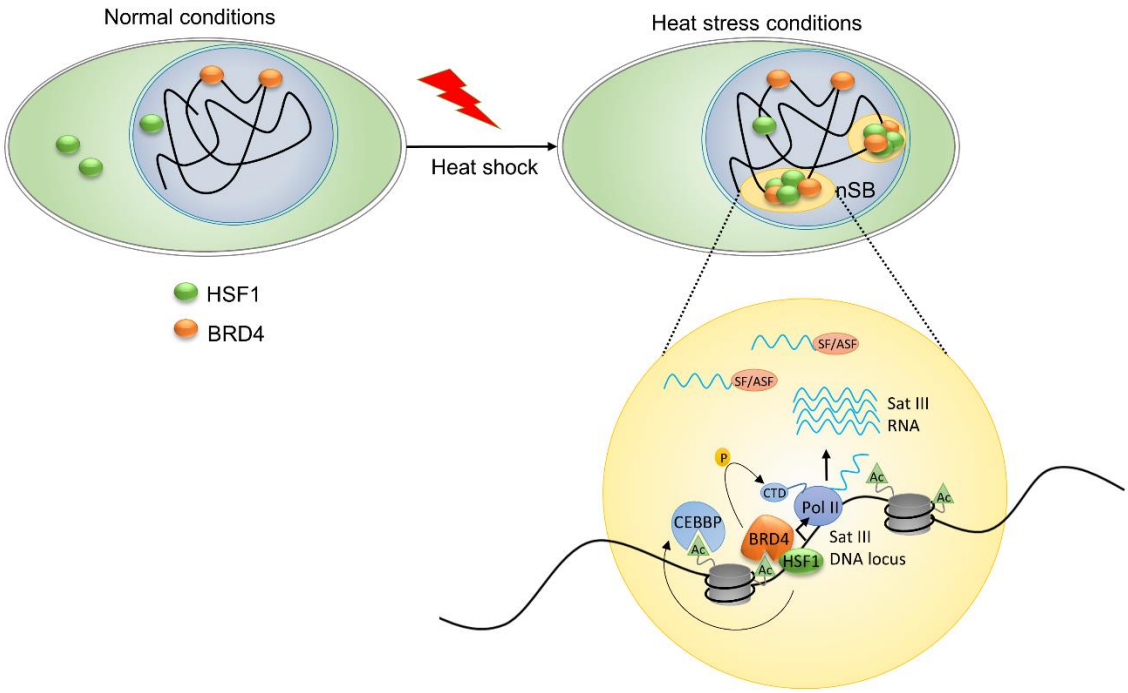

Figure 32 Schematic representation of the splicing regulatory network in nSB under HS. Under normal conditions HSF1 is captured in the cytoplasma and remains unbound to DNA. BRD4 is typically located in the nucleus and is important for the general transcription process. After the exposure to elevated temperatures (HS) HSF1 oligomerizes into a transcriptional active trimer, which binds to HS elements (HSE) of HS inducible genes and forms at pericentric heterochromatic regions (*Sat III* loci) nuclear stress bodies (nSB, yellow). BRD4 interacts with HSF1 in these nSB and regulates the expression of non-coding *Sat III* RNAs in an HSF1-dependent manner. These *Sat III* transcripts are important for the recruitment of splicing factors, such as SF2/ASF to the nSB.

Furthermore, the HSF1-dependent recruitment of BRD4 to nuclear stress bodies, supports this assumption. My analyses showed that the association of BRD4 with HSF1 in nSB seems to be required for the stress induced up-regulation of the non-coding *Sat III* RNA.

This regulation presumably allows BRD4 to influence splicing regulation during stress. The down-regulation of *Sat III* RNA expression by BRD4 depletion or inhibition may cause a defective recruitment of splicing factors to nSB that, in turn, potentially results in the observed splicing defects (Figure 32).

Taken together, this study uncovered a central role of BRD4 in the cellular stress response and improves our mechanistic understanding of BRD4 inhibitors. This is in particular important since alterations in stress response pathways are also found in numerous stress associated diseases including neurodegenerative and Alzheimer's diseases and BRD4 inhibitors might here be also therapeutically useful.

4 Material and Methods

4.1 Cell-biological methods

4.1.1 Human cell lines

Table 7 Human cell lines used in this study

cell line	*tissue*	*ATCC number*
WI38	lung fibroblasts	CCL-75
HEK293T	embryonic kidney	CRL-11268
HeLa	Cervix carcinoma; epithelial	CCL-2
DU145	prostate carcinoma; derived from metastatic site: brain	HTB-81
RWPE-1	prostate; normal epithelial	CRL-11609
LNCaP	prostate carcinoma; derived from metastatic site: left supraclavicular lymph node	CRL-1740
PC3	prostate carcinoma; derived from metastatic site: bone	CRL-1435
VCAP	prostate carcinoma; derived from metastatic site: vertebral metastasis	CRL-2876

4.1.2 Cultivation of human cell lines

Cells were cultivated at 37°C with 5% $C0_2$ in cell specific media containing 10% fetal calf serum (FCS), 2 mM L-glutamine and 100 U penicillin/streptomycin. Cultures at ~80% confluence were routinely split 1:3 in T75 culture flask as follows. The cells were washed twice in pre-warmed PBS. 1 ml Trypsin was added to the dishes. The dishes were placed at 37°C for 3-5 min. After the cells were detached from the ground, 12 ml pre-warmed culture medium was added to inactivate the Trypsin. 4 ml of the cells were transferred to a new flask and filled up with 9 ml fresh culture medium.

4.1.3 Cryo-preservation of human cell lines

Human cells can be stored in liquid nitrogen after culturing and manipulation. Freezing medium containing DMSO prevents water crystallization and subsequent cell lysis during thawing. This allows long term storage for future experiments.

Human cells were grown to approximately 80% confluence, washed once with PBS and detached by trypsin solution with subsequent inactivation by medium administration. A centrifugation step at 300*g for 5min and 4°C pelleted the cells which were afterwards gathered in 2ml of freezing medium. The cell solution was allocated à 1ml in cryo-vials and cooled in a cryo-container for 24h in a -80°C freezer (cooling frequency of 1°C per h) prior to their long term storage in a liquid nitrogen tank.

4.1.4 Transfection of human cell lines

The used transfection protocols for the corresponding cell lines are summarized in the following table.

Table 8 Seeding density of the cell lines and the corresponding transfection reagent.

cell line	Medium	seeding density per well (*10^3)					transfection reagents	
		96-well	24-well	12-well	6-well	6cm	plasmid DNA	siRNA
WI38	MEM	5	40	80	200	500	Attractene	Hiperfect
HEK293T	DMEM	10	80	120	500	1,200	X-treme Gene9	-
HeLa	DMEM	5	40	80	-	-	PEI	Lipo-fectamine
DU145	RPMI	5	-	-	-	500	-	-
RWPE-1	RPMI	5	-	-	-	500	-	-
LNCAP	RPMI	-	-	-	-	1,200	-	-
PC3	RPMI	5	-	-	-	500	-	-
VCAP	RPMI	-	-	-	-	1,200	-	-

4.1.4.1 Transfection of plasmid DNA

Attractene

The transfection reagent Attractene (Qiagen) shows relatively low cytotoxic side effects and was used in this study to transfect plasmid DNA into the WI38 fibroblast cell line. Cells were seeded in the appropriate cell culture vessel and retained in the incubator for 24h. For the transfection in 6 cm dishes 1 µg of Plasmid DNA was diluted in 175 µl of MEM medium without L-glutamine, FCS and antibiotics and subsequently mixed with 3.75 µl of Attractene reagent. To accomplish liposomal complex formation the mixture was incubated for 15 min at room temperature and added drop-wise onto the seeded cells. After gently swirling for uniform distribution the cells were placed back in the incubator until harvesting. Volumes for other well formats were adapted to the corresponding surface area.

X-tremeGENE9

X-tremeGENE9 (Roche) also exhibits low cytotoxic effects on the cells and was used for transfection of plasmid DNA into HEK293T cells according to the manufacturer's protocol. One day prior transfection cells were seeded in the chosen cell culture vessel. When the cells reached the desired density of 50 - 70% confluency the used medium was removed and replaced with fresh medium without FCS and antibiotics. For the transfection in a 6 cm dishes 6.9 µl of the transfection reagent was added to 2 ml serum-free medium and mixed cautiously by pipetting up and down. The mixture was incubated for 5 min at room temperature. Afterwards 2.3 µg of the DNA was added and the transfection reagent/DNA complex was incubated again at room temperature. After 15 min the transfection reagent/DNA complex was added drop-wise to the cells. The vessels were swirled cautiously to ensure distribution over the entire plate surface. Volumes for other well formats were adapted to the corresponding surface area.

Polyethylenimine (PEI)

The plasmid DNA transfection reagent PEI (Polyethyleneimine) was used for transfection of HeLa cells. Cells were seeded into the appropriate cell culture vessel and grown overnight in complete medium. After 24 h and 40-60% confluency, medium was changed to antibiotics free medium containing FCS. For the transfection in a 24-well plate 0.5 µM of plasmid DNA was mixed with 1.67 µl polyethyleneimine (PEI; 1mg/ml stock) and 50 µl

medium and was incubated for 20 min at room temperature and added drop-wise onto the seeded cells. After 3 h of incubation at 37°C, the medium was replaced with new complete medium. Volumes for other well formats were adapted to the corresponding surface area.

4.1.4.2 Transfection of siRNA

HiPerFect

The siRNA transfection reagent HiPerFect (Qiagen) was used in this study to transfect WI38 cells. The transfection was performed according to the manufacture's protocol. 24 h before transfection cells were seeded in the chosen cell culture vessel. For the transfection in a 6-well plate 20 nM of the siRNA was diluted in 100 µl culture medium without serum and antibiotics. After adding 80 µl HiPerFect Transfection Reagent to the diluted siRNA the mixture was incubated for 20 min at room temperature before adding the complexes drop-wise onto the cells. Volumes for other well formats were adapted to the corresponding surface area.

Lipofectamine LTX

The transfection reagent Lipofectamine LTX is a lipid-based technique for the transfection of siRNA into human cell lines. The transfection was carried out according to the manufacture's manual. In one tube lipofectamine LTX Reagent was diluted in Opti-MEM Medium, in a second tube the same amount of Opti-MEM Medium was used to dilute the DNA together with PLUS reagent. Finally, both tubes were mixed and incubated for 5 min at room temperature and added drop-wise onto the cells. Volumes for other well formats were adapted to the corresponding surface area.

4.1.5 Stimulation and treatment of human cell lines

4.1.5.1 Stimulation with cobalt protoporphyrine (CoPP)

Cells were cultivated as described above in medium containing FCS, antibiotic and L-glutamine. CoPP was dissolved to a final concentration of 10 mM in DMSO and stored at 4°C until use. For the stimulation the indicated amounts of CoPP was added to pre-warmed medium containing FCS, antibiotic and L-glutamine and mixed gently by vortexing. The used medium was removed and the fresh medium containing CoPP was

added to the cells. The vessels were swirled cautiously to ensure distribution over the entire plate surface. The cells were incubated at 37°C and 5% CO_2 until harvesting depending on the experiments.

4.1.5.2 Treatment with the BRD4 inhibitors JQ1 and I-BET 151

Cells were cultivated in their corresponding growth medium containing serum and antibiotics. Both BRD4 inhibitors (JQ1, Cayman Chemical: 1268524-70-4, Ann Arbor, MI, USA) and I-BET151 (Selleck Chemicals, Catalogue No.S2780) were dissolved in DMSO to a final concentration of 10 mM. For treatment the indicated amounts of the inhibitors were added to pre-warmed medium containing FCS, antibiotic and L-glutamine and mixed gently by vortexing. The cells were further cultured at 37°C and 5% CO_2 until harvesting.

4.1.5.3 Treatment with H_2O_2

Hydrogen peroxide was freshly diluted in PBS to a final concentration of 100 µM. The medium of the cultured cells was replaced with medium containing the indicated H_2O_2 concentrations. After 30 min of incubation at 37°C and 5% CO_2 the medium containing H_2O_2 was replaced with fresh medium without H_2O_2. The cells were further cultured at 37°C and 5% CO_2 until harvesting.

4.1.5.4 Heat shock treatment (HS)

The HS treatment was carried out in a cell culture incubator (4h of HS) or in a water bath (<1h of HS). The used medium of the cultured cells was removed and replaced with pre-warmed (42°C or 44°C) fresh medium and incubated for the indicated time at 42°C or 44°C, respectively until harvesting.

4.1.6 Luciferase reporter assay

Luciferase reporter systems are widely used to study eukaryotic gene expression and cellular physiology. Applications include the study of receptor activity, transcription factors, intracellular signalling, mRNA processing and protein folding. In this study the Dual-Luciferase® Reporter Assay System from Promega was used. The term “dual reporter” refers to the simultaneous expression and measurement of two individual reporter enzymes, the firefly and the renilla luciferase. The firefly luciferase reporter was measured first which represents the investigated promoter activity, while the activity of the co-

transfected “control” reporter, the renilla luciferase, provides an internal control that serves as the baseline response. Cells were seeded in 96 -well or 24-well plates, and co-transfected with the indicated luciferase promoter construct and the renilla luciferase plasmid by using the before mentioned transfection protocols. 24 h post transfection the Luciferase activities were measured according to the manufacturer’s protocol. Luciferase activities were normalized to the renilla luciferase activity.

4.1.7 ROS Detection

Cells were seeded in 12-well plates and treated with siRNAs or JQ1 inhibitor at various concentrations. After incubation for 72 h, 10 mM DHR (dihydrorhodamine 123) or 10 mM DHR + 1 mM H_2O_2 was added and incubated for 4 h to determine the levels of oxidative stress products. The absorbance of the green fluorescent rhodamine 123 was measured using an ACCURI C6 cytometer and analyzed with the free available Flowing Software 2 (http://www.flowingsoftware.com/).

4.1.8 Cell viability assay

Cell viability was measured using the Alamar Blue reagent from Life Technologies (Darmstadt, Germany). Cells were seeded in 96-well plates and treated with siRNAs or JQ1 inhibitor. After incubation for 72 h at 37°C, 10 µl of Alamar Blue cell viability reagent was added according to the manufacturer’s instructions, and the resulting fluorescence intensity was read using the fluorescence spectrometer LS55.

4.2 Microbiological methods

4.2.1 Transformation of *E.coli*

Transformation means the infiltration of a plasmid into a bacterial cell. Three different ways to introduce the DNA in the bacterial cell were commonly used: the electronic transformation, the chemical transformation and the transformation by heat shock. The last method was used in this study. Therefore, 5 µl of the ligation (see 4.4.6) or 1 µl of plasmid DNA and about 40 µl of competent bacteria cells were mixed together and incubated for 30 min on ice. After a short heat shock at 42°C for 45 seconds the cells were transferred back on ice for 2 min. 800 µl ml of LB medium was added to the cells.

Subsequently, the cells were incubated at 37°C on a shaker for 30 min to 1 h and then streaked out on LB agar plates containing antibiotics.

4.3 Protein chemical methods

4.3.1 Protein extraction from mammalian cells

The following description is for cell harvesting out of a 6 cm dish. The used medium was removed and cells were washed once with ice-cold PBS (0.14 M NaCl, 3.4 mM KCl, 10 mM Na2HPO4, 1.8 mM KH2PO4 before they were scraped in 1 ml ice-cold PBS. The cells were transferred to an Eppendorf tube and centrifuged for 3 min at 300 g at 4°C. The supernatant was discarded and the pellet was resuspended in 300 µl lysis buffer A (10 mM Hepes-KOH (pH 7.4), 10 mM NaCl, 1 mM DTT, 3 mM $MgCl_2$ and protease inhibitor cocktail (Roche)). The cells were incubated 10 min on ice before they were passed through a needle 10 times. Subsequently, NaCl was added to a final concentration of 300 mM and the lysate was rotated at 4°C for 20 min. After centrifugation for 5 min at 5,000 rpm at 4°C the supernatant was transferred to a new Eppendorf tube. The pellet, which contains insoluble proteins was resuspended in 300 µl lysis buffer B B (10 mM Hepes-KOH (pH 7.4), 300 mM NaCl, 1 mM DTT, 20 mM $MgCl_2$, 0.2 U DNase and Protease Inhibitor cocktail (Roche)) and incubated for 30 min at 37°C. The extract was centrifuged at 5,000 rpm at 4°C for 5 min and the supernatant was combined with the soluble protein fraction.

4.3.2 Protein quantification

To measure and determine protein concentrations the Bradford protein assay is a widely used technique [369]. This method is a sensitive and easy colorimetric assay to detect concentration as low as 1 µg per µl and is based on an absorbance shift of the dye Coomassie Brilliant Blue G-250. The Coomassie Brillant Blue G-250 has an absorption at 470 nm in its cationic (unbound) form. By binding proteins the absorption maximum is switched from 470 nm to 595 nm because of the stabilization of the blue anionic (bound) form of the Coomassie dye. The increase of absorbance at 595 nm is proportional to the amount of protein present in the sample. The protein concentration was determined with the help of a straight calibration line. As standard protein, bovine serum albumin (BSA) was used. Simultaneously, 2 µl of the investigated protein lysates was added to 18 µl H_2O and mixed with 1000 µl Bradford solution. The mixture was incubated for 5 min at room temperature and followed by measuring in a photometer at 595 nm.

4.3.3 SDS-PAGE

SDS-PAGE (sodium dodecyl sulphate polyacrylamide gel electrophoresis) is a method to separate proteins according to their electrophoretic mobility. Proteins were treated with an SDS containing buffer. The anionic detergent SDS denatures secondary and non–disulphide–linked tertiary structures, and applies a negative charge to each protein. The prescence of dithiothreitol (DTT) helps additionally to reduce the disulphide bonds that could provide dimer formation. First, 30 µg the proteins lysates from section 4.3.2 were treated with 4x SDS sample buffer (0.2 M Tris; pH 6.8, 8% (w/v) SDS, 40% (w/v) Glycerine, 0.4% (w/v) Bromphenol blue). The samples were heated up to 95°C for 5 min, helping SDS to bind, centrifuged briefly and loaded onto the SDS gel consisting of a resolving and a stacking gel (Table 9). After the electrophoretic run at 120 V for 90 min in SDS running buffer (0.25 M Glycine, 0.025 M Tris, 0.1% SDS) the proteins were transferred to a polyvinylidene difluoride (PVDF) membrane.

Table 9 Chemicals used for 10% and 12% SDS gels (resolving and stacking gel)

resolving gel (5 ml)	**10%**	**12%**
30% acrylamide	1.62 ml	2.0 ml
1.5 M Tris pH 8.8	1.25 ml	1.25 ml
ddH_2O	2.0 ml	1.62 ml
10% APS	16.25 µl	16.25 µl
TEMED	3.375 µl	3.375 µl

stacking gel (2 ml)	**5%**	**6%**
30% acrylamide	0.33 ml	0.4 ml
0.5 M Tris pH 6.8	0.5ml	0.5ml
ddH_2O	1.165 ml	1.1 ml
10% APS	20 µl	20 µl
TEMED	2 µl	2 µl

4.3.4 Western Blot

To detect specific proteins after SDS –PAGE the tank-blot technique was used. Before transfer, the PVDF membrane was activated in 100% methanol and equilibrated for 10 min in the transfer buffer (25 mM Tris, 192 mM Glycine). The transfer was run for 1 h at 100 V and 375 mA at 4°C. Before the membrane was blocked in 0.5% blocking solution (PBS (0.14 M NaCl, 3.4 mM KCl, 10 mM Na2HPO4, 1.8 mM KH2PO4), 0.5% milk powder) for 1 h at room temperature or over-night at 4°C, it was dried and activated again in methanol. Then the blocked membrane was incubated immediately with the primary antibody, diluted in PBS, over night at 4°C for endogenous proteins or for 1-3 h at room

temperature for recombinant proteins. The dilutions of the used antibodies are shown in Table 15. After repetitive washing steps with PBS-T (PBS containing 0.05% Tween20) the membrane was treated with the secondary antibody, diluted in PBS with 0.5% milk powder, for 1 h, which was coupled to the horse radish peroxidase (HRP). Afterwards the membrane was washed three times with PBS-T and once with PBS to reduce the concentration of the detergent. The proteins of interest were detected using the Western Lighting detection reagent according to manufacturer's protocol and exposed to chemiluminescence films.

4.3.5 Co-Immunoprecipitation

Co-Immunoprecipitation (Co-IP) is a valuable approach to identify physiological protein-protein interactions *in vivo* by using a target protein-specific antibody. The antibody binds its antigen (the target protein) and indirectly the bound interaction partners of the target protein as well. These protein complexes can be analyzed on SDS gel or Western Blot. For endogenous co-immunoprecipitation 500 µg of the lysed cells (see 4.3.1)105 pre-cleared by adding 50 µl protein G Dynabeads to the lysate and incubated for 1 h at 4°C. Subsequently, the bead/lysate emulsion is put on a magnetic rack and the pre-cleared supernatant was incubated with 3 µg of the target protein-specific antibodies over night at 4°C. The next day 10 µl of protein G Dynabeads were washed two times with 0.5% BSA/PBS, blocked with 0.5% BSA/PBS for 1 h and were added to the lysate/antibody mix. After 4 h the beads were washed three times with 0.5% BSA/PBS and concluding one time with PBS. The beads were diluted in 15 µl 1x SDS buffer (see section 4.3.3) and heated up to 95°C for 10 min. For analysis the whole solution was loaded on a SDS gel.

4.3.6 Immunofluorescence

Cells were seeded on cover slips and cultivated as described above at 37°C and 5% CO_2. After treatment, cells were washed twice with cold PBS PBS (0.14 M NaCl, 3.4 mM KCl, 10 mM Na2HPO4, 1.8 mM KH2PO4) and fixed for 30 min or over-night with 100% methanol at -20°C. Then the methanol was aspirated off and the cells were rehydrated in PBS containing 0.03% Triton X-100 at room temperature for 15 min. The cells were blocked for 30 min in PBS supplemented with 3% BSA. After blocking, the cover slips were incubated over night at 4°C with the first antibody, diluted in PBS. After 4 x 5 min washing with PBS containing 0.03% Triton X-100, the cover slips were incubated for 60 min with the secondary antibody, diluted in PBS at room temperature. Immediately after the

removal of the antibody solutions the nuclei were stained with 1µg/ml DAPI for 1 min. After 3 x 5 min washing with PBS containing 0.03% Triton X-100 the cover slips were briefly dip into ddH_20 to rinse of excess PBS and placed on glass slides. The coverslips were sealed with Flouromount-G (Southern Biotech) and stored at 4°C. Analysis of subcellular localizations was performed using a confocal fluorescence microscope (LSM 510 meta, Zeiss) and image analysis was carried out with the Axio vision software.

4.3.7 Quantitative high-content screening microscopy

For quantitative high-content screening microscopy analyses cells were plated at a density of 2000 cells/well in a 96-well imaging plate (Greiner µClear) and treated with a concentration gradient of I-BET or JQ1 as indicated and HS for 1h at 44°C. Cells were immunolabeled as described above and nuclei stained with DAPI (Sigma). Plates were scanned using a Thermo Fisher Cellomics ArrayScan VTI and images of 512x512pixels were acquired and analyzed using Cellomics softare package. Scanning and analyses were performed in the group of Prof. Dr. T. Hucho.

4.3.8 Chromatin-Immunoprecipitation

Chromatin immunoprecipitation, or ChIP, is a powerful method to determine whether a given protein, for example a transcription factor, binds to or is localized to a specific DNA sequence *in vivo*. ChIP was done according to the protocol of Dahl et al. 2009 [370]. Immediately before harvesting the cells sodium butyrate (Sigma-Aldrich) was added to the cell culture medium to a final concentration of 20 mM and mixed gently. The cells were harvested by trypsinization and cross-linked with 1% (v/v) formaldehyde for 10 min at room temperature on a shaker. The cross-link reaction was stopped by adding glycine to a final concentration of 125 mM for 5 min on a shaker. Subsequently, cells were pelleted by centrifugation at 500*g for 10 min. The cell pellet was lysed with 1 ml lysis buffer (50 mM Tris-HCl, 10 mM EDTA, 1% SDS, protease inhibitor cocktail and 20 mM sodium butyrate), by pipetting several times up and down. The chromatin was sheared by sonication using a Bioruptor (Diagenode) to a DNA fragment size of 200–600 bp with following set ups: intensity high, intervals of 10 sec on/off. To the sheared chromatin 1 ml RIPA buffer (10 mM Tris-HCl, 1 mM EDTA, 0.5 mM EGTA, 1% Triton-X100, 0,1% SDS, 0,1% sodium-deoxycholate and 140 mM NaCl) was added and the chromatin was precipitated by centrifugation at 12,000 g at 4°C for 10 min. For immunoprecipitations, 5 µg of each antibody or of a rabbit immunoglobulin G (IgG) control were incubated overnight with the

sheared chromatin. The next day, 50 µl protein G Dynabeads (Life Technologies) were added and incubated for 4 h at 4°C and collecting using a magnetic rack. The antibody/chromatin/beads complexes were washed four times with RIPA and once with TE-buffer (10 mM Tris-HCl, 10 mM EDTA). The entire chromatin was incubated with elution buffer (20 mM Tris-HCl, 5 mM EDTA, 20 mM sodium butyrate, 50 mM NaCl) containing 50 mg/ml proteinase K at 68°C for 2 h. DNA was purified using the Qiagen MinElute columns (Qiagen). For calculation of the enrichment, 300 pg of ChIP and input DNA were analysed using qPCR. The percentage of enrichment was calculated as (2*(CT input - CT IP sample)) × 100/CT input (CT=cycle threshold, IP= immunoprecipitation) and then normalized to the rabbit IgG control.

4.4 Molecular biological methods

4.4.1 Polymerase chain reaction (PCR)

The polymerase chain reaction, short PCR is a method that is used to amplify specific DNA fragments. It is based on the ability of a thermo-stable DNA polymerase to synthesize new strands of DNA complementary to a template strand. First the DNA template was denatured at 95°C, so that the primers were able to bind on their complementary sequence. The temperature for the annealing of the short oligonucleotides of usually 18-22 nucleotides in length, depends on their composition and length. The following formula can be used to calculate the annealing temperature: T_m= 69.3°C+0.41·(GC%) - (650$bp_{(primer)}$). Depending on the used DNA polymerase the annealing temperature has to be modified according to the manufacturer's protocol. The three steps, the denaturation, annealing and elongation, were repeated multiple times to amplify the desired DNA sequence. Table 10 and Table 11 show the pipetting scheme and the PCR program of the different DNA polymerases.

Table 10 Components and PCR protocol for Phusion® High-Fidelity DNA Polymerase (NEB)

Components	Vol. [µl]
Phusion DNA Polymerase	1.0
5x Phusion buffer	10.0
Primer 1 (10 pmol)	1.5
Primer 2 (10 pmol)	1.5
Template (10 – 50 ng)	X
dNTP (10 mM)	1.0
H_2O	ad to 50

Cycle	Temp. [°C]	Time [sec]	Repeat
Initial denaturation	98	30	1x
Denaturation	98	5 - 10	34x
Annealing	x-5	10 - 30	
Extension	72	15 – 30 per kb	
Final extension	72	5 – 10 min	1x

Table 11 Components and PCR protocol for Taq Polymerase (in house preparation)

Components	Vol. [µl]
Taq DNA Polymerase	1.0
10 x Taq buffer	5.0
Primer 1 (10 pmol)	1.25
Primer 2 (10 pmol)	1.25
Template (10 – 50 ng)	X
dNTP (10 mM)	1.0
H_2O	ad to 50

Cycle	Temp. [°C]	Time [min]	Repeat
Initial denaturation	95	2	1x
Denaturation	95	0.5	34x
Annealing	x-2	0.5	
Extension	72	1 min per kb	
Final extension	72	10	1x

4.4.2 Agarose-gel electrophoresis

Gel electrophoresis is used for separation of nucleic acid molecules such as DNA as well as RNA by applying an electric field. The DNA is then visualized in the gel by addition of ethidium bromide. These components binds strongly to DNA by intercalating between the

bases and can be visualized under UV light. For a 1% gel 1 g Agarose was dissolved in 100 ml TAE (0.4 M Tris, 0.2 M Acetate, 0.01 M EDTA) using a microwave. After a short cooling-down, the liquid gel was casted into a gel chamber. Approximately 3 µl of ethidium bromide was added and dispersed equally. Afterwards the combs were placed and the gel was cooled-down completely. Meanwhile the samples were prepared. To the desired volume of the sample 1/5 6x loading dye (Fermentas) was added and mixed. The electrophoresis was run at 90V for approximately 45 min.

4.4.3 Sanger-Sequencing

Sanger sequencing is a method to determine the nucleotide sequence in DNA molecules using the specific amplification by a DNA polymerase and an incorporation of dideoxynucleotides that terminate the strand elongation [371]. All generated constructs were validated by Sanger sequencing by the company Eurofins/MWG Operon.

4.4.4 Gel extraction

Most often for further analysis a desired fragment of DNA has to be isolated from the agarose gel. After DNA samples were run on the agarose gel, the ethidium bromide stained DNA was illuminated with UV light to identify the fragments of interest. The corresponding band was cut out of the gel and extracted using the Zymoclean Gel DNA Recovery Kit according to manufacturer's protocol. The excised gel fragment was weighed, three volumes of buffer ADB added to the gel slice and the gel dissolved for 10 min at 50°C. The solution was loaded Zymo-Spin™ Column in a Collection Tube and centrifuge for 30-60 seconds. 200 µl of DNA Wash Buffer was added to the column and centrifuge for 30 seconds. The flow-through was discarded and the wash step was repeated once. Finally, the DNA was eluted in 30 µl H2O or 10 mM Tris buffer (pH 8.5).

4.4.5 Restriction digest

A restriction digest is a process of cutting DNA molecules with special enzymes, called endonucleases. The enzymes recognize a specific DNA sequence and cut the DNA on specific restriction sites. In a cloning procedure the DNA digest was used to create the same overhangs to insert and vector. Therefore the specific restriction enzymes, the restriction buffer and the plasmid or DNA fragments were mixed together and incubated for 1 h or over-night at 37°C.

4.4.6 Ligation

The ligation is the step in the cloning procedure, where the DNA sequence, or insert, and the vector were connected. The inserts as well as the vectors were digested with specific restriction enzymes which constructed the same overhang. This overhang allows ligating both DNA molecules. The amount of the digested insert depends on the sizes of the fragment and the used vectors and was calculated by the following formula:

$m_{fragment} = 125\ ng \cdot (\frac{bp\ (fragment)}{bp\ (vector)})$.

The calculated amount of insert and 25 ng of the vector were added to 1 µl of T4 DNA ligase and 10 µl of 2x Quick ligase buffer. The mixture was filled up with H_2O to 20 µl and incubated at room temperature for 15 min. To test how many vectors combine without the insertion of the DNA sequence it was recommended to perform an additional control containing the vector and H_2O.

4.4.7 Plasmid-DNA extraction

Plasmid preparation is a method to isolate and purify plasmid DNA from bacteria. In this study the Qiagen Spin Miniprep Kit was used, which is based on the alkaline lysis method. The preparation was carried out according to the manufacturer's protocol. One bacteria colony was inoculated in 3 ml LB medium containing a selective antibiotic and grown for 16 h at 37°C and 160 rpm shaking. The bacteria were pelleted for 1 min at 13,000*g at room temperature and resuspended in 250 µl Buffer P1. The lysate was transferred to a micro-centrifuge tube before adding 250 µl Buffer P2 and mixing thoroughly by inverting the tube gently 4–6 times. The reaction was neutralized using 350 µl buffer N3. The cellular debris was separated by centrifugation for 10 min at 13,000*g at RT and plasmid DNA immobilized on a provided spin column. The DNA was eluted in 50 µl or 10 mM Tris buffer (pH 8.5).

4.4.8 Plasmid DNA extraction for cell culture

In this study the Qiagen Endo-free Plasmid Maxi Kit was used. The Plasmid extraction is based on a modified alkaline lysis procedure, followed by binding of plasmid DNA to Qiagen Anion-Exchange Resin under appropriate low-salt and pH conditions. RNA, proteins, dyes, and low-molecular weight impurities were removed by a medium-salt wash. Plasmid DNA was eluted in a high-salt buffer and then concentrated and desalted by isopropanol precipitation. The preparation was carried out according to manufacturer's

protocol. One bacteria colony was inoculated in a 5 ml starter culture (LB medium with a selective antibiotic), grown for 8-10 h at 37°C and 160 rpm shaking and subsequently diluted 1:750 in 100 ml LB medium with a selective antibiotic for an over-night culture. The bacteria were harvested by centrifugation for 15 min at 6000*g and 4°C, resuspended in buffer P1, lysed with buffer P2 and the reaction neutralized using buffer P3. The cellular debris was removed using a provided filter cartridge and a plunger and the endotoxins in the mixture eliminated by adding buffer ER. The plasmid DNA was immobilized on a column, two washing steps with buffer QC followed and then an elution with buffer QN by gravity flow at room temperature. Addition of isopropanol as well as centrifugation for 30 min at 17,000*g and 4°C precipitated the DNA contained in the solution and after washing (endotoxin-free 70% ethanol) and air-drying at room temperature the pellet was resuspended in 100-500 µl of endotoxin-free buffer TE.

4.4.9 RNA Extraction

The Quick-RNA MicroPrep Kit (Zymo research) enables total RNA preparation in ten min from tissue cultures using small cell numbers. The extraction protocol was performed at room temperature via Fast-Spin columns and without further use of organic solvents, beta-mercaptoethanol and proteases. The protocol was performed following the manufacturer's instructions. The cells were washed once in PBS and harvested in the same using a cell scraper. After pelleting the cells for 5 min at 500*g and 4°C they were lysed by resuspension in 400 µl RNA lysis buffer and afterwards spin for 1min at 13,000*g. The lysate was passed over the first provided spin column (Zymo-Spin IIIC) using a centrifuge for 30 sec at 8,000*g and the flow-through was combined with twice the volume of ethanol for small RNA recovery. The mixture was next passed over the second provided spin column (Zymo-Spin IC) for 1 min at 13,000*g and washed once with 400µl of RNA wash buffer. The remaining DNA was digested on the RNA bound column using DNase I. Therefore, 3 µl of RNase-free DNase I were mixed with 3 µl of 10x reaction buffer and 24 µl of RNA wash buffer and added to the column. After an incubation for 15 min at RT and a centrifugation for 30 sec at 13,000*g, a washing step with 400 µl of RNA prep buffer was performed. Two additional washing steps with 800 µl and 400 µl of RNA wash buffer, respectively, followed. The elution was performed into a new tube using > 6µl of nuclease free water. The concentration of the total RNA solution was determined by a NanoDrop (see section 4.4.10.1).

4.4.10 Quantification of nucleic acids

Spectrophotometers allow for quantification of nucleic acid and protein samples based on absorbance at 260 nm and 280 nm, respectively. In this study two different techniques were used to determine the concentration of nucleic acids.

4.4.10.1 NanoDrop™

A common spectrophotometric instrument used in the laboratory is the NanoDrop™. The sample was pipetted directly onto the measurement surface. The concentration was determined by measuring the optical density at 260 nm for DNA or 230 nm for RNA.

4.4.10.2 Quibit-iT™dsDNA HS assay

Invitrogen's Quant-iT™dsDNA HS Assay Kit enables researchers to quantitate as little as 25 pg/ml of dsDNA with a standard spectrofluorometer utilizing fluorescein excitation and emission wavelengths. The samples were prepared according to the manufacturer's protocol and measured using the Qubit™ fluorometer. The Qubit working solution was prepared containing HS reagent diluted 1:200 in HS buffer. The two DNA standards (Components A and B) as well as the samples were mixed 1:20 and 1:100 to a final volume of 200 µl in the set up working solution, respectively, and incubated for 2 min at room temperature. The fluorescence of the dye was subsequently measured using the Qubit fluorometer and the DNA concentration calculated as described below:

concentration of the sample in ng/ml = the value given by the fluorometer * (200/2)

4.4.11 Reverse transcription

Complementary DNA (cDNA) was generated from RNA using SuperScript II Reverse Transcriptase (Invitrogen) according to the manufacturer's instructions. Template RNAs were adjusted to a concentration of 60 ng/µl. In a 13 µl volume, 300 ng RNA were mixed with 5.6 µl Rnase-free water, 1.4 µl random hexamer primer for reverse transcription of mRNA or FSM13/RSM13 primer for reverse transcription of *Sat III* RNA, and 1 µl of 10 mM each dNTPs. After denaturation of the RNA at 65°C for 5 min, 4 µl 5x first-strand buffer, 1 µl 0.1 M DTT and 1 µl (200 U) of SuperScript II reverse transcriptase were added and mixed gently. Annealing of random primers took place at 25°C for 5 min, following 50°C for 60 min. The reverse transcriptase was heat inactivated at 70°C for 15 min. 1 µl (2 U) of *E.coli* RNase H was added to each sample to remove RNA which is bound to the

cDNA. RNA degradation was carried out at 37°C for 20 min and RNase H was inactivated at 65°C for 20 min. The resulting first-strand cDNA was stored at -80°C.

4.4.12 Quantitative PCR

Quantitative PCR (qPCR) allows the detection and quantification of genomic DNA and cDNA by measuring the intensity of a fluorescence dye during each PCR cycle. The higher the starting copy number of the DNA target, the sooner a significant increase in fluorescence is observed. In this study the SYBR Green dye, a highly specific, double stranded DNA binding dye, was used to detect PCR product as it accumulates during PCR cycles. The qPCR reactions were performed in 10 µl reaction volume composed of 5 ng of the cDNAs, 300 nM primers and 1x SYBR Green PCR Master Mix. The PCR program was performed as followed: 50°C for 2 min, 95°C for 10 min followed by 40 cycles at 94°C for 15 s and 60°C for 1 min. A final melting curve was recorded by cooling the reaction mixture to 60 °C for 15 s and then slowly heating the sample to 95 °C. The calculation of relative expression was carried out using the $\Delta\Delta C_t$ method. Therefore a common threshold value was chosen for all genes. Ct values were first normalized to the corresponding negative control and in second step to an internal control.

4.5 Next generation sequencing methods (NGS)

Next Generation Sequencing describes the high-throughput sequencing technique that allows the determination of the nucleotide sequence in DNA molecules on a high resolution level. In this study the Illumina Sequencing technology is used. This sequencing method is based on the sequencing by synthesis (SBS) technology, first described by Shankar Balasubramanian and David Klenerman at the University of Cambridge in the mid-1990s. It can be used for whole-genome and targeted enrichment-sequencing, transcriptome analysis, methylation profiling, and genome-wide protein-nucleic acid interaction analysis (ChIP).

4.5.1 RNA Sequencing

RNA library preparation and sequencing was performed by the sequencing core facility of the Max-Planck Institute for Molecular Genetics in Berlin on the Illumina HighSeq 2500.

4.5.2 ChIP Sequencing

Sequencing libraries of ChIP DNA (section 4.3.8) were prepared using the Illumina's TrueSeq ChIP- Sample Prep Kit (Illumina) according to manufacturer's instructions. After the generation of phosphorylated blunt ends, the ChIP DNA was purified using the QIAquick PCR Purifcation Kit and used for A-tailing. After purification using the MinElute PCR Purifcation Kit, the adapter ligation was performed and DNA was purified again using the MinElute PCR Purifcation Kit. The DNA size range between 150 and 250 bp was selected on an 2% agarose gel and extracted via the QIAquick

Gel Extraction Kit. In the end, the library was amplified, purifed using the MinElute Gel Extraction Kit and analysed on the Illumina Genome Analyzer IIx (Illumina, San Diego, CA, USA) by the Core Sequencing facility at the Max Planck Insitute for Molecular Geentics.

4.5.3 Bioinformatical analysis

Primary data analyses were performed by Dr. Martin Kerick and lists with counts of reads per genomic regions or RPKM values were provided for further analyses.

4.5.4 Pathway analyses

Pathway analyses were performed either with the over-representation analysis from "ConsensusPathDB" (http://consensuspathdb.org), developed by the Bioinformatics group of the Vertebrate Genomics Department at the Max-Planck-Institute for Molecular Genetics in Berlin, Germany, or with the Ingenuity Pathway Analysis software IPA (IPA®, Qiagen Redwood City, www. qiagen.com/ingenuity).

4.6 Material

4.6.1 Standard equipment

Table 12 Standard equipment and consumables.

Article	Distributor
Benchtop centrifuge 5424	Eppendorf
Centrifuge 5804	Eppendorf
Centrifuge 5810R	Eppendorf
Parafilm	Pechiney Plastic Packaging
pH meter Toledo MP220	Mettler
pipet filter tips TipOne RPT (10µl, 20µl, 200µl, 1250µl)	STARLAB
pipet tips TipOne RPT (10µl, 200µl, 1250µl)	STARLAB
pipetboy Pipetboy acu	IBS Integra biosciences
pipettes (sterile)	Sarstedt
reaction tubes (0.5ml, 1.5ml, 2ml)	Eppendorf
refrigerator economic	Bosch
rocking shaker PMR-30	Grant-Bio
surgical disposable scalpels	BRAUN
vortexer Vortex-Genie2	Scientific Industries

4.6.2 Cell-biological material

Table 13 Material and consumables used for cell-biological methods.

Article	Distributor	Catalogue number
10ml Serological Pipettes	Sarsted	#86.1253.001
25ml Serological Pipettes	Sarsted	#861685.001
5ml Serological Pipettes	Sarsted	#86.1254.001
96-Well Clear-Bottom Plates, Tissue culture treated; White	Fischer Scientific	#07-200-566
ACCURI C6 cytometer	BD Bioscience	
Alamar Blue reagent	Life Technologies	#DAL1025
Attractene	Qiagen	#301005
cell culture dishes 60 cm	TPP	#93060
cell culture flask 75 ml	TPP	#90076
cell culture plates 12-well	TPP	#92412
cell culture plates 24-well	TPP	#92424
cell culture plates 6-well	TPP	#92406
cell culture plates 96-well	TPP	#92496
Cobalt protoporphyrine (CoPP)	Frontier Scientific	#Co654-9
cryo-container "Mr. Frosty"	Nalgene	#5100-0001

Article	Distributor	Catalogue number
Dihydrorhodamine 123 (DHR)	Sigma	#D1054-2MG
DMSO	Sigma	#D8418-100ml
Dual-Luciferase Reporter Assay System	Promega	#E1910
Dulbecco's Modified Eagle's Medium (DMEM)	Biochrom	#F0415
Dulbecco's phosphat buffered saline (DPBS)	Sigma	#D8537
fetal bovine serum (FBS)	Biochrom	#S0113
H_2O_2	Sigma	#H1009
HiPerFect	Qiagen	#301704
I-BET 151	Selleckchem	#S2780
JQ1	Cayman Chemical	#1268524-70-4
L-glutamine solution	Biochrom	#K0283
Lipofectamine LTX	Invitrogen	#15338-100
LS55- Fluorescence Spectrometer	Perkin Elmer	#L2250107
Minimal essential Medium (MEM)	Biochrom	#F0325
Polyethylenimine (PEI)	Polysciences, Inc.	#23966-2
penicillin/streptomycin solution	Biochrom	#A2213
RPMI 1640	Life Technologies	#11875-085
TrypZean solution	Sigma	#T3449
X-tremeGENE9	Roche	#06365779001

4.6.3 Protein chemical material

Table 14 Material and consumables used for protein chemical methods.

Article	Distributor	Catalogue number
acrylamide/bis-acrylamide solution (30%)	Bio-Rad	#161-0154
ammonium persulfate (APS)	Merck	#2300-25GM
Axio Vision software	Zeiss	
bovine serum albumin (BSA)	AppliChem	#A6588,0025
Bradford reagent	Sigma	#B6916-500ML
Bromphenolblue	Sigma	#B-6131
Cell scraper	VWR	#734.2602
Complete Mini EDTA-free	Roche	#1186170001
cover slips	Menzel-Gläser	#CB00120RA1
RNase-free DNase set	Qiagen	#79254
dithiothreitol (DTT)	AppliChem	#A2948.0010
Dynalbeads-Protein G-Beads (magnetic)	Invitrogen	#100.03D
ECL solutions	Perkin Elmer	#NEL105001EA
EDTA	Applichem	#60-00-04
EGTA	Sigma	#E0396

Article	Distributor	Catalogue number
Fluoromount-G	Southern Biotech	#0100-01
formaldehyde solution (37%)	Sigma	#F1635-500ML
Glycerol	Merck	#1.04093.1000
Glycine	Merck	#1.04201.1000
HEPES	Calbiochem	#391338
Hoechst-33258	Sigma	#101200930
IgG	Jackson Immuno Research	#011-000-002
LSM 510 meta	Zeiss	
magnetic rack	Applied Biosystem	#AM10055
methanol	Roth	#00823
$MgCl_2$	Merck	#1.05833
microscope slides	Roth	#H868
MinElute PCR Purication Kit	Qiagen	#28004
Mini-PROTEAN Tetra Electrophoresis System	Biorad	#1658005EDU
NaCl	AppliChem	#A1149.5000
needle		
Page Ruler Plus Pre-stained Protein ladder	Fermentas	#26619
powdered milk	Roth	#T145.1
PowerPac™ Basic Power Supply	Biorad	#1645050
proteinase K	Roche	#3115852004
Polyvinylidenfluorid (PVDF, 0.45 µM)	Thermo Scientific	#88518
SDS	Roth	#4360.1
sodium butyrat	Sigma Aldrich	#303410
tetramethylethylenediamine (TEMED)	Invitrogen	#15524-010
Thermomixer	Eppendorf	
Tris	Roth	#4855.2
Triton-X 100	Sigma	#T8787
Tubes 1.5 ml	Eppendorf	# 0030120094
Tubes 2.0 ml	Eppendorf	# 0030120086
Tween20	Roth	#9127.1
Ultrospec 3000	Pharmacia Biotech	
Whatman (Chromatographypaper)	GE Healthcare	#3001-917

4.6.4 Antibodies

4.6.4.1 Primary antibodies

Antibodies were designed and generated for the detection of specific proteins or their fused tags. The provided list summarizes the used primary antibodies.

Table 15 Primary antibodies. Summary of used primary antibodies, the corresponding dilution for each application as well as the purchasing companies.

antibody	***Catalogue number***	***Distributor***	***dilution***			
			WB	IF	ChIP	Co-IP
BRD4	ab75898	Abcam	1:1000	1:300	5 µg	3 µg
HMOX1	ab13243	Abcam	1:1000	-	-	-
NRF2	sc13032, sc722	Santa Cruz Biotechnology	1:50	1:50	5 µg	-
KEAP1	K2769	Sigma-Aldrich	1:1000	-	-	-
TUBA	T9026	Sigma-Aldrich	1:10000	-	-	-
ACTB		Cell Signalling	1:10000	-	-	-
HSF1	AB1402812	Sigma-Aldrich	1:500	1:200	-	3 µg
anti-FLAG	M2, F7425	Sigma-Aldrich	1:1000	1:500	-	-
SC35	NB100-1774	Novus Biologicals	-	1:500	-	-
XPRESS	R910-25	Invitrogen	1:1000	1:500	-	-

4.6.4.2 Secondary antibodies

Secondary antibodies were generated for the binding to primary antibodies in a species specifc manner and conjugated with an enzyme for chemiluminescence detection or colorimetric staining.

Table 16 Secondary antibodies used in this study.

antibody	**Catalog number**	**Distributor**	**host**	**application**
Mouse IgG	A4416	Sigma-Aldrich	goat	WB
Rabbit IgG	A0545	Sigma-Aldrich	goat	WB
Alexa-488-α-mouse	A-11001	Molecular Probes	goat	IF
Alexa-594-α-rabbit	A-11012	Molecular Probes	goat	IF

4.6.5 Microbiological material

Table 17 Material and consumables for microbiological methods.

Article	Distributor	Catalogue number
Ampicillin	AppliChem	#A0839,0010
LB agar medium	MP Biomedicals,LLC	#3002-232
L-Broth	MP Biomedicals,LLC	#3001-032
Thermomixer	Eppendorf	
DH5α-bacteria	provided from Dr. Sylvia Krobitsch	
Petri dishes	Greiner Bio-One	

4.6.6 Molecular biological material

Table 18 Material and consumables used for molecular biological methods.

Article	Distributor	Catalogue number
7900 HT Fast Real Time PCR System	Applied Biosystems	#4329001
Agarose Standard	Roth	#T846.3
BamHI	Promega	#R6021
BglII	Promega	#R6081
dNTP's	Bioline	#BIO-39025
EDTA Dinatriumsalz Dihydrat (Titrierkomplex III)	Roth	#X986.2
Ethidium bromide	life technologies	#15585011
GeneRuler 100bp DNA Ladder	Fermentas	#SMO249
GeneRuler 1kb DNA Ladder	Fermentas	#SMO319
GoTaq®qPCR Master Mix	Promega	#A6001
HindIII	Promega	#R6041
MicroAmp Optical 384-Well Reaction Plate	Applied Biosystems	#4309849
MinElute PCR Purification Kit	Qiagen	#28006
NanoDrop 2000	ThermoScientific	ND-2000
NotI	Promega	#R6431
Orange DNA Loading Dye Solution (6x)	Fermentas	#R0631
PCR strips	VWR	#732-0545
Phusion DNA Polymerase	life technologies	#F-530L
Qiagen Plasmid Maxi Kit	Qiagen	#12165
Qiagen Spin Miniprep Kit	Qiagen	#12125
Quant-iT dsDNA HS Assay Kit	life technologies	#Q32851
QubitTM fluorometer	life technologies	
Quick ligase buffer	New England Biolabs	#B2200S
Quick-RNA Microprep Kit	Zymo Research	#R1060
thermal cycler PTC-100	MJ Research, Inc.	
Random Hexamere	Metabion	

Article	Distributor	Catalogue number
Ribonuclease H	Promega	#M4281
SalI	Promega	#R6051
SuperScript II Reverse Transcriptase Kit	life technologies	#18064-014
T4 DNA Ligase	New England Biolabs	#M0202S
Taq DNA Polymerase	in house preparation	
Zymoclean DNA Recovery Kit	Zymo Research	#D4001

4.6.6.1 Oligonucleotides

All oligonucleotides were purchased from Metabion.

Oligonucleotides for mRNA expression analyses

Table 19 Oligos used for mRNA expression analyses.

Gene	Sequence name	SEQUENCE
BRD4	BRD4-fwd	5'-AACCTGGCGTTTCCACGGTA-3'
	BRD4-rev	5'-GCCTGCACAGGAGGAGGATT-3'
HMOX1	HMOX1-fwd	5'-AGACGGCTTCAAGCTGGTGAT-3'
	HMOX1-rev	5'-CCTTGTTGCGCTCAATCTCCT-3'
NFE2L2	NRF2-fwd	5'-TACTCCCAGGTTGCCCACAT-3'
	NRF2-rev	5'-AATGTCTGCGCCAAAAGC-3'
KEAP1	KEAP1-fwd	5'-TGGCCAAGCAAGAGGAGTTC-3'
	KEAP1-rev	5'-GGCTGATGAGGGTCACCAGTT-3'
TUBB	TUBB-fwd	5'-GCTGGACCGCATCTCGTGTA-3'
	TUBB-rev	5'-CAGAGTCCATGGTCCCAGGTT-3'
HDAC6	HDAC6-fwd	5'-TGTCTCTGGAGGGTGGCTA-3'
	HDAC6-rev	5'-AGAAGGGTGTGGAGCGAAG-3'
MAPK3	MAPK3-fwd	5'-CCTGGAAGCCATGAGAGATG-3'
	MAPK3-rev	5'-AGGATCTGGTAGAGGAAGTAGC-3'
GSTP1	GSTP1-fwd	5'-CTCTATGGGAAGGACCAGCA-3'
	GSTP1-rev	5'-CCCGCCTCATAGTTGGTGTA-3'
SOD2	SOD2-fwd	5'-TTTGGGTTCTCCACCAC-3'
	SOD2-rev	5'-GTTGGCCAAGGGAGATG-3'
TXN2	TXN2-fwd	5'-GGGCCGAGGTTAGAGAAGAT-3'
	TXN2-rev	5'-CCGCTGACACCTCATACTCA-3'
SESN3	SESN3-fw	5'-GAGCACATTCAGAAACTTGTCA-3'
	SESN3-rev	5'-AGGACCACAGCATGTACCAG-3'
CAT	CAT-fwd	5'-GGGATCCCATATTGTTTCCAT-3'
	CAT-rev	5'-CAGGACGTAGGCTCCAGAAG-3'
GPX1	GPX1-fwd	5'-CGGGACTACACCCAGATGAA-3'
	GPX1-rev	5'-GATGCCCAAACTGGTTGC-3'

Gene	Sequence name	SEQUENCE
MDM2	MDM2-fwd	5'-CTACAGGGACGCCATCGAATC-3'
	MDM2-rev	5'-TCCTGATCCAACCAATCACCTG-3'
HSF1	HSF1-fwd	5'-CCATGAAGCATGAGAATGAG-3'
	HSF1-rev	5'-GCCACTGTCGTTCAGCATCA-3'
HSP70	HSP70-fwd	5'-AGAGCGGAGCCGACAGAG-3'
	HSP70-rev	5'-CACCTTGCCGTGTTGGAAC-3'

Oligonucleotides for ChIP analyses

Table 20 Oligos used for ChIP-qPCR analyses.

associated Gene	Sequence name	Sequence
HMOX1	HMOX1_Prom_fw	5'-GGATTCCAGCAGGTGACATT-3'
	HMOX1_Prom_rev	5'-GTGGGCAACATCAGGAACTT-3'
	HMOX1_E1_fw	5'-GAAGGCGGATTTTGCTAGATTT-3'
	HMOX1_E1_rev	5'-CTCCTGCCTACCATTAAAGCTG-3'
KEAP1	KEAP1_Prom_fw	5'-GAAAGGAGCGGCGATTCTC-3'
	KEAP1_Prom_rev	5'-TGGAAGGGACAGTGAGAAGG-3'
HDAC6	HDAC6_Prom_fw	5'-GCCAGTGTTTCCTGTGTACC-3'
	HDAC6_Prom_rev	5'-GTTGCCACTGGACGTTGG-3'
SESN3	SESN3_Prom_fw	5'-CCCTGCTCAGAAAGGAAGGT-3'
	SESN3_Prom_rev	5'-TGGACGCTAAAACCCTGACT-3'
MAPK3	MAPK3_Prom_fw	5'-CAGGCTGGAGTGTAGTGGTG-3'
	MAPK3_Prom_rev	5'-CACTCGTAGTCCCAGCTCTT-3'
VIM	VIM_Prom_fw	5'-GAAGAGCGAGAGGAGACCAG-3'
	VIM_Prom_rev	5'-CTCCCAGATCACGATTGCAC-3'
NON CODING REGION	NCR-fw	5'-TGCTGTTACTTTTTACAGGGAGTT-3'
	NCR-rev	5'-TTTGAGCAAAATGTTGAAAACAA-3'
GSTP1	GSTP1-fw	5'-GGGACCCTCCAGAAGAGC-3'
	GSTP1-rev	5'-ACTGGTGGCGAAGACTGC-3'
TXN2	TXN2-fw	5'-CCCACAGGGCTCCTACCT-3'
	TXN2-rev	5'-CTGTACCCGGAAGTGACGTT-3'

Oligonucleotides for cloning experiments

Table 21 Oligos used for cloning.

Experiment	*Gene*	Vector	Sequence name	Sequence	Restriction sites
Over-expression	*NFE2L2*	pTL-FlagC	NRF2-fw	5'-GAATGCGGCCGCCATGGCATAAAGCCCTACAGC-3'	Sal
			NRF2-rev	5'-TTACGCGTCGACAGAGCGTCCGCAACCCGACA-3'	Not
	SP1	pTL-FlagC	SP1-fw	5'-TTACGCGTCGACAAGCGACCAAGATCACTCCAT-3'	Sal
			SP1-rev	5'-GAATGCGGCCGCTCAGAAGCCATTGCCACTGATA-3'	Not
	BRD4	pTL-FlagC	BRD4-fw	5'- TTACGCGTCGACATCTGCGGAGAGCGGC -3'	Sal
			BRD4-rev	5'- TAGACTCGAGCGGCCG -3'	Not
	HSF1	pTL-FlagC	HSF1-fw	5'- TTACGCGTCGACGATCTGCCCGTGGGCCC-3'	Sal
			HSF1-rev	5'- GAATGCGGCCGCGGAGACAGTGGGGTCC-3'	Not
Reporter analyses	*HMOX1 Prom*	pGL3-basic	HMOX1-WT-fw	5'-TTTAGATCTCACCAGACCCAGACAGATTTACCT-3'	BglII
			HMOX1-rev	5'-TTTAAGCTTGTGCTGGGCTCGTTCGTGCTGGCT-3'	HindIII
	HMOX1 Prom_367	pGL3-basic	HMOX1-367-fw	5'-TTTAGATCTGAGCCTGCAGCTTCTCAGATTT-3'	BglII
	HMOX1 Prom_228	pGL3-basic	HMOX1-228-fw	5'-TTTAGATCTTATGACTGCTCCTCTCCACCCC-3'	BglII
	HMOX1_ E1_Prom	pGL3-basic	HMOX1-E1fw	5'-ACAATTGGCCCAGTCTATGG-3'	Sal
			HMOX1-E1rev	5'-GGAGTTCAAGACCAGCCTGA-3'	Not

Oligonucleotides for splicing analyses

Table 22 Oligos used for splicing analyses

Experiment	*Gene*	Sequence name	Sequence
Perfectly spliced transcripts	*LMLN*	LMLN_In4_Ex	5'-TCCCACAAGCGATTTCTT-3'
		LMLN_In4_ExEx	5'-GTTTGTTGCACATTGTCTGCTA-3'
		LMLN_In4_ExIn	5'-TCATGTGACATACCTGCTA-3'
	KIAA1462	KIAA1462_In3_Ex	5'-CTCTCTGTGTCCAAGGAC-3'
		KIAA1462_In3_ExEx	5'-CTGCTAGGGTCATAGGAAT-3'
		KIAA1462_In3_ExIn	5'-TGATTCCTCACCTGGGC-3'
	HMOX1	HMOX1_In3_ExIn	5'-GCTTTCAGCTGGTGATGGC-3'
		HMOX1_In3_ExEx	5'-AGACGGCTTCAAGCTGGTGAT-3'
		HMOX1_In3_Ex	5'-CCTTGTTGCGCTCAATCTCCT-3'
	POP1	POP1_In5_ExIn	5'-GTGGAACTCCTACCTCTTTCTG-3'
		POP1_In5_ExEx	5'-GTACGGCTTTCTCCGCCTCTT-3'
		POP1_In5_Ex	5'-CCATGAGCCACAACGTCAAAC-3'
	NFE2L2	NFE2L2_In3_Ex	5'-CAATGTCCTGTTGCATACCGTC-3'
		NFE2L2_In3_ExEx	5'-GACAATGAGGTTTCTTCGGCTACG-3'
		NFE2L2_In3_ExIn	5'-CAATTTTAGGTTTCTTCGGCTACG-3'
		NFE2L2_In2_ExIn	5'-ATCAGGTTGCCCACATTCCC-3'
		NFE2L2_In2_ExEx	5'-TACTCCCAGGTTGCCCACAT-3'
		NFE2L2_In2_Ex	5'-AATGTCTGCGCCAAAAGC-3'
	NA660	NA660_In1_Ex	5'-CCGGTTACATAACTCGTTGCGGG-3'
		NA660_In1_ExEx	5'-CCTCTGTCATTCACACCTCGTGG-3'
		NA660_In1_ExIn	5'-CCGCCACCTCACCTCGTG-3'
HS inhibited transcripts	*EDC4*	EDC4_In2_Ex	5'-GCTCTGCTCAGGTGATA-3'
		EDC4_In2_ExEx	5'-TCTCCTGAGAGACAGATGAC-3'
		EDC4_In2_ExIn	5'-CTCCTAGGTACTCACATGAC-3'
	NOB1	NOB1_In7_Ex	5'-GTTCTGCTGCAGATGGGGCT-3'
		NOB1_In7_ExEx	5'-GGCTCATGTCAGACGTTGTCTTGA-3'
		NOB1_In7_ExIn	5'-CAGGGCACCAGCTACATACTTGA-3'
	HSD17B7	HSD17B7_In4_Ex	5'-CATATGTTCTCCACAGCTGAAGGC-3'
		HSD17B7_In4_ExEx	5'-GCTCCAGTTCCCGAATCAGGAT-3'
		HSD17B7_In4_ExIn	5'-GCCCACAGCTTCTTTACCAGGAT-3'
	BAG3	BAG3_In2_Ex	5'-TCCTCAGAGGTCCCAGTCACC-3'
		BAG3_In2_ExEx	5'-AGACTGGGACCGCTCAGGT-3'
		BAG3_In2_ExIn	5'-GGCCTCTCCTTACCTCAGGTC-3'
	ST13	ST13_In1_Ex	5'-CCGCAAAGTGAACGAGCTTCG-3'
		ST13_In1_ExEx	5'-ACTTTACCACCCATGCTCTCCAC-3'
		ST13_In1_ExIn	5'-CCTGGGTCTCACCTCTCCAC-3'

Experiment	*Gene*	Sequence name	Sequence
	FAM72A	FAM72A_In1_Ex	5'-TGCGACGCCATGTCTACCAA-3'
		FAM72A_In1_ExEx	5'-AAGTCCACTGCGTTGGTAGGA-3'
		FAM72A_In1_ExIn	5'-AGCATGACTTACTTGGTAGGAGGG-3'
	MAML2	MAML2_Ex	5'-GATTCTCCCCAACACGAATTC-3'
		MAML2_Ex_In	5'-CTGTCTTTCAGCTCCAGGGT-3'
		MAML2_Ex_Ex	5'-CTGATTGCGCTCCAGGGTT-3'
	RAI2	RAI2_Ex	5'-GAATTCTGTGTCCAGGCAAG-3'
		RAI2_Ex_In	5'-CTTAACCCAGCAGGCTTC-3'
		RAI2_Ex_Ex	5'-CGGGCTTCCCAGGAAGAAT-3'
BRD4 HS inhibited	*KLHL25*	KLHL25_In2_ExIn	5'-CCAGGGACTCACCTGGCT-3'
		KLHL25_In2_Ex	5'-GCCCTACTCACTTATCCCCACG-3'
		KLHL25_In2_ExEx	5'-CTGAAGGCCGCGGTCTGG-3'
	PITX2	PITX2_In5_Ex	5'-GGACTCTCCTGAGAGCCGAA-3'
		PITX2_In5_ExEx	5'-ATCTTTCTCATTGGCGCCAGG-3'
		PITX2_In5_ExIn	5'-CCTCCCGGCCTTACCATTG-3'
	BCL6	BCL6_In8_Ex	5'-ATCCACACTGGTGAGAAGCCCTAT-3'
		BCL6_In8_ExEx	5'-GCAGGTTACACTTCTCACAATGGT-3'
		BCL6_In8_ExIn	5'-TCAAGAGGCTTACGTACATGGTAAG-3'
	ATF3	ATF3_In1_Ex	5'-GCGCACTGCACAGCTCTC-3'
		ATF3_In1_ExEx	5'-CAGAGACCTGGCCTCCAG-3'
		ATF3_In1_ExIn	5'-TCCAGCGCTCACCTCCAG-3'
		ATF3_In2_Ex	5'-GGATTTTGCTAACCTGACGCCCT-3'
		ATF3_In2_ExEx	5'-TTCAGGGGCTACCTCGGCT-3'
		ATF3_In2_ExIn	5'-TGATAGAACCCACCTCGGCT-3'
	CEP95	CEP95_In5_Ex	5'-GGTGTGTGCTGTGTCTCCAAG-3'
		CEP95_In5_ExEx	5'-TGGGAGGTGCTCCTTGTCTT-3'
		CEP95_In5_ExIn	5'-TGGGAGGTAGCACTTAGTGTCTC-3'
	LIAS	LIAS_In4_Ex	5'-GTATGTGAGGAAGCTCGATGTCCC-3'
		LIAS_In4_ExEx	5'-ATGTGTCACCCATCAACATGATCG-3'
		LIAS_In4_ExIn	5'-GCTGGCCCTACCATGATCG-3'
	EP300	EP300_Ex	5'-GTTGAATGTACAGAGTGCG-3'
		EP300_Ex_In	5'-CGTTAAGACTTACCCAGC-3'
		EP300_Ex_Ex	5'-CACAGACGAATCCAGCAG-3'
	SOD2	SOD2_Ex	5'-TTTGGGTTCTCCACCAC-3'
		SOD2_Ex_In	5'-GCATTTTAACTTTTCAGGAGATG-3'
		SOD2_Ex_Ex	5'-GTTGGCCAAGGGAGATG-3'
	ULK4	ULK4_Ex	5'-AGCCGCTCCAGAGCCC-3'
		ULK4_Ex_In	5'-CCTGCCCTTGCAGATCAC-3'
		ULK4_Ex_Ex	5'-GGGGAGTGTACCTTCAGTATCAC-3'
	SIK3	SIK3_Ex	5'-GAATTTGTTGCTGGAGAATTTG-3'

Experiment	*Gene*	Sequence name	Sequence
		SIK3_Ex_In	5'-TTCCCTTCAGGAGTGTGAG-3'
		SIK3_Ex_In	5'-TTGCAGCAGGAGTGTGAG-3'

4.6.6.2 Vector cards

Mammalian expression vectors

pcDNA4C-His-Max was used for the cloning of *BRD4* for overexpression experiments in cultured human cells. The *BRD4* construct was already available in our work group.

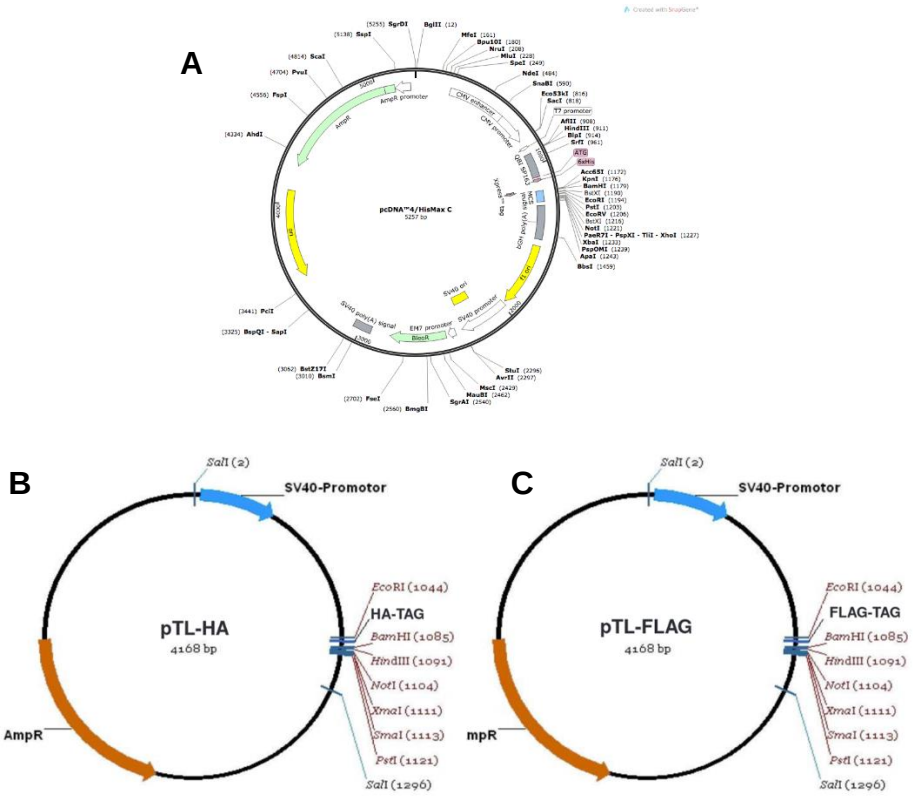

Figure 33 Mammalian expression vectors. **(A)** pcDNA4/His-Max-C is used for protein expression in Mammalia cells. The plasmid contains a 6xHis- and X-press-tag as well as an ampicillin resistance and a CMV promoter. The ~ 5,300 nucleotide long plasmid was purchased from Invitrogen. (**B)** pTL-HA and **(C)** pTL-Flag plasmids were used for protein expression in mammalia cells. They contain a C-terminal HA- and Flag-tag, respectively, an ampicillin resistance and a SV40 promoter. The plasmids were changed by adding a larger multiple cloning site, MCS, with BamHI, HindIII, XhoI, NotI, SmaI, PstI, SacI, KpnI and BglII restriction sites. The ~ 4,200 nucleotide long plasmids were provided by Dr. Sylvia Krobitsch (MPG Berlin). For cloning the following restriction sites were used: XhoI/SalI and NotI.

pTL-Flag was used for the cloning of *BRD4*, *NRF2*, *HSF1* and *SP1* for overexpression experiments in cultured human cells. pTL-HA was used for the cloning of *HSF1* and *HSF2*. These constructs were provided by the collaborating group of Dr. Sylvia Krobitsch.

Mammalian expression of interfering short hairpin RNAs (shRNAs)

shBRD4-1, shBRD4-2 and shCo were already available in the group. BRD4 and GFP (shCo) specific shRNAs had been cloned in pSUPER.retro.puro vectors for knockdown experiments in cultured human cells.

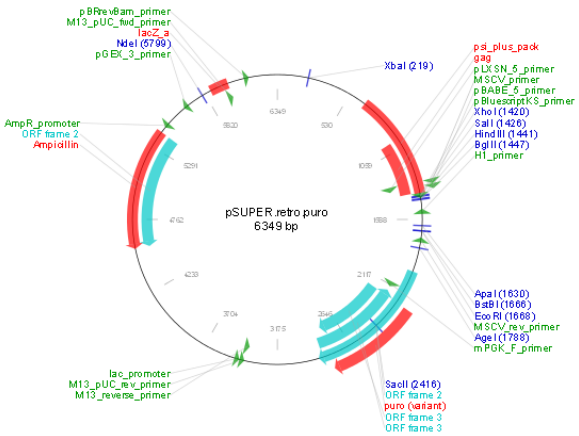

Figure 34 pSuper.retro.puro was used for RNAi experiments in mammalian cells. shBRD4-1, shBRD4-2 and shCo were already available in the group.

Luciferase promoter studies

pGL3-Basic was used for the cloning of *HMOX1* gene promoter fragments for the Dual-Luciferase Reporter Assay System (Promega).

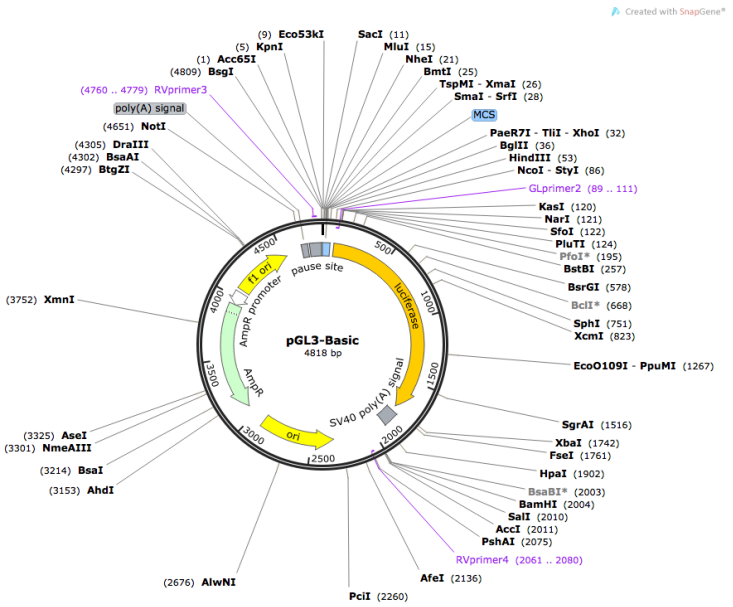

Figure 35 pGL3-basic vector was used for Luciferase reporter analysis. It contains the gene for the firefly luciferase, an ampicillin resistance and restriction sites for BglII and HindIII, which were used for cloning. The ~4,800 nucleotide long plasmid was purchased from Promega.

pRL-TK was used as a normalization plasmid in the Dual-Luciferase Reporter assay System (Promega). It was kindly provided by the collaborating group of Dr. Sylvia Krobitsch.

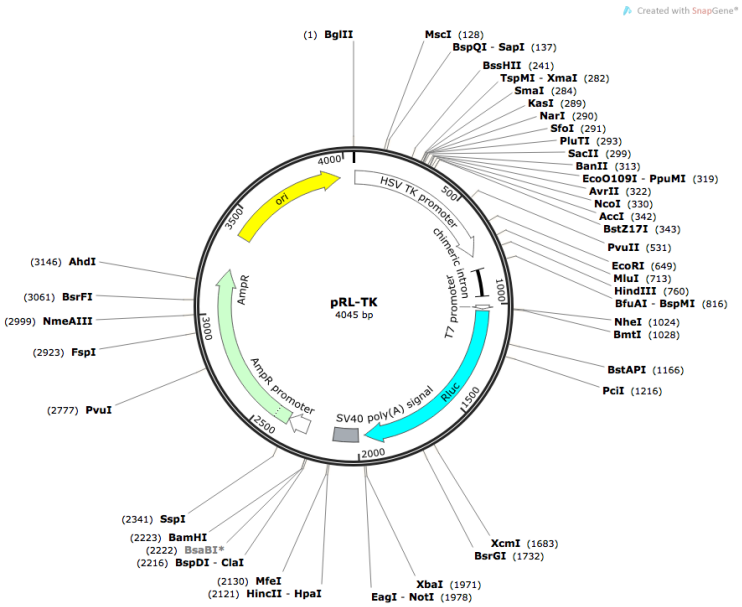

Figure 36 pRL-TK-Renilla-Luciferase was used for Luciferase reporter analysis. The ~ 4,000 nucleotide long plasmid contains a TK and T7 promoter, ampicillin resistance and the renilla luciferase gene.

4.6.7 Next generation sequencing material

Table 23 Material and consumables used for next generation sequencing methods

Article	Distributor	Catalogue number
TruSeq ChIP Sample Prep Kit	Illumina	#IP-202-1012
TruSeq RNA Library Preparation Kit	Illumina	#RS-122-2001
Illumina HighSeq 2500	Illumina	
Illumina Genome Analyzer IIx	Illumina	
MinElute PCR Purifcation Kit	Qiagen	#28004
QIAquick PCR Purifcation Kit	Qiagen	#28104
SuperScript II Reverse Transcriptase Kit	life technologies	#18064-014
MinElute Gel Extraction Kit	Qiagen	#28604

5 References

1. Team EE (2012) WHO launches the World Health Statistics 2012. Eurosurveillance 17: 15-15.

2. Hanahan D, Weinberg RA (2000) The hallmarks of cancer. Cell 100: 57-70.

3. Hanahan D, Weinberg RA (2011) Hallmarks of cancer: the next generation. Cell 144: 646-674.

4. Warburg O (1956) On the origin of cancer cells. Science 123: 309-314.

5. Lopez-Lazaro M (2008) The warburg effect: why and how do cancer cells activate glycolysis in the presence of oxygen? Anticancer Agents Med Chem 8: 305-312.

6. Fearon IM, Faux SP (2009) Oxidative stress and cardiovascular disease: novel tools give (free) radical insight. J Mol Cell Cardiol 47: 372-381.

7. Okamura DM, Himmelfarb J (2009) Tipping the redox balance of oxidative stress in fibrogenic pathways in chronic kidney disease. Pediatr Nephrol 24: 2309-2319.

8. Reddy VP, Zhu X, Perry G, Smith MA (2009) Oxidative stress in diabetes and Alzheimer's disease. J Alzheimers Dis 16: 763-774.

9. Wells PG, McCallum GP, Chen CS, Henderson JT, Lee CJ, et al. (2009) Oxidative stress in developmental origins of disease: teratogenesis, neurodevelopmental deficits, and cancer. Toxicol Sci 108: 4-18.

10. Valko M, Rhodes CJ, Moncol J, Izakovic M, Mazur M (2006) Free radicals, metals and antioxidants in oxidative stress-induced cancer. Chem Biol Interact 160: 1-40.

11. Kim SK, Yang JW, Kim MR, Roh SH, Kim HG, et al. (2008) Increased expression of Nrf2/ARE-dependent anti-oxidant proteins in tamoxifen-resistant breast cancer cells. Free Radic Biol Med 45: 537-546.

12. Ruiz-Ramos R, Lopez-Carrillo L, Rios-Perez AD, De Vizcaya-Ruiz A, Cebrian ME (2009) Sodium arsenite induces ROS generation, DNA oxidative damage, HO-1 and c-Myc proteins, NF-kappaB activation and cell proliferation in human breast cancer MCF-7 cells. Mutat Res 674: 109-115.

13. Mobley JA, Brueggemeier RW (2004) Estrogen receptor-mediated regulation of oxidative stress and DNA damage in breast cancer. Carcinogenesis 25: 3-9.

14. Rao AK, Ziegler YS, McLeod IX, Yates JR, Nardulli AM (2009) Thioredoxin and thioredoxin reductase influence estrogen receptor alpha-mediated gene expression in human breast cancer cells. J Mol Endocrinol 43: 251-261.

15. Khandrika L, Kumar B, Koul S, Maroni P, Koul HK (2009) Oxidative stress in prostate cancer. Cancer Lett 282: 125-136.

16. Frohlich DA, McCabe MT, Arnold RS, Day ML (2008) The role of Nrf2 in increased reactive oxygen species and DNA damage in prostate tumorigenesis. Oncogene 27: 4353-4362.

17. Bhattacharjee S, Rana T, Sengupta A (2007) Inhibition of lipid peroxidation and enhancement of GST activity by cardamom and cinnamon during chemically induced colon carcinogenesis in Swiss albino mice. Asian Pac J Cancer Prev 8: 578-582.

18. Palozza P, Serini S, Torsello A, Di Nicuolo F, Piccioni E, et al. (2003) Beta-carotene regulates NF-kappaB DNA-binding activity by a redox mechanism in human leukemia and colon adenocarcinoma cells. J Nutr 133: 381-388.

19. Hsu WH, Hsieh YS, Kuo HC, Teng CY, Huang HI, et al. (2007) Berberine induces apoptosis in SW620 human colonic carcinoma cells through generation of reactive oxygen species and activation of JNK/p38 MAPK and FasL. Arch Toxicol 81: 719-728.

20. Inokuma T, Haraguchi M, Fujita F, Tajima Y, Kanematsu T (2009) Oxidative stress and tumor progression in colorectal cancer. Hepatogastroenterology 56: 343-347.

21. Huang F, Nie C, Yang Y, Yue W, Ren Y, et al. (2009) Selenite induces redox-dependent Bax activation and apoptosis in colorectal cancer cells. Free Radic Biol Med 46: 1186-1196.

22. Pervaiz S, Clement MV (2004) Tumor intracellular redox status and drug resistance--serendipity or a causal relationship? Curr Pharm Des 10: 1969-1977.

23. Townsend DM, Tew KD (2003) The role of glutathione-S-transferase in anti-cancer drug resistance. Oncogene 22: 7369-7375.

24. Ramanathan B, Jan KY, Chen CH, Hour TC, Yu HJ, et al. (2005) Resistance to paclitaxel is proportional to cellular total antioxidant capacity. Cancer Res 65: 8455-8460.

25. Diehn M, Cho RW, Lobo NA, Kalisky T, Dorie MJ, et al. (2009) Association of reactive oxygen species levels and radioresistance in cancer stem cells. Nature 458: 780-783.

26. Brown NS, Bicknell R (2001) Hypoxia and oxidative stress in breast cancer. Oxidative stress: its effects on the growth, metastatic potential and response to therapy of breast cancer. Breast Cancer Res 3: 323-327.

27. Opazo C, Huang X, Cherny RA, Moir RD, Roher AE, et al. (2002) Metalloenzyme-like activity of Alzheimer's disease beta-amyloid. Cu-dependent catalytic conversion of dopamine, cholesterol, and biological reducing agents to neurotoxic H(2)O(2). J Biol Chem 277: 40302-40308.

28. Lotharius J, Brundin P (2002) Impaired dopamine storage resulting from alpha-synuclein mutations may contribute to the pathogenesis of Parkinson's disease. Hum Mol Genet 11: 2395-2407.

29. Bruijn LI, Houseweart MK, Kato S, Anderson KL, Anderson SD, et al. (1998) Aggregation and motor neuron toxicity of an ALS-linked SOD1 mutant independent from wild-type SOD1. Science 281: 1851-1854.

30. Chircop M, Speidel D (2014) Cellular stress responses in cancer and cancer therapy. Front Oncol 4: 304.

31. Poljsak B, Milisav I (2012) Clinical implications of cellular stress responses. Bosn J Basic Med Sci 12: 122-126.

32. Loschen G, Azzi A, Flohe L (1973) Mitochondrial H2O2 formation: relationship with energy conservation. FEBS Lett 33: 84-87.

33. Birben E, Sahiner UM, Sackesen C, Erzurum S, Kalayci O (2012) Oxidative stress and antioxidant defense. World Allergy Organ J 5: 9-19.

34. Moller P, Wallin H, Knudsen LE (1996) Oxidative stress associated with exercise, psychological stress and life-style factors. Chem Biol Interact 102: 17-36.

35. Esposito F, Ammendola R, Faraonio R, Russo T, Cimino F (2004) Redox control of signal transduction, gene expression and cellular senescence. Neurochem Res 29: 617-628.

36. Dhalla NS, Temsah RM, Netticadan T (2000) Role of oxidative stress in cardiovascular diseases. J Hypertens 18: 655-673.

37. Park HS, Kim SR, Lee YC (2009) Impact of oxidative stress on lung diseases. Respirology 14: 27-38.

38. Maritim AC, Sanders RA, Watkins JB, 3rd (2003) Diabetes, oxidative stress, and antioxidants: a review. J Biochem Mol Toxicol 17: 24-38.

39. Uttara B, Singh AV, Zamboni P, Mahajan RT (2009) Oxidative stress and neurodegenerative diseases: a review of upstream and downstream antioxidant therapeutic options. Curr Neuropharmacol 7: 65-74.

40. Reuter S, Gupta SC, Chaturvedi MM, Aggarwal BB (2010) Oxidative stress, inflammation, and cancer: how are they linked? Free Radic Biol Med 49: 1603-1616.

41. Aykin-Burns N, Ahmad IM, Zhu Y, Oberley LW, Spitz DR (2009) Increased levels of superoxide and H2O2 mediate the differential susceptibility of cancer cells versus normal cells to glucose deprivation. Biochem J 418: 29-37.

42. Visconti R, Grieco D (2009) New insights on oxidative stress in cancer. Curr Opin Drug Discov Devel 12: 240-245.

43. van Wetering S, van Buul JD, Quik S, Mul FP, Anthony EC, et al. (2002) Reactive oxygen species mediate Rac-induced loss of cell-cell adhesion in primary human endothelial cells. J Cell Sci 115: 1837-1846.

44. Storz P (2005) Reactive oxygen species in tumor progression. Front Biosci 10: 1881-1896.

45. Colavitti R, Finkel T (2005) Reactive oxygen species as mediators of cellular senescence. IUBMB Life 57: 277-281.

46. Ushio-Fukai M, Alexander RW (2004) Reactive oxygen species as mediators of angiogenesis signaling: role of NAD(P)H oxidase. Mol Cell Biochem 264: 85-97.

47. Mates JM, Sanchez-Jimenez FM (2000) Role of reactive oxygen species in apoptosis: implications for cancer therapy. Int J Biochem Cell Biol 32: 157-170.

48. McCubrey JA, Steelman LS, Chappell WH, Abrams SL, Wong EW, et al. (2007) Roles of the Raf/MEK/ERK pathway in cell growth, malignant transformation and drug resistance. Biochim Biophys Acta 1773: 1263-1284.

49. Steelman LS, Abrams SL, Whelan J, Bertrand FE, Ludwig DE, et al. (2008) Contributions of the Raf/MEK/ERK, PI3K/PTEN/Akt/mTOR and Jak/STAT pathways to leukemia. Leukemia 22: 686-707.

50. Roberts PJ, Der CJ (2007) Targeting the Raf-MEK-ERK mitogen-activated protein kinase cascade for the treatment of cancer. Oncogene 26: 3291-3310.

51. Wang X, Liu JZ, Hu JX, Wu H, Li YL, et al. (2011) ROS-activated p38 MAPK/ERK-Akt cascade plays a central role in palmitic acid-stimulated hepatocyte proliferation. Free Radic Biol Med 51: 539-551.

52. Chan DW, Liu VW, Tsao GS, Yao KM, Furukawa T, et al. (2008) Loss of MKP3 mediated by oxidative stress enhances tumorigenicity and chemoresistance of ovarian cancer cells. Carcinogenesis 29: 1742-1750.

53. Choi SY, Lim JW, Shimizu T, Kuwano K, Kim JM, et al. (2012) Reactive oxygen species mediate Jak2/Stat3 activation and IL-8 expression in pulmonary epithelial cells stimulated with lipid-associated membrane proteins from Mycoplasma pneumoniae. Inflamm Res 61: 493-501.

54. Ye SF, Wu YH, Hou ZQ, Zhang QQ (2009) ROS and NF-kappaB are involved in upregulation of IL-8 in A549 cells exposed to multi-walled carbon nanotubes. Biochem Biophys Res Commun 379: 643-648.

55. Fay J, Varoga D, Wruck CJ, Kurz B, Goldring MB, et al. (2006) Reactive oxygen species induce expression of vascular endothelial growth factor in chondrocytes and human articular cartilage explants. Arthritis Res Ther 8: R189.

56. Xia C, Meng Q, Liu LZ, Rojanasakul Y, Wang XR, et al. (2007) Reactive oxygen species regulate angiogenesis and tumor growth through vascular endothelial growth factor. Cancer Res 67: 10823-10830.

57. Barnouin K, Dubuisson ML, Child ES, Fernandez de Mattos S, Glassford J, et al. (2002) H2O2 induces a transient multi-phase cell cycle arrest in mouse fibroblasts through modulating cyclin D and p21Cip1 expression. J Biol Chem 277: 13761-13770.

58. Ben Mahdi MH, Andrieu V, Pasquier C (2000) Focal adhesion kinase regulation by oxidative stress in different cell types. IUBMB Life 50: 291-299.

59. Chiarugi P, Pani G, Giannoni E, Taddei L, Colavitti R, et al. (2003) Reactive oxygen species as essential mediators of cell adhesion: the oxidative inhibition of a FAK tyrosine phosphatase is required for cell adhesion. J Cell Biol 161: 933-944.

60. Wu WS, Wu JR, Hu CT (2008) Signal cross talks for sustained MAPK activation and cell migration: the potential role of reactive oxygen species. Cancer Metastasis Rev 27: 303-314.

61. Schreck R, Rieber P, Baeuerle PA (1991) Reactive oxygen intermediates as apparently widely used messengers in the activation of the NF-kappa B transcription factor and HIV-1. EMBO J 10: 2247-2258.

62. McMahon M, Itoh K, Yamamoto M, Hayes JD (2003) Keap1-dependent proteasomal degradation of transcription factor Nrf2 contributes to the negative regulation of antioxidant response element-driven gene expression. J Biol Chem 278: 21592-21600.

63. Andrews NC, Erdjument-Bromage H, Davidson MB, Tempst P, Orkin SH (1993) Erythroid transcription factor NF-E2 is a haematopoietic-specific basic-leucine zipper protein. Nature 362: 722-728.

64. Igarashi K, Kataoka K, Itoh K, Hayashi N, Nishizawa M, et al. (1994) Regulation of transcription by dimerization of erythroid factor NF-E2 p45 with small Maf proteins. Nature 367: 568-572.

65. Motohashi H, Katsuoka F, Engel JD, Yamamoto M (2004) Small Maf proteins serve as transcriptional cofactors for keratinocyte differentiation in the Keap1-Nrf2 regulatory pathway. Proc Natl Acad Sci U S A 101: 6379-6384.

66. Nguyen T, Sherratt PJ, Nioi P, Yang CS, Pickett CB (2005) Nrf2 controls constitutive and inducible expression of ARE-driven genes through a dynamic pathway involving nucleocytoplasmic shuttling by Keap1. J Biol Chem 280: 32485-32492.

67. Moi P, Chan K, Asunis I, Cao A, Kan YW (1994) Isolation of NF-E2-related factor 2 (Nrf2), a NF-E2-like basic leucine zipper transcriptional activator that binds to the tandem NF-E2/AP1 repeat of the beta-globin locus control region. Proc Natl Acad Sci U S A 91: 9926-9930.

68. Venugopal R, Jaiswal AK (1996) Nrf1 and Nrf2 positively and c-Fos and Fra1 negatively regulate the human antioxidant response element-mediated expression of NAD(P)H:quinone oxidoreductase1 gene. Proc Natl Acad Sci U S A 93: 14960-14965.

69. Nguyen T, Sherratt PJ, Huang HC, Yang CS, Pickett CB (2003) Increased protein stability as a mechanism that enhances Nrf2-mediated transcriptional activation of the antioxidant response element. Degradation of Nrf2 by the 26 S proteasome. J Biol Chem 278: 4536-4541.

70. Stewart D, Killeen E, Naquin R, Alam S, Alam J (2003) Degradation of transcription factor Nrf2 via the ubiquitin-proteasome pathway and stabilization by cadmium. J Biol Chem 278: 2396-2402.

71. Zhang DD, Hannink M (2003) Distinct cysteine residues in Keap1 are required for Keap1-dependent ubiquitination of Nrf2 and for stabilization of Nrf2 by chemopreventive agents and oxidative stress. Mol Cell Biol 23: 8137-8151.

72. Itoh K, Wakabayashi N, Katoh Y, Ishii T, O'Connor T, et al. (2003) Keap1 regulates both cytoplasmic-nuclear shuttling and degradation of Nrf2 in response to electrophiles. Genes Cells 8: 379-391.

73. Kobayashi A, Ohta T, Yamamoto M (2004) Unique function of the Nrf2-Keap1 pathway in the inducible expression of antioxidant and detoxifying enzymes. Methods Enzymol 378: 273-286.

74. Zhang DD, Lo SC, Cross JV, Templeton DJ, Hannink M (2004) Keap1 is a redox-regulated substrate adaptor protein for a Cul3-dependent ubiquitin ligase complex. Mol Cell Biol 24: 10941-10953.

75. Cho HY, Jedlicka AE, Reddy SP, Kensler TW, Yamamoto M, et al. (2002) Role of NRF2 in protection against hyperoxic lung injury in mice. Am J Respir Cell Mol Biol 26: 175-182.

76. Lau A, Wang XJ, Zhao F, Villeneuve NF, Wu T, et al. (2010) A noncanonical mechanism of Nrf2 activation by autophagy deficiency: direct interaction between Keap1 and p62. Mol Cell Biol 30: 3275-3285.

77. Apopa PL, He X, Ma Q (2008) Phosphorylation of Nrf2 in the transcription activation domain by casein kinase 2 (CK2) is critical for the nuclear translocation and transcription activation function of Nrf2 in IMR-32 neuroblastoma cells. J Biochem Mol Toxicol 22: 63-76.

78. Jain AK, Jaiswal AK (2006) Phosphorylation of tyrosine 568 controls nuclear export of Nrf2. J Biol Chem 281: 12132-12142.

79. Kaspar JW, Niture SK, Jaiswal AK (2012) Antioxidant-induced INrf2 (Keap1) tyrosine 85 phosphorylation controls the nuclear export and degradation of the INrf2-Cul3-Rbx1 complex to allow normal Nrf2 activation and repression. J Cell Sci 125: 1027-1038.

80. Kawai Y, Garduno L, Theodore M, Yang J, Arinze IJ (2011) Acetylation-deacetylation of the transcription factor Nrf2 (nuclear factor erythroid 2-related factor 2) regulates its transcriptional activity and nucleocytoplasmic localization. J Biol Chem 286: 7629-7640.

81. Sun Z, Chin YE, Zhang DD (2009) Acetylation of Nrf2 by p300/CBP augments promoter-specific DNA binding of Nrf2 during the antioxidant response. Mol Cell Biol 29: 2658-2672.

82. Sporn MB, Liby KT (2012) NRF2 and cancer: the good, the bad and the importance of context. Nat Rev Cancer 12: 564-571.

83. Boutten A, Goven D, Artaud-Macari E, Boczkowski J, Bonay M (2011) NRF2 targeting: a promising therapeutic strategy in chronic obstructive pulmonary disease. Trends Mol Med 17: 363-371.

84. Cho HY, Kleeberger SR (2010) Nrf2 protects against airway disorders. Toxicol Appl Pharmacol 244: 43-56.

85. Aleksunes LM, Goedken MJ, Rockwell CE, Thomale J, Manautou JE, et al. (2010) Transcriptional regulation of renal cytoprotective genes by Nrf2 and its potential use as a therapeutic target to mitigate cisplatin-induced nephrotoxicity. J Pharmacol Exp Ther 335: 2-12.

86. Yoo NJ, Kim HR, Kim YR, An CH, Lee SH (2012) Somatic mutations of the KEAP1 gene in common solid cancers. Histopathology 60: 943-952.

87. Ohta T, Iijima K, Miyamoto M, Nakahara I, Tanaka H, et al. (2008) Loss of Keap1 function activates Nrf2 and provides advantages for lung cancer cell growth. Cancer Res 68: 1303-1309.

88. Konstantinopoulos PA, Spentzos D, Fountzilas E, Francoeur N, Sanisetty S, et al. (2011) Keap1 mutations and Nrf2 pathway activation in epithelial ovarian cancer. Cancer Res 71: 5081-5089.

89. Nioi P, Nguyen T (2007) A mutation of Keap1 found in breast cancer impairs its ability to repress Nrf2 activity. Biochem Biophys Res Commun 362: 816-821.

90. Kim YR, Oh JE, Kim MS, Kang MR, Park SW, et al. (2010) Oncogenic NRF2 mutations in squamous cell carcinomas of oesophagus and skin. J Pathol 220: 446-451.

91. Solis LM, Behrens C, Dong W, Suraokar M, Ozburn NC, et al. (2010) Nrf2 and Keap1 abnormalities in non-small cell lung carcinoma and association with clinicopathologic features. Clin Cancer Res 16: 3743-3753.

92. Shibata T, Ohta T, Tong KI, Kokubu A, Odogawa R, et al. (2008) Cancer related mutations in NRF2 impair its recognition by Keap1-Cul3 E3 ligase and promote malignancy. Proc Natl Acad Sci U S A 105: 13568-13573.

93. Singh A, Misra V, Thimmulappa RK, Lee H, Ames S, et al. (2006) Dysfunctional KEAP1-NRF2 interaction in non-small-cell lung cancer. PLoS Med 3: e420.

94. (2012) Comprehensive genomic characterization of squamous cell lung cancers. Nature 489: 519-525.

95. Shibata T, Kokubu A, Gotoh M, Ojima H, Ohta T, et al. (2008) Genetic alteration of Keap1 confers constitutive Nrf2 activation and resistance to chemotherapy in gallbladder cancer. Gastroenterology 135: 1358-1368, 1368 e1351-1354.

96. Wang R, An J, Ji F, Jiao H, Sun H, et al. (2008) Hypermethylation of the Keap1 gene in human lung cancer cell lines and lung cancer tissues. Biochem Biophys Res Commun 373: 151-154.

97. Burdelski C, Reiswich V, Hube-Magg C, Kluth M, Minner S, et al. (2015) Cytoplasmic Accumulation of Sequestosome 1 (p62) Is a Predictor of Biochemical Recurrence, Rapid Tumor Cell Proliferation, and Genomic Instability in Prostate Cancer. Clin Cancer Res 21: 3471-3479.

98. DeNicola GM, Karreth FA, Humpton TJ, Gopinathan A, Wei C, et al. (2011) Oncogene-induced Nrf2 transcription promotes ROS detoxification and tumorigenesis. Nature 475: 106-109.

99. Lenormand P, Pages G, Sardet C, L'Allemain G, Meloche S, et al. (1993) MAP kinases: activation, subcellular localization and role in the control of cell proliferation. Adv Second Messenger Phosphoprotein Res 28: 237-244.

100. Wolf G (2005) Role of reactive oxygen species in angiotensin II-mediated renal growth, differentiation, and apoptosis. Antioxid Redox Signal 7: 1337-1345.

101. Meloche S, Pouyssegur J (2007) The ERK1/2 mitogen-activated protein kinase pathway as a master regulator of the G1- to S-phase transition. Oncogene 26: 3227-3239.

102. Lee YJ, Cho HN, Soh JW, Jhon GJ, Cho CK, et al. (2003) Oxidative stress-induced apoptosis is mediated by ERK1/2 phosphorylation. Exp Cell Res 291: 251-266.

103. Terry CM, Clikeman JA, Hoidal JR, Callahan KS (1998) Effect of tumor necrosis factor-alpha and interleukin-1 alpha on heme oxygenase-1 expression in human endothelial cells. Am J Physiol 274: H883-891.

104. Torre LA, Bray F, Siegel RL, Ferlay J, Lortet-Tieulent J, et al. (2015) Global cancer statistics, 2012. CA Cancer J Clin 65: 87-108.

105. Fleshner NE, Klotz LH (1998) Diet, androgens, oxidative stress and prostate cancer susceptibility. Cancer Metastasis Rev 17: 325-330.

106. Khor TO, Fuentes F, Shu L, Paredes-Gonzalez X, Yang AY, et al. (2014) Epigenetic DNA methylation of antioxidative stress regulator NRF2 in human prostate cancer. Cancer Prev Res (Phila) 7: 1186-1197.

107. Rylander MN, Feng Y, Zhang Y, Bass J, Jason Stafford R, et al. (2006) Optimizing heat shock protein expression induced by prostate cancer laser therapy through predictive computational models. J Biomed Opt 11: 041113.

108. Hartl FU (1996) Molecular chaperones in cellular protein folding. Nature 381: 571-579.

109. Morimoto RI, Kline MP, Bimston DN, Cotto JJ (1997) The heat-shock response: regulation and function of heat-shock proteins and molecular chaperones. Essays Biochem 32: 17-29.

110. Cornford PA, Dodson AR, Parsons KF, Desmond AD, Woolfenden A, et al. (2000) Heat shock protein expression independently predicts clinical outcome in prostate cancer. Cancer Res 60: 7099-7105.

111. van de Vijver MJ, He YD, van't Veer LJ, Dai H, Hart AA, et al. (2002) A gene-expression signature as a predictor of survival in breast cancer. N Engl J Med 347: 1999-2009.

112. Blagosklonny MV (2001) Re: Role of the heat shock response and molecular chaperones in oncogenesis and cell death. J Natl Cancer Inst 93: 239-240.

113. Kapranos N, Kominea A, Konstantinopoulos PA, Savva S, Artelaris S, et al. (2002) Expression of the 27-kDa heat shock protein (HSP27) in gastric carcinomas and adjacent normal,

metaplastic, and dysplastic gastric mucosa, and its prognostic significance. J Cancer Res Clin Oncol 128: 426-432.

114. Ciocca DR, Jorge AD, Jorge O, Milutin C, Hosokawa R, et al. (1991) Estrogen receptors, progesterone receptors and heat-shock 27-kD protein in liver biopsy specimens from patients with hepatitis B virus infection. Hepatology 13: 838-844.

115. Rocchi P, So A, Kojima S, Signaevsky M, Beraldi E, et al. (2004) Heat shock protein 27 increases after androgen ablation and plays a cytoprotective role in hormone-refractory prostate cancer. Cancer Res 64: 6595-6602.

116. Mestiri S, Bouaouina N, Ahmed SB, Khedhaier A, Jrad BB, et al. (2001) Genetic variation in the tumor necrosis factor-alpha promoter region and in the stress protein hsp70-2: susceptibility and prognostic implications in breast carcinoma. Cancer 91: 672-678.

117. Syrigos KN, Harrington KJ, Karayiannakis AJ, Sekara E, Chatziyianni E, et al. (2003) Clinical significance of heat shock protein-70 expression in bladder cancer. Urology 61: 677-680.

118. Abd el All H, Rey A, Duvillard P (1998) Expression of heat shock protein 70 and c-myc in cervical carcinoma. Anticancer Res 18: 1533-1536.

119. Kurepa J, Wang S, Li Y, Smalle J (2009) Proteasome regulation, plant growth and stress tolerance. Plant Signal Behav 4: 924-927.

120. Bonner JJ, Carlson T, Fackenthal DL, Paddock D, Storey K, et al. (2000) Complex regulation of the yeast heat shock transcription factor. Mol Biol Cell 11: 1739-1751.

121. Mendillo ML, Santagata S, Koeva M, Bell GW, Hu R, et al. (2012) HSF1 drives a transcriptional program distinct from heat shock to support highly malignant human cancers. Cell 150: 549-562.

122. Santagata S, Hu R, Lin NU, Mendillo ML, Collins LC, et al. (2011) High levels of nuclear heat-shock factor 1 (HSF1) are associated with poor prognosis in breast cancer. Proc Natl Acad Sci U S A 108: 18378-18383.

123. Sandqvist A, Bjork JK, Akerfelt M, Chitikova Z, Grichine A, et al. (2009) Heterotrimerization of heat-shock factors 1 and 2 provides a transcriptional switch in response to distinct stimuli. Mol Biol Cell 20: 1340-1347.

124. Hoj A, Jakobsen BK (1994) A short element required for turning off heat shock transcription factor: evidence that phosphorylation enhances deactivation. EMBO J 13: 2617-2624.

125. Hong Y, Rogers R, Matunis MJ, Mayhew CN, Goodson ML, et al. (2001) Regulation of heat shock transcription factor 1 by stress-induced SUMO-1 modification. J Biol Chem 276: 40263-40267.

126. Lis JT, Mason P, Peng J, Price DH, Werner J (2000) P-TEFb kinase recruitment and function at heat shock loci. Genes Dev 14: 792-803.

127. Sarge KD, Murphy SP, Morimoto RI (1993) Activation of heat shock gene transcription by heat shock factor 1 involves oligomerization, acquisition of DNA-binding activity, and nuclear localization and can occur in the absence of stress. Mol Cell Biol 13: 1392-1407.

128. Sengupta S, Parihar R, Ganesh S (2009) Satellite III non-coding RNAs show distinct and stress-specific patterns of induction. Biochem Biophys Res Commun 382: 102-107.

129. Grady DL, Ratliff RL, Robinson DL, McCanlies EC, Meyne J, et al. (1992) Highly conserved repetitive DNA sequences are present at human centromeres. Proc Natl Acad Sci U S A 89: 1695-1699.

130. Jones KW, Prosser J, Corneo G, Ginelli E (1973) The chromosomal location of human satellite DNA 3. Chromosoma 42: 445-451.

131. Valgardsdottir R, Chiodi I, Giordano M, Rossi A, Bazzini S, et al. (2008) Transcription of Satellite III non-coding RNAs is a general stress response in human cells. Nucleic Acids Res 36: 423-434.

132. Biamonti G (2004) Nuclear stress bodies: a heterochromatin affair? Nat Rev Mol Cell Biol 5: 493-498.

133. Jolly C, Metz A, Govin J, Vigneron M, Turner BM, et al. (2004) Stress-induced transcription of satellite III repeats. J Cell Biol 164: 25-33.

134. Rizzi N, Denegri M, Chiodi I, Corioni M, Valgardsdottir R, et al. (2004) Transcriptional activation of a constitutive heterochromatic domain of the human genome in response to heat shock. Mol Biol Cell 15: 543-551.

135. Metz A, Soret J, Vourc'h C, Tazi J, Jolly C (2004) A key role for stress-induced satellite III transcripts in the relocalization of splicing factors into nuclear stress granules. J Cell Sci 117: 4551-4558.

136. Valgardsdottir R, Chiodi I, Giordano M, Cobianchi F, Riva S, et al. (2005) Structural and functional characterization of noncoding repetitive RNAs transcribed in stressed human cells. Mol Biol Cell 16: 2597-2604.

137. Green MR (1986) Pre-mRNA splicing. Annu Rev Genet 20: 671-708.

138. Patel AA, Steitz JA (2003) Splicing double: insights from the second spliceosome. Nat Rev Mol Cell Biol 4: 960-970.

139. Wahl MC, Will CL, Luhrmann R (2009) The spliceosome: design principles of a dynamic RNP machine. Cell 136: 701-718.

140. Will CL, Luhrmann R (2011) Spliceosome structure and function. Cold Spring Harb Perspect Biol 3.

141. Fairbrother WG, Yeh RF, Sharp PA, Burge CB (2002) Predictive identification of exonic splicing enhancers in human genes. Science 297: 1007-1013.

142. Wang Z, Burge CB (2008) Splicing regulation: from a parts list of regulatory elements to an integrated splicing code. RNA 14: 802-813.

143. Mazin P, Xiong J, Liu X, Yan Z, Zhang X, et al. (2013) Widespread splicing changes in human brain development and aging. Mol Syst Biol 9: 633.

144. Pan Q, Shai O, Lee LJ, Frey BJ, Blencowe BJ (2008) Deep surveying of alternative splicing complexity in the human transcriptome by high-throughput sequencing. Nat Genet 40: 1413-1415.

145. Boutz PL, Stoilov P, Li Q, Lin CH, Chawla G, et al. (2007) A post-transcriptional regulatory switch in polypyrimidine tract-binding proteins reprograms alternative splicing in developing neurons. Genes Dev 21: 1636-1652.

146. Makeyev EV, Zhang J, Carrasco MA, Maniatis T (2007) The MicroRNA miR-124 promotes neuronal differentiation by triggering brain-specific alternative pre-mRNA splicing. Mol Cell 27: 435-448.

147. Breitbart RE, Andreadis A, Nadal-Ginard B (1987) Alternative splicing: a ubiquitous mechanism for the generation of multiple protein isoforms from single genes. Annu Rev Biochem 56: 467-495.

148. Kim E, Magen A, Ast G (2007) Different levels of alternative splicing among eukaryotes. Nucleic Acids Res 35: 125-131.

149. Rajan P, Elliott DJ, Robson CN, Leung HY (2009) Alternative splicing and biological heterogeneity in prostate cancer. Nat Rev Urol 6: 454-460.

150. Hsin JP, Manley JL (2012) The RNA polymerase II CTD coordinates transcription and RNA processing. Genes Dev 26: 2119-2137.

151. Ghosh S, Garcia-Blanco MA (2000) Coupled in vitro synthesis and splicing of RNA polymerase II transcripts. RNA 6: 1325-1334.

152. Das R, Dufu K, Romney B, Feldt M, Elenko M, et al. (2006) Functional coupling of RNAP II transcription to spliceosome assembly. Genes Dev 20: 1100-1109.

153. David CJ, Boyne AR, Millhouse SR, Manley JL (2011) The RNA polymerase II C-terminal domain promotes splicing activation through recruitment of a U2AF65-Prp19 complex. Genes Dev 25: 972-983.

154. Yuryev A, Patturajan M, Litingtung Y, Joshi RV, Gentile C, et al. (1996) The C-terminal domain of the largest subunit of RNA polymerase II interacts with a novel set of serine/arginine-rich proteins. Proc Natl Acad Sci U S A 93: 6975-6980.

155. Huang Y, Li W, Yao X, Lin QJ, Yin JW, et al. (2012) Mediator complex regulates alternative mRNA processing via the MED23 subunit. Mol Cell 45: 459-469.

156. Lin S, Coutinho-Mansfield G, Wang D, Pandit S, Fu XD (2008) The splicing factor SC35 has an active role in transcriptional elongation. Nat Struct Mol Biol 15: 819-826.

157. Ji X, Zhou Y, Pandit S, Huang J, Li H, et al. (2013) SR proteins collaborate with 7SK and promoter-associated nascent RNA to release paused polymerase. Cell 153: 855-868.

158. Schmidt U, Basyuk E, Robert MC, Yoshida M, Villemin JP, et al. (2011) Real-time imaging of cotranscriptional splicing reveals a kinetic model that reduces noise: implications for alternative splicing regulation. J Cell Biol 193: 819-829.

159. Schor IE, Gomez Acuna LI, Kornblihtt AR (2013) Coupling between transcription and alternative splicing. Cancer Treat Res 158: 1-24.

160. de la Mata M, Alonso CR, Kadener S, Fededa JP, Blaustein M, et al. (2003) A slow RNA polymerase II affects alternative splicing in vivo. Mol Cell 12: 525-532.

161. Fong N, Bird G, Vigneron M, Bentley DL (2003) A 10 residue motif at the C-terminus of the RNA pol II CTD is required for transcription, splicing and 3' end processing. EMBO J 22: 4274-4282.

162. Hirose Y, Tacke R, Manley JL (1999) Phosphorylated RNA polymerase II stimulates pre-mRNA splicing. Genes Dev 13: 1234-1239.

163. Munoz MJ, de la Mata M, Kornblihtt AR (2010) The carboxy terminal domain of RNA polymerase II and alternative splicing. Trends Biochem Sci 35: 497-504.

164. Kolasinska-Zwierz P, Down T, Latorre I, Liu T, Liu XS, et al. (2009) Differential chromatin marking of introns and expressed exons by H3K36me3. Nat Genet 41: 376-381.

165. Andersson R, Enroth S, Rada-Iglesias A, Wadelius C, Komorowski J (2009) Nucleosomes are well positioned in exons and carry characteristic histone modifications. Genome Res 19: 1732-1741.

166. Schwartz S, Meshorer E, Ast G (2009) Chromatin organization marks exon-intron structure. Nat Struct Mol Biol 16: 990-995.

167. Spies N, Nielsen CB, Padgett RA, Burge CB (2009) Biased chromatin signatures around polyadenylation sites and exons. Mol Cell 36: 245-254.

168. Huff JT, Plocik AM, Guthrie C, Yamamoto KR (2010) Reciprocal intronic and exonic histone modification regions in humans. Nat Struct Mol Biol 17: 1495-1499.

169. Schwartz S, Gal-Mark N, Kfir N, Oren R, Kim E, et al. (2009) Alu exonization events reveal features required for precise recognition of exons by the splicing machinery. PLoS Comput Biol 5: e1000300.

170. Bieberstein NI, Carrillo Oesterreich F, Straube K, Neugebauer KM (2012) First exon length controls active chromatin signatures and transcription. Cell Rep 2: 62-68.

171. Kim S, Kim H, Fong N, Erickson B, Bentley DL (2011) Pre-mRNA splicing is a determinant of histone H3K36 methylation. Proc Natl Acad Sci U S A 108: 13564-13569.

172. Choi JK (2010) Contrasting chromatin organization of CpG islands and exons in the human genome. Genome Biol 11: R70.

173. Li Z, Guo J, Wu Y, Zhou Q (2013) The BET bromodomain inhibitor JQ1 activates HIV latency through antagonizing Brd4 inhibition of Tat-transactivation. Nucleic Acids Res 41: 277-287.

174. Belkina AC, Denis GV (2012) BET domain co-regulators in obesity, inflammation and cancer. Nat Rev Cancer 12: 465-477.

175. Florence B, Faller DV (2001) You bet-cha: a novel family of transcriptional regulators. Front Biosci 6: D1008-1018.

176. Wu SY, Chiang CM (2007) The double bromodomain-containing chromatin adaptor Brd4 and transcriptional regulation. J Biol Chem 282: 13141-13145.

177. Nakamura Y, Umehara T, Nakano K, Jang MK, Shirouzu M, et al. (2007) Crystal structure of the human BRD2 bromodomain: insights into dimerization and recognition of acetylated histone H4. J Biol Chem 282: 4193-4201.

178. Lin YJ, Umehara T, Inoue M, Saito K, Kigawa T, et al. (2008) Solution structure of the extraterminal domain of the bromodomain-containing protein BRD4. Protein Sci 17: 2174-2179.

179. Hassan AH, Awad S, Al-Natour Z, Othman S, Mustafa F, et al. (2007) Selective recognition of acetylated histones by bromodomains in transcriptional co-activators. Biochem J 402: 125-133.

180. Garabedian MV, Noguchi C, Ziegler MA, Das MM, Singh T, et al. (2012) The double-bromodomain proteins Bdf1 and Bdf2 modulate chromatin structure to regulate S-phase stress response in Schizosaccharomyces pombe. Genetics 190: 487-500.

181. Matangkasombut O, Buratowski RM, Swilling NW, Buratowski S (2000) Bromodomain factor 1 corresponds to a missing piece of yeast TFIID. Genes Dev 14: 951-962.

182. Lygerou Z, Conesa C, Lesage P, Swanson RN, Ruet A, et al. (1994) The yeast BDF1 gene encodes a transcription factor involved in the expression of a broad class of genes including snRNAs. Nucleic Acids Res 22: 5332-5340.

183. Volanakis A, Passoni M, Hector RD, Shah S, Kilchert C, et al. (2013) Spliceosome-mediated decay (SMD) regulates expression of nonintronic genes in budding yeast. Genes Dev 27: 2025-2038.

184. Fu J, Hou J, Liu L, Chen L, Wang M, et al. (2013) Interplay between BDF1 and BDF2 and their roles in regulating the yeast salt stress response. FEBS J 280: 1991-2001.

185. Liu X, Yang H, Zhang X, Liu L, Lei M, et al. (2009) Bdf1p deletion affects mitochondrial function and causes apoptotic cell death under salt stress. FEMS Yeast Res 9: 240-246.

186. Florence B, McGinnis W (1998) A genetic screen of the Drosophila X chromosome for mutations that modify Deformed function. Genetics 150: 1497-1511.

187. Digan ME, Haynes SR, Mozer BA, Dawid IB, Forquignon F, et al. (1986) Genetic and molecular analysis of fs(1)h, a maternal effect homeotic gene in Drosophila. Dev Biol 114: 161-169.

188. Kellner WA, Van Bortle K, Li L, Ramos E, Takenaka N, et al. (2013) Distinct isoforms of the Drosophila Brd4 homologue are present at enhancers, promoters and insulator sites. Nucleic Acids Res 41: 9274-9283.

189. Denis GV, Vaziri C, Guo N, Faller DV (2000) RING3 kinase transactivates promoters of cell cycle regulatory genes through E2F. Cell Growth Differ 11: 417-424.

190. Sinha A, Faller DV, Denis GV (2005) Bromodomain analysis of Brd2-dependent transcriptional activation of cyclin A. Biochem J 387: 257-269.

191. LeRoy G, Rickards B, Flint SJ (2008) The double bromodomain proteins Brd2 and Brd3 couple histone acetylation to transcription. Mol Cell 30: 51-60.

192. Shang E, Wang X, Wen D, Greenberg DA, Wolgemuth DJ (2009) Double bromodomain-containing gene Brd2 is essential for embryonic development in mouse. Dev Dyn 238: 908-917.

193. Hnilicova J, Hozeifi S, Stejskalova E, Duskova E, Poser I, et al. (2013) The C-terminal domain of Brd2 is important for chromatin interaction and regulation of transcription and alternative splicing. Mol Biol Cell 24: 3557-3568.

194. Belkina AC, Nikolajczyk BS, Denis GV (2013) BET protein function is required for inflammation: Brd2 genetic disruption and BET inhibitor JQ1 impair mouse macrophage inflammatory responses. J Immunol 190: 3670-3678.

195. Nicodeme E, Jeffrey KL, Schaefer U, Beinke S, Dewell S, et al. (2010) Suppression of inflammation by a synthetic histone mimic. Nature 468: 1119-1123.

196. Lamonica JM, Deng W, Kadauke S, Campbell AE, Gamsjaeger R, et al. (2011) Bromodomain protein Brd3 associates with acetylated GATA1 to promote its chromatin occupancy at erythroid target genes. Proc Natl Acad Sci U S A 108: E159-168.

197. Berkovits BD, Wolgemuth DJ (2011) The first bromodomain of the testis-specific double bromodomain protein Brdt is required for chromocenter organization that is modulated by genetic background. Dev Biol 360: 358-368.

198. Berkovits BD, Wang L, Guarnieri P, Wolgemuth DJ (2012) The testis-specific double bromodomain-containing protein BRDT forms a complex with multiple spliceosome components and is required for mRNA splicing and 3'-UTR truncation in round spermatids. Nucleic Acids Res 40: 7162-7175.

199. Della Rovere F, Airoldi CA, Falasca G, Ghiani A, Fattorini L, et al. (2010) The Arabidopsis BET bromodomain factor GTE4 regulates the mitotic cell cycle. Plant Signal Behav 5: 677-680.

200. Chua YL, Channeliere S, Mott E, Gray JC (2005) The bromodomain protein GTE6 controls leaf development in Arabidopsis by histone acetylation at ASYMMETRIC LEAVES1. Genes Dev 19: 2245-2254.

201. Yang Z, He N, Zhou Q (2008) Brd4 recruits P-TEFb to chromosomes at late mitosis to promote G1 gene expression and cell cycle progression. Mol Cell Biol 28: 967-976.

202. Dey A, Nishiyama A, Karpova T, McNally J, Ozato K (2009) Brd4 marks select genes on mitotic chromatin and directs postmitotic transcription. Mol Biol Cell 20: 4899-4909.

203. Mochizuki K, Nishiyama A, Jang MK, Dey A, Ghosh A, et al. (2008) The bromodomain protein Brd4 stimulates G1 gene transcription and promotes progression to S phase. J Biol Chem 283: 9040-9048.

204. Hargreaves DC, Horng T, Medzhitov R (2009) Control of inducible gene expression by signal-dependent transcriptional elongation. Cell 138: 129-145.

205. Jang MK, Mochizuki K, Zhou M, Jeong HS, Brady JN, et al. (2005) The bromodomain protein Brd4 is a positive regulatory component of P-TEFb and stimulates RNA polymerase II-dependent transcription. Mol Cell 19: 523-534.

206. Reines D, Conaway RC, Conaway JW (1999) Mechanism and regulation of transcriptional elongation by RNA polymerase II. Curr Opin Cell Biol 11: 342-346.

207. Yang Z, Yik JH, Chen R, He N, Jang MK, et al. (2005) Recruitment of P-TEFb for stimulation of transcriptional elongation by the bromodomain protein Brd4. Mol Cell 19: 535-545.

208. Bryant JM, Donahue G, Wang X, Meyer-Ficca M, Luense LJ, et al. (2015) Characterization of BRD4 during mammalian postmeiotic sperm development. Mol Cell Biol 35: 1433-1448.

209. Floyd SR, Pacold ME, Huang Q, Clarke SM, Lam FC, et al. (2013) The bromodomain protein Brd4 insulates chromatin from DNA damage signalling. Nature 498: 246-250.

210. Maruyama T, Farina A, Dey A, Cheong J, Bermudez VP, et al. (2002) A Mammalian bromodomain protein, brd4, interacts with replication factor C and inhibits progression to S phase. Mol Cell Biol 22: 6509-6520.

211. Wang R, Li Q, Helfer CM, Jiao J, You J (2012) Bromodomain protein Brd4 associated with acetylated chromatin is important for maintenance of higher-order chromatin structure. J Biol Chem 287: 10738-10752.

212. Dey A, Ellenberg J, Farina A, Coleman AE, Maruyama T, et al. (2000) A bromodomain protein, MCAP, associates with mitotic chromosomes and affects G(2)-to-M transition. Mol Cell Biol 20: 6537-6549.

213. Nishiyama A, Dey A, Miyazaki J, Ozato K (2006) Brd4 is required for recovery from antimicrotubule drug-induced mitotic arrest: preservation of acetylated chromatin. Mol Biol Cell 17: 814-823.

214. Dey A, Chitsaz F, Abbasi A, Misteli T, Ozato K (2003) The double bromodomain protein Brd4 binds to acetylated chromatin during interphase and mitosis. Proc Natl Acad Sci U S A 100: 8758-8763.

215. Rahman S, Sowa ME, Ottinger M, Smith JA, Shi Y, et al. (2011) The Brd4 extraterminal domain confers transcription activation independent of pTEFb by recruiting multiple proteins, including NSD3. Mol Cell Biol 31: 2641-2652.

216. Liu W, Ma Q, Wong K, Li W, Ohgi K, et al. (2013) Brd4 and JMJD6-associated anti-pause enhancers in regulation of transcriptional pause release. Cell 155: 1581-1595.

217. Heim A, Grimm C, Muller U, Haussler S, Mackeen MM, et al. (2014) Jumonji domain containing protein 6 (Jmjd6) modulates splicing and specifically interacts with arginine-serine-rich (RS) domains of SR- and SR-like proteins. Nucleic Acids Res 42: 7833-7850.

218. Farina A, Hattori M, Qin J, Nakatani Y, Minato N, et al. (2004) Bromodomain protein Brd4 binds to GTPase-activating SPA-1, modulating its activity and subcellular localization. Mol Cell Biol 24: 9059-9069.

219. McPhillips MG, Oliveira JG, Spindler JE, Mitra R, McBride AA (2006) Brd4 is required for e2-mediated transcriptional activation but not genome partitioning of all papillomaviruses. J Virol 80: 9530-9543.

220. Shi J, Whyte WA, Zepeda-Mendoza CJ, Milazzo JP, Shen C, et al. (2013) Role of SWI/SNF in acute leukemia maintenance and enhancer-mediated Myc regulation. Genes Dev 27: 2648-2662.

221. Liu W, Stein P, Cheng X, Yang W, Shao NY, et al. (2014) BRD4 regulates Nanog expression in mouse embryonic stem cells and preimplantation embryos. Cell Death Differ 21: 1950-1960.

222. Pott S, Lieb JD (2015) What are super-enhancers? Nat Genet 47: 8-12.

223. Hnisz D, Abraham BJ, Lee TI, Lau A, Saint-Andre V, et al. (2013) Super-enhancers in the control of cell identity and disease. Cell 155: 934-947.

224. Pulakanti K, Pinello L, Stelloh C, Blinka S, Allred J, et al. (2013) Enhancer transcribed RNAs arise from hypomethylated, Tet-occupied genomic regions. Epigenetics 8: 1303-1320.

225. Loven J, Hoke HA, Lin CY, Lau A, Orlando DA, et al. (2013) Selective inhibition of tumor oncogenes by disruption of super-enhancers. Cell 153: 320-334.

226. Wang CY, Filippakopoulos P (2015) Beating the odds: BETs in disease. Trends Biochem Sci 40: 468-479.

227. Garnier JM, Sharp PP, Burns CJ (2014) BET bromodomain inhibitors: a patent review. Expert Opin Ther Pat 24: 185-199.

228. Prinjha RK, Witherington J, Lee K (2012) Place your BETs: the therapeutic potential of bromodomains. Trends Pharmacol Sci 33: 146-153.

229. Filippakopoulos P, Qi J, Picaud S, Shen Y, Smith WB, et al. (2010) Selective inhibition of BET bromodomains. Nature 468: 1067-1073.

230. Dawson MA, Prinjha RK, Dittmann A, Giotopoulos G, Bantscheff M, et al. (2011) Inhibition of BET recruitment to chromatin as an effective treatment for MLL-fusion leukaemia. Nature 478: 529-533.

231. You J, Croyle JL, Nishimura A, Ozato K, Howley PM (2004) Interaction of the bovine papillomavirus E2 protein with Brd4 tethers the viral DNA to host mitotic chromosomes. Cell 117: 349-360.

232. Ottinger M, Christalla T, Nathan K, Brinkmann MM, Viejo-Borbolla A, et al. (2006) Kaposi's sarcoma-associated herpesvirus LANA-1 interacts with the short variant of BRD4 and releases cells from a BRD4- and BRD2/RING3-induced G1 cell cycle arrest. J Virol 80: 10772-10786.

233. Lin A, Wang S, Nguyen T, Shire K, Frappier L (2008) The EBNA1 protein of Epstein-Barr virus functionally interacts with Brd4. J Virol 82: 12009-12019.

234. Wang X, Li J, Schowalter RM, Jiao J, Buck CB, et al. (2012) Bromodomain protein Brd4 plays a key role in Merkel cell polyomavirus DNA replication. PLoS Pathog 8: e1003021.

235. Venkataraman S, Alimova I, Balakrishnan I, Harris P, Birks DK, et al. (2014) Inhibition of BRD4 attenuates tumor cell self-renewal and suppresses stem cell signaling in MYC driven medulloblastoma. Oncotarget 5: 2355-2371.

236. Bandopadhayay P, Bergthold G, Nguyen B, Schubert S, Gholamin S, et al. (2014) BET bromodomain inhibition of MYC-amplified medulloblastoma. Clin Cancer Res 20: 912-925.

237. Kumar K, Raza SS, Knab LM, Chow CR, Kwok B, et al. (2015) GLI2-dependent c-MYC upregulation mediates resistance of pancreatic cancer cells to the BET bromodomain inhibitor JQ1. Sci Rep 5: 9489.

238. Sahai V, Kumar K, Knab LM, Chow CR, Raza SS, et al. (2014) BET bromodomain inhibitors block growth of pancreatic cancer cells in three-dimensional collagen. Mol Cancer Ther 13: 1907-1917.

239. Wong C, Laddha SV, Tang L, Vosburgh E, Levine AJ, et al. (2014) The bromodomain and extra-terminal inhibitor CPI203 enhances the antiproliferative effects of rapamycin on human neuroendocrine tumors. Cell Death Dis 5: e1450.

240. Sengupta D, Kannan A, Kern M, Moreno MA, Vural E, et al. (2015) Disruption of BRD4 at H3K27Ac-enriched enhancer region correlates with decreased c-Myc expression in Merkel cell carcinoma. Epigenetics 10: 460-466.

241. Shimamura T, Chen Z, Soucheray M, Carretero J, Kikuchi E, et al. (2013) Efficacy of BET bromodomain inhibition in Kras-mutant non-small cell lung cancer. Clin Cancer Res 19: 6183-6192.

242. Zuber J, Shi J, Wang E, Rappaport AR, Herrmann H, et al. (2011) RNAi screen identifies Brd4 as a therapeutic target in acute myeloid leukaemia. Nature 478: 524-528.

243. Bhadury J, Nilsson LM, Muralidharan SV, Green LC, Li Z, et al. (2014) BET and HDAC inhibitors induce similar genes and biological effects and synergize to kill in Myc-induced murine lymphoma. Proc Natl Acad Sci U S A 111: E2721-2730.

244. Wedeh G, Cerny-Reiterer S, Eisenwort G, Herrmann H, Blatt K, et al. (2015) Identification of bromodomain-containing protein-4 as a novel marker and epigenetic target in mast cell leukemia. Leukemia.

245. Segura MF, Fontanals-Cirera B, Gaziel-Sovran A, Guijarro MV, Hanniford D, et al. (2013) BRD4 sustains melanoma proliferation and represents a new target for epigenetic therapy. Cancer Res 73: 6264-6276.

246. Gallagher SJ, Mijatov B, Gunatilake D, Tiffen JC, Gowrishankar K, et al. (2014) The epigenetic regulator I-BET151 induces BIM-dependent apoptosis and cell cycle arrest of human melanoma cells. J Invest Dermatol 134: 2795-2805.

247. Lockwood WW, Zejnullahu K, Bradner JE, Varmus H (2012) Sensitivity of human lung adenocarcinoma cell lines to targeted inhibition of BET epigenetic signaling proteins. Proc Natl Acad Sci U S A 109: 19408-19413.

248. De Raedt T, Beert E, Pasmant E, Luscan A, Brems H, et al. (2014) PRC2 loss amplifies Ras-driven transcription and confers sensitivity to BRD4-based therapies. Nature 514: 247-251.

249. Tang Y, Gholamin S, Schubert S, Willardson MI, Lee A, et al. (2014) Epigenetic targeting of Hedgehog pathway transcriptional output through BET bromodomain inhibition. Nat Med 20: 732-740.

250. Seton-Rogers S (2014) Prostate cancer: BETting on epigenetic therapy. Nat Rev Cancer 14: 384-385.

251. Zhang P, Dong Z, Cai J, Zhang C, Shen Z, et al. (2015) BRD4 promotes tumor growth and epithelial-mesenchymal transition in hepatocellular carcinoma. Int J Immunopathol Pharmacol 28: 36-44.

252. Pastori C, Daniel M, Penas C, Volmar CH, Johnstone AL, et al. (2014) BET bromodomain proteins are required for glioblastoma cell proliferation. Epigenetics 9: 611-620.

253. Lee DH, Qi J, Bradner JE, Said JW, Doan NB, et al. (2015) Synergistic effect of JQ1 and rapamycin for treatment of human osteosarcoma. Int J Cancer 136: 2055-2064.

254. Rodriguez RM, Huidobro C, Urdinguio RG, Mangas C, Soldevilla B, et al. (2012) Aberrant epigenetic regulation of bromodomain BRD4 in human colon cancer. J Mol Med (Berl) 90: 587-595.

255. Hu Y, Zhou J, Ye F, Xiong H, Peng L, et al. (2015) BRD4 inhibitor inhibits colorectal cancer growth and metastasis. Int J Mol Sci 16: 1928-1948.

256. Crawford NP, Alsarraj J, Lukes L, Walker RC, Officewala JS, et al. (2008) Bromodomain 4 activation predicts breast cancer survival. Proc Natl Acad Sci U S A 105: 6380-6385.

257. Shi J, Wang Y, Zeng L, Wu Y, Deng J, et al. (2014) Disrupting the interaction of BRD4 with diacetylated Twist suppresses tumorigenesis in basal-like breast cancer. Cancer Cell 25: 210-225.

258. Yan Y, Yang FQ, Zhang HM, Li J, Li W, et al. (2014) Bromodomain 4 protein is a predictor of survival for urothelial carcinoma of bladder. Int J Clin Exp Pathol 7: 4231-4238.

259. Parikh SA, French CA, Costello BA, Marks RS, Dronca RS, et al. (2013) NUT Midline Carcinoma An Aggressive Intrathoracic Neoplasm. Journal of Thoracic Oncology 8: 1335-1338.

260. Coude MM, Braun T, Berrou J, Dupont M, Bertrand S, et al. (2015) BET inhibitor OTX015 targets BRD2 and BRD4 and decreases c-MYC in acute leukemia cells. Oncotarget 6: 17698-17712.

261. Stewart HJ, Horne GA, Bastow S, Chevassut TJ (2013) BRD4 associates with p53 in DNMT3A-mutated leukemia cells and is implicated in apoptosis by the bromodomain inhibitor JQ1. Cancer Med 2: 826-835.

262. Stratikopoulos EE, Dendy M, Szabolcs M, Khaykin AJ, Lefebvre C, et al. (2015) Kinase and BET Inhibitors Together Clamp Inhibition of PI3K Signaling and Overcome Resistance to Therapy. Cancer Cell 27: 837-851.

263. Fowler T, Ghatak P, Price DH, Conaway R, Conaway J, et al. (2014) Regulation of MYC expression and differential JQ1 sensitivity in cancer cells. PLoS One 9: e87003.

264. Cheng Z, Gong Y, Ma Y, Lu K, Lu X, et al. (2013) Inhibition of BET bromodomain targets genetically diverse glioblastoma. Clin Cancer Res 19: 1748-1759.

265. Gopalakrishnan R, Matta H, Tolani B, Triche T, Jr., Chaudhary PM (2015) Immunomodulatory drugs target IKZF1-IRF4-MYC axis in primary effusion lymphoma in a cereblon-dependent manner and display synergistic cytotoxicity with BRD4 inhibitors. Oncogene.

266. Lenhart R, Kirov S, Desilva H, Cao J, Lei M, et al. (2015) Sensitivity of Small-Cell Lung Cancer to BET Inhibition is Mediated by Regulation of ASCL1 Gene Expression. Mol Cancer Ther.

267. Xu C, Buczkowski KA, Zhang Y, Asahina H, Beauchamp EM, et al. (2015) NSCLC Driven by DDR2 Mutation is Sensitive to Dasatinib and JQ1 Combination Therapy. Mol Cancer Ther.

268. Sun B, Shah B, Fiskus W, Qi J, Rajapakshe K, et al. (2015) Synergistic activity of BET protein antagonist-based combinations in mantle cell lymphoma cells sensitive or resistant to ibrutinib. Blood.

269. Henssen A, Thor T, Odersky A, Heukamp L, El-Hindy N, et al. (2013) BET bromodomain protein inhibition is a therapeutic option for medulloblastoma. Oncotarget 4: 2080-2095.

270. Long J, Li B, Rodriguez-Blanco J, Pastori C, Volmar CH, et al. (2014) The BET bromodomain inhibitor I-BET151 acts downstream of smoothened protein to abrogate the growth of hedgehog protein-driven cancers. J Biol Chem 289: 35494-35502.

271. Heinemann A, Cullinane C, De Paoli-Iseppi R, Wilmott JS, Gunatilake D, et al. (2015) Combining BET and HDAC inhibitors synergistically induces apoptosis of melanoma and suppresses AKT and YAP signaling. Oncotarget.

272. Wyspianska BS, Bannister AJ, Barbieri I, Nangalia J, Godfrey A, et al. (2014) BET protein inhibition shows efficacy against JAK2V617F-driven neoplasms. Leukemia 28: 88-97.

273. Patel AJ, Liao CP, Chen Z, Liu C, Wang Y, et al. (2014) BET bromodomain inhibition triggers apoptosis of NF1-associated malignant peripheral nerve sheath tumors through Bim induction. Cell Rep 6: 81-92.

274. Siegel MB, Liu SQ, Davare MA, Spurgeon SE, Loriaux MM, et al. (2015) Small molecule inhibitor screen identifies synergistic activity of the bromodomain inhibitor CPI203 and bortezomib in drug resistant myeloma. Oncotarget 6: 18921-18932.

275. Wang R, Liu W, Helfer CM, Bradner JE, Hornick JL, et al. (2014) Activation of SOX2 expression by BRD4-NUT oncogenic fusion drives neoplastic transformation in NUT midline carcinoma. Cancer Res 74: 3332-3343.

276. Baker EK, Taylor S, Gupte A, Sharp PP, Walia M, et al. (2015) BET inhibitors induce apoptosis through a MYC independent mechanism and synergise with CDK inhibitors to kill osteosarcoma cells. Sci Rep 5: 10120.

277. Lamoureux F, Baud'huin M, Rodriguez Calleja L, Jacques C, Berreur M, et al. (2014) Selective inhibition of BET bromodomain epigenetic signalling interferes with the bone-associated tumor vicious cycle. Nat Commun 5: 3511.

278. Baratta MG, Schinzel AC, Zwang Y, Bandopadhayay P, Bowman-Colin C, et al. (2015) An in-tumor genetic screen reveals that the BET bromodomain protein, BRD4, is a potential therapeutic target in ovarian carcinoma. Proc Natl Acad Sci U S A 112: 232-237.

279. Lochrin SE, Price DK, Figg WD (2014) BET bromodomain inhibitors--a novel epigenetic approach in castration-resistant prostate cancer. Cancer Biol Ther 15: 1583-1585.

280. Patel MC, Debrosse M, Smith M, Dey A, Huynh W, et al. (2013) BRD4 coordinates recruitment of pause release factor P-TEFb and the pausing complex NELF/DSIF to regulate transcription elongation of interferon-stimulated genes. Mol Cell Biol 33: 2497-2507.

281. Huang B, Yang XD, Zhou MM, Ozato K, Chen LF (2009) Brd4 coactivates transcriptional activation of NF-kappaB via specific binding to acetylated RelA. Mol Cell Biol 29: 1375-1387.

282. Ai N, Hu X, Ding F, Yu B, Wang H, et al. (2011) Signal-induced Brd4 release from chromatin is essential for its role transition from chromatin targeting to transcriptional regulation. Nucleic Acids Res 39: 9592-9604.

283. Schweiger MR, Ottinger M, You J, Howley PM (2007) Brd4-independent transcriptional repression function of the papillomavirus e2 proteins. J Virol 81: 9612-9622.

284. Kamburov A, Wierling C, Lehrach H, Herwig R (2009) ConsensusPathDB--a database for integrating human functional interaction networks. Nucleic Acids Res 37: D623-628.

285. Shan Y, Lambrecht RW, Donohue SE, Bonkovsky HL (2006) Role of Bach1 and Nrf2 in up-regulation of the heme oxygenase-1 gene by cobalt protoporphyrin. FASEB J 20: 2651-2653.

286. Bailey TL, Elkan C (1994) Fitting a mixture model by expectation maximization to discover motifs in biopolymers. Proc Int Conf Intell Syst Mol Biol 2: 28-36.

287. Borno ST, Fischer A, Kerick M, Falth M, Laible M, et al. (2012) Genome-wide DNA methylation events in TMPRSS2-ERG fusion-negative prostate cancers implicate an EZH2-dependent mechanism with miR-26a hypermethylation. Cancer Discov 2: 1024-1035.

288. Kumar B, Koul S, Khandrika L, Meacham RB, Koul HK (2008) Oxidative stress is inherent in prostate cancer cells and is required for aggressive phenotype. Cancer Res 68: 1777-1785.

289. Schneider CA, Rasband WS, Eliceiri KW (2012) NIH Image to ImageJ: 25 years of image analysis. Nat Methods 9: 671-675.

290. Alaoui-Jamali MA, Bismar TA, Gupta A, Szarek WA, Su J, et al. (2009) A novel experimental heme oxygenase-1-targeted therapy for hormone-refractory prostate cancer. Cancer Res 69: 8017-8024.

291. Wang ET, Sandberg R, Luo S, Khrebtukova I, Zhang L, et al. (2008) Alternative isoform regulation in human tissue transcriptomes. Nature 456: 470-476.

292. Quesada V, Conde L, Villamor N, Ordonez GR, Jares P, et al. (2012) Exome sequencing identifies recurrent mutations of the splicing factor SF3B1 gene in chronic lymphocytic leukemia. Nat Genet 44: 47-52.

293. Yoshida K, Sanada M, Shiraishi Y, Nowak D, Nagata Y, et al. (2011) Frequent pathway mutations of splicing machinery in myelodysplasia. Nature 478: 64-69.

294. Wang L, Lawrence MS, Wan Y, Stojanov P, Sougnez C, et al. (2011) SF3B1 and other novel cancer genes in chronic lymphocytic leukemia. N Engl J Med 365: 2497-2506.

295. Graubert TA, Shen D, Ding L, Okeyo-Owuor T, Lunn CL, et al. (2012) Recurrent mutations in the U2AF1 splicing factor in myelodysplastic syndromes. Nat Genet 44: 53-57.

296. Kanno T, Kanno Y, LeRoy G, Campos E, Sun HW, et al. (2014) BRD4 assists elongation of both coding and enhancer RNAs by interacting with acetylated histones. Nat Struct Mol Biol 21: 1047-1057.

297. Pastori C, Kapranov P, Penas C, Peschansky V, Volmar CH, et al. (2015) The Bromodomain protein BRD4 controls HOTAIR, a long noncoding RNA essential for glioblastoma proliferation. Proc Natl Acad Sci U S A 112: 8326-8331.

298. Diamant G, Dikstein R (2013) Transcriptional control by NF-kappaB: elongation in focus. Biochim Biophys Acta 1829: 937-945.

299. Ott CJ, Kopp N, Bird L, Paranal RM, Qi J, et al. (2012) BET bromodomain inhibition targets both c-Myc and IL7R in high-risk acute lymphoblastic leukemia. Blood 120: 2843-2852.

300. Fiaschi T, Chiarugi P (2012) Oxidative stress, tumor microenvironment, and metabolic reprogramming: a diabolic liaison. Int J Cell Biol 2012: 762825.

301. Gullett NP, Ruhul Amin AR, Bayraktar S, Pezzuto JM, Shin DM, et al. (2010) Cancer prevention with natural compounds. Semin Oncol 37: 258-281.

302. Xia Z, Dickens M, Raingeaud J, Davis RJ, Greenberg ME (1995) Opposing effects of ERK and JNK-p38 MAP kinases on apoptosis. Science 270: 1326-1331.

303. Zhu X, Assoian RK (1995) Integrin-dependent activation of MAP kinase: a link to shape-dependent cell proliferation. Mol Biol Cell 6: 273-282.

304. Lee DS, Kim KS, Ko W, Li B, Jeong GS, et al. (2014) The cytoprotective effect of sulfuretin against tert-butyl hydroperoxide-induced hepatotoxicity through Nrf2/ARE and JNK/ERK MAPK-mediated heme oxygenase-1 expression. Int J Mol Sci 15: 8863-8877.

305. Lee KM, Kang K, Lee SB, Nho CW (2013) Nuclear factor-E2 (Nrf2) is regulated through the differential activation of ERK1/2 and PKC alpha/betaII by Gymnasterkoreayne B. Cancer Lett 330: 225-232.

306. Gao AM, Ke ZP, Shi F, Sun GC, Chen H (2013) Chrysin enhances sensitivity of BEL-7402/ADM cells to doxorubicin by suppressing PI3K/Akt/Nrf2 and ERK/Nrf2 pathway. Chem Biol Interact 206: 100-108.

307. Haupt Y, Maya R, Kazaz A, Oren M (1997) Mdm2 promotes the rapid degradation of p53. Nature 387: 296-299.

308. Sablina AA, Budanov AV, Ilyinskaya GV, Agapova LS, Kravchenko JE, et al. (2005) The antioxidant function of the p53 tumor suppressor. Nat Med 11: 1306-1313.

309. Tan M, Li S, Swaroop M, Guan K, Oberley LW, et al. (1999) Transcriptional activation of the human glutathione peroxidase promoter by p53. J Biol Chem 274: 12061-12066.

310. Faraonio R, Vergara P, Di Marzo D, Pierantoni MG, Napolitano M, et al. (2006) p53 suppresses the Nrf2-dependent transcription of antioxidant response genes. J Biol Chem 281: 39776-39784.

311. Wade M, Li YC, Wahl GM (2013) MDM2, MDMX and p53 in oncogenesis and cancer therapy. Nat Rev Cancer 13: 83-96.

312. Zhang P, Singh A, Yegnasubramanian S, Esopi D, Kombairaju P, et al. (2010) Loss of Kelch-like ECH-associated protein 1 function in prostate cancer cells causes chemoresistance and radioresistance and promotes tumor growth. Mol Cancer Ther 9: 336-346.

313. Singh A, Bodas M, Wakabayashi N, Bunz F, Biswal S (2010) Gain of Nrf2 function in non-small-cell lung cancer cells confers radioresistance. Antioxid Redox Signal 13: 1627-1637.

314. Taguchi K, Motohashi H, Yamamoto M (2011) Molecular mechanisms of the Keap1-Nrf2 pathway in stress response and cancer evolution. Genes Cells 16: 123-140.

315. Uruno A, Motohashi H (2011) The Keap1-Nrf2 system as an in vivo sensor for electrophiles. Nitric Oxide 25: 153-160.

316. Kobayashi M, Li L, Iwamoto N, Nakajima-Takagi Y, Kaneko H, et al. (2009) The antioxidant defense system Keap1-Nrf2 comprises a multiple sensing mechanism for responding to a wide range of chemical compounds. Mol Cell Biol 29: 493-502.

317. Shapiro TA, Fahey JW, Dinkova-Kostova AT, Holtzclaw WD, Stephenson KK, et al. (2006) Safety, tolerance, and metabolism of broccoli sprout glucosinolates and isothiocyanates: a clinical phase I study. Nutr Cancer 55: 53-62.

318. Hong F, Freeman ML, Liebler DC (2005) Identification of sensor cysteines in human Keap1 modified by the cancer chemopreventive agent sulforaphane. Chem Res Toxicol 18: 1917-1926.

319. Shankar S, Ganapathy S, Srivastava RK (2008) Sulforaphane enhances the therapeutic potential of TRAIL in prostate cancer orthotopic model through regulation of apoptosis, metastasis, and angiogenesis. Clin Cancer Res 14: 6855-6866.

320. Singh AV, Xiao D, Lew KL, Dhir R, Singh SV (2004) Sulforaphane induces caspase-mediated apoptosis in cultured PC-3 human prostate cancer cells and retards growth of PC-3 xenografts in vivo. Carcinogenesis 25: 83-90.

321. Lawson TE, Redlak MJ, Yager DR (2011) Preconditioning with cobalt protoporphyrin protects human gastric mucosal cells from deoxycholate-induced apoptosis. Wound Repair Regen 19: 241-249.

322. Fowler T, Sen R, Roy AL (2011) Regulation of primary response genes. Mol Cell 44: 348-360.

323. Szatrowski TP, Nathan CF (1991) Production of large amounts of hydrogen peroxide by human tumor cells. Cancer Res 51: 794-798.

324. Patel BP, Rawal UM, Dave TK, Rawal RM, Shukla SN, et al. (2007) Lipid peroxidation, total antioxidant status, and total thiol levels predict overall survival in patients with oral squamous cell carcinoma. Integr Cancer Ther 6: 365-372.

325. Tsao SM, Yin MC, Liu WH (2007) Oxidant stress and B vitamins status in patients with non-small cell lung cancer. Nutr Cancer 59: 8-13.

326. Oberley TD, Oberley LW (1997) Antioxidant enzyme levels in cancer. Histol Histopathol 12: 525-535.

327. Hu Y, Rosen DG, Zhou Y, Feng L, Yang G, et al. (2005) Mitochondrial manganese-superoxide dismutase expression in ovarian cancer: role in cell proliferation and response to oxidative stress. J Biol Chem 280: 39485-39492.

328. Saydam N, Kirb A, Demir O, Hazan E, Oto O, et al. (1997) Determination of glutathione, glutathione reductase, glutathione peroxidase and glutathione S-transferase levels in human lung cancer tissues. Cancer Lett 119: 13-19.

329. Murawaki Y, Tsuchiya H, Kanbe T, Harada K, Yashima K, et al. (2008) Aberrant expression of selenoproteins in the progression of colorectal cancer. Cancer Lett 259: 218-230.

330. van Hogerlinden M, Rozell BL, Ahrlund-Richter L, Toftgard R (1999) Squamous cell carcinomas and increased apoptosis in skin with inhibited Rel/nuclear factor-kappaB signaling. Cancer Res 59: 3299-3303.

331. Marullo R, Werner E, Degtyareva N, Moore B, Altavilla G, et al. (2013) Cisplatin induces a mitochondrial-ROS response that contributes to cytotoxicity depending on mitochondrial redox status and bioenergetic functions. PLoS One 8: e81162.

332. Asangani IA, Dommeti VL, Wang X, Malik R, Cieslik M, et al. (2014) Therapeutic targeting of BET bromodomain proteins in castration-resistant prostate cancer. Nature 510: 278-282.

333. Jayakumar S, Kunwar A, Sandur SK, Pandey BN, Chaubey RC (2014) Differential response of DU145 and PC3 prostate cancer cells to ionizing radiation: role of reactive oxygen species, GSH and Nrf2 in radiosensitivity. Biochim Biophys Acta 1840: 485-494.

334. Hoshida Y, Moriyama M, Otsuka M, Kato N, Taniguchi H, et al. (2007) Gene expressions associated with chemosensitivity in human hepatoma cells. Hepatogastroenterology 54: 489-492.

335. Cui W, Bai Y, Miao X, Luo P, Chen Q, et al. (2012) Prevention of diabetic nephropathy by sulforaphane: possible role of Nrf2 upregulation and activation. Oxid Med Cell Longev 2012: 821936.

336. Kensler TW, Egner PA, Agyeman AS, Visvanathan K, Groopman JD, et al. (2013) Keap1-nrf2 signaling: a target for cancer prevention by sulforaphane. Top Curr Chem 329: 163-177.

337. Alfieri A, Srivastava S, Siow RC, Cash D, Modo M, et al. (2013) Sulforaphane preconditioning of the Nrf2/HO-1 defense pathway protects the cerebral vasculature against blood-brain barrier disruption and neurological deficits in stroke. Free Radic Biol Med 65: 1012-1022.

338. Calkins MJ, Johnson DA, Townsend JA, Vargas MR, Dowell JA, et al. (2009) The Nrf2/ARE pathway as a potential therapeutic target in neurodegenerative disease. Antioxid Redox Signal 11: 497-508.

339. Lee JY, Koga H, Kawaguchi Y, Tang W, Wong E, et al. (2010) HDAC6 controls autophagosome maturation essential for ubiquitin-selective quality-control autophagy. EMBO J 29: 969-980.

340. Boyault C, Zhang Y, Fritah S, Caron C, Gilquin B, et al. (2007) HDAC6 controls major cell response pathways to cytotoxic accumulation of protein aggregates. Genes Dev 21: 2172-2181.

341. Bellot G, Garcia-Medina R, Gounon P, Chiche J, Roux D, et al. (2009) Hypoxia-induced autophagy is mediated through hypoxia-inducible factor induction of BNIP3 and BNIP3L via their BH3 domains. Mol Cell Biol 29: 2570-2581.

342. Scherz-Shouval R, Shvets E, Fass E, Shorer H, Gil L, et al. (2007) Reactive oxygen species are essential for autophagy and specifically regulate the activity of Atg4. EMBO J 26: 1749-1760.

343. van der Zee J (2002) Heating the patient: a promising approach? Ann Oncol 13: 1173-1184.

344. Yost HJ, Lindquist S (1986) RNA splicing is interrupted by heat shock and is rescued by heat shock protein synthesis. Cell 45: 185-193.

345. Bond U (1988) Heat shock but not other stress inducers leads to the disruption of a sub-set of snRNPs and inhibition of in vitro splicing in HeLa cells. EMBO J 7: 3509-3518.

346. Maquat LE (2004) Nonsense-mediated mRNA decay: splicing, translation and mRNP dynamics. Nat Rev Mol Cell Biol 5: 89-99.

347. Wang D, Zavadil J, Martin L, Parisi F, Friedman E, et al. (2011) Inhibition of nonsense-mediated RNA decay by the tumor microenvironment promotes tumorigenesis. Mol Cell Biol 31: 3670-3680.

348. Kawaguchi T, Tanigawa A, Naganuma T, Ohkawa Y, Souquere S, et al. (2015) SWI/SNF chromatin-remodeling complexes function in noncoding RNA-dependent assembly of nuclear bodies. Proc Natl Acad Sci U S A 112: 4304-4309.

349. Albulescu LO, Sabet N, Gudipati M, Stepankiw N, Bergman ZJ, et al. (2012) A quantitative, high-throughput reverse genetic screen reveals novel connections between Pre-mRNA splicing and 5' and 3' end transcript determinants. PLoS Genet 8: e1002530.

350. Simon JM, Hacker KE, Singh D, Brannon AR, Parker JS, et al. (2014) Variation in chromatin accessibility in human kidney cancer links H3K36 methyltransferase loss with widespread RNA processing defects. Genome Res 24: 241-250.

351. Ward AJ, Cooper TA (2010) The pathobiology of splicing. J Pathol 220: 152-163.

352. Klamt B, Koziell A, Poulat F, Wieacker P, Scambler P, et al. (1998) Frasier syndrome is caused by defective alternative splicing of WT1 leading to an altered ratio of WT1 +/-KTS splice isoforms. Hum Mol Genet 7: 709-714.

353. Fu RH, Liu SP, Huang SJ, Chen HJ, Chen PR, et al. (2013) Aberrant alternative splicing events in Parkinson's disease. Cell Transplant 22: 653-661.

354. Pagani F, Buratti E, Stuani C, Romano M, Zuccato E, et al. (2000) Splicing factors induce cystic fibrosis transmembrane regulator exon 9 skipping through a nonevolutionary conserved intronic element. J Biol Chem 275: 21041-21047.

355. Mordes D, Luo X, Kar A, Kuo D, Xu L, et al. (2006) Pre-mRNA splicing and retinitis pigmentosa. Mol Vis 12: 1259-1271.

356. Kuyumcu-Martinez NM, Cooper TA (2006) Misregulation of alternative splicing causes pathogenesis in myotonic dystrophy. Prog Mol Subcell Biol 44: 133-159.

357. Oltean S, Bates DO (2014) Hallmarks of alternative splicing in cancer. Oncogene 33: 5311-5318.

358. Makishima H, Visconte V, Sakaguchi H, Jankowska AM, Abu Kar S, et al. (2012) Mutations in the spliceosome machinery, a novel and ubiquitous pathway in leukemogenesis. Blood 119: 3203-3210.

359. Malcovati L, Papaemmanuil E, Bowen DT, Boultwood J, Della Porta MG, et al. (2011) Clinical significance of SF3B1 mutations in myelodysplastic syndromes and myelodysplastic/myeloproliferative neoplasms. Blood 118: 6239-6246.

360. Zhang J, Manley JL (2013) Misregulation of pre-mRNA alternative splicing in cancer. Cancer Discov 3: 1228-1237.

361. Dvinge H, Bradley RK (2015) Widespread intron retention diversifies most cancer transcriptomes. Genome Med 7: 45.

362. Zhang Q, Li H, Jin H, Tan H, Zhang J, et al. (2014) The global landscape of intron retentions in lung adenocarcinoma. BMC Med Genomics 7: 15.

363. Kierlin-Duncan MN, Sullenger BA (2007) Using 5'-PTMs to repair mutant beta-globin transcripts. RNA 13: 1317-1327.

364. Fernandez Alanis E, Pinotti M, Dal Mas A, Balestra D, Cavallari N, et al. (2012) An exon-specific U1 small nuclear RNA (snRNA) strategy to correct splicing defects. Hum Mol Genet 21: 2389-2398.

365. Hartmann L, Neveling K, Borkens S, Schneider H, Freund M, et al. (2010) Correct mRNA processing at a mutant TT splice donor in FANCC ameliorates the clinical phenotype in patients and is enhanced by delivery of suppressor U1 snRNAs. Am J Hum Genet 87: 480-493.

366. Kotake Y, Sagane K, Owa T, Mimori-Kiyosue Y, Shimizu H, et al. (2007) Splicing factor SF3b as a target of the antitumor natural product pladienolide. Nat Chem Biol 3: 570-575.

367. Albert BJ, McPherson PA, O'Brien K, Czaicki NL, Destefino V, et al. (2009) Meayamycin inhibits pre-messenger RNA splicing and exhibits picomolar activity against multidrug-resistant cells. Mol Cancer Ther 8: 2308-2318.

368. Venables JP, Klinck R, Koh C, Gervais-Bird J, Bramard A, et al. (2009) Cancer-associated regulation of alternative splicing. Nat Struct Mol Biol 16: 670-676.

369. Bradford MM (1976) A rapid and sensitive method for the quantitation of microgram quantities of protein utilizing the principle of protein-dye binding. Anal Biochem 72: 248-254.

370. Dahl JA, Reiner AH, Collas P (2009) Fast genomic muChIP-chip from 1,000 cells. Genome Biol 10: R13.

371. Sanger F, Coulson AR (1975) A rapid method for determining sequences in DNA by primed synthesis with DNA polymerase. J Mol Biol 94: 441-448.

6 Supplement

BRD4 target list

Supplement Table S 1 Integration of RNA-Seq and ChIP-Seq data sets: 52 top candidate genes positively regulated by BRD4. Shown are the log2 fold change expressions of both BRD4 knockdown approaches (siBRD4-1 and siBRD4-2), the log2 fold enrichment of BRD4 in the ChIP data and the presence of an SP1-binding site for each identified BRD4 target gene.

gene name	log2FC (siBRD4-1)	log2FC (siBRD4-2)	log2FC (average)	FC (peak)	SP1- binding site
DHRS3	-0.84	-0.95	-0.90	11.25	no
ARSG	-1.11	-0.80	-0.95	10.32	no
EZR	-0.45	-0.90	-0.67	9	yes
AMACR	-0.71	-0.92	-0.82	8.97	yes
PRSS23	-0.76	-0.89	-0.82	8.75	no
AHCYL2	-0.75	-1.04	-0.90	7	no
DNAJB2	-0.51	-1.00	-0.76	7	yes
LAP3	-0.79	-1.30	-1.05	6.83	yes
MDM2	-0.55	-0.87	-0.71	6.16	yes
ITGB3BP	-0.48	-0.67	-0.57	6.12	no
CCDC112	-0.59	-1.04	-0.82	6.1	no
PIGP	-0.54	-0.76	-0.65	5.98	no
ZMYM3	-0.60	-0.87	-0.73	5.83	no
TPD52	-0.82	-1.74	-1.28	5.71	no
CCDC91	-0.91	-0.64	-0.78	5.71	no
KEAP1	-0.47	-0.92	-0.69	5.71	yes
MAPK3	-0.94	-0.79	-0.87	5.62	yes
AAAS	-0.61	-0.46	-0.53	5.58	yes
ARHGEF3	-0.58	-1.18	-0.88	5.56	no
HOXC10	-0.80	-0.41	-0.61	5.56	yes
TXN2	-0.59	-0.54	-0.56	5.42	yes
WDR34	-0.79	-0.97	-0.88	5.41	no
PPAP2B	-1.11	-1.69	-1.40	5.29	no
C3ORF14	-0.96	-0.79	-0.88	5	no
SNX15	-0.91	-0.75	-0.83	5	yes
HDAC6	-0.75	-0.79	-0.77	5	yes
TMEM116	-0.83	-0.54	-0.69	5	yes
ABR	-0.50	-0.91	-0.71	4.95	no
SESN3	-0.52	-0.53	-0.53	4.8	yes
MRPL40	-0.56	-0.86	-0.71	4.67	yes
SOD2	-0.63	-0.70	-0.67	4.5	yes
AC007563.5	-2.34	-0.46	-1.40	4.49	no
MRPS18C	-0.40	-1.07	-0.73	4.45	no
VPS52	-0.77	-0.99	-0.88	4.38	no

gene name	log2FC (siBRD4-1)	log2FC (siBRD4-2)	log2FC (average)	FC (peak)	SP1- binding site
EPM2A	-0.64	-0.74	-0.69	4.23	no
GSTP1	-0.68	-0.98	-0.83	4.05	yes
INTS4	-0.69	-0.76	-0.73	4	no
C22ORF13	-0.41	-0.73	-0.57	3.96	no
UBE2E1	-0.44	-1.04	-0.74	3.93	no
CIZ1	-0.72	-0.74	-0.73	3.92	yes
EPHX1	-0.61	-0.57	-0.59	3.92	no
ALDH4A1	-0.93	-0.54	-0.73	3.89	no
UCK2	-0.82	-0.92	-0.87	3.79	no
ZBTB16	-1.55	-1.03	-1.29	3.75	yes
PHACTR4	-0.58	-0.49	-0.54	3.75	no
UCK1	-0.45	-0.76	-0.60	3.64	no
DDR1	-1.22	-1.78	-1.50	3.57	yes
COPS7A	-0.62	-1.35	-0.98	3.53	no
ZNF689	-0.41	-0.68	-0.55	3.42	no
VIM	-0.70	-0.70	-0.70	3.33	yes
GPX1	-0.63	-0.82	-0.72	3.18	no
DCAF6	-0.53	-0.53	-0.53	2.74	no

GO:0034599 - target genes list

Supplement Table S 2 GO:0034599 cellular response to oxidative stress. Oxidative stress responsive genes of of the Gene ontology pathway GO:0034599. Top 16 genes overlapping with the 887 down regulated genes in BRD4 knock down cells.

gene symbol	gene name	siBRD4
SOD2	Superoxide dismutase [Mn], mitochondrial	yes
HDAC6	Histone deacetylase 6	yes
AGAP3	Arf-GAP with GTPase, ANK repeat and PH domain-containing protein 3	yes
PML	Protein PML	yes
TP53	Cellular tumor antigen p53	yes
EPAS1	Endothelial PAS domain-containing protein 1	yes
FBLN5	Fibulin-5	yes
BMP7	Bone morphogenetic protein 7	yes
G6PD	Glucose-6-phosphate 1-dehydrogenase	yes
TMEM161A	Transmembrane protein 161A	yes
CAT	Catalase	yes
GPX1	Glutathione peroxidase 1	yes
PXDN	Peroxidasin homolog	yes
mdm2	E3 ubiquitin-protein ligase Mdm2	yes
ANXA1	Annexin A1	yes
TNFAIP3	Tumor necrosis factor alpha-induced protein 3	yes
NFE2L2	Nuclear factor erythroid 2-related factor 2	no
SNCA	Alpha-synuclein	no
ADNP2	ADNP homeobox protein 2	no
COQ7	Ubiquinone biosynthesis protein COQ7 homolog	no
MGMT	Methylated-DNA--protein-cysteine methyltransferase	no
MT3	Metallothionein-3	no
PRDX2	Peroxiredoxin-2	no
PYCR1	Pyrroline-5-carboxylate reductase 1, mitochondrial	no
LONP1	Lon protease homolog, mitochondrial	no
ETV5	ETS translocation variant 5	no
ALDH3B1	Aldehyde dehydrogenase family 3 member B1	no
SLC11A2	Natural resistance-associated macrophage protein 2	no
FOXO1	Forkhead box protein O1	no
TRAP1	Heat shock protein 75 kDa, mitochondrial	no
DHRS2	Dehydrogenase/reductase SDR family member 2	no
STX3	Syntaxin-3	no
PRKD1	Serine/threonine-protein kinase D1	no
VRK2	Serine/threonine-protein kinase VRK2	no
PNPT1	Polyribonucleotide nucleotidyltransferase 1, mitochondrial	no
VIMP	Selenoprotein S	no
PPARGC1A	Peroxisome proliferator-activated receptor gamma coactivator 1-alpha	no

BRD4 expression in cancer cell lines

Supplement Table S 3 BRD4 mRNA expression in 18 cell lines. BRD4 expression was calculated using qPCR experiments and normalized to WI38 cells. This table is related to Figure 17)

Tumor entitiy	Cell line	BRD4 expression	STDEV
Controls	HEK293T	1.23	± 0.51
	WI38	1.00	± 0.07
Lung	A549	1.08	± 0.08
	HCC827	3.54	± 0.23
Colon	CaCo2	8.85	± 1.34
	HTC116	3.96	± 0.16
	SW480	4.17	± 0.35
	SW620	3.24	± 0.42
Prostate	DU145	5.18	± 2.36
	LNCAP	14.64	± 0.12
	PC3	5.23	± 1.05
	VCAP	16.78	± 1.83
Cervix	HELA	1.97	± 0.05
	C33A	1.69	± 0.06
Breast	MCF7	5.23	± 0.38
	SKBR3	0.64	± 0.18
Bone	U2OS	0.83	± 0.06
Liver	HepG2	2.85	0.39

IR in BRD4 knockdown cells following HS

Supplement Table S 4 Expression values of introns were calculated using the percent spliced in index (PSI) corresponding to Wang et al for each condition and the relative intron inclusion level was estimated by normalising to the untreated control. Columns 1 -3 represents the chromosomal location of the putative intron. Columns 4 - 5 mark the gene IDs and gene name. Columns 6 -11 contain the relative expression level (ΔPSI) of the corresponding intron from siCo+HS and siBRD4+HS compared to the untreated control.

					ΔPSI(siCo+HS)			**ΔPSI(siBRD4+HS)**		
chr	**start**	**end**	**ensg**	**name**	**rep1**	**rep2**	**rep3**	**rep1**	**rep2**	**rep3**
1	237789104	237791107	ENSG00000198626	*RYR2*	1.0	0.5	-1.1	-10.1	1.4	0.9
11	130180369	130184270	ENSG00000196323	*ZBTB44*	0.5	0.9	1.1	-10.1	1.6	3.1
15	29131424	29139020	ENSG00000034053	*APBA2*	NA	14.3	10.7	NA	15.3	16.5
15	42632952	42635276	ENSG00000214013	*GANC*	11.5	1.3	0.1	NA	2.4	1.1
16	747419	755512	ENSG00000102854	*MSLN*	NA	14.3	10.7	NA	15.3	16.5
16	31885585	31886473	ENSG00000185947	*ZNF267*	NA	0.3	10.7	NA	1.5	16.5
17	28442641	28443664	ENSG00000126653	*NSRP1*	1.5	1.3	0.5	-10.1	2.0	1.1
19	1295857	1298550	ENSG00000160953	*MUM1*	NA	14.3	0.6	NA	15.3	2.4

					ΔPSI(siCo+HS)			ΔPSI(siBRD4+HS)		
chr	**start**	**end**	**ensg**	**name**	**rep1**	**rep2**	**rep3**	**rep1**	**rep2**	**rep3**
2	24247163	24248302	ENSG00000205639	*MFSD2B*	11.5	1.6	10.7	NA	2.6	16.5
2	30454630	30455019	ENSG00000213626	*LBH*	-1.1	1.5	0.4	-10.1	2.2	1.6
22	47022858	47033737	ENSG00000075240	*GRAMD4*	-0.5	0.8	0.2	-10.1	1.6	1.1
3	31750656	31750763	ENSG00000144645	*OSBPL10*	0.3	14.3	10.7	-10.1	15.3	16.5
4	77678241	77679202	ENSG00000138771	*SHROOM3*	11.5	2.6	10.7	NA	3.8	16.5
5	139030751	139039140	ENSG00000171604	*CXXC5*	4.7	3.9	0.0	-10.1	4.6	0.9
5	171789873	171800794	ENSG00000174705	*SH3PXD2B*	0.9	-0.1	-0.5	-10.1	0.7	0.7
6	160109380	160111951	ENSG00000112096	*SOD2*	11.5	14.3	0.7	NA	15.3	1.7
7	116599871	116605900	ENSG00000004866	*ST7*	11.5	1.3	-0.3	NA	2.9	0.6
7	127232291	127233552	ENSG00000179562	*GCC1*	11.5	1.4	0.2	NA	4.1	1.4
7	127232291	127233552	ENSG00000106328	*FSCN3*	11.5	1.9	0.5	NA	4.6	1.6
7	127234051	127234548	ENSG00000106328	*FSCN3*	NA	2.7	0.7	NA	3.5	2.3
7	143098698	143104704	ENSG00000146904	*EPHA1*	NA	3.9	0.8	NA	5.1	2.3
8	17396431	17400827	ENSG00000003989	*SLC7A2*	1.5	-0.2	-15.5	-10.1	0.9	1.1
8	26372195	26405185	ENSG00000092964	*DPYSL2*	-1.7	0.5	0.5	-10.1	1.3	1.3
8	99449436	99466867	ENSG00000104375	*STK3*	11.5	0.9	0.2	NA	1.9	1.1
9	35665284	35669581	ENSG00000137135	*ARHGEF39*	NA	-0.9	10.7	NA	2.8	16.5
X	18593610	18597968	ENSG00000008086	*CDKL5*	0.7	-1.4	-2.2	-10.1	0.7	1.0
10	114287164	114293289	ENSG00000151532	*VTI1A*	0.4	-0.7	0.7	-0.4	0.9	1.4
13	46054425	46055365	ENSG00000136152	*COG3*	11.5	0.2	1.2	12.2	1.3	1.9
17	71303453	71305894	ENSG00000179604	*CDC42EP4*	-0.4	3.1	0.9	-1.4	3.8	3.0
19	46088100	46093022	ENSG00000125741	*OPA3*	2.5	1.5	10.7	0.9	3.3	16.5
19	36448284	36449116	ENSG00000267786	*AF038458.3*	NA	0.2	1.1	12.2	2.7	2.9
2	61145741	61147176	ENSG00000162924	*REL*	-0.4	-0.5	0.7	-1.5	0.8	1.4
20	34680891	34697595	ENSG00000088367	*EPB41L1*	2.2	2.2	0.3	0.0	2.8	2.4
22	47185368	47188417	ENSG00000054611	*TBC1D22A*	-11.5	-0.6	2.1	0.8	1.1	3.5
22	30954377	30956264	ENSG00000100330	*MTMR3*	11.5	1.8	10.7	12.2	2.7	16.5
3	31746462	31748684	ENSG00000144645	*OSBPL10*	2.4	14.3	10.7	-0.4	15.3	16.5
3	50127527	50127803	ENSG00000004534	*RBM6*	11.5	14.3	10.7	12.2	15.3	16.5
3	50127527	50127803	ENSG00000003756	*RBM5*	11.5	14.3	10.7	12.2	15.3	16.5
3	137816689	137820320	ENSG00000158163	*DZIP1L*	1.3	2.3	4.2	0.5	3.5	5.0
6	155632473	155634272	ENSG00000029639	*TFB1M*	-0.6	0.0	0.6	-2.2	0.7	1.4
7	134343420	134345173	ENSG00000172331	*BPGM*	-11.5	14.3	10.7	-0.1	15.3	16.5
8	128808317	128815396	ENSG00000249859	*PVT1*	0.0	0.0	0.3	-3.0	1.0	1.5
12	51476893	51477012	ENSG00000110925	*CSRNP2*	0.9	1.7	10.7	0.7	3.3	16.5
12	64488984	64491021	ENSG00000255886	*RP11-196H14.2*	0.0	-1.7	1.0	-1.5	0.7	1.6
12	112699940	112701888	ENSG00000173064	*HECTD4*	-2.0	-0.2	-2.4	-0.9	1.0	0.6
14	50146518	50148020	ENSG00000100479	*POLE2*	11.5	0.4	0.0	12.2	1.5	0.8
14	75746234	75746346	ENSG00000170345	*FOS*	-0.7	14.3	10.7	-1.2	15.3	16.5
16	58150982	58153037	ENSG00000070761	*C16orf80*	11.5	0.2	0.2	12.2	1.3	1.5
16	58150982	58153037	ENSG00000260545	*CTB-134F13.1*	11.5	0.1	0.1	12.2	1.2	1.4
17	55509975	55518051	ENSG00000153944	*MSI2*	1.2	14.3	10.7	-0.3	15.3	16.5

					ΔPSI(siCo+HS)			ΔPSI(siBRD4+HS)		
chr	**start**	**end**	**ensg**	**name**	**rep1**	**rep2**	**rep3**	**rep1**	**rep2**	**rep3**
19	1286307	1295544	ENSG00000160953	*MUM1*	11.5	14.3	3.2	12.2	15.3	3.9
19	49644770	49645291	ENSG00000177380	*PPFIA3*	11.5	1.1	-1.8	12.2	1.7	1.1
2	71891568	71892292	ENSG00000135636	*DYSF*	-1.5	-0.3	0.2	0.1	0.6	0.9
21	43332549	43334707	ENSG00000157617	*C2CD2*	0.2	0.2	0.7	-1.3	1.0	1.5
22	30962148	30968674	ENSG00000100330	*MTMR3*	11.5	14.3	10.7	12.2	15.3	16.5
22	30956763	30959217	ENSG00000100330	*MTMR3*	NA	14.3	10.7	12.2	15.3	16.5
3	164924947	165063260	ENSG00000244128	*RP11-85M11.2*	-0.2	0.2	-0.9	-2.1	1.0	0.9
3	33482415	33482761	ENSG00000153560	*UBP1*	-1.1	2.0	10.7	-2.3	2.7	16.5
3	145912242	145912911	ENSG00000114698	*PLSCR4*	-0.3	0.1	0.4	0.3	1.2	1.0
4	2825300	2826340	ENSG00000087266	*SH3BP2*	1.7	0.3	0.8	3.1	1.1	1.8
4	141622096	141622658	ENSG00000109436	*TBC1D9*	-0.7	1.0	-0.8	-1.4	1.9	0.9
5	133642393	133643692	ENSG00000006837	*CDKL3*	1.2	0.9	10.7	0.2	2.1	16.5
6	119150416	119177534	ENSG00000111877	*MCM9*	0.6	-2.4	-0.2	-0.4	1.2	0.8
6	158423415	158438236	ENSG00000078269	*SYNJ2*	-11.5	-1.0	0.1	1.0	0.7	1.1
6	29545525	29550026	ENSG00000204681	*GABBR1*	11.5	2.6	10.7	12.2	3.4	16.5
7	27170418	27173700	ENSG00000254369	*HOXA-AS3*	0.8	0.2	0.2	-1.1	1.7	1.0
7	143088868	143090764	ENSG00000146904	*EPHA1*	-0.2	0.7	0.5	-0.5	1.3	1.6
8	9008206	9008857	ENSG00000173281	*PPP1R3B*	-0.1	1.3	10.7	-1.3	2.8	16.5
10	51291433	51295110	ENSG00000244393	*RP11-592B15.3*	11.5	0.6	1.0	12.2	2.5	3.0
10	51291433	51295110	ENSG00000225784	*RP11-592B15.4*	11.5	0.2	0.9	12.2	2.2	3.0
10	81933157	81935863	ENSG00000122359	*ANXA11*	3.8	0.1	1.4	2.8	1.5	2.1
11	110034104	110035066	ENSG00000149289	*ZC3H12C*	-0.5	0.0	0.0	0.5	0.6	0.7
12	19283064	19283644	ENSG00000052126	*PLEKHA5*	2.2	0.4	10.7	2.5	1.2	16.5
13	42501485	42524072	ENSG00000102763	*VWA8*	2.1	-1.9	-2.2	2.0	0.6	0.7
13	39596549	39597189	ENSG00000120685	*PROSER1*	-0.4	-0.9	0.0	-0.6	0.7	0.9
14	64476834	64483191	ENSG00000054654	*SYNE2*	0.8	1.4	-1.6	0.4	2.3	0.7
15	66604239	66606377	ENSG00000166938	*DIS3L*	-1.0	0.5	0.8	-0.4	1.4	1.8
15	86313051	86313727	ENSG00000183655	*KLHL25*	11.5	2.4	10.7	12.2	4.2	16.5
17	80888519	80889825	ENSG00000141556	*TBCD*	-0.2	0.1	0.7	0.4	1.1	1.7
19	40318296	40318937	ENSG00000105204	*DYRK1B*	0.3	-0.5	-0.1	0.0	1.0	1.1
2	217577192	217629612	ENSG00000236886	*AC007563.5*	11.5	3.4	1.2	12.2	4.2	2.5
2	236414444	236415597	ENSG00000157985	*AGAP1*	11.5	14.3	10.7	12.2	15.3	16.5
4	41420811	41455582	ENSG00000064042	*LIMCH1*	1.5	1.2	1.0	0.3	2.5	1.7
4	48807347	48832594	ENSG00000109180	*OCIAD1*	2.0	1.4	-0.3	0.7	2.1	1.7
4	84039124	84055688	ENSG00000145287	*PLAC8*	1.4	0.9	-0.1	0.4	1.5	0.6
4	170991803	170994287	ENSG00000109576	*AADAT*	0.9	1.5	1.0	0.3	2.3	2.3
7	16685929	16700839	ENSG00000136261	*BZW2*	0.7	2.1	0.1	0.8	3.3	1.2
7	40277325	40314110	ENSG00000175600	*C7orf10*	-0.8	-0.9	-0.4	-0.5	1.1	0.7
7	76671655	76672910	ENSG00000265479	*DTX2P1*	-0.8	1.1	-0.9	1.1	2.4	0.6
7	76671655	76672910	ENSG00000186704	*DTX2P1*	-1.0	1.2	-1.0	1.2	2.4	0.6
8	23389438	23398983	ENSG00000147454	*SLC25A37*	11.5	-1.8	10.7	12.2	2.3	16.5

					ΔPSI(siCo+HS)			ΔPSI(siBRD4+HS)		
chr	**start**	**end**	**ensg**	**name**	**rep1**	**rep2**	**rep3**	**rep1**	**rep2**	**rep3**
1	46348067	46365545	ENSG00000086015	*MAST2*	-0.6	14.3	0.2	0.8	15.3	1.4
1	204043517	204047257	ENSG00000143842	*SOX13*	11.5	1.8	1.1	12.2	2.9	2.3
1	58939640	58946391	ENSG00000162600	*OMA1*	11.5	-1.3	-1.1	12.2	0.8	0.9
1	148255973	148256693	ENSG00000203832	*NBPF20*	0.9	1.3	-0.1	0.8	2.5	1.3
1	155051545	155057567	ENSG00000143590	*EFNA3*	1.2	1.5	1.7	1.0	2.7	2.3
1	155051545	155057567	ENSG00000251246	*RP11-540D14.8*	0.6	1.6	1.5	0.7	2.9	2.2
10	104352481	104353393	ENSG00000107882	*SUFU*	0.6	-0.1	-0.1	0.9	1.3	0.9
12	64238663	64265522	ENSG00000196935	*SRGAP1*	-2.2	1.2	0.3	-1.3	2.2	1.8
13	107212005	107214180	ENSG00000134884	*ARGLU1*	-0.1	-0.4	0.4	-0.7	0.6	1.3
15	81212640	81213373	ENSG00000103888	*KIAA1199*	0.2	0.4	0.2	2.4	1.0	0.7
19	6166030	6175302	ENSG00000087903	*RFX2*	-11.5	0.3	0.1	0.0	1.0	1.6
2	218343281	218464335	ENSG00000231672	*DIRC3*	-0.1	0.7	0.6	1.3	1.3	1.6
2	25862197	25872706	ENSG00000138101	*DTNB*	11.5	14.3	3.5	12.2	15.3	4.1
2	39570593	39583306	ENSG00000011566	*MAP4K3*	-2.8	-0.3	-0.1	-0.7	0.8	1.0
22	23604258	23605323	ENSG00000186716	*BCR*	11.5	1.0	-0.2	12.2	2.1	1.5
22	38352908	38354381	ENSG00000100142	*POLR2F*	-0.9	0.2	0.3	-1.0	2.4	2.9
22	40984007	40990678	ENSG00000196588	*MKL1*	1.1	4.2	0.3	1.1	5.0	1.7
3	17566186	17588508	ENSG00000131374	*TBC1D5*	2.0	0.2	0.4	1.8	1.3	1.0
5	492186	524227	ENSG00000066230	*SLC9A3*	-11.5	1.1	10.7	0.2	2.8	16.5
7	90193177	90219933	ENSG00000058091	*CDK14*	4.9	2.2	10.7	2.5	2.9	16.5
8	25745488	25747268	ENSG00000221818	*EBF2*	-0.7	1.4	-0.1	-0.2	2.0	1.4
8	131016847	131020580	ENSG00000153310	*FAM49B*	-0.7	2.0	1.6	1.1	3.3	2.6
9	82191735	82194975	ENSG00000106829	*TLE4*	NA	14.3	3.7	12.2	15.3	4.3
10	33271613	33274551	ENSG00000150093	*ITGB1*	0.4	-0.2	10.7	-0.2	1.4	16.5
10	51837912	51838435	ENSG00000099290	*FAM21A*	-0.1	0.8	0.1	0.6	1.5	0.9
12	95531454	95535164	ENSG00000180263	*FGD6*	-0.4	0.3	0.3	-1.0	1.2	1.6
16	12391180	12450020	ENSG00000048471	*SNX29*	2.8	-0.1	0.5	2.4	2.9	1.4
16	69383554	69385444	ENSG00000259900	*RP11-343C2.7*	11.5	-0.1	-1.8	12.2	1.7	0.6
2	135888291	135890465	ENSG00000115839	*RAB3GAP1*	-1.2	0.2	0.4	-0.6	0.8	1.0
2	175324816	175326130	ENSG00000163328	*GPR155*	0.4	0.4	-0.8	0.5	1.3	1.1
2	29356682	29358414	ENSG00000115295	*CLIP4*	2.4	0.2	0.2	2.5	1.5	1.0
2	220119330	220130945	ENSG00000127824	*TUBA4A*	1.2	1.1	10.7	2.0	2.6	16.5
4	154265892	154266505	ENSG00000121211	*MND1*	-1.3	0.1	0.1	1.1	1.6	1.1
5	111284685	111305149	ENSG00000134986	*NREP*	-2.1	-0.4	-0.6	-0.4	0.7	0.6
1	116925215	116925992	ENSG00000163399	*ATP1A1*	2.3	1.1	0.8	1.4	2.3	1.9
1	171773099	171783015	ENSG00000010165	*METTL13*	11.5	14.3	-15.5	12.2	15.3	1.7
12	125324589	125343129	ENSG00000073060	*SCARB1*	-0.7	1.5	0.5	2.3	2.9	1.1
13	66897693	67204847	ENSG00000184226	*PCDH9*	0.1	-0.1	1.3	0.3	0.8	2.0
14	73359357	73360765	ENSG00000205683	*DPF3*	0.4	-0.4	0.8	1.3	1.1	1.8
15	31696113	31712331	ENSG00000169926	*KLF13*	3.2	14.3	10.7	2.2	15.3	16.5
15	90736795	90744551	ENSG00000185033	*SEMA4B*	11.5	14.3	10.7	12.2	15.3	16.5
16	69951786	69958893	ENSG00000198373	*WWP2*	0.7	2.1	1.2	1.0	4.0	2.2

					ΔPSI(siCo+HS)			ΔPSI(siBRD4+HS)		
chr	**start**	**end**	**ensg**	**name**	**rep1**	**rep2**	**rep3**	**rep1**	**rep2**	**rep3**
17	76183514	76186792	ENSG00000183077	*AFMID*	2.3	0.2	-0.2	1.4	1.2	0.7
19	44580557	44585168	ENSG00000267022	*AC084219.2*	0.0	-1.0	-0.5	0.1	0.7	1.4
19	45932468	45952431	ENSG00000012061	*ERCC1*	1.2	1.2	0.3	0.6	2.1	1.0
2	65601259	65604747	ENSG00000198369	*SPRED2*	11.5	14.3	10.7	12.2	15.3	16.5
2	111902097	111903526	ENSG00000153094	*BCL2L11*	11.5	1.5	10.7	12.2	2.7	16.5
2	242651795	242658898	ENSG00000168395	*ING5*	0.0	0.2	0.1	0.1	1.1	0.8
20	17971765	17977205	ENSG00000125850	*OVOL2*	NA	14.3	10.7	12.2	15.3	16.5
3	49530406	49547657	ENSG00000173402	*DAG1*	2.0	0.0	1.0	0.8	1.1	1.9
3	128370372	128393578	ENSG00000163902	*RPN1*	2.0	0.2	0.4	0.6	1.4	1.4
3	48485616	48486432	ENSG00000244380	*RP11-24C3.2*	11.5	-1.7	-0.4	12.2	0.9	0.7
4	166161616	166173732	ENSG00000109466	*KLHL2*	11.5	14.3	10.7	12.2	15.3	16.5
4	83858451	83859566	ENSG00000189308	*LIN54*	-1.2	-0.4	0.2	1.4	0.7	1.4
4	146404328	146405665	ENSG00000170365	*SMAD1*	11.5	14.3	10.7	12.2	15.3	16.5
5	110891678	110907799	ENSG00000246859	*STARD4-AS1*	11.5	-0.1	1.4	12.2	0.7	2.2
5	61604338	61607640	ENSG00000068796	*KIF2A*	2.1	2.6	0.4	0.7	3.2	1.1
7	40234659	40256996	ENSG00000175600	*C7orf10*	-0.3	-0.2	-0.4	1.0	1.1	1.2
1	165769272	165788590	ENSG00000143183	*TMCO1*	0.8	2.1	0.6	0.5	3.4	1.4
1	178838445	178839876	ENSG00000116191	*RALGPS2*	11.5	3.3	10.7	12.2	3.9	16.5
11	78239982	78244222	ENSG00000137513	*NARS2*	0.3	0.0	-0.8	-0.4	0.9	0.6
13	23948155	23949258	ENSG00000151835	*SACS*	2.5	2.0	-0.2	1.5	2.7	0.7
14	58877806	58878620	ENSG00000258378	*RP11-517O13.1*	11.5	-1.2	-0.5	12.2	1.0	1.0
14	58877806	58878620	ENSG00000100575	*TIMM9*	11.5	-1.2	-0.6	12.2	0.9	0.9
15	42551188	42553156	ENSG00000103978	*TMEM87A*	0.4	0.3	-0.6	0.9	1.0	0.8
15	102244140	102245886	ENSG00000185418	*TARSL2*	2.8	-0.2	-0.5	3.7	0.7	1.0
16	69008071	69040955	ENSG00000103047	*TMCO7*	1.0	0.2	-0.2	2.2	0.8	0.8
17	20862034	20867035	ENSG00000233098	*RP11-344E13.3*	-0.8	-0.3	-15.5	0.7	0.7	0.7
17	79027591	79030162	ENSG00000175866	*BAIAP2*	11.5	1.7	-1.3	12.2	2.4	1.0
2	70322298	70323036	ENSG00000226505	*AC016700.3*	11.5	14.3	10.7	12.2	15.3	16.5
20	10623249	10624426	ENSG00000101384	*JAG1*	-0.7	1.7	1.3	0.2	2.4	2.0
20	10643154	10644611	ENSG00000101384	*JAG1*	11.5	4.1	1.5	12.2	4.9	2.4
21	47088946	47148590	ENSG00000183570	*PCBP3*	0.4	0.9	0.0	1.9	1.8	1.3
6	144033473	144070065	ENSG00000112419	*PHACTR2*	-1.7	-0.5	-0.2	-0.7	0.7	0.9
6	155230002	155265250	ENSG00000146426	*TIAM2*	-0.9	0.0	-0.4	-1.8	0.9	0.7
8	22256310	22262030	ENSG00000104635	*SLC39A14*	11.5	14.3	10.7	12.2	15.3	16.5
8	68018210	68024207	ENSG00000104218	*CSPP1*	-0.6	0.7	1.2	1.9	1.7	2.3
X	70748575	70749366	ENSG00000147133	*TAF1*	3.7	14.3	10.7	3.7	15.3	16.5
1	6420767	6445554	ENSG00000097021	*ACOT7*	11.5	-0.1	1.0	12.2	0.7	2.3
10	123629553	123658356	ENSG00000107669	*ATE1*	-0.9	-0.2	-0.3	0.4	0.6	0.6
10	126822181	126826576	ENSG00000175029	*CTBP2*	2.1	0.6	-0.2	2.4	1.5	0.7
11	59387945	59402893	ENSG00000255139	*AP000442.1*	0.5	-2.2	-0.4	0.5	0.6	0.7
11	47292692	47293513	ENSG00000110514	*MADD*	11.5	1.6	2.3	12.2	2.3	3.0

					ΔPSI(siCo+HS)			ΔPSI(siBRD4+HS)		
chr	**start**	**end**	**ensg**	**name**	**rep1**	**rep2**	**rep3**	**rep1**	**rep2**	**rep3**
11	116733043	116734384	ENSG00000160584	*SIK3*	-0.8	-0.3	-0.1	0.5	0.6	0.9
12	89853815	89854487	ENSG00000139323	*POC1B*	0.7	0.0	-1.1	1.3	1.5	0.7
12	96780972	96792871	ENSG00000059758	*CDK17*	1.2	1.2	-15.5	0.2	2.6	1.0
16	67907361	67909641	ENSG00000038358	*EDC4*	11.5	-0.3	0.5	12.2	0.6	1.3
17	15165906	15168471	ENSG00000109099	*PMP22*	11.5	14.3	10.7	12.2	15.3	16.5
19	2255350	2256382	ENSG00000167476	*JSRP1*	11.5	14.3	10.7	12.2	15.3	16.5
19	44860834	44871241	ENSG00000267173	*CTC-512J12.6*	1.9	-0.7	0.0	0.6	1.6	0.7
19	44860834	44871241	ENSG00000062370	*ZFP112*	1.6	-0.6	0.2	0.3	1.6	0.8
2	65604884	65605081	ENSG00000198369	*SPRED2*	11.5	14.3	10.7	12.2	15.3	16.5
2	65605263	65607760	ENSG00000198369	*SPRED2*	11.5	14.3	3.5	12.2	15.3	4.1
2	160252345	160253585	ENSG00000223642	*AC008277.1*	11.5	0.7	1.1	12.2	1.7	1.9
2	160252345	160253585	ENSG00000123636	*BAZ2B*	11.5	0.7	1.5	12.2	1.5	2.1
2	242352836	242357377	ENSG00000006607	*FARP2*	2.8	-0.1	0.1	2.4	0.7	1.0
21	45158742	45160897	ENSG00000160209	*PDXK*	4.1	2.6	10.7	3.3	3.2	16.5
3	124931708	124944405	ENSG00000221955	*SLC12A8*	-11.5	-0.2	1.4	1.5	1.8	2.2
3	125011637	125029725	ENSG00000163848	*ZNF148*	-0.3	-0.1	0.0	-0.2	1.4	0.6
3	188443292	188461435	ENSG00000145012	*LPP*	11.5	14.3	10.7	12.2	15.3	16.5
3	50651548	50654562	ENSG00000114738	*MAPKAPK3*	1.9	0.3	0.7	1.8	2.0	1.8
4	141889027	141918112	ENSG00000170153	*RNF150*	-0.2	0.8	-0.2	0.7	2.1	0.9
4	151561018	151600740	ENSG00000198589	*LRBA*	-11.5	-0.9	-0.5	2.0	1.0	1.4
7	1127957	1131043	ENSG00000146540	*C7orf50*	1.9	3.2	0.1	2.9	4.7	1.1
1	221879808	221884979	ENSG00000143507	*DUSP10*	-0.6	0.0	0.6	1.1	0.7	1.4
10	31288446	31320762	ENSG00000183621	*ZNF438*	0.5	1.8	0.0	1.1	2.9	1.2
10	73973109	73975535	ENSG00000138303	*ASCC1*	1.9	-1.2	2.3	3.3	1.8	3.3
15	49065728	49073393	ENSG00000103995	*CEP152*	-1.6	-0.5	-0.1	-0.2	0.8	0.7
20	35093770	35101522	ENSG00000080845	*DLGAP4*	1.8	0.1	-0.5	1.0	1.1	1.0
21	16343890	16346536	ENSG00000180530	*NRIP1*	1.8	2.8	0.1	2.5	3.8	1.6
6	43613062	43618112	ENSG00000172426	*RSPH9*	11.5	3.4	10.7	12.2	4.1	16.5
10	7795565	7795915	ENSG00000151657	*KIN*	0.0	1.4	1.7	2.0	2.2	2.3
12	6982945	6984667	ENSG00000111671	*SPSB2*	1.1	0.5	0.4	1.4	1.4	1.0
12	6982945	6984667	ENSG00000240370	*RPL13P5*	0.2	0.1	-0.3	1.3	0.9	0.9
12	6982945	6984667	ENSG00000010626	*LRRC23*	0.3	0.1	-0.2	0.6	0.9	0.9
14	35297929	35314506	ENSG00000198604	*BAZ1A*	2.3	-0.1	0.8	2.4	0.7	1.4
14	35452421	35462450	ENSG00000100883	*SRP54*	-0.7	-0.5	0.3	-1.1	0.7	1.0
15	52264003	52296377	ENSG00000069956	*MAPK6*	1.1	0.3	-0.1	0.5	1.1	0.8
16	2973231	2978825	ENSG00000059122	*FLYWCH1*	11.5	-1.6	0.6	12.2	0.7	1.2
16	84853739	84861869	ENSG00000103196	*CRISPLD2*	1.8	3.5	0.2	2.7	4.6	0.8
19	15391262	15443101	ENSG00000141867	*BRD4*	0.2	-0.8	0.3	2.4	1.0	1.1
2	192242643	192245730	ENSG00000128641	*MYO1B*	1.1	0.8	-0.1	0.5	2.3	1.4
21	37447900	37451603	ENSG00000185917	*SETD4*	11.5	14.3	10.7	12.2	15.3	16.5
21	37447900	37451603	ENSG00000230212	*AP000688.14*	11.5	14.3	10.7	12.2	15.3	16.5
3	43514088	43526464	ENSG00000160746	*ANO10*	1.2	2.2	0.3	1.8	3.1	2.6

					ΔPSI(siCo+HS)			ΔPSI(siBRD4+HS)		
chr	**start**	**end**	**ensg**	**name**	**rep1**	**rep2**	**rep3**	**rep1**	**rep2**	**rep3**
5	142421455	142434004	ENSG00000145819	*ARHGAP26*	0.1	-0.2	0.7	0.7	1.0	1.5
8	141944689	141950661	ENSG00000169398	*PTK2*	0.5	0.2	-0.5	2.9	2.4	1.2
1	97189150	97215087	ENSG00000117569	*PTBP2*	-0.4	-0.7	0.5	0.8	-0.4	1.6
1	197684204	197703139	ENSG00000213047	*DENND1B*	11.5	0.5	-0.2	12.2	1.1	-0.7
1	110274972	110276554	ENSG00000241720	*RP4-735C1.4*	1.4	0.4	0.0	2.8	1.1	-0.1
1	146462830	146463540	ENSG00000186275	*NBPF12*	1.7	0.7	-0.9	2.8	-0.5	1.5
1	173803657	173806078	ENSG00000117593	*DARS2*	1.1	0.3	-0.6	1.9	1.0	-0.3
1	173819617	173820974	ENSG00000117593	*DARS2*	-2.2	-0.5	0.3	0.9	-0.1	1.0
10	95806882	95841707	ENSG00000138193	*PLCE1*	2.2	2.3	10.7	1.6	2.9	16.5
10	13542679	13544861	ENSG00000165626	*BEND7*	1.9	14.3	10.7	1.2	15.3	16.5
10	90708710	90712488	ENSG00000107796	*ACTA2*	-0.9	0.2	-0.5	1.3	-0.4	1.3
10	96064402	96066184	ENSG00000138193	*PLCE1*	0.8	1.3	-0.3	1.6	2.3	0.8
10	104861083	104865115	ENSG00000076685	*NT5C2*	-1.1	-0.2	-0.3	1.2	-0.6	0.8
10	114166432	114168180	ENSG00000197142	*ACSL5*	-11.5	1.0	10.7	3.8	1.7	16.5
11	180404	185902	ENSG00000177951	*BET1L*	11.5	5.3	5.9	12.2	6.5	6.4
11	67011287	67012549	ENSG00000173120	*KDM2A*	11.5	0.3	1.1	12.2	-0.2	1.7
12	52416723	52430961	ENSG00000123358	*NR4A1*	11.5	2.2	0.6	12.2	1.2	1.4
12	15837236	15865787	ENSG00000151491	*EPS8*	-1.2	0.5	-1.5	0.9	1.2	-0.4
12	69252851	69260605	ENSG00000135678	*CPM*	-0.4	-3.9	1.2	1.0	-12.4	1.9
12	9578716	9580229	ENSG00000214826	*DDX12P*	1.5	-0.3	-0.2	2.2	-0.9	0.9
12	11126320	11138512	ENSG00000212127	*TAS2R14*	0.0	-0.4	0.3	1.0	0.8	0.3
12	11126320	11138512	ENSG00000111215	*PRR4*	-0.2	-0.3	0.2	1.3	0.7	0.2
14	51060614	51062294	ENSG00000198513	*ATL1*	-0.7	1.1	2.5	0.7	1.9	1.7
14	55749361	55754316	ENSG00000178974	*FBXO34*	11.5	1.3	5.0	12.2	3.2	3.8
14	101406974	101407463	ENSG00000225746	*AL132709.5*	11.5	14.3	10.7	12.2	15.3	16.5
15	64795257	64820866	ENSG00000180357	*ZNF609*	1.3	0.3	0.5	2.2	1.1	-0.1
16	18458491	18462115	ENSG00000205746	*RP11-1212A22.1*	-1.3	-0.3	-1.1	1.3	1.1	0.1
16	18458491	18462115	ENSG00000254681	*PKD1P5*	-1.2	-0.3	-0.8	1.0	1.0	0.2
16	70376002	70380102	ENSG00000261777	*RP11-529K1.2*	2.0	-0.7	0.2	2.9	-0.9	1.2
17	6510590	6511668	ENSG00000198920	*KIAA0753*	0.2	-0.3	0.2	1.3	0.7	-0.4
17	74073622	74075263	ENSG00000186919	*ZACN*	11.5	14.3	0.8	12.2	15.3	1.4
19	11531880	11532345	ENSG00000198003	*CCDC151*	11.5	2.5	1.2	12.2	2.4	2.0
19	54059162	54067017	ENSG00000130844	*ZNF331*	-0.4	0.8	0.0	2.0	0.6	0.7
2	47206046	47220589	ENSG00000068724	*TTC7A*	0.3	0.3	-0.7	1.3	1.3	-0.6
2	39515421	39517433	ENSG00000011566	*MAP4K3*	-0.3	1.3	1.0	0.7	0.9	1.6
2	43456755	43457975	ENSG00000115970	*THADA*	-0.4	-0.2	2.6	0.6	-0.5	3.5
2	43456755	43457975	ENSG00000234936	*AC010883.5*	-0.4	-0.1	2.2	1.1	-0.2	3.4
2	160571109	160572192	ENSG00000136536	*MARCH7*	0.7	0.3	1.4	1.6	0.9	0.4
20	47860614	47861122	ENSG00000124201	*ZNFX1*	2.2	3.2	1.7	3.7	2.9	3.0
21	33959683	33964389	ENSG00000265590	*AP000275.65*	11.5	1.2	10.7	12.2	0.9	16.5
21	33957843	33959623	ENSG00000265590	*AP000275.65*	0.1	1.2	1.1	1.9	2.1	2.3
22	41560134	41562603	ENSG00000100393	*EP300*	-0.8	0.6	0.0	-0.2	1.3	0.7

					ΔPSI(siCo+HS)			ΔPSI(siBRD4+HS)		
chr	**start**	**end**	**ensg**	**name**	**rep1**	**rep2**	**rep3**	**rep1**	**rep2**	**rep3**
3	195388712	195389442	ENSG00000215837	*SDHAP2*	0.3	1.1	0.5	2.8	0.6	1.4
4	126384822	126389667	ENSG00000196159	*FAT4*	1.0	0.5	-0.1	1.0	2.3	0.9
4	8376879	8383219	ENSG00000087008	*ACOX3*	-1.6	-0.3	0.0	0.6	1.0	-0.8
4	106602133	106603618	ENSG00000236699	*ARHGEF38*	1.9	2.0	-0.1	2.9	1.2	0.6
4	107114927	107115875	ENSG00000145348	*TBCK*	0.7	-0.5	0.7	1.5	1.3	0.5
5	70331623	70333334	ENSG00000145736	*GTF2H2*	-0.5	-0.1	-0.4	1.6	0.7	0.0
5	121356497	121358065	ENSG00000151304	*SRFBP1*	2.3	2.3	3.9	3.9	3.1	2.9
6	126924797	126964634	ENSG00000260527	*RP11-73O6.4*	-1.9	-0.4	-0.9	0.6	0.6	0.3
6	31514750	31515358	ENSG00000213760	*ATP6V1G2*	0.7	1.5	1.9	1.4	2.5	0.9
6	31514750	31515358	ENSG00000204498	*NFKBIL1*	0.8	2.0	2.1	1.9	2.7	1.4
6	38050233	38056107	ENSG00000156639	*ZFAND3*	0.1	-0.1	0.7	0.2	0.7	1.4
6	114281203	114283531	ENSG00000196591	*HDAC2*	0.4	0.7	0.1	1.7	0.3	0.9
6	121560334	121562611	ENSG00000146350	*C6orf170*	-0.2	14.3	0.5	0.9	15.3	3.6
7	8010136	8019943	ENSG00000106415	*GLCCI1*	0.5	0.5	0.2	0.7	2.2	1.0
7	28452536	28475234	ENSG00000146592	*CREB5*	-11.5	2.8	1.6	1.8	1.8	2.4
7	158716424	158718878	ENSG00000126870	*WDR60*	2.7	-0.2	-15.5	3.5	0.8	1.1
8	74885228	74888065	ENSG00000175606	*TMEM70*	11.5	-1.3	0.2	12.2	1.8	0.9
8	100844880	100847425	ENSG00000132549	*VPS13B*	-0.1	-0.3	0.7	0.8	1.0	0.4
8	100871708	100874004	ENSG00000132549	*VPS13B*	0.4	-0.5	-0.3	3.8	0.6	0.0
X	129350075	129354323	ENSG00000056277	*ZNF280C*	-0.4	0.0	-15.5	2.6	-0.9	0.8
X	153193873	153194695	ENSG00000089820	*ARHGAP4*	-1.1	-1.5	-2.2	1.7	1.2	-1.8
1	40840380	40862507	ENSG00000084070	*SMAP2*	0.8	0.2	-0.1	2.1	1.5	0.7
1	45363116	45378740	ENSG00000070785	*EIF2B3*	0.7	-1.6	-0.5	1.6	0.7	-0.7
1	46365660	46379260	ENSG00000086015	*MAST2*	-0.6	-0.7	0.8	1.4	-0.3	2.4
1	45403020	45406301	ENSG00000070785	*EIF2B3*	11.5	-0.5	-2.8	12.2	1.0	0.0
1	100905554	100908490	ENSG00000079335	*CDC14A*	0.8	-1.0	1.3	1.4	-0.1	1.9
1	110236367	110244274	ENSG00000241720	*RP4-735C1.4*	1.1	-0.2	-1.7	2.9	0.9	-1.2
1	110236367	110244274	ENSG00000134184	*GSTM1*	1.5	-0.3	-1.7	3.6	0.9	-1.2
1	110268690	110274797	ENSG00000241720	*RP4-735C1.4*	11.5	1.3	2.5	12.2	2.4	2.1
1	153538341	153539178	ENSG00000196754	*S100A2*	0.3	0.7	1.1	3.8	1.6	0.8
10	518489	530721	ENSG00000151240	*DIP2C*	-1.1	-0.6	-0.5	1.0	-0.5	0.6
10	99923154	99946224	ENSG00000166024	*R3HCC1L*	11.5	0.0	0.8	12.2	1.4	1.8
11	47130869	47144655	ENSG00000149179	*C11orf49*	1.2	-0.5	1.2	2.0	0.6	0.7
11	64649417	64655700	ENSG00000110047	*EHD1*	0.8	2.2	10.7	3.1	2.7	16.5
11	71842953	71846756	ENSG00000110203	*FOLR3*	1.4	-0.8	-0.7	2.3	0.3	0.8
12	42566011	42592938	ENSG00000015153	*YAF2*	-1.3	1.0	0.0	0.6	0.7	1.3
12	70595784	70612912	ENSG00000257815	*RP11-611E13.2*	11.5	0.6	0.1	12.2	1.8	0.4
12	64475704	64480779	ENSG00000255886	*RP11-196H14.2*	11.5	1.8	-15.5	12.2	-0.7	1.2
12	64475704	64480779	ENSG00000196935	*SRGAP1*	11.5	1.5	-15.5	12.2	-0.9	1.1
12	99097277	99100263	ENSG00000120868	*APAF1*	-0.8	-0.1	0.1	0.9	0.8	-0.5
13	36129239	36141042	ENSG00000172915	*NBEA*	1.2	1.2	1.0	2.4	1.9	2.6

					ΔPSI(siCo+HS)			ΔPSI(siBRD4+HS)		
chr	**start**	**end**	**ensg**	**name**	**rep1**	**rep2**	**rep3**	**rep1**	**rep2**	**rep3**
14	64932331	64933825	ENSG00000089775	*ZBTB25*	-0.5	1.5	3.8	2.4	2.2	3.7
14	68937436	68938750	ENSG00000182185	*RAD51B*	-1.5	0.4	0.9	0.9	-0.2	1.5
14	100344956	100349578	ENSG00000066629	*EML1*	0.8	-0.2	-1.2	1.7	1.0	0.5
15	72186119	72189231	ENSG00000066933	*MYO9A*	-11.5	-0.1	-0.2	1.2	-0.2	1.0
15	42213939	42218279	ENSG00000103966	*EHD4*	1.7	-0.9	1.1	2.4	1.1	0.5
15	45974859	45980535	ENSG00000137767	*SQRDL*	1.0	0.2	0.5	2.5	0.6	1.3
15	89436343	89438690	ENSG00000140511	*HAPLN3*	0.7	-1.4	-1.4	1.9	1.6	-0.9
16	11343635	11348262	ENSG00000175643	*RMI2*	0.5	1.4	3.2	2.3	3.4	3.5
16	19071318	19073100	ENSG00000170537	*TMC7*	-1.7	1.2	-0.2	1.5	-0.7	0.6
16	71919279	71924472	ENSG00000182149	*IST1*	1.1	0.3	-0.1	0.9	1.0	0.7
17	49302585	49326940	ENSG00000011258	*MBTD1*	11.5	2.7	0.1	12.2	2.5	1.2
17	443816	454874	ENSG00000141252	*VPS53*	1.0	2.3	0.8	2.0	3.1	1.6
18	8635797	8636187	ENSG00000206418	*RAB12*	1.1	2.1	10.7	2.7	0.8	16.5
18	8635797	8636187	ENSG00000266708	*RP11-661O13.1*	0.9	1.8	10.7	2.8	0.7	16.5
18	21063104	21066072	ENSG00000101782	*RIOK3*	2.6	4.1	10.7	3.7	3.2	16.5
19	58341932	58350391	ENSG00000198466	*ZNF587*	1.5	-0.3	0.5	2.9	1.1	-0.3
19	9641743	9643521	ENSG00000130818	*ZNF426*	-0.1	-0.8	1.1	1.0	0.2	2.4
19	37080603	37084748	ENSG00000233527	*AC092295.7*	-0.4	0.3	-3.9	1.7	1.1	-1.3
19	37080603	37084748	ENSG00000186020	*ZNF529*	-1.3	0.7	-3.5	1.0	1.5	-0.7
2	112552617	112558374	ENSG00000153107	*ANAPC1*	1.6	-0.1	-0.1	2.2	1.0	0.1
2	197767466	197777606	ENSG00000197121	*PGAP1*	0.1	-0.2	-0.7	1.0	0.2	0.9
2	159195597	159196754	ENSG00000153237	*CCDC148*	11.5	-0.4	-2.5	12.2	-1.2	0.8
2	208591600	208598671	ENSG00000163249	*CCNYL1*	1.0	-1.5	0.8	1.8	1.8	1.1
2	219146931	219148762	ENSG00000127838	*PNKD*	1.5	1.0	1.0	2.9	2.8	0.1
2	219146931	219148762	ENSG00000135926	*TMBIM1*	2.0	1.1	1.3	3.1	2.9	0.4
2	220060091	220065154	ENSG00000158552	*ZFAND2B*	2.0	14.3	3.0	2.7	15.3	3.8
3	43129560	43131980	ENSG00000144647	*GTDC2*	11.5	-0.7	-0.7	12.2	1.3	0.0
4	75231092	75245165	ENSG00000124882	*EREG*	2.5	-0.6	2.1	3.7	1.4	2.4
4	83803093	83811848	ENSG00000138674	*SEC31A*	0.6	1.5	0.6	1.3	1.5	1.2
4	153271276	153273622	ENSG00000109670	*FBXW7*	-0.9	0.2	1.1	2.1	0.9	0.0
4	78695870	78697425	ENSG00000138767	*CNOT6L*	-0.3	0.3	0.9	1.1	1.2	1.2
4	113479465	113481889	ENSG00000138658	*C4orf21*	0.1	-0.9	0.5	0.8	0.7	-0.2
4	154547377	154548757	ENSG00000121210	*KIAA0922*	1.0	0.5	-1.9	2.5	0.2	0.9
5	56517223	56526531	ENSG00000062194	*GPBP1*	11.5	1.0	0.0	12.2	1.5	0.3
6	144665440	144719095	ENSG00000152818	*UTRN*	0.6	0.3	0.9	1.6	1.4	0.6
6	128313854	128316394	ENSG00000152894	*PTPRK*	-0.7	1.5	1.7	0.6	1.6	2.6
7	8021859	8043527	ENSG00000106415	*GLCCI1*	1.5	14.3	-0.8	2.9	15.3	0.8
8	131020699	131028616	ENSG00000153310	*FAM49B*	11.5	2.0	2.8	12.2	2.6	2.7
8	136533598	136550777	ENSG00000131773	*KHDRBS3*	-0.4	-1.9	-1.0	1.5	-0.8	0.7
8	17354746	17359766	ENSG00000003989	*SLC7A2*	0.6	-0.2	1.4	1.5	0.9	1.1
9	130854368	130856596	ENSG00000148339	*SLC25A25*	1.2	14.3	1.4	2.8	15.3	1.1
1	39361741	39376994	ENSG00000228436	*RP5-864K19.4*	1.7	-0.4	-0.5	2.4	-0.9	0.6

					ΔPSI(siCo+HS)			ΔPSI(siBRD4+HS)		
chr	**start**	**end**	**ensg**	**name**	**rep1**	**rep2**	**rep3**	**rep1**	**rep2**	**rep3**
1	117635523	117637265	ENSG00000116830	*TTF2*	1.1	0.2	0.4	2.2	1.2	-0.4
1	212561074	212583468	ENSG00000065600	*TMEM206*	0.6	-0.2	2.4	1.3	0.6	0.6
1	59007281	59008155	ENSG00000162600	*OMA1*	11.5	-1.4	-0.8	12.2	-1.2	0.9
1	144159043	144159763	ENSG00000162825	*RP3-377D14.1*	1.0	0.9	2.3	2.6	1.8	1.5
1	148325966	148326676	ENSG00000203832	*NBPF20*	-0.1	-1.0	-15.5	2.1	0.8	1.0
1	185245800	185249976	ENSG00000116668	*SWT1*	0.1	1.9	0.4	1.8	1.3	1.6
10	46112019	46113213	ENSG00000172671	*ZFAND4*	1.0	0.4	-0.1	2.0	1.2	0.5
10	101668903	101673710	ENSG00000107554	*DNMBP*	-0.3	0.8	0.3	1.1	1.6	-0.4
10	106207575	106209829	ENSG00000120051	*CCDC147*	2.2	-0.2	0.0	3.4	-0.1	0.7
11	45907472	45918101	ENSG00000121653	*MAPK8IP1*	0.9	0.3	1.0	3.1	1.4	0.1
11	33573787	33581295	ENSG00000110427	*KIAA1549L*	0.9	-0.1	2.1	1.5	0.7	2.8
12	49627921	49650180	ENSG00000167553	*TUBA1C*	0.6	0.4	0.4	1.7	0.6	1.0
12	51868990	51873776	ENSG00000050438	*SLC4A8*	-0.3	0.4	-0.1	1.1	0.7	0.6
12	56721415	56721677	ENSG00000135473	*PAN2*	-1.9	0.7	1.4	1.7	2.0	0.4
13	48939107	48941630	ENSG00000139687	*RB1*	0.3	0.1	0.0	0.3	0.8	0.6
15	57182365	57208924	ENSG00000137871	*ZNF280D*	-11.5	0.1	3.2	3.9	1.6	3.3
16	70253894	70254624	ENSG00000261556	*RP11-296I10.6*	0.9	1.2	-1.6	1.6	0.3	0.9
16	88893524	88898406	ENSG00000141012	*GALNS*	-0.1	-0.2	0.2	0.6	-0.6	1.1
17	1718089	1731155	ENSG00000186532	*SMYD4*	0.6	-0.2	0.0	1.9	0.9	0.6
17	18077235	18079879	ENSG00000266677	*RP11-258F1.1*	11.5	3.1	0.1	12.2	3.9	-0.7
19	45690998	45702147	ENSG00000007047	*MARK4*	2.0	-0.7	0.4	3.1	1.0	0.6
2	24236280	24239026	ENSG00000205639	*MFSD2B*	0.7	1.5	0.6	1.5	2.1	1.6
2	69748120	69752165	ENSG00000115977	*AAK1*	-0.7	-0.3	0.6	0.6	0.7	0.1
20	44536543	44538155	ENSG00000100979	*PLTP*	0.3	0.4	1.7	3.6	2.5	0.9
3	196033883	196042953	ENSG00000213123	*TCTEX1D2*	0.6	0.2	0.5	1.4	0.8	0.4
3	8817350	8819163	ENSG00000070950	*RAD18*	1.9	1.5	1.3	3.1	1.9	3.3
3	113675353	113676421	ENSG00000184307	*ZDHHC23*	11.5	0.6	1.0	12.2	0.8	2.1
3	129100279	129101765	ENSG00000244932	*RP11-529F4.1*	-0.5	0.4	1.8	0.8	1.8	1.1
3	141006296	141010430	ENSG00000155893	*ACPL2*	1.1	0.4	-0.7	1.8	1.6	-0.3
5	142006755	142023678	ENSG00000113578	*FGF1*	-1.6	-0.7	-0.5	1.8	-0.2	2.1
5	118811568	118812143	ENSG00000133835	*HSD17B4*	11.5	1.3	0.2	12.2	1.4	1.3
8	41134522	41155682	ENSG00000104332	*SFRP1*	1.6	-1.2	-0.1	2.2	0.1	0.6
8	38259201	38260043	ENSG00000165046	*LETM2*	0.1	0.7	-0.4	1.4	1.2	0.8
8	145775057	145780944	ENSG00000147799	*ARHGAP39*	0.2	2.1	1.8	3.0	1.7	2.4
X	153006173	153008441	ENSG00000101986	*ABCD1*	3.0	-0.8	0.3	2.9	0.6	1.1
1	19751163	19775328	ENSG00000077549	*CAPZB*	2.2	-0.1	0.9	2.8	0.9	0.8
1	32398301	32398621	ENSG00000184007	*PTP4A2*	4.5	1.1	1.5	4.3	3.1	3.1
1	47046299	47048486	ENSG00000079277	*MKNK1*	-0.7	0.3	0.4	1.2	1.2	0.2
1	54707182	54707837	ENSG00000157216	*SSBP3*	3.0	1.2	0.3	2.0	2.0	0.9
1	84641490	84644518	ENSG00000142875	*PRKACB*	0.2	0.8	-0.3	0.8	0.5	0.7
1	117658311	117659238	ENSG00000134253	*TRIM45*	-1.3	-1.0	0.0	0.9	-1.6	0.8

					ΔPSI(siCo+HS)			ΔPSI(siBRD4+HS)		
chr	**start**	**end**	**ensg**	**name**	**rep1**	**rep2**	**rep3**	**rep1**	**rep2**	**rep3**
1	144341077	144341670	ENSG00000231360	*AL592284.2*	-0.2	0.6	2.1	2.6	-0.1	3.5
1	146431261	146431971	ENSG00000186275	*NBPF12*	1.5	0.7	-0.2	2.5	1.9	0.2
1	153957838	153958493	ENSG00000143545	*RAB13*	1.2	-0.2	-0.1	2.6	0.9	0.6
1	224906810	224910169	ENSG00000143786	*CNIH3*	11.5	1.8	2.1	12.2	2.5	1.7
10	33559784	33577234	ENSG00000099250	*NRP1*	1.9	1.3	-0.4	2.7	0.7	0.6
11	9950810	9978115	ENSG00000133812	*SBF2*	-0.3	1.7	1.2	1.4	2.3	0.9
11	10860120	10871444	ENSG00000236287	*ZBED5*	1.8	0.3	0.5	2.5	-0.4	1.9
11	47144892	47152259	ENSG00000149179	*C11orf49*	0.9	-2.6	-2.1	1.9	-0.9	1.2
13	33274006	33275121	ENSG00000083642	*PDS5B*	-1.6	1.1	0.7	2.2	1.9	1.7
13	114133393	114134781	ENSG00000150401	*DCUN1D2*	0.7	1.9	-0.8	1.4	-0.7	1.4
14	88971715	88974267	ENSG00000070778	*PTPN21*	-0.1	0.6	0.6	0.6	0.1	1.2
14	89689686	89697072	ENSG00000053254	*FOXN3*	11.5	0.8	10.7	12.2	2.1	16.5
14	101452077	101452394	ENSG00000232018	*AL132709.8*	11.5	3.7	10.7	12.2	2.8	16.5
15	43147398	43149593	ENSG00000128881	*TTBK2*	-2.6	-0.8	0.1	0.9	-12.4	1.0
15	72543692	72545778	ENSG00000137817	*PARP6*	0.4	-0.3	0.2	1.2	-0.5	1.5
16	16477649	16481256	ENSG00000214967	*RP11-467M13.1*	0.8	0.3	-0.1	1.4	-1.0	0.6
16	23406267	23409367	ENSG00000168434	*COG7*	3.0	0.1	0.1	4.4	1.0	0.3
16	72841091	72843246	ENSG00000140836	*ZFHX3*	-0.3	0.1	-0.5	0.8	-1.6	0.7
17	63800553	63822256	ENSG00000154240	*CEP112*	1.3	0.6	0.2	2.0	1.6	0.2
17	30222030	30226665	ENSG00000108651	*UTP6*	0.8	1.2	1.4	1.6	2.1	1.3
17	35787108	35796488	ENSG00000108264	*TADA2A*	-0.2	-0.2	0.5	0.8	-0.4	1.8
18	12326618	12328943	ENSG00000176014	*TUBB6*	0.0	-0.7	-0.6	0.9	0.8	-0.7
19	36704294	36705504	ENSG00000196357	*ZNF565*	11.5	0.2	-0.2	12.2	1.8	-1.0
19	46133304	46135779	ENSG00000125746	*EML2*	1.2	-0.1	-0.9	1.9	1.2	-0.1
19	55544233	55549571	ENSG00000267149	*CTC-550B14.6*	2.2	2.4	0.6	3.6	2.4	1.2
2	39811950	39814156	ENSG00000231312	*AC007246.3*	2.3	0.6	0.3	2.4	1.5	1.7
2	165522411	165536698	ENSG00000082438	*COBLL1*	0.8	1.7	-0.5	2.1	1.4	1.1
2	179257265	179259040	ENSG00000079156	*OSBPL6*	-0.4	-0.6	0.2	0.8	0.7	1.4
2	203086729	203096266	ENSG00000116030	*SUMO1*	-0.4	-0.4	-0.7	0.8	0.9	-1.0
2	234328067	234343026	ENSG00000077044	*DGKD*	-0.1	-0.6	-0.1	1.2	0.6	0.0
2	61546462	61552510	ENSG00000115464	*USP34*	0.2	0.2	0.0	0.9	1.4	0.3
2	95963201	95964431	ENSG00000115041	*KCNIP3*	11.5	3.8	10.7	12.2	3.3	16.5
2	197706096	197707445	ENSG00000197121	*PGAP1*	0.6	-0.2	-0.5	1.0	0.8	0.7
20	45523626	45529782	ENSG00000064655	*EYA2*	1.6	0.3	-1.0	2.3	1.2	0.5
21	34841990	34851105	ENSG00000159128	*IFNGR2*	11.5	-0.1	-0.3	12.2	-0.1	1.3
21	34841990	34851105	ENSG00000142188	*TMEM50B*	11.5	-0.1	-0.4	12.2	-0.1	1.0
3	14523349	14526375	ENSG00000131389	*SLC6A6*	1.0	0.2	-0.2	2.7	0.8	0.1
3	14693385	14695933	ENSG00000154781	*C3orf19*	-0.2	0.2	-0.4	0.9	-0.6	0.7
3	41291065	41292414	ENSG00000168036	*CTNNB1*	11.5	-0.4	-0.6	12.2	0.1	1.3
3	41291065	41292414	ENSG00000168038	*ULK4*	11.5	-0.6	-0.8	12.2	0.0	1.0
3	155611488	155613202	ENSG00000163655	*GMPS*	0.4	-0.2	-0.1	1.1	0.7	0.0
4	89653710	89657512	ENSG00000138640	*FAM13A*	-1.2	-0.6	-2.0	0.8	0.6	-0.7

					ΔPSI(siCo+HS)			ΔPSI(siBRD4+HS)		
chr	**start**	**end**	**ensg**	**name**	**rep1**	**rep2**	**rep3**	**rep1**	**rep2**	**rep3**
5	148691938	148695203	ENSG00000157510	*AFAP1L1*	0.1	0.6	-1.0	1.7	1.6	-1.4
5	167843527	167849013	ENSG00000113645	*WWC1*	1.1	0.5	1.9	3.4	1.1	1.4
5	172186156	172189218	ENSG00000253295	*RP11-779O18.1*	11.5	14.3	3.1	12.2	15.3	3.5
5	174937315	174938439	ENSG00000164466	*SFXN1*	0.5	0.5	1.4	1.2	1.4	1.1
5	178999742	179004076	ENSG00000176783	*RUFY1*	0.4	0.0	-0.7	1.3	0.8	-0.2
6	45127248	45165411	ENSG00000196284	*SUPT3H*	0.5	-0.2	-0.6	3.3	1.9	-0.9
6	52906206	52916789	ENSG00000112144	*ICK*	-0.3	0.2	-0.7	1.0	0.9	0.2
6	84871628	84872863	ENSG00000135315	*KIAA1009*	-1.0	1.4	0.8	0.7	2.0	0.1
7	19095788	19152097	ENSG00000122691	*TWIST1*	1.0	2.4	4.3	2.6	3.4	4.2
7	72138146	72159677	ENSG00000254184	*TYW1B*	11.5	1.5	2.8	12.2	2.2	2.2
7	102969958	102975689	ENSG00000105821	*DNAJC2*	-0.2	-1.3	0.8	0.4	0.7	1.7
8	66683496	66691955	ENSG00000205268	*PDE7A*	1.2	-0.8	0.1	1.9	0.3	0.8
9	5123121	5125965	ENSG00000096968	*JAK2*	11.5	0.6	-0.3	12.2	1.2	1.1
9	37832138	37835659	ENSG00000122741	*DCAF10*	11.5	-0.7	1.1	12.2	-12.4	2.4
9	37832138	37835659	ENSG00000255872	*RP11-613M10.9*	11.5	-0.9	0.9	12.2	-12.4	2.3
9	135487700	135493717	ENSG00000125485	*DDX31*	-1.0	0.7	-0.1	1.2	0.8	1.2
9	139777162	139780517	ENSG00000127191	*TRAF2*	0.9	0.6	-0.3	2.3	1.0	1.0
1	65730615	65745139	ENSG00000116675	*DNAJC6*	3.1	2.5	0.2	4.9	3.5	0.4
1	227916487	227918126	ENSG00000143740	*SNAP47*	1.3	0.1	-0.4	2.5	1.6	0.9
1	28844087	28844648	ENSG00000180198	*RCC1*	1.5	-0.5	-1.9	3.1	0.9	-1.4
1	36913488	36915859	ENSG00000116885	*OSCP1*	1.1	0.1	0.0	2.3	-0.3	1.0
1	146036740	146037450	ENSG00000232637	*WI2-3658N16.1*	-0.8	0.2	1.0	1.8	0.3	1.9
1	146036740	146037450	ENSG00000152042	*NBPF11*	-0.8	0.3	0.8	1.7	0.4	1.8
1	222988513	222997198	ENSG00000228106	*RP11-452F19.3*	-0.5	-0.2	0.8	0.7	0.6	1.1
12	29435293	29444349	ENSG00000064763	*FAR2*	11.5	-0.9	-0.1	12.2	0.7	0.7
13	111811436	111837285	ENSG00000102606	*ARHGEF7*	-11.5	1.1	2.6	3.1	2.7	2.8
15	74905852	74907170	ENSG00000179335	*CLK3*	11.5	1.0	2.4	12.2	1.9	2.4
16	28900274	28903636	ENSG00000196296	*ATP2A1*	0.1	0.3	0.7	1.1	1.2	0.5
16	68287420	68288256	ENSG00000103066	*PLA2G15*	0.6	1.2	0.5	3.2	1.8	1.1
17	2935743	2936375	ENSG00000132359	*RAP1GAP2*	1.2	0.0	1.0	1.9	-0.1	2.2
18	19757082	19760073	ENSG00000141448	*GATA6*	1.7	14.3	2.7	3.1	15.3	2.9
2	100185377	100194789	ENSG00000144218	*AFF3*	1.4	1.0	0.9	2.9	2.6	1.9
2	190430325	190436441	ENSG00000138449	*SLC40A1*	1.9	-0.1	-0.1	4.2	0.4	0.8
2	191221534	191224372	ENSG00000151689	*INPP1*	-1.2	0.6	4.4	2.0	1.8	4.2
20	4781708	4795748	ENSG00000101265	*RASSF2*	1.7	1.0	-0.2	3.9	0.4	0.8
3	139163205	139169122	ENSG00000248932	*RP11-319G6.1*	11.5	-0.3	0.5	12.2	0.8	0.1
3	15313178	15314623	ENSG00000131370	*SH3BP5*	11.5	-0.3	2.4	12.2	0.8	2.0
3	183956661	183957182	ENSG00000145191	*EIF2B5*	2.2	0.0	3.2	3.7	1.1	2.9
4	113532175	113533680	ENSG00000138658	*C4orf21*	11.5	14.3	4.3	12.2	15.3	4.1
5	145694581	145718587	ENSG00000091009	*RBM27*	1.9	-0.3	0.1	4.2	-0.8	1.0
6	42153535	42156320	ENSG00000112599	*GUCA1B*	0.5	1.4	10.7	1.5	-0.2	16.5

					ΔPSI(siCo+HS)			ΔPSI(siBRD4+HS)		
chr	**start**	**end**	**ensg**	**name**	**rep1**	**rep2**	**rep3**	**rep1**	**rep2**	**rep3**
6	143097328	143100680	ENSG00000010818	*HIVEP2*	-1.2	0.0	0.6	1.4	0.2	1.6
6	43457766	43465619	ENSG00000137221	*TJAP1*	0.3	0.7	-0.1	1.0	1.3	-0.4
7	138230223	138235808	ENSG00000122779	*TRIM24*	0.1	1.7	-0.1	1.8	2.0	0.8
8	6420930	6475996	ENSG00000147316	*MCPH1*	1.1	1.2	-0.5	3.1	1.8	0.8
8	109261031	109321251	ENSG00000104408	*EIF3E*	-0.3	-0.1	10.7	1.8	-0.3	16.5
9	132872705	132876856	ENSG00000148358	*GPR107*	-0.1	0.3	-1.1	1.1	1.5	0.0
9	33348721	33351558	ENSG00000086102	*NFX1*	0.7	-0.8	1.4	2.3	1.6	1.3
9	37762682	37763626	ENSG00000255872	*RP11-613M10.9*	1.5	14.3	-0.1	2.3	15.3	0.8
9	139795128	139796396	ENSG00000127191	*TRAF2*	11.5	2.2	0.1	12.2	2.0	1.5
X	67913668	67932756	ENSG00000130052	*STARD8*	2.5	0.7	0.3	2.2	1.6	1.6
X	70712847	70747664	ENSG00000147133	*TAF1*	2.6	0.4	2.3	2.0	1.9	3.1
1	155452240	155490016	ENSG00000116539	*ASH1L*	-0.9	-0.2	0.1	1.2	-0.7	0.8
1	240990472	241031887	ENSG00000182901	*RGS7*	-0.3	0.1	-0.2	2.0	0.9	-0.3
1	244541941	244552253	ENSG00000240963	*RP11-518L10.2*	0.3	-0.4	4.0	2.7	0.9	3.2
1	169838269	169839396	ENSG00000000457	*SCYL3*	0.8	1.4	-0.1	1.7	1.9	1.2
10	129183173	129201319	ENSG00000150760	*DOCK1*	-0.1	0.2	0.7	1.3	1.2	0.0
10	50679166	50680422	ENSG00000225830	*ERCC6*	-0.2	-0.2	-0.4	2.5	-0.4	1.0
11	118280560	118301123	ENSG00000167283	*ATP5L*	-1.0	1.0	1.5	0.8	1.9	1.6
11	58956796	58958587	ENSG00000110042	*DTX4*	1.9	1.0	0.4	2.6	1.7	0.9
12	12707593	12713700	ENSG00000111266	*DUSP16*	1.4	2.6	2.3	2.7	1.8	2.9
13	47273538	47275256	ENSG00000136141	*LRCH1*	1.1	0.5	-0.1	1.7	1.1	0.0
14	59732879	59757935	ENSG00000100592	*DAAM1*	0.0	0.6	0.6	0.6	1.4	-0.2
14	55739023	55749014	ENSG00000178974	*FBXO34*	2.0	0.6	3.0	2.9	1.4	2.4
15	80353082	80364906	ENSG00000086666	*ZFAND6*	-0.3	0.2	0.4	1.2	0.9	0.2
15	102166766	102173146	ENSG00000184277	*TM2D3*	1.4	0.8	0.1	1.5	2.2	1.2
15	44066971	44067504	ENSG00000128886	*ELL3*	-0.2	0.4	2.0	1.2	1.6	1.2
15	44066971	44067504	ENSG00000262560	*RP11-296A16.1*	-0.3	0.3	2.0	1.3	1.5	1.1
17	20833359	20834906	ENSG00000233098	*RP11-344E13.3*	-0.2	1.1	-1.6	2.5	1.2	1.0
17	46180751	46184911	ENSG00000002919	*SNX11*	1.3	2.6	-15.5	2.6	1.8	3.0
18	9735599	9757960	ENSG00000168461	*RAB31*	11.5	1.8	1.4	12.2	4.1	1.5
19	36027892	36029209	ENSG00000105679	*GAPDHS*	11.5	2.3	1.0	12.2	3.7	2.0
2	217629733	217650497	ENSG00000236886	*AC007563.5*	2.8	14.3	4.0	5.5	15.3	4.7
2	70321610	70322091	ENSG00000226505	*AC016700.3*	11.5	14.3	10.7	12.2	15.3	16.5
2	110596570	110597954	ENSG00000015568	*RGPD5*	-2.1	-11.9	1.5	1.0	1.3	-1.0
2	234184648	234185794	ENSG00000085978	*ATG16L1*	0.4	0.4	0.9	1.2	1.2	0.3
21	38739930	38782872	ENSG00000157540	*DYRK1A*	-0.3	0.9	-0.2	0.7	0.9	0.8
22	28702631	28838874	ENSG00000100154	*TTC28*	0.3	0.1	0.4	2.1	0.8	0.3
3	31748912	31750207	ENSG00000144645	*OSBPL10*	2.9	14.3	5.0	3.6	15.3	5.1
4	146424123	146425004	ENSG00000170365	*SMAD1*	11.5	14.3	10.7	12.2	15.3	16.5
5	56147901	56152427	ENSG00000095015	*MAP3K1*	0.8	1.9	4.0	1.7	3.0	3.2
5	56147901	56152427	ENSG00000237705	*AC008937.2*	1.0	1.6	3.8	2.2	3.1	2.8

					ΔPSI(siCo+HS)			ΔPSI(siBRD4+HS)		
chr	**start**	**end**	**ensg**	**name**	**rep1**	**rep2**	**rep3**	**rep1**	**rep2**	**rep3**
5	177312347	177335466	ENSG00000170089	*RP11-423H2.1*	0.5	0.0	-0.6	1.1	0.6	-0.3
5	7904275	7905860	ENSG00000124275	*MTRR*	2.9	0.9	0.4	3.5	1.5	0.0
6	10764839	10770310	ENSG00000137210	*TMEM14B*	-0.7	-1.4	-0.2	3.2	0.8	0.3
7	151079067	151082174	ENSG00000187260	*WDR86*	1.5	-1.5	-0.3	2.1	1.3	-0.3
8	56618205	56637678	ENSG00000167904	*TMEM68*	11.5	0.6	2.2	12.2	1.7	1.7
8	6366583	6371199	ENSG00000147316	*MCPH1*	2.3	-1.3	2.5	4.2	0.9	2.3
9	5073785	5077453	ENSG00000096968	*JAK2*	1.8	2.6	2.5	3.9	3.3	1.0
9	37525169	37529121	ENSG00000147912	*FBXO10*	11.5	1.0	1.1	12.2	2.6	1.5
9	37525169	37529121	ENSG00000256966	*RP11-613M10.8*	11.5	0.9	0.9	12.2	2.6	1.5
1	77763710	77779480	ENSG00000154027	*AK5*	-0.9	1.7	1.4	3.8	3.4	1.8
1	110260888	110268442	ENSG00000241720	*RP4-735C1.4*	11.5	14.3	10.7	12.2	15.3	16.5
10	74928144	74934445	ENSG00000138286	*FAM149B1*	0.9	0.5	-0.2	1.6	1.2	0.3
10	99915904	99922640	ENSG00000166024	*R3HCC1L*	0.0	0.4	0.7	2.3	1.3	1.2
11	71177812	71183495	ENSG00000172890	*NADSYN1*	-0.1	0.1	0.3	3.1	0.8	0.7
12	46149788	46169864	ENSG00000189079	*ARID2*	-1.4	0.2	-3.5	1.1	1.1	0.2
14	19851016	19854098	ENSG00000257898	*RP11-496I2.3*	1.5	0.9	0.8	2.2	0.7	1.8
16	3536963	3543484	ENSG00000263212	*LA16c-306E5.3*	1.1	0.6	0.8	1.8	1.5	0.8
17	4857520	4858370	ENSG00000108515	*ENO3*	1.8	1.3	0.4	2.9	1.3	1.4
19	36694444	36703921	ENSG00000196357	*ZNF565*	0.1	0.1	0.4	1.9	1.2	-0.2
19	16766179	16769969	ENSG00000214046	*C19orf42*	11.5	0.6	2.1	12.2	1.8	1.0
19	57985789	57986392	ENSG00000197128	*ZNF772*	1.0	-0.8	0.7	1.7	0.7	-0.6
2	191557492	191564441	ENSG00000228509	*AC006460.2*	-1.7	0.2	-1.1	1.3	1.0	-0.7
2	203851060	203879280	ENSG00000138442	*WDR12*	2.0	-0.5	-0.1	2.7	0.9	0.8
2	27850784	27851114	ENSG00000243943	*ZNF512*	2.1	3.9	10.7	2.8	4.3	16.5
2	27850784	27851114	ENSG00000259080	*RP11-158I13.2*	2.3	3.8	10.7	2.9	4.3	16.5
3	41237197	41240136	ENSG00000168036	*CTNNB1*	0.5	0.5	0.0	1.2	0.7	0.6
3	57317467	57321929	ENSG00000239388	*ASB14*	1.7	1.6	0.0	3.7	3.3	0.4
3	187452735	187453878	ENSG00000113916	*BCL6*	1.3	2.6	1.5	2.5	2.6	2.2
4	183090531	183111370	ENSG00000218336	*ODZ3*	0.7	0.2	0.4	2.1	1.2	1.7
4	169785737	169798874	ENSG00000129116	*PALLD*	2.2	-2.2	0.5	3.7	-2.0	1.2
4	169785737	169798874	ENSG00000145439	*CBR4*	1.7	-2.2	0.4	2.7	-2.0	1.1
4	39472926	39474720	ENSG00000121897	*LIAS*	0.7	0.7	-0.1	1.2	0.4	1.3
6	1931233	1959940	ENSG00000112699	*GMDS*	1.7	1.6	1.9	1.2	2.2	2.9
6	99936696	99949619	ENSG00000123552	*USP45*	0.0	0.2	-1.2	2.1	0.8	-0.9
6	128770446	128812877	ENSG00000152894	*PTPRK*	1.8	1.0	0.5	1.2	1.9	1.1
6	126243980	126248809	ENSG00000260527	*RP11-73O6.4*	0.3	1.0	0.4	0.9	2.1	0.0
7	4201488	4213854	ENSG00000146555	*SDK1*	0.7	-0.1	-0.2	1.8	-0.4	0.7
7	44092550	44096339	ENSG00000136279	*DBNL*	0.0	-0.4	-0.2	2.6	1.2	-0.3
8	74746277	74782504	ENSG00000258677	*RP11-463D19.2*	0.6	-0.5	1.6	1.4	0.6	0.9
X	224547	228086	ENSG00000178605	*GTPBP6*	1.3	-0.7	-0.9	2.3	1.2	0.0
1	169631761	169652610	ENSG00000000460	*C1orf112*	1.4	0.9	1.4	3.5	1.4	2.3

					ΔPSI(siCo+HS)			ΔPSI(siBRD4+HS)		
chr	**start**	**end**	**ensg**	**name**	**rep1**	**rep2**	**rep3**	**rep1**	**rep2**	**rep3**
1	179993717	180000455	ENSG00000135837	*CEP350*	0.2	-0.3	-0.3	1.1	0.8	-1.2
1	241100006	241146379	ENSG00000182901	*RGS7*	1.4	0.2	0.2	3.0	1.8	0.1
1	145823596	145826388	ENSG00000117262	*GPR89A*	11.5	14.3	10.7	12.2	15.3	16.5
10	51764480	51767785	ENSG00000204149	*AGAP6*	1.4	-0.8	-15.5	2.1	0.9	0.4
11	64043231	64043820	ENSG00000002330	*BAD*	2.2	0.7	-1.0	3.3	2.3	-1.0
11	64043231	64043820	ENSG00000173264	*GPR137*	2.0	0.7	-0.9	2.8	2.0	-1.0
12	82702094	82736375	ENSG00000133773	*CCDC59*	11.5	5.6	10.7	12.2	4.8	16.5
12	122409975	122413150	ENSG00000158023	*WDR66*	0.9	0.0	-2.2	2.2	0.5	0.8
13	51929279	51935414	ENSG00000102786	*INTS6*	0.9	-0.2	-0.4	1.8	0.8	-0.8
14	101435359	101435796	ENSG00000232018	*AL132709.8*	2.0	0.4	2.2	3.4	0.2	3.1
15	102202019	102204373	ENSG00000185418	*TARSL2*	0.1	0.1	0.4	1.7	1.0	1.1
15	102177137	102182049	ENSG00000184277	*TM2D3*	1.2	2.5	2.1	1.8	3.3	2.3
16	29803835	29808207	ENSG00000079616	*KIF22*	0.7	-0.1	0.5	4.3	1.1	0.6
17	62126562	62130140	ENSG00000178607	*ERN1*	1.0	0.2	-2.3	1.6	0.9	-1.4
19	15355573	15357847	ENSG00000141867	*BRD4*	2.2	0.0	0.2	3.9	1.9	1.4
2	20527144	20531478	ENSG00000055917	*PUM2*	1.0	1.1	2.4	3.3	2.4	2.0
2	24011517	24021008	ENSG00000119778	*ATAD2B*	2.0	-0.2	1.9	2.6	0.6	1.3
2	73718625	73746902	ENSG00000116127	*ALMS1*	-0.8	0.2	-0.2	1.5	0.8	-0.4
3	183979251	183993799	ENSG00000145194	*ECE2*	-0.6	-0.6	-1.0	1.3	-0.2	0.6
3	183957824	183958215	ENSG00000145191	*EIF2B5*	11.5	-0.2	1.7	12.2	1.1	1.4
4	164069586	164078116	ENSG00000145414	*NAF1*	0.6	2.0	2.4	1.5	2.6	2.2
5	77339962	77352448	ENSG00000132842	*AP3B1*	2.1	0.4	2.2	2.5	1.1	3.3
6	90329923	90330933	ENSG00000083099	*LYRM2*	0.9	-0.9	0.0	3.1	-0.1	0.8
7	127672160	127682355	ENSG00000197157	*SND1*	11.5	14.3	10.7	12.2	15.3	16.5
8	141919720	141930913	ENSG00000169398	*PTK2*	0.4	-0.1	0.8	1.2	0.8	0.2
1	160201197	160206925	ENSG00000258465	*RP11-574F21.3*	-0.4	0.2	0.1	0.9	0.8	-0.1
1	160201197	160206925	ENSG00000132716	*DCAF8*	-0.5	0.3	0.2	0.8	0.9	0.0
10	74891586	74893414	ENSG00000122882	*ECD*	0.8	0.0	0.7	1.9	0.8	0.0
12	65637249	65639080	ENSG00000174106	*LEMD3*	1.0	1.0	2.3	1.8	1.0	3.1
15	44925835	44941064	ENSG00000104133	*SPG11*	0.3	0.5	0.5	1.7	1.6	1.3
18	8810196	8811129	ENSG00000168502	*SOGA2*	2.6	2.9	1.9	3.7	3.5	1.1
19	12639510	12659527	ENSG00000196826	*CTD-2192J16.17*	0.4	-0.9	1.2	2.7	-0.9	1.8
19	45721577	45728036	ENSG00000007047	*MARK4*	3.1	-0.3	10.7	4.2	2.1	16.5
2	132250713	132254783	ENSG00000152117	*AC093838.4*	-0.5	0.3	0.4	2.7	0.9	0.2
2	9618499	9621000	ENSG00000134330	*IAH1*	3.5	1.3	1.0	4.8	4.0	1.6
2	238965891	238969530	ENSG00000258984	*RP11-526L8.1*	-0.5	-0.9	-0.3	1.2	1.2	-0.3
20	11891155	11893962	ENSG00000132640	*BTBD3*	-0.4	0.0	0.3	0.9	1.0	0.2
20	11891155	11893962	ENSG00000236526	*RP4-742J24.2*	-0.4	0.1	0.2	1.0	1.1	0.3
3	29529990	29628605	ENSG00000144642	*RBMS3*	0.6	0.0	-0.2	1.2	0.6	-0.6
4	87857633	87869650	ENSG00000172493	*AFF1*	2.2	2.4	2.8	2.8	2.2	3.4
5	1800009	1801448	ENSG00000171421	*MRPL36*	1.1	-0.1	0.4	2.0	0.7	0.5

					ΔPSI(siCo+HS)			ΔPSI(siBRD4+HS)		
chr	**start**	**end**	**ensg**	**name**	**rep1**	**rep2**	**rep3**	**rep1**	**rep2**	**rep3**
5	112889719	112891749	ENSG00000047188	*YTHDC2*	1.6	1.4	1.3	2.4	2.2	1.0
5	132109904	132111427	ENSG00000164402	*Sep 08*	11.5	1.6	2.2	12.2	2.3	2.7
6	109935683	109940295	ENSG00000155085	*AKD1*	0.8	2.6	-0.9	2.6	1.0	0.8
6	88032795	88038856	ENSG00000111850	*C6orf162*	0.4	-0.6	1.5	1.6	1.0	1.5
7	1869300	1878222	ENSG00000002822	*MAD1L1*	11.5	2.0	0.8	12.2	-12.4	2.8
8	66647129	66651737	ENSG00000205268	*PDE7A*	-1.0	-0.4	-0.6	1.1	0.7	-0.8
8	88648878	88659145	ENSG00000253500	*AF121898.3*	2.1	2.0	10.7	2.9	1.6	16.5
8	145999990	146002843	ENSG00000196378	*ZNF34*	0.1	-2.0	-1.8	2.1	0.7	0.0
11	5663736	5664047	ENSG00000258588	*TRIM6-TRIM34*	11.5	-1.0	1.3	12.2	-0.4	2.1
11	5663736	5664047	ENSG00000258659	*TRIM34*	11.5	-1.0	1.3	12.2	-0.4	2.1
12	124212456	124215189	ENSG00000185344	*ATP6V0A2*	0.0	0.3	0.0	0.8	0.9	-0.4
13	31115102	31115780	ENSG00000189403	*HMGB1*	11.5	14.3	1.5	12.2	15.3	1.5
14	30127122	30132905	ENSG00000184304	*PRKD1*	2.6	0.7	0.3	3.6	2.3	0.6
15	30919152	30922906	ENSG00000187951	*ARHGAP11B*	-0.4	0.1	0.3	1.0	0.8	0.0
2	95969251	95975970	ENSG00000115041	*KCNIP3*	11.5	1.1	1.2	12.2	1.8	1.9
3	182817375	182833262	ENSG00000078070	*MCCC1*	-0.3	1.0	-0.5	1.4	2.5	1.0
3	185407415	185410487	ENSG00000073792	*IGF2BP2*	0.1	-0.2	0.1	0.5	0.9	0.8
4	99831110	99847123	ENSG00000151247	*EIF4E*	0.0	0.7	0.3	1.8	1.5	0.0
5	135483595	135488364	ENSG00000113658	*SMAD5*	0.3	3.5	0.0	1.8	3.6	0.9
7	736739	750966	ENSG00000188191	*PRKAR1B*	1.0	0.0	0.7	2.5	0.7	0.7
8	6484831	6492363	ENSG00000147316	*MCPH1*	0.1	-0.9	-0.7	2.0	1.6	0.9
9	37753849	37761900	ENSG00000255872	*RP11-613M10.9*	11.5	14.3	2.5	12.2	15.3	2.9
9	127691569	127693595	ENSG00000136935	*GOLGA1*	0.4	-1.3	-0.2	2.1	-0.5	0.6
9	132623891	132625465	ENSG00000136878	*USP20*	5.3	0.6	0.8	5.2	1.7	2.1
X	101860820	101870406	ENSG00000125962	*ARMCX5*	0.2	-0.7	-0.5	1.4	0.7	-0.2
13	99556960	99566582	ENSG00000088387	*DOCK9*	1.4	1.2	0.6	2.1	1.7	1.9
17	62534069	62538192	ENSG00000258890	*CEP95*	1.1	0.1	-0.1	0.7	1.0	0.6
2	9621576	9624561	ENSG00000134330	*IAH1*	2.6	0.0	0.6	3.3	0.9	0.4
2	70096996	70098877	ENSG00000087338	*GMCL1*	1.7	0.4	-0.3	3.1	-0.3	0.6
2	191537937	191541670	ENSG00000138386	*NAB1*	0.6	1.4	0.0	1.9	2.1	-0.3
2	200870500	200873189	ENSG00000162972	*C2orf47*	11.5	3.4	10.7	12.2	3.1	16.5
21	35515334	35552978	ENSG00000214955	*AP000318.2*	0.6	-1.2	-0.1	1.3	-0.6	1.4
3	20027674	20038295	ENSG00000183977	*PP2D1*	0.8	0.4	-0.2	1.6	1.1	-0.2
3	33076302	33079407	ENSG00000170266	*GLB1*	2.2	-3.5	-0.2	4.0	0.7	-1.2
3	46967025	46982105	ENSG00000160799	*CCDC12*	-0.1	-0.2	-0.1	1.4	0.7	0.1
3	185485692	185531843	ENSG00000073792	*IGF2BP2*	1.0	1.5	1.3	1.7	2.2	1.1
4	1901122	1902346	ENSG00000109685	*WHSC1*	11.5	-0.2	-1.5	12.2	1.1	-1.5
5	733954	741709	ENSG00000188818	*ZDHHC11*	11.5	14.3	0.8	12.2	15.3	3.2
7	4051867	4056803	ENSG00000146555	*SDK1*	1.1	0.5	0.4	1.8	0.5	1.2
1	224411530	224415036	ENSG00000237101	*RP11-365O16.6*	3.3	-0.4	-0.8	4.1	0.8	0.1
1	52507269	52509625	ENSG00000223390	*RP11-91A18.4*	1.1	0.7	0.0	3.3	0.8	1.0

					ΔPSI(siCo+HS)			ΔPSI(siBRD4+HS)		
chr	**start**	**end**	**ensg**	**name**	**rep1**	**rep2**	**rep3**	**rep1**	**rep2**	**rep3**
1	201694043	201702534	ENSG00000231871	*IPO9-AS1*	2.6	0.4	-0.9	3.3	0.9	0.8
1	201694043	201702534	ENSG00000134369	*NAV1*	2.8	0.6	-0.7	3.8	0.9	1.0
11	128858020	128863132	ENSG00000134909	*ARHGAP32*	1.2	2.5	0.5	1.9	1.9	1.2
12	3324521	3382078	ENSG00000011105	*TSPAN9*	0.8	-0.3	-0.5	1.5	1.1	-0.8
12	32717223	32727660	ENSG00000139132	*FGD4*	3.5	4.3	1.8	4.2	4.7	2.6
12	30877385	30878900	ENSG00000110888	*CAPRIN2*	0.3	1.4	2.1	1.3	2.2	1.5
14	58770479	58771662	ENSG00000032219	*ARID4A*	2.6	0.7	0.4	3.6	0.8	1.2
15	45859241	45878376	ENSG00000179362	*HMGN2P46*	0.3	2.0	0.4	1.5	1.3	1.2
15	91500955	91502982	ENSG00000166965	*RCCD1*	1.7	0.1	-0.3	2.5	1.0	1.0
17	47801889	47809642	ENSG00000121104	*FAM117A*	0.6	-2.6	-1.9	1.2	1.2	-0.5
18	56224420	56233694	ENSG00000198796	*ALPK2*	11.5	14.3	2.7	12.2	15.3	2.0
19	33487367	33490492	ENSG00000131941	*RHPN2*	0.4	0.3	0.4	2.1	1.0	0.5
2	17969188	17978832	ENSG00000163029	*SMC6*	1.9	-0.7	0.3	4.2	1.1	1.3
2	122363756	122406948	ENSG00000074054	*CLASP1*	1.3	0.2	0.6	0.8	1.2	1.2
21	35206728	35208745	ENSG00000205726	*ITSN1*	0.8	-0.4	-0.7	1.6	0.8	-1.1
22	28208730	28247657	ENSG00000180957	*PITPNB*	0.4	0.2	0.6	1.1	1.1	0.0
3	149696011	149696939	ENSG00000070087	*PFN2*	11.5	1.9	-1.6	12.2	2.8	0.2
5	86565104	86590008	ENSG00000145715	*RASA1*	3.0	0.0	2.3	4.2	0.5	2.9
5	133695782	133702050	ENSG00000006837	*CDKL3*	-1.1	0.3	0.6	1.4	2.1	0.5
6	36411500	36418692	ENSG00000112078	*KCTD20*	0.5	-0.1	1.6	1.3	1.5	1.1
6	87862587	87864909	ENSG00000188994	*ZNF292*	0.0	0.5	0.4	1.1	0.5	1.1
7	6414401	6415490	ENSG00000136238	*RAC1*	11.5	14.3	10.7	12.2	15.3	16.5
8	100880693	100883013	ENSG00000132549	*VPS13B*	0.7	0.3	0.0	2.0	1.2	-0.3
9	94374774	94398533	ENSG00000169071	*ROR2*	1.8	0.6	-1.0	2.7	0.9	1.2
1	26620822	26623410	ENSG00000158062	*UBXN11*	1.4	-1.1	0.4	2.6	0.6	-0.2
1	156309582	156314371	ENSG00000163468	*CCT3*	0.1	0.2	-0.4	2.9	1.3	1.0
10	51787123	51807962	ENSG00000235618	*RP11-324H6.5*	1.3	-0.7	-1.1	2.0	0.8	-0.5
13	103486902	103490993	ENSG00000134897	*BIVM*	-0.1	-1.0	-0.2	0.8	-0.9	0.8
14	101412057	101413371	ENSG00000225746	*AL132709.5*	11.5	2.4	2.0	12.2	2.8	2.7
16	30320322	30346296	ENSG00000183604	*RP11-347C12.2*	-0.3	0.2	-0.6	0.8	0.6	1.3
2	66689019	66691241	ENSG00000143995	*MEIS1*	1.0	0.5	0.0	2.0	0.8	0.7
20	13550233	13561544	ENSG00000089123	*TASP1*	1.6	-0.8	2.2	3.5	0.6	1.3
21	47979019	47980635	ENSG00000160305	*DIP2A*	3.1	0.8	0.3	3.5	1.5	0.9
22	42952680	42954354	ENSG00000183569	*SERHL2*	0.4	0.1	1.6	1.8	1.6	1.6
22	42952680	42954354	ENSG00000182841	*RRP7B*	0.6	-0.3	1.1	1.8	1.4	1.3
3	196793625	196795373	ENSG00000075711	*DLG1*	2.1	-0.1	-0.1	2.8	0.1	1.0
4	148582469	148589690	ENSG00000164169	*PRMT10*	0.1	0.2	0.1	1.3	1.2	0.0
4	151412187	151500241	ENSG00000198589	*LRBA*	2.3	0.3	0.6	3.6	0.8	1.2
8	38260162	38261858	ENSG00000165046	*LETM2*	-0.1	-0.7	0.3	1.3	0.9	0.3
X	70750375	70752115	ENSG00000147133	*TAF1*	4.3	1.5	10.7	4.4	2.4	16.5
14	80971363	80993028	ENSG00000100629	*CEP128*	2.0	0.3	0.7	2.9	1.0	1.3
14	69585947	69588934	ENSG00000139990	*DCAF5*	0.3	0.1	0.3	1.0	0.8	0.8

					ΔPSI(siCo+HS)			ΔPSI(siBRD4+HS)		
chr	**start**	**end**	**ensg**	**name**	**rep1**	**rep2**	**rep3**	**rep1**	**rep2**	**rep3**
15	33360363	33381000	ENSG00000248905	*FMN1*	0.9	1.2	-0.4	1.9	1.4	1.0
19	44503384	44506417	ENSG00000266921	*RP11-15A1.7*	0.7	1.7	0.3	2.0	2.0	1.2
3	29410912	29432339	ENSG00000144642	*RBMS3*	11.5	0.1	1.0	12.2	0.7	0.2
3	184296254	184297265	ENSG00000145191	*EIF2B5*	1.7	-0.6	-0.2	2.4	0.2	1.2
4	20734408	20736251	ENSG00000163138	*PACRGL*	0.6	-0.1	-0.6	1.5	1.0	-0.9
6	2176225	2245555	ENSG00000112699	*GMDS*	0.5	0.0	2.8	1.6	-0.1	4.5
6	157473538	157488174	ENSG00000049618	*ARID1B*	0.5	-0.4	0.1	1.2	0.7	-0.2
6	116443124	116446502	ENSG00000178425	*NT5DC1*	1.7	-0.4	0.1	2.5	-1.8	0.9
X	48448675	48455866	ENSG00000101940	*WDR13*	3.4	14.3	-0.1	6.0	15.3	0.4
1	28304985	28314984	ENSG00000158161	*EYA3*	-0.3	0.0	0.4	0.9	0.7	0.5
1	77806566	77811731	ENSG00000154027	*AK5*	0.3	-0.3	0.5	1.7	0.7	0.2
1	229685769	229693883	ENSG00000135776	*ABCB10*	1.5	-0.2	-0.5	2.2	0.7	-0.1
11	103280385	103306671	ENSG00000187240	*DYNC2H1*	0.5	0.4	0.1	1.8	1.0	0.5
11	74209578	74303575	ENSG00000077514	*POLD3*	1.3	1.3	0.7	2.3	1.8	1.6
12	132448187	132464239	ENSG00000183495	*EP400*	0.5	1.6	1.3	1.4	1.1	2.1
12	6986764	6991354	ENSG00000240370	*RPL13P5*	-1.4	1.0	0.6	2.4	1.6	0.8
12	6986764	6991354	ENSG00000111671	*SPSB2*	-0.5	1.5	1.3	2.6	2.1	1.0
14	23459336	23463019	ENSG00000100802	*C14orf93*	0.1	-0.2	-0.7	1.4	0.7	0.9
15	45927306	45938079	ENSG00000260170	*RP11-96O20.4*	11.5	2.5	4.9	12.2	2.7	5.6
15	45927306	45938079	ENSG00000137767	*SQRDL*	11.5	2.2	4.8	12.2	2.5	5.5
4	30989429	31144095	ENSG00000169851	*PCDH7*	1.1	0.4	1.0	2.6	1.6	1.2
4	90641190	90645250	ENSG00000251095	*RP11-115D19.1*	1.8	0.1	0.3	2.2	1.1	2.1
5	130769351	130771454	ENSG00000158987	*RAPGEF6*	-0.2	0.3	0.8	1.4	1.5	0.6
5	130769351	130771454	ENSG00000217128	*FNIP1*	-0.8	0.4	0.7	1.1	1.5	0.5
6	149642526	149663786	ENSG00000055208	*TAB2*	2.1	0.5	1.7	2.8	1.5	1.4
9	34655934	34656736	ENSG00000137070	*IL11RA*	2.0	-0.1	0.1	2.8	-0.5	0.8
9	34655934	34656736	ENSG00000258728	*RP11-195F19.29*	2.3	0.0	0.0	3.6	-0.4	0.7
1	184706198	184706745	ENSG00000116406	*EDEM3*	2.0	0.3	-0.2	2.9	0.7	1.3
10	24875035	24878200	ENSG00000107863	*ARHGAP21*	2.0	1.3	0.1	2.8	0.5	1.2
11	1977839	1983469	ENSG00000214026	*MRPL23*	1.4	0.1	0.9	2.4	0.5	1.6
15	74002030	74003473	ENSG00000103855	*CD276*	1.1	-0.2	1.2	2.5	1.0	1.4
17	264457	270463	ENSG00000187624	*C17orf97*	11.5	0.0	0.0	12.2	1.6	0.8
19	11533529	11534546	ENSG00000198003	*CCDC151*	11.5	1.3	2.1	12.2	2.1	1.9
2	29037552	29038863	ENSG00000163806	*SPDYA*	3.8	2.8	0.8	4.6	3.9	0.9
20	39928767	39945502	ENSG00000174306	*ZHX3*	1.3	0.3	-0.2	1.9	1.2	-0.2
22	21193019	21212858	ENSG00000241973	*PI4KA*	0.2	0.3	0.0	0.9	1.0	0.3
3	135722335	135741577	ENSG00000073711	*PPP2R3A*	0.8	-0.4	-0.9	1.6	0.7	-0.1
4	6912328	6925100	ENSG00000132405	*TBC1D14*	0.8	0.5	-0.5	2.3	0.8	0.9
4	81106672	81110903	ENSG00000152784	*PRDM8*	0.1	0.2	-0.3	1.2	1.2	0.5
5	159466207	159470140	ENSG00000113312	*TTC1*	1.3	-0.7	-0.3	2.9	1.9	-0.2
6	46293405	46406047	ENSG00000172348	*RCAN2*	0.9	0.7	0.3	2.5	1.9	1.6

					ΔPSI(siCo+HS)			ΔPSI(siBRD4+HS)		
chr	**start**	**end**	**ensg**	**name**	**rep1**	**rep2**	**rep3**	**rep1**	**rep2**	**rep3**
8	48243484	48273386	ENSG00000164808	*KIAA0146*	11.5	1.0	3.3	12.2	1.3	4.0
8	130902901	130906733	ENSG00000153310	*FAM49B*	1.1	-1.4	-1.2	2.2	2.3	-0.4
9	37529257	37531906	ENSG00000147912	*FBXO10*	0.3	0.8	-0.4	1.4	1.7	-0.1
9	37529257	37531906	ENSG00000256966	*RP11-613M10.8*	0.2	0.6	-0.5	1.5	1.7	-0.2
9	139290222	139291429	ENSG00000165684	*SNAPC4*	1.3	0.4	0.5	2.8	0.5	1.1
1	12538928	12557280	ENSG00000048707	*VPS13D*	11.5	-0.1	0.8	12.2	0.7	0.4
1	212787474	212788360	ENSG00000162772	*ATF3*	0.7	2.0	2.8	2.0	2.6	2.9
14	19720595	19724389	ENSG00000257898	*RP11-496I2.3*	-1.1	0.5	0.5	1.6	1.4	1.3
2	87772404	87777641	ENSG00000222041	*LINC00152*	0.3	0.3	0.7	1.2	1.3	0.5
22	22058414	22064776	ENSG00000100027	*YPEL1*	3.3	-1.4	0.3	4.9	1.5	0.4
4	139144478	139153421	ENSG00000151012	*SLC7A11*	-0.2	0.2	0.4	0.8	0.8	-0.1
5	68882183	68886155	ENSG00000183474	*GTF2H2C*	1.1	-1.2	-1.0	2.4	-0.3	0.6
1	47060731	47069837	ENSG00000079277	*MKNK1*	0.9	0.5	-0.7	2.4	1.5	0.7
1	104078816	104079964	ENSG00000185946	*RNPC3*	-0.2	1.6	0.0	1.9	0.8	1.0
11	71615127	71616153	ENSG00000254469	*RP11-849H4.2*	2.5	0.1	0.9	2.0	0.8	1.5
13	21311944	21321174	ENSG00000150456	*N6AMT2*	1.0	0.7	0.4	2.8	1.4	-0.4
14	101411497	101411986	ENSG00000225746	*AL132709.5*	11.5	2.0	4.2	12.2	3.2	4.1
17	29634977	29640997	ENSG00000185862	*EVI2B*	0.4	0.1	0.2	1.4	-0.3	0.8
17	29634977	29640997	ENSG00000265118	*CTD-2370N5.3*	0.5	0.0	-0.1	1.6	-0.3	0.7
19	20038122	20042817	ENSG00000184635	*ZNF93*	0.7	0.0	0.4	1.6	1.2	0.8
2	228762997	228767718	ENSG00000123977	*WDR69*	1.5	0.0	-0.9	2.4	0.6	-0.7
2	242534145	242541230	ENSG00000176946	*THAP4*	2.3	-0.7	0.2	2.9	0.9	0.0
7	73803762	73811404	ENSG00000106665	*CLIP2*	0.8	0.1	0.0	1.5	0.3	0.7
8	132999949	133008637	ENSG00000132294	*EFR3A*	-0.4	-0.3	-0.4	1.0	0.6	-0.6
9	15474235	15478475	ENSG00000164985	*PSIP1*	0.1	-0.4	-0.5	1.1	0.8	0.1
1	41984159	41990406	ENSG00000127124	*HIVEP3*	1.5	-0.5	0.2	2.1	0.6	0.4
11	63886682	63894326	ENSG00000133315	*MACROD1*	1.3	0.6	-0.3	1.8	1.5	0.6
12	54394510	54396214	ENSG00000172789	*HOXC5*	3.0	0.5	0.0	4.3	1.2	0.8
12	54394510	54396214	ENSG00000197757	*HOXC6*	2.5	0.2	-0.1	4.4	0.9	0.7
12	42842425	42848522	ENSG00000134283	*PPHLN1*	3.2	2.2	-0.3	4.0	3.0	0.3
13	113401754	113408808	ENSG00000068650	*ATP11A*	11.5	14.3	5.0	12.2	15.3	4.4
14	61997313	62004226	ENSG00000258989	*RP11-47I22.4*	-0.2	-0.2	-0.5	1.1	0.7	0.5
15	42531929	42536248	ENSG00000103978	*TMEM87A*	0.9	0.1	0.3	1.6	0.2	0.9
17	79057709	79058632	ENSG00000175866	*BAIAP2*	-0.1	0.3	1.1	3.1	1.0	1.4
19	52592255	52597099	ENSG00000197608	*ZNF841*	2.8	-1.7	0.1	4.0	-0.2	0.8
19	36029585	36031640	ENSG00000105679	*GAPDHS*	2.0	1.4	1.1	4.6	1.7	1.7
19	45978437	45981994	ENSG00000012061	*ERCC1*	1.3	1.5	0.1	2.1	1.4	0.9
2	160569172	160571068	ENSG00000136536	*MARCH7*	2.0	0.0	-0.8	3.4	1.1	0.5
2	228741210	228750067	ENSG00000123977	*WDR69*	0.8	0.4	-0.1	1.7	0.3	1.0
4	81112723	81115267	ENSG00000152784	*PRDM8*	1.9	1.1	0.8	2.9	1.4	1.7
7	2233110	2239900	ENSG00000002822	*MAD1L1*	1.5	-1.9	-0.4	2.7	0.0	0.7

					ΔPSI(siCo+HS)			ΔPSI(siBRD4+HS)		
chr	**start**	**end**	**ensg**	**name**	**rep1**	**rep2**	**rep3**	**rep1**	**rep2**	**rep3**
15	101100997	101104897	ENSG00000140471	*LINS*	0.3	-11.9	-1.0	1.0	0.8	-1.2
17	35501387	35506788	ENSG00000132142	*ACACA*	1.4	0.6	0.6	2.0	1.4	0.7
5	139893064	139903651	ENSG00000254996	*ANKHD1-EIF4EBP3*	0.7	0.4	0.6	1.3	1.0	0.7
5	139893064	139903651	ENSG00000131503	*ANKHD1*	0.8	0.4	0.6	1.4	1.0	0.7
6	41538132	41545724	ENSG00000137166	*FOXP4*	3.2	0.1	1.5	4.4	0.7	1.3
9	88932191	88933873	ENSG00000083223	*ZCCHC6*	0.6	0.3	0.6	1.4	1.0	0.4
13	33010542	33012789	ENSG00000244754	*N4BP2L2*	3.4	2.1	2.5	4.0	3.1	2.6
13	33010542	33012789	ENSG00000139617	*RP11-298P3.4*	1.2	1.1	0.7	1.8	1.8	0.6
16	70417138	70422270	ENSG00000260111	*RP11-529K1.4*	0.4	0.2	-0.9	1.4	1.2	-0.4
16	70417138	70422270	ENSG00000157350	*ST3GAL2*	0.6	0.2	-1.2	1.4	1.2	-0.6
16	22376510	22378367	ENSG00000140743	*CDR2*	0.3	-0.4	1.0	1.3	0.8	0.6
17	270888	273271	ENSG00000187624	*C17orf97*	3.3	4.2	3.3	4.7	5.0	3.5
17	73031452	73034958	ENSG00000180901	*KCTD2*	-0.4	0.7	0.7	2.8	1.4	0.7
19	16506278	16509477	ENSG00000127527	*EPS15L1*	2.8	0.6	0.2	3.6	1.4	0.4
19	52580337	52588040	ENSG00000197608	*ZNF841*	0.0	0.0	1.0	1.1	0.9	0.6
3	195997412	196010346	ENSG00000213123	*TCTEX1D2*	1.2	0.2	0.7	1.8	0.9	0.8
7	72598764	72602009	ENSG00000233369	*RP11-396K3.1*	1.0	-0.6	0.1	2.3	0.7	0.6
X	133554353	133559231	ENSG00000156531	*PHF6*	0.5	-0.1	0.0	1.3	0.7	0.1
11	19961319	19967947	ENSG00000166833	*NAV2*	4.1	0.4	-0.2	5.1	1.0	0.6
12	65762806	65812511	ENSG00000174099	*MSRB3*	0.6	-0.4	0.3	1.3	1.0	-1.2
14	31806820	31809656	ENSG00000129493	*HEATR5A*	1.4	0.1	-0.2	2.6	0.7	-0.2
14	31806820	31809656	ENSG00000203546	*RP11-176H8.1*	1.5	0.1	-0.2	2.8	0.7	-0.2
15	44070314	44077608	ENSG00000140264	*SERF2*	1.2	0.1	-0.9	3.0	1.4	0.2
16	30240431	30242761	ENSG00000198064	*RP11-347C12.1*	1.9	0.0	-0.1	2.8	0.6	0.5
2	40482349	40564465	ENSG00000183023	*SLC8A1*	0.2	-0.9	0.1	2.0	0.6	0.6
2	95945745	95946990	ENSG00000155066	*PROM2*	11.5	1.7	1.8	12.2	2.3	2.6
2	231359175	231363176	ENSG00000067066	*SP100*	2.3	0.2	0.1	2.9	0.3	1.2
4	111559310	111563075	ENSG00000164093	*PITX2*	11.5	14.3	2.3	12.2	15.3	3.2
8	6312773	6331366	ENSG00000147316	*MCPH1*	1.8	-0.5	1.1	2.4	0.6	1.2
1	160195453	160201087	ENSG00000132716	*DCAF8*	0.2	0.2	-0.7	1.2	0.8	-0.2
1	160195453	160201087	ENSG00000258465	*RP11-574F21.3*	0.3	0.1	-0.8	1.3	0.8	-0.4
10	95100006	95101666	ENSG00000138119	*MYOF*	11.5	-0.2	0.8	12.2	0.7	0.4
12	96266238	96271989	ENSG00000139343	*SNRPF*	11.5	1.6	0.7	12.2	2.1	1.4
15	92700471	92704805	ENSG00000176463	*SLCO3A1*	1.9	0.5	0.3	1.7	1.3	1.1
16	1697056	1702497	ENSG00000007545	*CRAMP1L*	1.5	-0.1	0.3	1.2	0.8	1.1
16	1697056	1702497	ENSG00000261732	*LA16c-431H6.6*	1.5	-0.2	0.2	1.5	0.7	1.0
20	32224514	32226545	ENSG00000078699	*CBFA2T2*	4.7	0.1	0.4	5.6	0.8	0.3
1	155620061	155629237	ENSG00000125459	*MSTO1*	2.0	1.1	0.0	3.0	1.8	1.0
1	155620061	155629237	ENSG00000203761	*RP11-243J18.3*	2.0	1.1	0.1	2.7	1.7	1.1
1	155620061	155629237	ENSG00000246203	*RP11-29H23.5*	2.0	0.4	-0.5	3.0	1.2	0.6

					ΔPSI(siCo+HS)			ΔPSI(siBRD4+HS)		
chr	**start**	**end**	**ensg**	**name**	**rep1**	**rep2**	**rep3**	**rep1**	**rep2**	**rep3**
11	85981199	85987174	ENSG00000074266	*EED*	2.3	0.8	0.8	1.9	1.4	1.4
12	7365467	7370998	ENSG00000139197	*PEX5*	0.7	0.5	0.2	1.5	0.2	0.9
13	103317286	103320108	ENSG00000134900	*TPP2*	2.0	-0.3	-0.5	2.7	0.6	-0.5
16	54088495	54097549	ENSG00000140718	*FTO*	3.2	1.2	1.6	4.6	2.5	0.9
19	2770779	2777491	ENSG00000104969	*SGTA*	1.6	0.4	0.1	1.9	1.0	1.0
20	37630485	37631415	ENSG00000101452	*DHX35*	1.8	-0.6	0.2	3.6	0.0	1.6
3	9852393	9854627	ENSG00000250151	*ARPC4-TTLL3*	1.9	1.8	1.2	3.2	2.8	1.7
3	9852393	9854627	ENSG00000241553	*ARPC4*	2.0	1.6	1.0	3.5	2.8	1.5
4	16290668	16309079	ENSG00000263327	*RP11-783N5.1*	1.6	0.4	0.3	4.5	0.4	1.3
X	154014675	154018229	ENSG00000130830	*MPP1*	0.2	0.1	-0.1	1.0	0.8	-0.1
1	43255605	43258476	ENSG00000164008	*C1orf50*	2.0	0.5	-0.1	2.6	0.2	0.6
1	247053361	247054258	ENSG00000153207	*AHCTF1*	11.5	3.6	3.6	12.2	3.4	4.4
11	63744015	63753325	ENSG00000256100	*AP000721.4*	1.4	0.0	-0.5	2.4	1.2	-0.3
14	32295920	32312950	ENSG00000151413	*NUBPL*	0.8	-0.1	0.5	2.0	0.6	0.6
22	37164598	37168447	ENSG00000100360	*IFT27*	1.7	0.1	-0.7	2.4	0.8	0.0
9	37205365	37284160	ENSG00000147905	*ZCCHC7*	0.5	0.0	-0.2	2.1	0.6	-0.4
X	3533933	3539300	ENSG00000183943	*PRKX*	3.9	1.4	0.5	3.4	2.1	1.5
14	72065048	72085473	ENSG00000197555	*SIPA1L1*	0.6	0.9	1.5	2.0	1.5	1.1
16	22535269	22538887	ENSG00000243716	*RP11-368J21.2*	3.1	-0.9	-0.2	2.8	1.2	0.6
19	2778011	2782568	ENSG00000104969	*SGTA*	0.7	0.6	0.4	1.4	0.9	1.1
4	1259951	1281393	ENSG00000196810	*CTBP1-AS1*	1.6	1.1	1.1	2.6	2.5	1.2
7	129083939	129091454	ENSG00000128578	*FAM40B*	0.6	0.4	0.9	1.6	1.2	0.1
10	46395874	46405997	ENSG00000234596	*RP11-175I17.2*	0.9	0.8	0.6	2.0	1.4	0.4
2	234174805	234178648	ENSG00000085978	*ATG16L1*	1.5	0.2	1.1	2.7	0.8	0.4
6	117829278	117840979	ENSG00000164465	*DCBLD1*	0.7	-0.8	0.1	1.5	1.1	-0.1
6	57025950	57029679	ENSG00000226803	*RP11-203B9.4*	0.9	-0.8	-1.6	1.8	-0.4	1.3
7	148544397	148580289	ENSG00000106462	*EZH2*	2.1	0.8	1.2	2.0	1.4	1.9
10	89527480	89530709	ENSG00000138138	*ATAD1*	0.8	-0.2	-0.6	1.7	0.7	-0.6
11	57420263	57424488	ENSG00000172409	*CLP1*	0.1	-0.4	-0.4	1.5	0.8	0.3
15	33129527	33149216	ENSG00000248905	*FMN1*	1.4	0.5	1.6	2.1	1.2	0.6
16	84630432	84649630	ENSG00000103187	*COTL1*	1.3	1.4	1.1	2.7	2.0	1.5
6	29556745	29570005	ENSG00000204681	*GABBR1*	0.9	0.6	-0.8	2.1	1.5	-0.4
1	185250954	185259806	ENSG00000116668	*SWT1*	1.8	0.6	0.9	2.8	1.6	0.4
10	114182199	114185096	ENSG00000197142	*ACSL5*	0.9	0.9	1.8	2.6	1.8	1.3
11	3692646	3696240	ENSG00000110713	*NUP98*	1.5	1.0	0.0	3.2	1.5	1.1
12	112194903	112204691	ENSG00000257767	*RP11-162P23.2*	3.2	2.9	2.1	5.6	3.8	1.3
2	191542244	191548464	ENSG00000138386	*NAB1*	-0.4	0.2	0.2	0.3	1.0	0.9
2	191542244	191548464	ENSG00000228509	*AC006460.2*	-0.1	0.3	0.2	0.6	1.1	1.0
2	118696687	118698765	ENSG00000125633	*CCDC93*	0.8	1.0	1.5	2.1	1.9	1.8
7	128441563	128444704	ENSG00000128596	*CCDC136*	0.4	0.3	0.5	3.3	1.2	0.7
16	30243168	30246769	ENSG00000198064	*RP11-347C12.1*	3.8	1.5	0.2	4.7	-0.3	1.2

					ΔPSI(siCo+HS)			ΔPSI(siBRD4+HS)		
chr	**start**	**end**	**ensg**	**name**	**rep1**	**rep2**	**rep3**	**rep1**	**rep2**	**rep3**
16	30243168	30246769	ENSG00000183604	*RP11-347C12.2*	4.0	1.1	0.0	4.7	-0.4	0.9
1	23163342	23189530	ENSG00000133216	*EPHB2*	0.8	-0.2	-0.1	1.5	0.6	-0.5
16	5097965	5105247	ENSG00000033011	*ALG1*	3.0	-0.6	-0.6	3.5	1.3	0.8
17	27104167	27117396	ENSG00000173065	*FAM222B*	2.8	0.9	-0.1	4.6	1.5	0.5
2	66691352	66723158	ENSG00000143995	*MEIS1*	1.1	-0.6	0.7	2.5	1.1	-0.1
13	33765020	33779956	ENSG00000249121	*RP11-81F11.3*	11.5	2.4	2.8	12.2	2.4	3.4
15	102161958	102166651	ENSG00000184277	*TM2D3*	0.2	0.3	2.2	2.4	1.6	2.2
8	99046538	99047880	ENSG00000156482	*RPL30*	3.0	1.7	-0.1	3.6	2.5	0.1
12	109902700	109906867	ENSG00000110906	*KCTD10*	1.3	0.0	1.6	1.9	0.7	1.5
18	8811254	8812843	ENSG00000168502	*SOGA2*	3.2	1.3	2.2	4.9	2.1	2.2
1	119762719	119776081	ENSG00000231365	*RP11-418J17.1*	-0.7	-0.5	0.8	1.4	0.8	0.1
16	21855114	21858733	ENSG00000185864	*RP11-645C24.1*	3.2	0.0	0.0	4.0	0.0	1.3
16	1884367	1887685	ENSG00000180185	*FAHD1*	11.5	-0.7	1.6	12.2	1.0	2.0
17	79061647	79071379	ENSG00000175866	*BAIAP2*	2.4	0.4	1.7	3.0	1.0	1.9
10	126811437	126822081	ENSG00000175029	*CTBP2*	3.2	0.5	2.1	3.9	1.9	2.2
11	75155540	75159537	ENSG00000158555	*GDPD5*	1.4	0.1	0.4	2.8	0.9	0.8
9	91947901	91948940	ENSG00000187742	*SECISBP2*	-0.4	-1.4	-0.1	2.8	1.0	-1.4
X	137798779	137821404	ENSG00000129682	*FGF13*	0.1	-0.3	-0.2	1.5	0.6	-0.4
12	14614067	14619044	ENSG00000171681	*ATF7IP*	1.4	0.3	-0.2	2.5	0.7	1.0
8	132947764	132952128	ENSG00000132294	*EFR3A*	5.1	14.3	2.2	6.8	15.3	2.6
14	62463260	62536236	ENSG00000139973	*SYT16*	0.6	1.2	0.9	1.4	1.8	0.9
2	106006684	106013104	ENSG00000115641	*FHL2*	0.0	1.1	0.6	0.6	1.7	0.6
4	26386230	26387975	ENSG00000168214	*RBPJ*	2.5	-1.5	-0.1	3.8	-0.8	1.0
7	44842716	44861593	ENSG00000196262	*PPIA*	3.0	0.0	0.2	4.1	0.8	0.3
11	14542242	14632400	ENSG00000129084	*PSMA1*	-0.3	-0.2	0.2	1.3	1.0	0.8
8	22857618	22861557	ENSG00000245025	*RP11-875O11.1*	2.3	0.6	1.4	3.6	1.5	1.8
8	22857618	22861557	ENSG00000008853	*RHOBTB2*	2.0	0.6	1.4	3.5	1.4	1.8
1	201688755	201692422	ENSG00000231871	*IPO9-AS1*	3.5	1.8	0.5	5.0	1.3	2.0
1	201688755	201692422	ENSG00000134369	*NAV1*	3.8	2.0	0.7	5.6	1.3	2.2
10	69826974	69828762	ENSG00000148634	*HERC4*	11.5	0.3	1.5	12.2	1.1	1.2
3	156881721	156886806	ENSG00000241770	*RP11-555M1.3*	-0.2	-0.6	-1.0	1.9	1.0	-0.4
8	54852284	54857885	ENSG00000147509	*RGS20*	1.8	0.5	1.4	2.4	1.7	2.5
12	7499743	7507556	ENSG00000177675	*CD163L1*	0.3	0.3	0.7	1.1	1.0	0.3
2	242021779	242026509	ENSG00000122085	*MTERFD2*	2.4	-0.1	-1.1	3.0	0.8	-0.8
3	44894753	44903361	ENSG00000163808	*KIF15*	0.1	-1.1	-1.2	1.3	0.6	-0.5
14	23551045	23559191	ENSG00000100813	*ACIN1*	1.2	0.2	0.8	2.0	1.2	1.4
2	170684562	170728746	ENSG00000144357	*UBR3*	0.9	1.0	0.5	1.9	1.8	1.1
3	183901879	183903811	ENSG00000145191	*EIF2B5*	1.2	0.4	1.0	3.0	1.1	0.5
X	67414340	67417028	ENSG00000079482	*OPHN1*	1.8	0.4	0.1	2.4	1.4	0.5
2	97001586	97007130	ENSG00000121152	*NCAPH*	3.0	0.2	1.5	3.6	1.1	1.2
6	116676979	116687246	ENSG00000111817	*DSE*	0.4	0.0	-0.6	2.0	0.7	-0.1

					ΔPSI(siCo+HS)			ΔPSI(siBRD4+HS)		
chr	**start**	**end**	**ensg**	**name**	**rep1**	**rep2**	**rep3**	**rep1**	**rep2**	**rep3**
2	220065364	220068515	ENSG00000158552	*ZFAND2B*	2.7	2.8	3.0	4.1	4.2	3.3
3	9397543	9404524	ENSG00000254485	*RP11-380O24.1*	0.0	-0.1	-0.6	0.6	0.9	-1.0
14	65002693	65007035	ENSG00000126803	*HSPA2*	0.7	1.2	3.8	1.7	2.4	3.1
11	115069160	115078022	ENSG00000182985	*CADM1*	0.0	0.3	-0.1	0.6	0.9	-0.3
21	43414217	43422459	ENSG00000173276	*ZNF295*	0.3	1.3	0.1	1.7	1.2	0.7
1	120840676	120841975	ENSG00000188610	*FAM72B*	0.9	0.8	0.4	2.0	1.6	1.0
4	146419218	146424028	ENSG00000170365	*SMAD1*	11.5	14.3	5.1	12.2	15.3	4.8
2	238954425	238965799	ENSG00000258984	*RP11-526L8.1*	0.4	0.7	0.3	1.8	0.2	0.9
1	32399576	32401190	ENSG00000184007	*PTP4A2*	2.6	2.7	2.8	3.7	3.3	2.7
11	12265659	12270731	ENSG00000133816	*MICAL2*	0.4	-0.6	-1.6	3.2	1.0	-0.6
2	75749613	75753238	ENSG00000115363	*FAM176A*	1.2	1.4	0.4	2.0	1.2	1.1
1	109325328	109336204	ENSG00000116266	*STXBP3*	1.0	0.5	0.2	1.7	1.2	-0.1
1	229773994	229779280	ENSG00000135763	*URB2*	1.8	1.0	1.0	2.5	2.0	1.0
13	31117598	31127807	ENSG00000189403	*HMGB1*	11.5	14.3	3.6	12.2	15.3	3.6
15	49663596	49688172	ENSG00000166262	*FAM227B*	0.7	0.5	-0.2	2.3	1.2	-0.2
7	93601975	93605216	ENSG00000105829	*BET1*	4.5	2.2	10.7	5.4	2.7	16.5
10	115479402	115480757	ENSG00000165806	*CASP7*	11.5	5.6	10.7	12.2	5.7	16.5
12	123451056	123457590	ENSG00000150967	*ABCB9*	2.1	-0.5	-0.5	3.1	0.7	-0.1
6	5113651	5132952	ENSG00000214113	*LYRM4*	2.9	2.5	2.5	3.5	3.1	2.6
1	244558962	244571796	ENSG00000240963	*RP11-518L10.2*	0.9	0.6	0.2	2.0	1.6	0.2
21	45551063	45553487	ENSG00000248354	*AP001055.7*	1.6	-0.5	-0.4	3.5	0.8	0.6
6	43507440	43511881	ENSG00000124571	*XPO5*	1.3	-0.5	-0.4	2.5	0.8	-0.3
15	64388371	64403657	ENSG00000028528	*SNX1*	1.3	0.0	0.6	2.2	0.9	0.7
15	42814293	42820141	ENSG00000092531	*SNAP23*	4.3	0.0	0.1	5.0	-1.0	0.9
4	182827620	182896309	ENSG00000177822	*AC108142.1*	1.2	-0.1	0.0	2.1	0.5	0.7
1	65282192	65296522	ENSG00000162437	*RAVER2*	0.1	0.0	0.4	0.8	0.7	0.0
7	96136010	96251874	ENSG00000127922	*SHFM1*	2.8	0.3	0.4	3.4	1.1	0.6
12	49583107	49602329	ENSG00000167553	*TUBA1C*	0.9	-0.2	0.1	2.7	-0.4	0.8
1	233297109	233313548	ENSG00000135749	*PCNXL2*	2.2	0.6	1.0	3.2	1.4	0.7
18	72633014	72772111	ENSG00000215421	*ZNF407*	2.1	1.7	0.8	3.2	2.1	1.9
6	38145069	38160295	ENSG00000183826	*BTBD9*	1.1	-0.1	-0.7	2.1	0.7	-0.2
2	95964868	95968792	ENSG00000115041	*KCNIP3*	3.0	0.8	0.9	5.8	1.9	1.5
11	64858008	64863587	ENSG00000149823	*VPS51*	3.3	0.7	0.5	5.1	1.4	0.8
14	72043304	72052998	ENSG00000197555	*SIPA1L1*	1.4	-0.7	-0.9	2.8	0.2	0.7
8	48424703	48459366	ENSG00000164808	*KIAA0146*	1.6	0.4	1.3	2.3	1.2	1.4
17	38474700	38479243	ENSG00000131759	*RARA*	1.7	-0.1	-0.2	3.5	0.3	0.7
13	100962162	100982815	ENSG00000175198	*PCCA*	2.6	0.4	1.3	3.3	1.0	1.3
8	130892704	130902711	ENSG00000153310	*FAM49B*	2.2	0.0	0.4	3.1	1.0	0.3
3	158501859	158519654	ENSG00000118855	*MFSD1*	1.9	1.1	0.0	3.7	1.9	0.3
5	36986403	36995252	ENSG00000164190	*NIPBL*	0.4	0.4	0.1	1.1	1.1	0.1
15	74901068	74905535	ENSG00000179335	*CLK3*	1.5	0.6	1.0	3.5	1.2	1.6

					ΔPSI(siCo+HS)			ΔPSI(siBRD4+HS)		
chr	**start**	**end**	**ensg**	**name**	**rep1**	**rep2**	**rep3**	**rep1**	**rep2**	**rep3**
22	46202984	46207578	ENSG00000130638	*ATXN10*	1.7	0.2	0.6	3.1	1.1	0.7
10	99120375	99123611	ENSG00000052749	*RRP12*	2.5	-0.2	0.2	3.4	0.5	1.5
17	38479511	38482727	ENSG00000131759	*RARA*	1.7	-0.1	0.0	3.5	0.8	0.5
15	89430576	89436205	ENSG00000140511	*HAPLN3*	1.3	0.0	-0.3	2.8	1.0	-0.1
7	66221064	66233818	ENSG00000154710	*RABGEF1*	1.9	0.0	0.6	2.6	0.6	0.6
14	54950778	54955325	ENSG00000197045	*GMFB*	1.6	-0.5	2.2	2.5	0.6	1.7
1	184695523	184701917	ENSG00000116406	*EDEM3*	3.8	3.0	1.9	4.6	3.6	2.2
2	198318970	198324656	ENSG00000115520	*COQ10B*	2.1	1.8	1.8	3.4	2.6	1.9
5	54529868	54552073	ENSG00000251307	*RP11-506H20.1*	2.3	1.1	2.6	2.9	1.7	2.4
4	48504862	48506123	ENSG00000075539	*FRYL*	2.9	2.3	2.7	4.8	2.3	3.4
1	180924023	180933647	ENSG00000243155	*RP11-46A10.5*	1.1	-0.5	-1.1	2.3	0.7	-0.6
3	67705526	67718671	ENSG00000241316	*RP11-81N13.1*	1.1	0.0	0.9	2.0	0.6	1.1
11	3361860	3379157	ENSG00000005801	*ZNF195*	1.8	0.6	0.5	2.5	1.3	1.2
20	20392792	20452081	ENSG00000188559	*RALGAPA2*	3.8	0.8	0.2	4.7	1.5	0.2
3	179096602	179103357	ENSG00000171109	*MFN1*	3.7	0.6	1.1	4.7	1.1	0.9
17	41623800	41656660	ENSG00000175832	*ETV4*	2.6	2.1	1.7	3.3	2.2	2.4
2	37839401	37869032	ENSG00000236213	*AC006369.2*	0.7	-0.1	-0.3	1.9	0.7	0.2
2	169699627	169707346	ENSG00000152253	*SPC25*	1.0	0.0	-0.2	1.9	0.8	0.1
14	21702990	21704532	ENSG00000092199	*HNRNPC*	2.3	-1.4	-0.1	4.2	-2.0	0.8
14	89094302	89100813	ENSG00000165521	*EML5*	2.1	1.8	1.3	2.7	2.4	1.6
6	88198270	88205793	ENSG00000213204	*C6orf165*	3.1	1.1	0.0	4.4	1.7	0.5
6	88198270	88205793	ENSG00000164414	*SLC35A1*	3.1	1.0	0.0	4.3	1.7	0.5
3	9367852	9372212	ENSG00000254485	*RP11-380O24.1*	3.5	3.5	3.3	4.5	4.1	3.8
5	177643992	177649356	ENSG00000175309	*AGXT2L2*	1.4	0.6	0.9	2.0	1.2	0.7
2	192711981	192745908	ENSG00000233766	*AC098617.2*	3.6	3.7	3.6	5.5	4.8	4.5
2	232329305	232347395	ENSG00000115053	*NCL*	2.2	0.3	1.1	3.1	0.1	1.7
7	93598978	93601695	ENSG00000105829	*BET1*	2.2	0.0	0.4	3.2	-0.1	1.2
1	71514671	71524006	ENSG00000235079	*ZRANB2-AS1*	1.1	1.4	0.2	2.7	1.4	0.8
11	85376146	85393760	ENSG00000137504	*CREBZF*	0.7	0.6	-0.1	1.6	1.7	0.3
12	96290406	96292163	ENSG00000139343	*SNRPF*	11.5	5.5	10.7	12.2	5.4	16.5
3	25825647	25831258	ENSG00000151092	*NGLY1*	2.0	0.0	0.2	3.4	0.2	1.1
2	200828848	200870466	ENSG00000162972	*C2orf47*	0.2	0.1	0.7	1.0	0.8	0.6
2	122176305	122182715	ENSG00000074054	*CLASP1*	2.5	1.2	2.0	3.2	1.6	2.7
3	9335013	9367694	ENSG00000254485	*RP11-380O24.1*	0.2	0.1	-0.4	2.5	1.0	0.1
2	122168545	122176198	ENSG00000074054	*CLASP1*	3.2	1.1	1.8	3.9	2.0	2.5
19	46032714	46049539	ENSG00000125741	*OPA3*	0.5	0.4	0.2	1.3	1.3	0.2
1	94898208	94921289	ENSG00000117528	*ABCD3*	2.5	1.6	0.6	3.5	1.9	1.3
8	130883742	130891635	ENSG00000153310	*FAM49B*	1.5	0.4	-0.1	3.2	1.2	0.2
1	184703777	184706159	ENSG00000116406	*EDEM3*	3.9	1.1	1.6	4.5	1.8	1.9
2	47357399	47378397	ENSG00000143933	*CALM2*	2.2	0.6	0.8	2.9	1.9	1.2
7	26217742	26223321	ENSG00000050344	*NFE2L3*	2.6	1.5	1.3	3.5	2.2	1.4

					ΔPSI(siCo+HS)			ΔPSI(siBRD4+HS)		
chr	**start**	**end**	**ensg**	**name**	**rep1**	**rep2**	**rep3**	**rep1**	**rep2**	**rep3**
14	67309434	67346657	ENSG00000171723	*GPHN*	2.5	0.8	0.1	3.7	0.1	0.7
4	81222483	81256874	ENSG00000138675	*FGF5*	1.5	0.1	0.9	2.8	1.1	1.5
2	217124491	217130244	ENSG00000144583	*MARCH4*	1.8	0.5	0.9	2.9	1.5	0.9
2	217124491	217130244	ENSG00000231092	*AC012513.6*	1.6	0.7	0.8	2.5	1.5	1.0
5	37516692	37605166	ENSG00000082068	*WDR70*	2.2	0.1	0.6	2.9	0.7	0.7
7	26192688	26217563	ENSG00000050344	*NFE2L3*	1.9	0.0	0.1	2.8	0.9	0.5
2	217385497	217393993	ENSG00000197756	*RPL37A*	5.2	1.9	3.5	5.8	2.5	3.5
2	217385497	217393993	ENSG00000241836	*AC073321.5*	5.0	1.9	3.4	5.7	2.5	3.5

IPA pathway analysis of IR genes

Supplement Table S 5 IPA analaysis of 824 IR genes. *Canonical pathways and their associated genes are listed.*

Ingenuity Canonical Pathways	Genes in dataset
Sonic Hedgehog Signalling	*SUFU, DYRK1B, PRKAR1B, PRKACB, DYRK1A*
TNFR1 Signalling	*FOS, TRAF2, APAF1, MADD, MAP3K1, CASP7*
Molecular Mechanisms of Cancer	*APAF1,J AK2, BCL2L11, CTNNB1, RBPJ, EP300, TAB2, PRKACB, PTK2, BAD, FOS, SUFU, ARHGEF7, SMAD5, ITGB1, SMAD1, PRKAR1B, PRKD1, RASA1, RB1, RAC1, CASP7*
ERK/MAPK Signalling	*EP300, PPP2R3A, PRKACB, PTK2, BAD, DOCK1, FOS, CREB5, ITGB1, MKNK1, PRKAR1B, EIF4E, RAC1*
Proein Kinase A Signalling	*DUSP10, CALM1, EYA2, CTNNB1, EP300, PLCE1, PRKACB, PTK2, MTMR3, EYA3, BAD, ANAPC1, PTPRK, PDE7A, CREB5, MAP3K1, PTPN21, PRKAR1B, PRKD1, RYR2, DUSP16*
FAK Signalling	*ARHGEF7, ITGB1, ACTA2, PTK2, ARHGAP26, RAC1, DOCK1*
Nucleotide Excision Repair Pathway	*ERCC1, GTF2H2, POLR2F, ERCC6*
Endoplasmic Reticulum Stress Pathway	*TRAF2, ERN1, CASP7*

Eigenständigkeitserklärung

Hiermit versichere ich, dass ich die vorliegende Dissertation mit dem Titel “THE TRANSCRIPTIONAL AND EPIGENETIC ROLE OF BRD4 IN THE REGULATION OF THE CELLULAR STRESS RESPONSE” selbständig verfasst und keine weiteren als die angegebenen Hilfsmittel verwendet habe. In der Arbeit verwendete Aussagen anderer Autoren habe ich durch Quellenangabe kenntlich gemacht. Die vorliegende Arbeit wurde in keinem früheren Promotionsverfahren eingereicht oder als ungenügend beurteilt.

Berlin, den

Publication Record

Hussong M, Kaehler C, Kerick M, Grimm C, Franz A, Timmermann B, Welzel F, Isensee J, Hucho T, Krobitsch S, Schweiger MR. The bromodomain protein BRD4 regulates splicing during heat shock. (2016) Nucleic Acids Res. 2016 Aug 17.

Hussong, M. and Schweiger, MR. Oxidative stress and Cancer Epigenomics. (2016) Epigenetics: A Different Way of Looking at Genetics, Springer-Verlag, ISBN-13 9783319271842

Hussong, M., Borno, S. T., Kerick, M., Wunderlich, A., Franz, A., Sultmann, H., Timmermann, B., Lehrach, H., Hirsch-Kauffmann, M., Schweiger, M. R. The bromodomain protein BRD4 regulates the KEAP1/NRF2-dependent oxidative stress response. (2014) Cell Death Dis, 5, e1195. doi:10.1038/cddis.2014.157

Schweiger, M. R., **Hussong, M**., Rohr, C., & Lehrach, H. Genomics and epigenomics of colorectal cancer. (2013) Wiley Interdiscip Rev Syst Biol Med, 5(2), 205-219. doi: 10.1002/wsbm.1206